Polymer Immobilised Ionic Liquid Supported Catalysts: Synthesis, Characterisation and Applications

Tina See Tin Tran

A thesis submitted in the partial fulfilment of the requirements for the award of

Doctor of Philosophy

School of Natural and Environmental Sciences

(Chemistry)

Newcastle University

September 2020

Abstract

Due to increasing demand for synthetic commodities, to reduce the overall environmental impact of existing chemical processes, a sustainable approach is required. In order to accomplish this, it will be necessary to use highly efficient, durable, and scalable catalyst technologies which are low in energy consumption and waste production. In addition, bio-renewable feedstock will also be required due its abundancy and availability. In this regard, chapter 1 provides an overview of the unique physicochemical properties and concepts of ionic liquids (ILs). The incorporation of ILs can produce functional materials, which in turn, can be used for the sustainable conversion of bio-renewable feedstock.

Chapter 2 discusses the rational design and synthesis of a range of ruthenium nanoparticle (RuNP) catalysts, in which, the catalysts were tested in the hydrogenation of the benchmark substrate acetophenone. The overall aim of this work was to investigate the effect of the interactions between the ruthenium and the polymer support on the catalyst performance and selectivity. The resulting catalysts were highly active and selective in the hydrogenation of a range of α,β-unsaturated ketones, aldehydes, and the study was extended to include bio-derived substrates. In total four reactions were tested, namely the hydrogenation of acetophenone, furfural, levulinic acid and ethyl levulinate. The low ruthenium loadings and the reusability of these heterogenous catalysts, in addition to the use of water as the co-solvent/solvent, has provided a sustainable hydrogenation method, which is among one of the highest reported on comparison with the literature. Chapter 3 covers the application of the RuNPs for the hydrazine-mediated reduction of a broad range of nitroaromatics to their corresponding aromatic amines under mild conditions with low catalyst loadings.

Chapter 4 details the synthesis of a set of imidazolium polystyrene-based Brønsted acid catalysts immobilised with peroxophosphotungstate anions. These efficient and selective catalysts were tested, as catalysts for the alcoholysis of furfuryl alcohol to produce alkyl levulinates, under batch as well as continuous flow regimes. Such generated levulinates are highly desirable as bio-renewable fuel additives.

Acknowledgements

First of all, I would like to express my sincere gratitude and appreciation to my supervisor, Dr Simon Doherty, for his daily guidance, support and patience over the last four years, both in and out of the lab. As well as Dr Julian Knight for his co-supervision, valuable advice, and insights.

My thanks and appreciation to my past colleagues, Dr Tom Backhouse, Dr Phillip Layford, Francesca Stals, Dominic Shiels, Dr Graeme Bowling and Dr Kate Phipps for providing a supportive working environment, friendship and the endless gossip/tea breaks.

I would also like to thank the academic collaborators for their expertise and for carrying out the chemical analysis that was crucial to this work. Dr John Mallows (Newcastle University) for providing all the TGA in chapters 2-3. Dr Tom Chamberlain (Leeds University), for providing all the TEMs in chapter 2. Prof Chris Hardacre (Manchester University), who provided the XPS spectra for chapter 2. Dr Haresh Manyar (Queens University, Belfast) for the use of his GC-MS in chapter 3. Dr Michael Carroll for allowing me to use of his FlowSyn apparatus and for offering me advice for the work carried out in chapter 3 and Dr Nick Rees (Oxford University), for providing all of the solid-state NMR spectra.

Last, and most importantly, I would like to give a special thanks to my parents and sisters: Karen and Cindy – Thank you all, for your endless support, encouragement and all your belief in me.

Table of Contents

List of Figures

for 1-phenylethanol (**B**) = [% 1-phenylethanol / (% 1-phenylethanol + % cyclohexylethanol)].

Figure 2.20: Conversion and selectivity for the hydrogenation of acetophenone as a function of the catalyst loading. Reaction conditions: 1 mmol substrate, RuNP@OPPh$_2$PEGPIILP (**2.20**) (specified amount), 0.1 mmol K$_2$CO$_3$, 50 ℃, 70 psi H$_2$, 12 mL 1:1 EtOH/water, reaction time = 1 hour. Conversion and selectivity determined by ^{1}H NMR spectroscopy with 1,3-dinitrobenzene as the internal standard. Selectivity for 1-phenylethanol (**B**) = [% 1-phenylethanol / (% 1-phenylethanol + % cyclohexylethanol)].

Figure 2.21: Monitoring of the catalytic hydrogenation of acetophenone as a function of time. Reaction conditions: 1 mmol acetophenone, 0.1 mol% RuNP@OPPh$_2$PEGPIILP (**2.20**), 0.1 mmol K$_2$CO$_3$, 70 psi H$_2$, 50 ℃, 12 mL 1:1 EtOH/water, reaction time = 3 hour. Conversion and selectivity determined by ^{1}H NMR spectroscopy with 1,3-dinitrobenzene as the internal standard. Selectivity for 1-phenylethanol (**B**) = [% 1-phenylethanol / (% 1-phenylethanol + % cyclohexylethanol)].

Figure 2.22: Recycling profile for the hydrogenation of benzaldehyde catalysed by **2.20**. Reaction conditions: 1 mmol benzaldehyde, 0.1 mol% RuNP@(O)PPh$_2$PEGPIILP (**2.20**), 70 psi H$_2$, 50 ℃, 12 mL water, reaction time = 90 mins. Conversion and selectivity determined by ^{1}H NMR spectroscopy with 1,3-dinitrobenzene as the internal standard. Selectivity for benzyl alcohol = [% benzyl alcohol / (% benzyl alcohol + % other products)].

Figure 2.23: (a) HRTEM image of the catalyst after the 10th recycle for the hydrogenation of benzaldehyde in water catalysed by **2.20** and (b) particle size distribution for RuNP@O=PPh$_2$-PEGPIILP (**2.20**) after 10 recycles showing an average NP diameter of 1.31 ± 0.42 nm. Scale bars are 5 nm (white).

Figure 2.24: Monitoring of the complete catalytic hydrogenation of acetophenone as a function of time. Reaction conditions: 1 mmol acetophenone, 0.1 mol% RuNP@OPPh$_2$PEGPIILP (**2.20**), 0.1 mmol K$_2$CO$_3$, 12 mL 1:1 EtOH/water, 70 ℃, 400 psi H$_2$, reaction time = 70 minutes. Conversion and selectivity determined by ^{1}H NMR spectroscopy with 1,3-dinitrobenzene as the internal standard. Selectivity for 1-

cyclohexylethanol (**D**) = [% 1-cyclohexylethanol / (% 1-phenylethanol + % cyclohexylethanol)].

Figure 2.25: Conversion and selectivity for the hydrogenation of furfural as a function of hydrogen pressure. Reaction conditions: 1 mmol furfural, 0.1 mol% RuNP@(O)PPh$_2$PEGPIILP (**2.20**), H$_2$ (specified), 50 ℃, 12 mL water, reaction time = 45 mins. Conversion and selectivity determined by ^{1}H NMR spectroscopy with 1,3-dinitrobenzene as the internal standard. Selectivity for furfuryl alcohol (**F**) = [% furfuryl alcohol / (% furfuryl alcohol + % tetrahydrofurfuryl alcohol)].

Figure 2.26: Product distribution for the catalytic hydrogenation of levulinic acid (**H**) as a function of time. Reaction conditions: 1 mmol levulinic acid, 0.1 mol % RuNP@(O)PPh$_2$PEGPIILP **2.20**, 12 mL water, 100 ℃, 400 psi H$_2$. Conversion and selectivity determined by ^{1}H NMR spectroscopy with 1,3-dinitrobenzene as the internal standard. Selectivity for γ-valerolactone (**J**) = [% γ-valerolactone / (% 4-hydroxypentanoic acid + % γ-valerolactone)].

Figure 2.27: Product distribution for the hydrogenation of levulinic acid catalysed by **2.20** with a base additive as a function of time. Reaction conditions: 1 mmol levulinic acid, 0.1 mol % RuNP@(O)PPh$_2$PEGPIILP **2.20**, 0.1 mmol K$_2$CO$_3$, 12 mL water, 100 ℃, 400 psi H$_2$. Conversion and selectivity determined by ^{1}H NMR spectroscopy with 1,3-dinitrobenzene as the internal standard. Selectivity for γ-valerolactone (**J**) = [% γ-valerolactone / (% 4-hydroxypentanoic acid + % γ-valerolactone)].

Figure 2.28: Reuse study for the hydrogenation of levulinic acid (**H**) catalysed by **2.20**. Reaction conditions: 1 mmol levulinic acid, 0.1 mol % RuNP@(O)PPh$_2$PEGPIILP **2.20**, 1 mmol Amberlyst-15, 12 mL water, 100 ℃, 400 psi H$_2$, 4h. Conversion and selectivity determined by ^{1}H NMR spectroscopy with 1,3-dinitrobenzene as the internal standard. Selectivity for γ-valerolactone (**J**) = [% γ-valerolactone / (% 4-hydroxypentanoic acid + % γ-valerolactone)].

Figure 2.29: Product distribution for the hydrogenation of ethyl levulinate (**K**) catalysed by **2.20** with a base additive as a function of time. Reaction conditions: 1 mmol ethyl levulinate, 0.1 mol % RuNP@(O)PPh$_2$-PEGPIILP **2.20**, 0.1 mmol K$_2$CO$_3$, 12 mL water, 100 ℃, 400 psi H$_2$. Conversion and selectivity determined by ^{1}H NMR spectroscopy with 1,3-dinitrobenzene as the internal standard. Selectivity for γ-

valerolactone = [% γ-valerolactone / (% 4-hydroxypentanoic acid ethyl ester + % γ-valerolactone)].

Chapter 3: RuNP-Catalysed Reduction of Nitroarenes

RuNP@(O)PPh$_2$PEGPIILP (2.20), 3 mmol reducing agent, 2 mL EtOH, 40 ℃, 1 h. Conversion and selectivity determined by ^{1}H NMR spectroscopy with dioxane as the internal standard. Average of 3 runs. Selectivity for aniline = [% aniline / (% aniline + % *N*-phenylhydroxylamine + % azoxybenzene)].

of 3 runs. Selectivity for aniline = [% aniline / (% aniline + % *N*-phenylhydroxylamine + % azoxybenzene)].

Chapter 4: Brønsted Acid Ionic Liquid Catalysed Alcoholysis of Furfuryl Alcohol

the internal standard. Selectivity for *n*-butyl levulinate = [% *n*-butyl levulinate / (% *n*-butyl levulinate + % 2-butoxymethylfuran)]. Average of 3 runs.

Figure 4.33: Conversion-selectivity profile as a function of the time-on-stream (6 hours) for the continuous flow alcoholysis of FFA catalysed by **4.10**/SiO$_2$, **4.11**/SiO$_2$ and **Amberlyst-15**/SiO$_2$. Reaction conditions: catalyst, 1.0 g on 1.0 g of silica; 0.32 M FFA in *n*-butanol; temperature, 130 ℃; flow rate, 1.1 mL min^{-1}; injection volume, 360 mL. Conversion and selectivity determined by ^{1}H NMR spectroscopy with 1,4-dioxane as the internal standard. Selectivity for *n*-butyl levulinate = [% *n*-butyl levulinate / (% *n*-butyl levulinate + % 2-butoxymethylfuran)]. Average of 2 runs.

List of Tables

List of Schemes

List of symbols and abbreviations

δ	Chemical shift
AIBN	Azobisisobutyronitrile
AL	Alkyl Levulinate
AMF	Alkoxy methyl furan
AN	Aniline
AYB	Azoxybenzene
BET	Brunauer-Emmett-Teller
BL	Butyl Levulinate
[BMIM]	1-butyl-3-methylimidazolium
CNT	Carbon Nanotubes
COD	1,5-cyclooctadiene
COT	1,3,5-cyclooctatriene
d	doublet
DFNS	Dendritic fibrous nanosilica
DLS	Dynamic Light Scattering
DRIFTS	Diffuse Reflectance Infrared Fourier Transform Spectroscopy
DSC	Differential Scanning Calorimetry
DVB	Divinylbenzene
DLVO	Derjaugin-Landau-Verwey-Overbeek
EL	Ethyl Levulinate
equiv.	equivalent(s)
FF	Furfural
FFA	Furfuryl Alcohol
FIL	functionalised ionic liquids
FT-IR	Fourier Transform InfraRed
GVL	γ-valerolactone
h	hour
HPA	Heteropoly Acid
ICP-OES	Inductively Coupled Plasma Optical Emission Spectrometry
ID	Inner diameter
IL	Ionic liquid

J	Coupling constant
LA	Levulinic acid
m	multiplet
MIMBS	1-(4-sulfonic acid) methylimidazolium
NB	Nitrobenzene
NHC	*N*-heterocyclic carbene
NMR	Nuclear magnetic resonance
NP	Nanoparticle
NPHA	*N*-phenylhydroxylamine
PEG	Polyethylene Glycol
PFIL	Phosphine-Functionalised Ionic Liquid
PIIL	Polymer-Immobilised Ionic Liquid
PIILP	Polymer-Immobilised Ionic Liquid Phase
PIL	Polyionic Liquid
POM	Polyoxometalate
ppm	parts per million
PTA	phosphotungstic acid
PyOx	pyridine-oxazoline
q	quartet
rpm	revolutions per minute
ROMP	Ring-Opening Metathesis Polymerisation
RTIL	Room Temperature Ionic Liquid
RuNP	Ruthenium Nanoparticle
s	singlet
SCILL	Solid Catalyst with Ionic Liquid Layer
SEM	Scanning Electron Microscopy
SFILs	Sulfonated-Functionalised Ionic Liquids
SILP	Supported Ionic Liquid Phase
SMSI	Strong Metal-Support Interactions
t	triplet
TBA	tetra n-butylammonium
TEM	Transmission Electron Microscopy
TGA	Thermal Gravimetric Analysis
TMNP	Transition Metal Nanoparticles

TOF	Turnover Frequency
TON	Turnover Number
TPPTS	trisulphonated triphenylphosphine
TSIL	Task Specific Ionic Liquid
wt. %	weight percentage of total mass
XAS	X-ray Absorption Spectroscopy
XPS	X-ray Photoelectron Spectroscopy
XRD	X-ray Diffraction

Chapter 1

Ionic Liquids, Nanoparticles, SILP and PIILP Catalysis

1.1 Introduction

The efficient synthesis of organic compounds is an important goal across a wide range of scientific fields, ranging from biology, chemistry and materials. Currently, there is a great drive to develop sustainable and more environmentally-benign processes in line with the "12 Principles of Green Chemistry"[1] and atom efficiency.[2] The intent of Green Chemistry is to design chemicals and processes that will be less damaging to the environment and human health. To this end, catalysis is a vital tool in the development of "greener" processes. The utilisation of molecular homogeneous catalysts is well-documented, particularly with regards to the use of single well-defined active sites that are considerably more active and selective than their heterogeneous counterparts. Given this, the use of molecular catalysts has been widely applied throughout the chemical industry in processes such as hydroformylation, oxidation, metathesis, oligomerisation and carbonylation.[3] However, the challenging separation and recycling of the catalyst is a considerable drawback that has prevented the widespread use of homogeneous catalysts as it often results in the contamination of both the products and catalyst. Recovery of the catalyst often requires expensive purification procedures, which in general, are counter to the previously mentioned green principles in addition to adding further costs to the process. In contrast, the use of a heterogeneous catalyst avoids this problem as the catalyst can be filtered in a straightforward procedure and provided that leaching is negligible the catalyst can be recovered and recycled. However, there is an overall reduction in the catalyst performance, partially due to the ill-defined active sites of the catalyst, which are less efficient at reactant and/or reaction intermediate adsorption;[3b] as a matter of fact, quite a few of the above industrial transformations lack a heterogeneous counterpart.

In addition to the use of catalysis to improve the "green" credentials of a process, the solvents that are used in these processes are now under more scrutiny. In terms of conventional volatile organic solvents, additional concerns arise from their flammability and lasting environmental impact. For example, the use of conventional solvents constitutes 60% of the energy that is consumed in an industrial pharmaceutical process and 50% of the emissions of post-treatment greenhouse gases.[4] In an effort to address the issues associated with organic solvents, several alternative non-conventional reaction media have been examined where the homogeneous catalyst is immobilised to allow for catalyst recycling, such as ionic

liquids, supercritical carbon dioxide (scCO$_2$), perfluorinated solvents and water.[5] In general, these alternative reaction media have been successfully applied to a variety of transformations such as oxidation, hydroformylation, hydrogenation and metal-catalysed C-C bond coupling which form biphasic systems whereupon the product can be either extracted by a gaseous reagent stream or with a solvent.[6] Despite their successful applications there are severe drawbacks to this approach which include the solubility/miscibility of the catalyst or reagent and, in the case of fluorous solvents, hydrofluoric acid is generated under the harsh reaction conditions. Based on all of the investigated non-conventional reaction media, it is ionic liquids which have received the greatest attention and have demonstrated the most promise due to their tuneable and unique physicochemical properties.

1.2 Ionic Liquids

1.2.1 History of ionic liquids

Ionic liquids (ILs) are salts with melting points below 100°C that are comprised entirely of ions, which form weakly coordinating ion pairs.[7] In 1914, Walden reported the first ever room temperature molten salt, ethylammonium nitrate [C$_2$H$_5$NH$_3$][NO$_3$] with a melting point of 12-14 °C.[8] In 1940, Hurley and Weir were searching for an easier and cheaper method to electroplate aluminium and developed the first ILs with chloroaluminate anions by heating and mixing aluminium chloride with powdered pyridinium halides to produce a clear colourless liquid.[9] In the late 1970s, Osteryoung et al.[10] and 1980s, Hussey et al.[11] undertook exhaustive studies into room temperature chloroaluminate melts which are considered as the first generation of ILs (Figure 1.1). However, these melts did not find much use as a result of their hygroscopic nature and the fact that they must be prepared and used under an inert atmosphere. During that time, the focus of the research and development was on the electrochemical applications of these ILs.[12]

In the early 1980s, Hussey, Seddon and co-workers[13] started to explore the use of chloroaluminate melts as non-aqueous polar solvents for transition metal complexes and in the mid-1980s, Fry, Pienta,[14] and Boon et al.[15] put forward low melting point ILs as solvents for organic synthesis. In the 1990s, molten salts which had melting points below 100 ℃ were used as unique chemical reaction media and were termed "room

temperature ionic liquids" (RTILs). Then in 1990, Chauvin *et. al.*[16] and Carlin *et al.*[17] reported the first use of ILs for homogeneous catalysis. In regard to the works by Wilkes and Zaworotko,[18] it became apparent that ILs were no longer limited to only chloroaluminate melts and they prepared and developed the first air-stable IL which was composed of the 1-ethyl-3-methylimidazolium cation and the tetrafluoroborate anion (Figure 1.1). In contrast to the previously mentioned chloroaluminate melts, these ILs could be prepared and stored safely without an inert atmosphere and became known as the "second generation" ILs, which have been used as reaction media for a range of organic and inorganic transformations due to their ease of handling.[19]

1st generation — 1980s - Air and water sensitive chloroaluminate Ionic Liquids

$AlCl_4^-$

2nd generation — 1990s - Air and moisture stable Ionic Liquids

BF_4^-

3rd generation — 2000s - Task Specific Ionic Liquids

BF_4^-

Widespread application:
-Catalysts
-Synthesis
-Electrochemistry
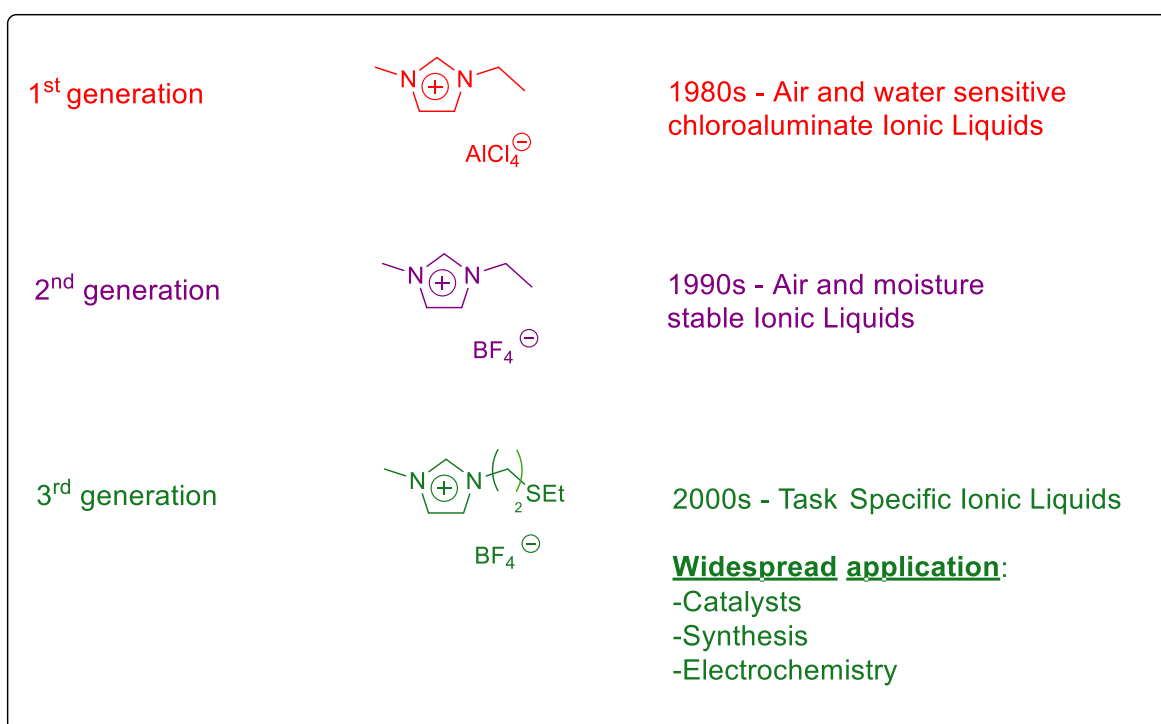
Figure 1.1: The 1st, 2nd and 3rd generation ILs and their widespread application.

In 1996, Bonhôte *et al.*[21] published the synthesis of an IL with CF_3^- containing anions and other fluorinated alkyl groups. These water stable ILs have highly suitable properties, however the $Li[(CF_3SO_2)_2N]$ starting material is potentially prohibitively expensive and could impose a huge problem for their large-scale application. The third generation ILs have functional groups tethered to their cations or anions and are typically referred to as Task Specific Ionic Liquids (TSILs) (Figure 1.1). Most of the studies have focused on functionalisation of the cation, in particular with imidazolium

cations.[22] For example, Mirkhani *et al.* designed a catalytic system composed of a MIL−101(Cr) support with a TSIL for CO_2 cycloaddition to form epoxides (Figure 1.2). The imidazolium cation of this TSIL was covalently bound to a carboxylic acid moiety. The imidazolium component of the IL led to CO_2 activation due to electrostatic interactions, whilst the carboxylic acid moiety was incorporated to activate the epoxide *via* hydrogen bonding.
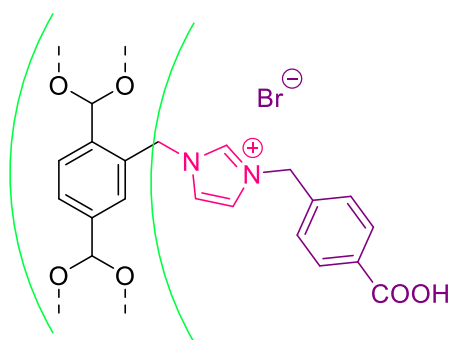
Figure 1.2: MIL-101(Cr)-TSIL for the cycloadditon of CO_2 to form epoxides.

Currently, the number of synthesised RTILs has surpassed 500. In particular, in the past few years, the dialkylimidazolium cation is the most widely investigated heterocyclic cation for developing new ILs. Due to the facile derivatisation of the imidazolium ring, low viscosity as well as their stability to oxidative and reductive reaction conditions.

There is practically an unlimited number of salts with low melting points, though Earle and Seddon[23] have valued this number to be in the order of a billion and the research carried out on their uses and properties has intensified over the years. Figure 1.3 illustrates the number of publications in the last 30 years, including the words in the title, "molten salts" and/or "ionic liquids". As can be seen, the average number of publications has increased constantly representing the rising interest in ILs. The ability to fine-tune the ILs physiochemical properties together with their low volatility has resulted in their implementation in a wide range of applications and it has been estimated that more than half of all publications involving ILs are on their use in synthesis and catalysis.[24] Therefore this part of this thesis will solely focus on assessing their use in this capacity.
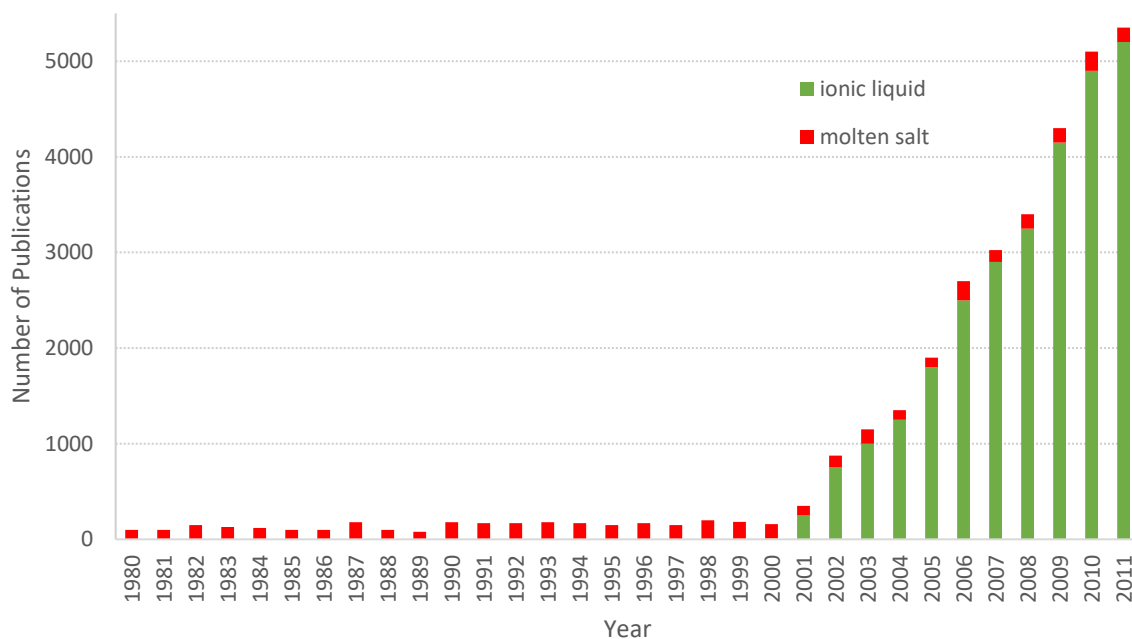
Figure 1.3: The number of papers including the words "molten salts" and/or "ionic liquids" in the title, as a function of time, determined using Scopus.

1.2.2 Physical and Chemical Properties of Ionic Liquids

As the ionic liquids name implies they are liquids made from ions, however, unlike other ionic compounds found in nature (see Table 1.1), ILs have melting points below 100 ℃. It is this remarkable property that makes them extremely unique compounds. Their low melting points arise from a combination of van-der-Waals, coulombic and hydrogen bonding interactions between their ions.

Compound	Melting point/ ℃
Sodium fluoride (cleaning agent)	993
Calcium carbonate (calcium source)	825
Sodium chloride (salt)	801
Potassium bromide (sedative)	734
Potassium iodide (nutritional supplement)	680
Lithium chloride (desiccant)	605

Table 1.1: Ionic compounds in nature with their applications in parenthesis and melting points.

Ionic compounds in nature form a closed packed lattice of cations and anions (Figure 1.4a) and as such they possess high melting points and therefore are solids at room temperature which cannot serve as a solvent. On the other hand, ILs have both the liquid state and ionic character which renders them extraordinary as solvents. ILs are liquids at room temperature because they cannot pack well into a crystal lattice due to the unsymmetrical bulky nature of the organic cation and the charge-delocalised inorganic anion (Figure 1.4b).

a) *Typical inorganic salt structure*   **b)** *Ionic liquid structure*
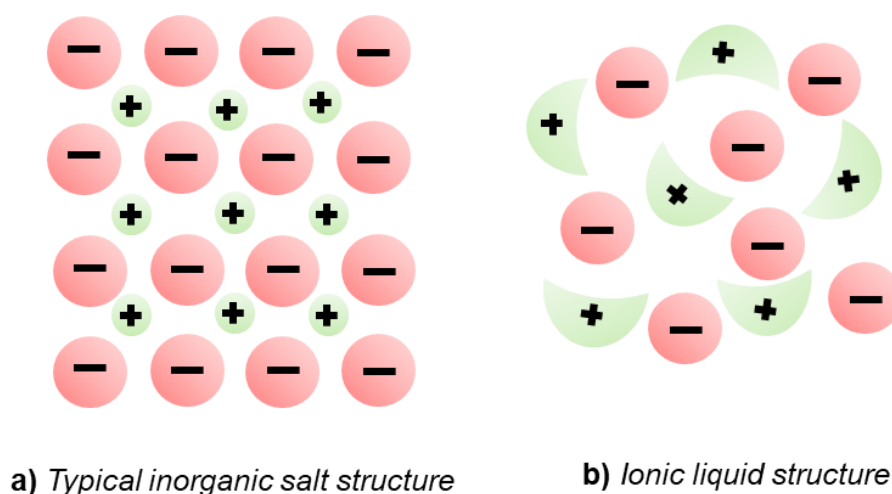
Figure 1.4: The crystal packing of a) a typical inorganic salt and b) an ionic liquid.

ILs are comprised of poorly coordinating ions which makes them highly polar but non-coordinating solvents. They are frequently found to be immiscible with non-polar organic solvents creating an opportunity for a two-phase (biphasic) system operation. In addition, they have the ability to form unique ionic microenvironments which can create both hydrophobic and hydrophilic domains from their alkyl side chains and ionic regions of the IL fragments, respectively.[25a]

Part of the major challenge of conventional volatile organic solvents is that they evaporate into the atmosphere and their resulting vapours are toxic and flammable. This does not occur with ILs as they have very low vapour pressures. This in turn, reduces the exposure to the toxic solvent vapours associated with conventional volatile organic solvents. This at the same time allows for the effective immobilisation of the reaction solvent with a suitable thermally stable catalyst, thereby allowing the products

to be isolated by distillation. The lack of vapour pressure can also be beneficial in catalysis with moisture- and/or air-sensitive transition metal catalysts as water can be removed by heating the solvent under a high vacuum before the reaction. In addition, in contrast to traditional organic solvents, ILs are non-explosive, can be repeatedly used, avoids air pollution problems and hazardous exposure.

At the same time, their main disadvantage is that at room temperature ILs have high viscosities and can be a hundred times higher than those of conventional organic solvents; this makes them challenging to handle and can have a severe detrimental effect on the kinetics and the dynamics of a catalytic process. Highly viscous ILs impose mass transport limitations which can significantly impede the rate determining step of a catalytic reaction and consequently the entire reaction. However, it is possible to lower the viscosity of an IL by tuning the anion.[25b]

The density of ILs can be higher or lower than that of water, varying between 1 and 1.6 g/cm^2. Some physical and chemical properties of ILs can be modified by altering the alkyl chain length in the cation and/or the anion. For example, the solubility of water in ILs can be altered, from being immiscible, to soluble, by merely switching the anion from Cl^- to PF_6^-. Figure 1.5 shows some cations where different alkyl chains may be attached and various anions. By rational selection of the cation and anion, ILs have been shown to enhance activity and selectivity of a reaction by stabilising the reactive intermediates or catalytic species.[26] By cation-anion pairings, approximately 10^{18} different ILs can be generated.[27] It is this extraordinary potential for structural diversity which has led to one of the main aspects of IL application, enabling for the fine-tuning of their physicochemical properties to fit any intended application.
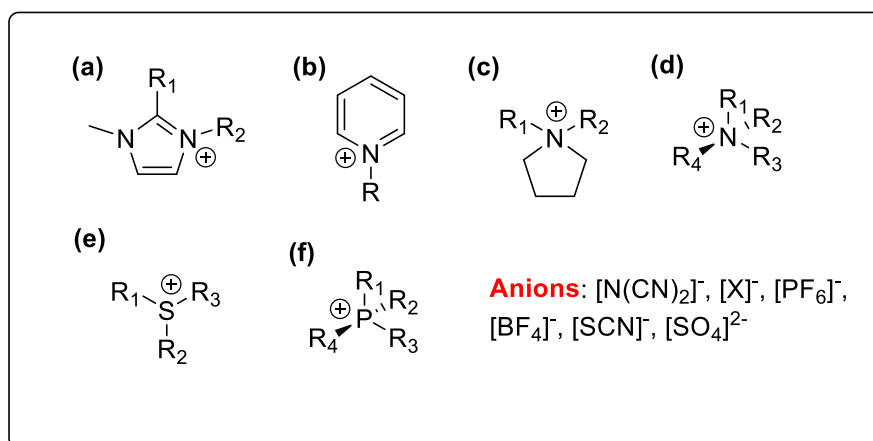
Figure 1.5: A range of common IL cations and anions; a) imidazolium, b) pyridinium, c) pyrrolidinium, d) ammonium, e) sulfonium and f) phosphonium.

Wasserscheid indicated that the good thermal stability of ILs, of up to 450 ℃ is due to the strength of their N-H and N-C bonds. However, high temperatures are only tolerated for brief periods and eventually decomposition occurs after long periods of exposure.[28] Furthermore, ILs have high conductivities (~10 mS cm^{-1}) owing to the fact that the ILs are composed entirely of ions, in addition they have comparatively large electrochemical windows and as a result they can act as electrolytes.

1.2.3 Synthesis and Applications of Ionic Liquids

As illustrated in figure 1.5, various types of IL architectures are possible, however, those based on the dialkylimidazolium cation are the most common as alkylimidazole is synthesised on an industrial scale. There are 5 main synthetic pathways to generate this class of IL (Scheme 1.1), each of which has associated benefits and drawbacks. The most commonly used method for the synthesis of ILs involves quaternisation of an imidazole with an alkyl halide followed by the metathesis with an appropriate metal-counter anion (MA) (Scheme 1.1, Route 1).
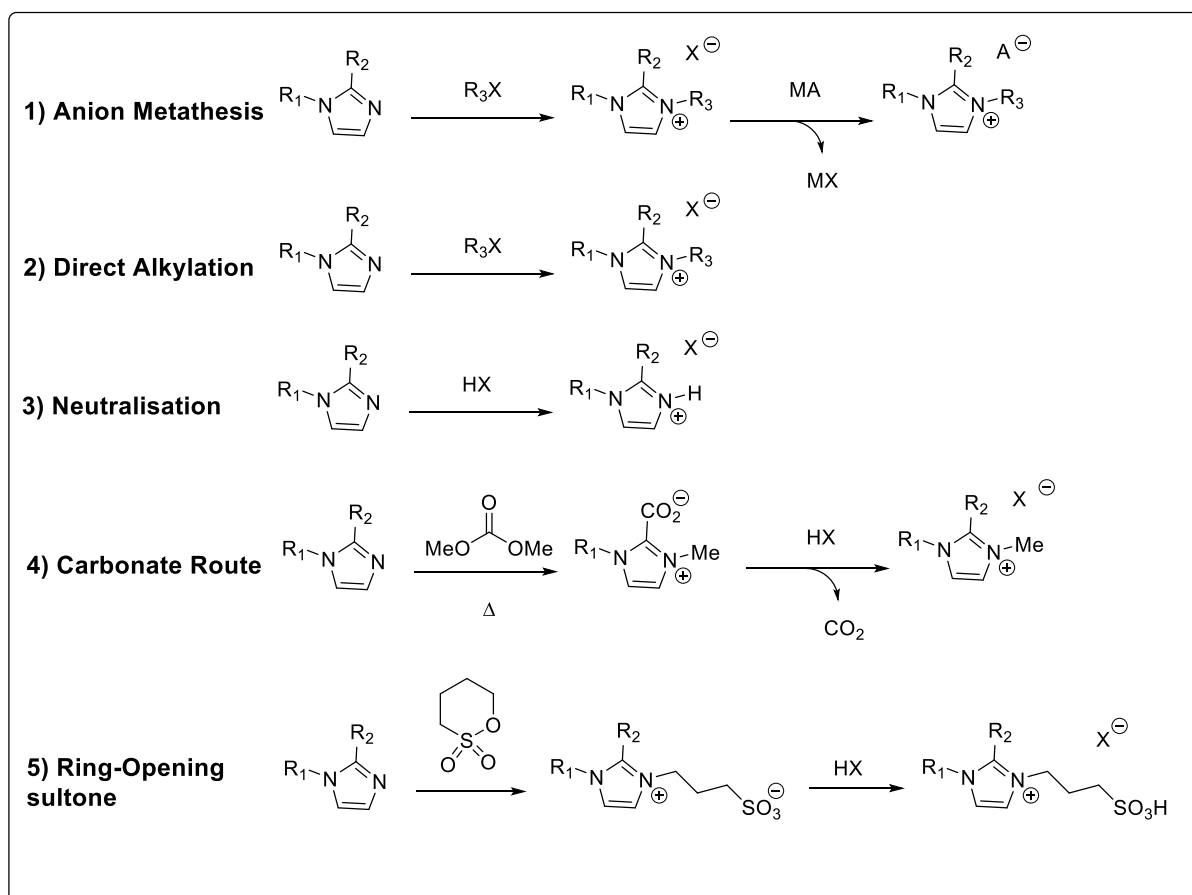
Scheme 1.1: The general routes employed to synthesise imidazolium-based ionic liquids.

While this chemistry is fairly straightforward, it significantly reduces any 'green' merits of the IL in question by the stoichiometric formation of metal halide (MX) byproduct which can often be labour intensive, costly and time consuming to remove. This can often be problematic in particular for hydrophilic ILs, as both the aqueous extraction and the filtration to remove the metal salt by-product are rendered impractical. Other common routes for the synthesis of ILs include direct alkylation (Scheme 1.1, Route 2) or base neutralisation with a Brønsted acid (Scheme 1.1, Route 3). Although these approaches have high atom efficiency they often form impurities which are challenging to remove. The functionality that can be incorporated into the IL is limited by the availability of the alkylating agent and the reaction is usually nonquantitative. These methods have been used to prepare phosphate-, sulfate- and sulfonate-based ILs. Alternatively, the use of a dimethyl carbonate has recently been employed as an alternative alkylating agent to alkyl halides (Scheme 1.1, Route 4). Subsequent anion exchange with either water or a suitable Brønsted acid can generate

numerous ILs with different physicochemical properties; this approach avoids the use of metal-based reagents.[30a] An anion-functionalised IL can be directly accessed *via* a one-step ring-opening reaction of sultones to form zwitterions with high melting points (Scheme 1.1, Route 5). These zwitterions can then be reacted with acids to generate functionalised ILs.[30b]

The purity of ILs has been demonstrated to have a significant role in their catalytic performance. The presence of impurities such as unreacted alkyl halides, protic reagents (especially water) and inorganic halides can considerably alter both the chemical and physical properties of the IL and therefore influence the catalyst performance.[31] Although, the presence of water is problematic as a result of the general hygroscopic nature of ILs, the other impurities are artefacts which arise during the synthesis of an IL.

In recent years the fine-tuning of the ILs physicochemical properties such as its polarity, hydrophobicity, density and viscosity has attracted considerable interest throughout the academic literature.[32] Moreover, ILs can be easily modified to possess properties which can optimise their performance in a range of different chemical applications due to their high thermal stability, ionic conductivity and broad electrochemical window.[33] These properties allow for safe IL storage, facile product separation, catalyst recovery and solvent recycling. Owing to their properties, ILs have a wide range of applications in multiple processes. Currently, ILs are not only used as solvents but also as catalyst activators or catalysts, lubricants and/or electrolytes for batteries.[34]

As previously stated in section 1.1.1, over half of all publications related to ILs focus on their use in catalysis. Nowadays, catalysis is defined as the presence of a catalyst which accelerates a chemical reaction. The purpose of the catalyst is to provide an alternative reaction mechanism, consisting of a different transition state, typically with a lower activation energy (Ea). As a result, more molecules possess enough energy to overcome this barrier enabling them to react and form the product. Catalysis can be split into three main types; homogeneous, where the catalyst and substrates are all dissolved in the same phase; heterogeneous, where the catalyst is separate as a solid to the reagents and products and biological, in which naturally occurring enzymes are used. From an economical approach, there is a strong interest

in homogeneous catalysis as higher activities and product selectivities can be achieved whilst extremely small amounts of the precious and expensive catalysts are used.[35] However, the major problem with homogeneous catalysis involves the separation and recyclability of the catalyst after the reaction.[36] Common approaches to avoid this problem include the use of an IL as the solvent, either in a biphasic or in a Supported Ionic Liquid Phase (SILP)-based system; the latter is discussed in section 1.3.

ILs can be fine-tuned to become hydrophilic, entirely hydrophobic, or partially water miscible allowing them to be used for biphasic extractions. In an optimal liquid-liquid biphasic system (Figure 1.6), the IL homogenously dissolves the starting materials and catalyst. The final product can be extracted using an immiscible organic solvent leaving the catalyst in the IL phase.
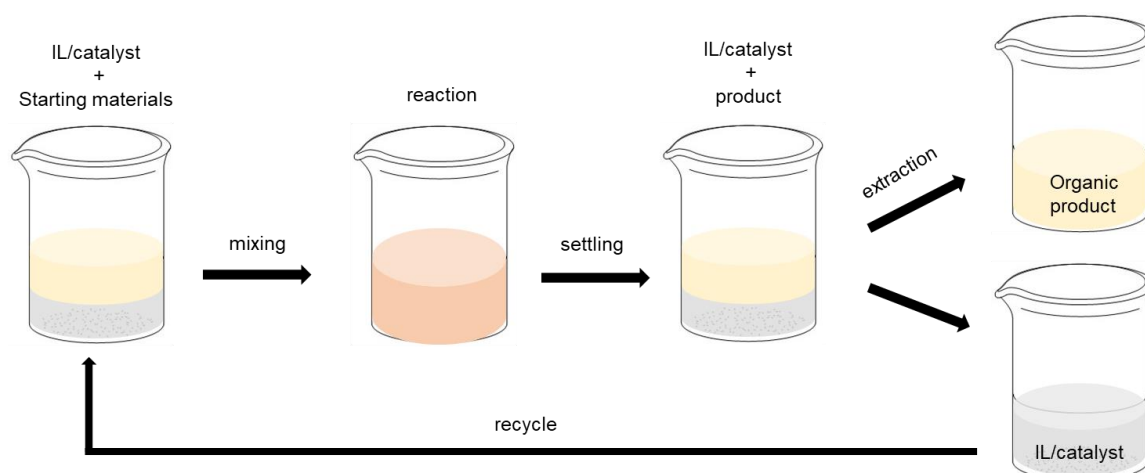
Figure 1.6: An ideal biphasic ionic liquid-based liquid-liquid catalytic system.

Besides simplifying product separation, liquid-liquid biphasic systems are often employed as the IL combines the advantages of homogeneous catalysis with the immobilisation benefits associated with heterogeneous catalysis which allows the catalyst to be recovered, recycled and reused. In practice, once the product has been decanted or extracted, the IL phase can be directly reused after a further purification/drying step. This is particularly beneficial as the IL or the catalyst are often the most expensive aspect of a reaction. However, in most cases the catalyst activity and selectivity often drops after successive reuse which is usually a result of ligand and/or catalyst leaching due to the mutual solubilities of the two phases during the extraction and/or purification processes between the catalytic cycles. As a result the

product can be contaminated by the IL/catalyst. Whilst conventional organic solvents have been successfully used to extract unreacted reactants and products from the IL, their use can significantly diminish the green/environmentally benign aspects of a biphasic liquid-liquid system. In this context, the use of ILs as a bulk solvent can significantly facilitate product separation through their unique solubilities and non-volatile nature enabling product extraction and/or distillation. Again, in this regard, the IL's tuneable nature enables the performance to be optimised in terms of catalyst activity, selectivity, stability and retention. In a thermoregulated system, a homogeneous mixture of IL and co-solvent allows for the efficient mixing of the reactant and the catalyst at high temperatures, while after cooling, the mixture separates to create a biphasic system which enables the organic product-containing layer to be separated as described above. Such examples include the use of IL-water systems in hydrogenation[37] and a fluorous-tagged IL-toluene system in hydrosilylation.[38]

Due to the ILs beneficial role in catalysis in terms of the potential improvements in the reaction performance, catalyst immobilisation and product separation, they have found application in new process technologies across all chemical sectors in industry, whether at the pilot plant or at the full commercial scale.[39] Continuous flow systems have been frequently used and extensively studied for organic and/or inorganic synthesis, in comparison to batch reactions these systems enable facile reaction scale-up and product separation. These flow systems act as an intermediary between bench-top chemistry and the industrial manufacturing scale. ILs are extensively used worldwide in industry for many processes employed by different companies. One of the main applications and possibly the most accomplished example of an industrial process that uses an IL is BASF's BASIL™ (Biphasic Acid Scavenging utilising Ionic Liquids) process. In this method, 1-methylimidazole is used to scavenge the acid that is formed during the synthesis of alkoxyphenylphosphines from the corresponding chlorophosphine which is then recycled and introduced back into the system (Figure 1.7).
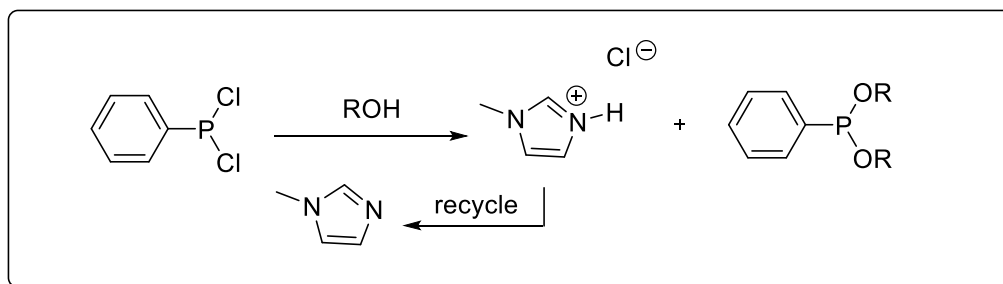
Figure 1.7: The BASF's BASIL™ process.

The previous process used triethylamine to scavenge the acid and produced triethyammonium chloride with a 50% yield and a space time yield of 8 Kg m^{-3} h^{-1} as a thick insoluble paste which made the mixture hard to handle. The replacement of the triethylamine with methylimidazole, meant that the by-product salt could be easily separated as a liquid and the yield increased to 98% along with an improved space time yield of 690,000 kg m^{-3} h^{-1}.[39] This process has also been extended to various other acid scavenger processes such as acylation, elimination, phosphorylation, sulfurylation, silylation and deprotonation.[40,41]

To close, ILs possess unique properties and have a range of application for catalytic processes which allows for enhancements in the catalyst performance. As well as being able to be recycled, reused and optimised for specific processes. Nevertheless, their effect and role on a reaction is often extremely complex, such that, making predictions about their reactivities becomes particularly difficult. While definitely advantageous under the appropriate conditions, the common severe limitations of ILs, particularly their high viscosity and significant cost prevents their large-scale application. As a result, there has been intense interest in the chemical community to develop novel, alternative approaches which use less IL for their application. Concerning the synthesis of ILs, the purity of the final product can often be complex, as previously mentioned, as a result of the nonquantitative nature of IL synthesis. Unreacted inorganic salts, imidazolium bases and water impurities which are formed during IL synthesis can all have a significant influence on the catalyst performance. Although this impact is not always unfavourable it does emphasise the need for a better understanding of the implementation of ILs and their purity when they are employed in catalysis. Additional issues arise regarding IL synthesis when their

overall 'green credentials' are considered. As ILs have largely been found to be green alternatives to organic solvents, the often-lengthy synthesis could likely outweigh any positive effects. The high viscosity of ILs could be argued as one of their obvious drawbacks which impose mass transport limitations on the system. Whilst this problem can be minimised through ion pair fine-tuning, the added complication to a procedure does highlight that ILs used in the liquid phase, either in a biphasic liquid-liquid system or as a bulk solvent are far from ideal. Other issues can also arise with regards to the biphasic system because of the prerequisite of a co-solvent, again, potentially invalidating the 'green credentials' of ILs. While it should be possible to recycle and reuse the IL/catalyst phase this process is far from perfect as the IL and/or catalyst often leaches.

1.2.4 Ionic Liquids for the Conversion of Biomass

An increase in the environmental pollution and CO_2 emissions along with the diminishing fossil fuel resources have triggered efforts to generate renewable biofuels for biorefinery and commodity chemicals.[42] Of the vast number of biomass resources, nonedible lignocellulose is the most abundant carbon-containing resource on earth.[43] Cellulose is a polymer consisting of glucose units attached through β-1,4-glycosidic bonds, however, the polymer is insoluble due to the extensive intra- and intermolecular hydrogen bond networks.[44] Irrespective of its challenging nature, cellulose can be deconstructed into glucose that can then be converted into several biofuels and platform molecules such as levulinic acid, γ-valerolactone, sorbitol, lactic acid, 5-hydroxymethylfurfural (HMF) and hydrocarbons for facile synthetic diversification (Scheme 1.2).
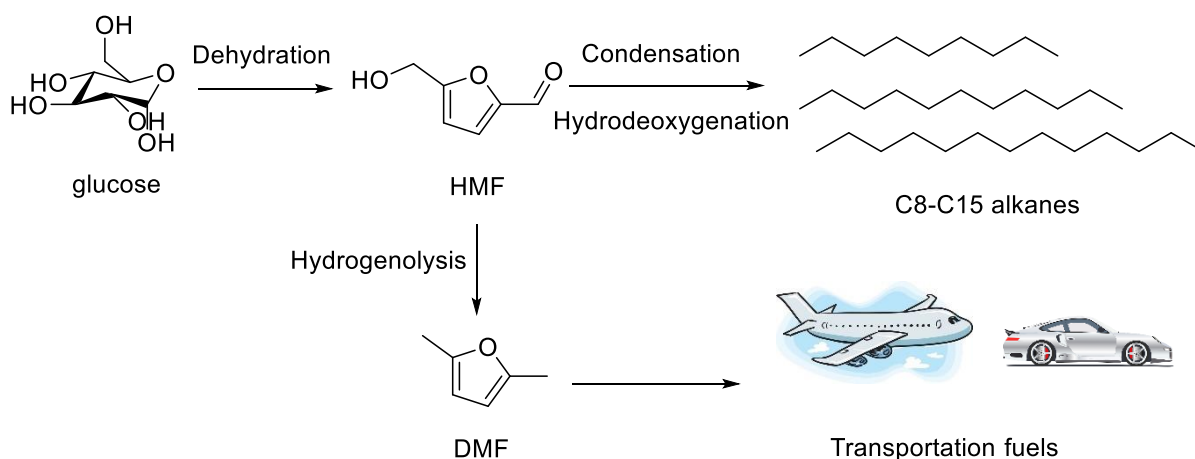
Scheme 1.2: Conversion of glucose to platform molecules for biofuels.

A primary goal going forward for green chemistry is targeting molecules that are essential to industrial processes that could be retro-synthetically associated to bioderived feedstock. The challenging defunctionalisation of highly oxygenated substrates must be addressed for the utilisation of biomass as a renewable source of carbon. To this end, the green credentials, tuneable physical properties and their ability to solvate oxygenated species renders ILs ideal solvents for these transformations. Furthermore, the high thermal stability of ILs makes them a good practical medium since the reaction temperatures needed for these processes are above those of conventional volatile organic solvents. As an example of the use of ILs in green chemistry, Leitner and co-workers showed that ILs could serve as either a stabiliser or a reaction medium for the selective RuNP-catalysed hydrogenation of bioderived aldehydes and ketones (Scheme 1.3).[45] By altering the nature of the IL, particularly the anion, the selectivity could be fine-tuned to either the C=O, arene, C=C or heteroaromatic functionality. The nanoparticles size was shown to be dependent on the particle's interaction and the nature of the IL both of which were important for the high catalyst activity that was comparable to the homogeneous system but with the added advantage of catalyst recyclability in supercritical CO_2.
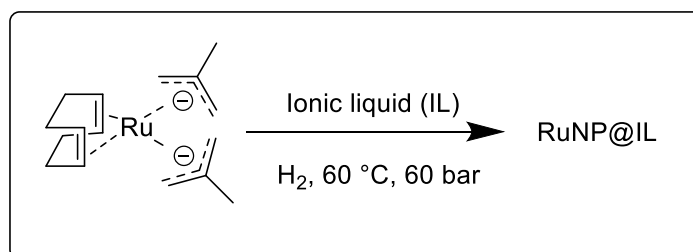
Scheme 1.3: Synthesis of RuNPs stabilised by ILs that are used as catalysts for the hydrogenation of bioderived aldehydes and ketones.[45]

Selective hydrogenation of CO_2 to formic acid is an atom-economic transformation. Driven by the global drive to reduce CO_2 levels this reaction has gained plenty of consideration as CO_2 acts as a feedstock, therefore reducing CO_2 levels together with utilising it as a source of organic carbon. Lui *et al.* reported the efficient direct hydrogenation of CO_2 catalysed by Pd/C in 1-butyl-3-methylimidazolium acetate under mild conditions.[46] The authors demonstrated that the IL modifies the PdNPs, activates CO_2 and stabilises the formic acid that is produced.

A recent study by Branco *et al.* demonstrated the use of fluorinated imidazolium-based ILs as reaction solvents with [Ru(COD)(2-methylallyl)$_2$] which can overcome the high thermodynamic and kinetic barriers with respect to CO_2 hydrogenation to methane.[47] The authors demonstrated that the catalysts performance could be improved by imidazolium cations bearing longer alkyl side chains. The formation of methane was found to be heavily dependent on the solubility of CO_2 in the IL media and the IL's capability to form and stabilse the RuNPs.

Dyson and co-workers synthesised a series of bifunctional NP:IL catalysts which were stabilised by Brønsted-acid ILs with a SO_3H group and various *N*-alkyl chain lengths for the efficient conversion of lignin-derived phenolic substrates to cycloalkanes (Figure 1.8).[48] The Brønsted-acid IL catalysed the dehydration reaction and the metal NPs catalysed the hydrogenation reaction to reduce phenolic substrates to the corresponding cycloalkanes in a single reaction vessel. The ILs acidity was shown to be affected by the *N*-alkyl chain length and the nature of the counter anion.

1: R = $(CH_2)_4SO_3H$, A = CF_3SO_3
2: R = $(CH_2)_4SO_3H$, A = BF_4
3: R = $(CH_2)_4SO_3H$, A = CF_3COO
4: R = $(CH_2)_4SO_3H$, A = CH_3SO_3
5: R = $(CH_2)_4SO_3H$, A = Tf_2N
6: R = $(CH_2)_4SO_3H$, A = HSO_4
7: R = $(CH_2)_4SO_3H$, A = H_2PO_4
8: R = H, A = HSO_4
9: R = H, A = H_2PO_4
10: R = CH_2SO_3H, A = CF_3SO_3
11: R = $(CH_2)_2SO_3H$, A = CF_3SO_3
12: R = $(CH_2)_3SO_3H$, A = CF_3SO_3
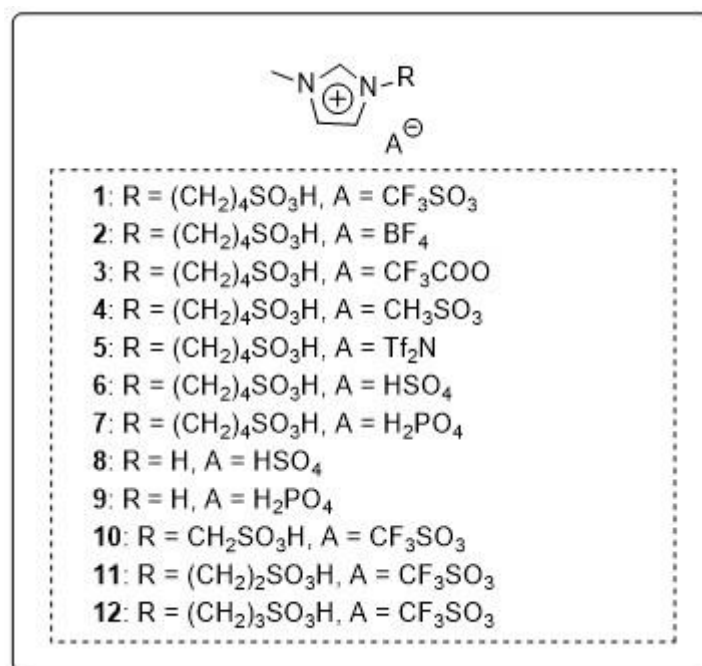
Figure 1.8: Brønsted acid ILs used in the study by Dyson *et al.* for the dehydration of phenolic substrates.

Furthermore, new valuable biofuels are also produced in the alcoholysis of lignocellulose such as levulinates, alkyl glucosides and xylosides. Methanol, ethanol,

2-propanol and 1-butanol are often used as solvents in alcoholysis processes, because of their low boiling points and prices.[49] These alcohols are simply separated from the reaction mixture by distillation and can therefore be recycled. Over the last decade, several studies have reported the alcoholysis of lignocellulose. In addition to lignocellulose, several platform molecules such as furfuryl alcohol (FFA) have been used as substrates to synthesise valuable products through alcoholysis.[50]

1.2.5 Task Specific and Functionalised Ionic Liquids

Functionalised ionic liquids (FILs), which are also known as task specific ILs (TSILs), have been used for the synthesis of metal nanoparticles. For instance, ionic liquids can be readily functionalised by decorating them with heteroatom donors (HAD). This concept has been extensively explored on the basis that the advantageous features of ILs combined with the donor's positive effects may enable the electronic properties of the catalyst to be modulated in a rational manner. To this end, reactions using donor modified ILs as the solvent have been reported to improve catalyst performance for several benchmark transformations. For example, Dyson *et al.* reported that the selectivity and the efficiency of palladium-catalysed Heck reactions between aryl bromides and electron-deficient olefins were significantly enhanced using diol-functionalised ILs as a result of strong interactions with multiple coordination sites on the PdNPs.[51] The active Pd catalyst could be retained during reaction workup as the IL acted as a ligand and therefore improved the catalyst recyclability by preventing Pd leaching. Hou *et al.* demonstrated that amino-functionalised ILs formed NiNPs that catalysed selective hydrogenation of the C=C bond in various functionalised alkenes.[52] The FILs were proposed to control the size and dispersion of the NiNPs in the aqueous phase. The catalysts showed better catalytic performance than the conventional Raney/Ni catalyst. Similarly, Moores *et al.* demonstrated that phosphine-functionalised ionic liquids (PFILs) could be used as ligands when combined with [Rh(acac)(CO)$_2$] to produce a highly efficient biphasic hydroformylation catalyst for higher alkenes (Scheme 1.4). In the absence of a PFIL, the catalyst was shown to be considerably less active due to the aggregated nature of the metal NPs. Both the counteranion and the length of the *N*-alkyl chain of the PFILs affected the catalytic activity of the stabilised NPs.[53]
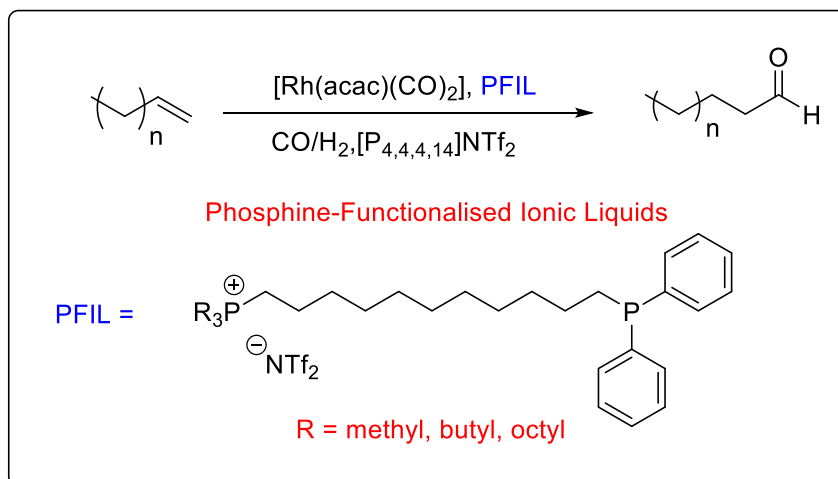
Scheme 1.4: RhNPs stabilised by phosphine-functionalised ILs for the hydroformylation of alkenes.

During the development of TSILs far less attention has been given to the incorporation of functional groups into the anion. Although, in industry easily separable heterogeneous catalysts are preferred these have some drawbacks such as heat and mass transfer and lower stereo- and chemo- selectivties. This can be circumvented by combining organic cations with catalytically active polyoxometalates (POMs) to form POM-based ILs (POM-ILs) which are an emerging class of catalyst. These attractive organic-inorganic hybrid materials have properties of both an IL cation and a POM anion. These POM-ILs can undergo electron transfer, possess Brønsted-acid properties and are excellent co-catalysts and strong reactant activators in coupling reactions. Bourlinos *et al.* first reported an ionic liquid-based POM (POM-IL)[54] by partial proton exchange of the POM with a PEG-based quaternary ammonium salt. This POM-IL has similar properties to other ILs such as comparable viscosities, low melting points and high conductivities. An alternative simple way to obtain POM-ILs proved by Rickert *et al.* was the pairing of a POM anion with a tetraalkylphosphonium cation.[55] Recently, several "IL-like" imidazolium-based polyoxometalates have also been reported and used as catalysts for epoxidation and oxidation reactions.[56]

1.3   Nanoparticles Synthesis, Stabilisation and Application for Catalysis

Alternatively, ILs can be used as immobilising agents instead of as a solvent. Transition metal nanoparticle (TMNP) catalysis is evolving as a powerful and adaptable technology. By virtue of their nanoscale dimensions (1-100 nm) and the quantum confinement effect, it is their unique physical properties that drives their application in medicine,[57] drug delivery,[58] electrochemistry,[59] fuel cells[60] and catalysis. The outstanding activity of NP-based catalysts originates from their large surface-area to volume ratio relative to their bulk counterparts, which in turn, increases the availability of their accessible active sites. As a result of their small size and high catalytic activity NPs are deemed as the interface between heterogeneous and homogeneous catalysis. Over the past decade, a huge amount of publications have documented a variety of synthetic methodologies that have been designed strategically to yield NPs with tuneable surface and size properties heralding a new era of heterogeneous catalysis. Additionally, NPs can be immobilised or incorporated into many materials such as silica, polymers, carbon nanotubes and metal-organic frameworks which assists their reuse and improves their "green" credentials.

Preventing aggregation under the reaction conditions is one of the major obstacles in NP catalysis. NPs often agglomerate into larger particles because they are kinetically unstable which reduces their activity. This process is referred to as "Otswald ripening" which is the result of the co-ordinately unsaturated surface atoms being less stable compared to the highly-ordered bulk atoms. The particles aggregate to create larger, thermodynamically more stable particles by separation of the small particle atoms and attachment onto the larger particles to reduce the overall energy of the system (Figure 1.9).
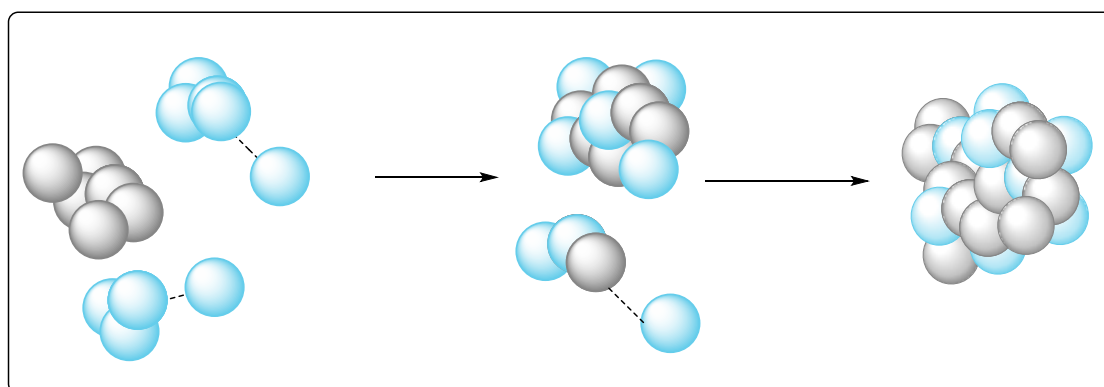
Figure 1.9: The Otswald ripening process for NPs.

As NPs have a large surface atom to bulk ratio they need further stabilisation which has commonly been achieved by surfactants,[61] donor ligands[62] or surface ligating anions.[63] While stabilisers assist in improving the NP's isolation or solubility it is essential that it does not restrict the substrate's access to the surface of the catalysts.[64] There are two approaches for the synthesis and optimisation of metal NPs. By reducing the overall amount of expensive precious metal this will enhance the efficiency of the approach. In addition, the favourable interactions with the stabiliser or support increases the particle's kinetic and thermal stability.[65] The "top down" approach involves breaking the bulk metal into NPs by chemical, mechanical or thermal means.[66] However, the more conventional "bottom up approach" is achieved by the decomposition or reduction of an organometallic precursor in the presence of a stabiliser followed by NP aggregation. This also allows for a more logical catalyst design through controlling the NPs size, shape and dispersity which generally affects the selectivity and activity of the catalyst.[67] Furthermore, this method is applicable for scale-up industrial production.[68] Hence, metal NP stabilisation is an essential feature in the generation of highly active and selective catalysts.

Despite the current abundance of research regarding the development of NP stabilisers such as ionic liquids,[69] metal organic frameworks,[70] inorganic polyoxometalates,[71] carbon nanotubes,[72] organic heteroatom donor-functionalised polymers[73] and fullerenes[74] the basic principles regarding their stabilisation fall into three main subcategories (Figure 1.10).

Electrostatic   *Steric*   *Electrosteric*
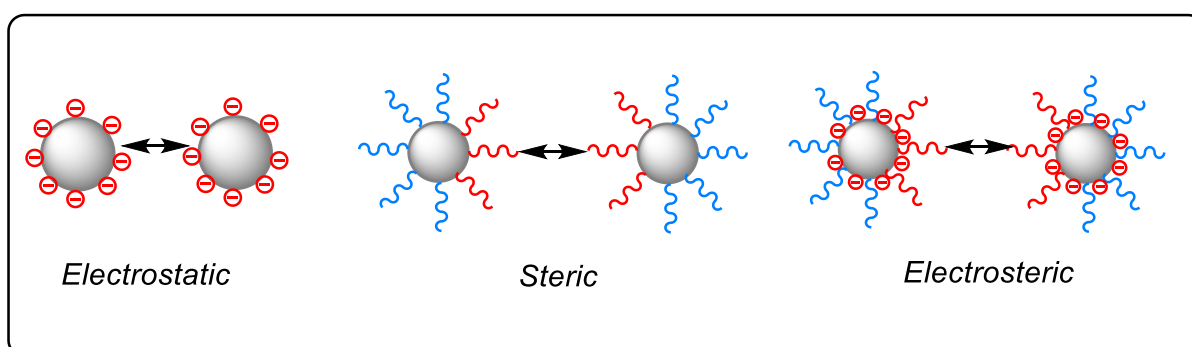
Figure 1.10: Different stabilisation strategies for NPs.

i) Electrostatic stabilisation

The stability of colloids is rationalised by the Derjaugin-Landau-Verwey-Overbeek (DLVO) theory. This indicates that anions in ionic media are adsorbed onto the NP's electrophilic surface and coulombic repulsion between neighbouring particles is provided by the anionic layer. Agglomeration with neighbouring particles is therefore hindered by the unfavourable electrostatic repulsion.[75] This form of stabilisation can be achieved through a variety of salts dissolved in solution or by using TSILs. In TSILs, the IL unit is decorated with a remote ligand which coordinates to the metal and this functionalisation can be incorporated either on the cation or the anion (Figure 1.11). The incorporation of an IL fragment into the catalyst's architecture greatly improves its miscibility with the IL media. The high activity associated with NP:IL catalysts arises from the loosely bound IL stabiliser which is readily displaced from the surface of the metal to provide access to the active site.

[A-R-FG][B]

A = amine, arsine, heterocycle, phosphine, thioether
R = linker
FG = functional group
B = BF_4^-, PF_6^-, NTf_2^- ....
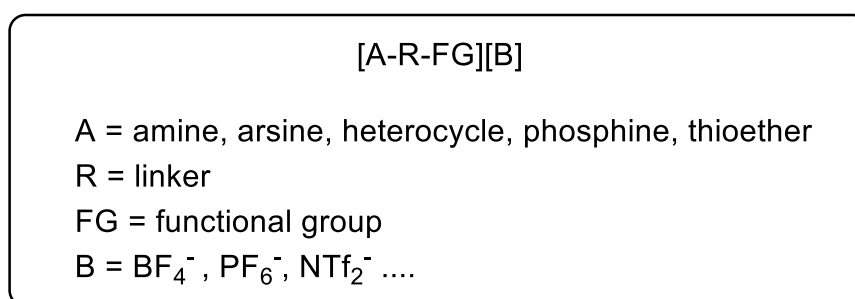
Figure 1.11: General composition of a task-specific ionic liquid.

Glorius and Ravoo reported the synthesis of highly active, chemoselective and recyclable NHC-stabilised Pd- and AuNPs for aqueous phase hydrogenations.[76] The NHC-stabilised MNPs exhibited long-term stability in water. By varying the pH from pH 1 to pH 4, the carboxylate NHC stabilised MNPs showed in water, a reversibility between the aggregated and soluble form due to the partial protonation of the carboxylate moiety which resulted in the loss in electrostatic repulsion between the MNPs. This led to NP clustering which demonstrated the fundamental concept of electrostatic stabilisation.

ii) Steric stabilisation

The FILs can covalently anchor themselves to the surface of a metal which alleviates the lability problem associated with non-functionalised ILs. A steric stabilisation layer which is provided by the alkyl spacer of a FIL further enhances the stabilisation of the metal NPs. Nanoparticles can be stabilised by sterics by performing the reduction step in the presence of a designer supramolecular material or with bulky protecting groups; this will restrict approach of the neighbouring particles and prevent aggregation (Figure 1.10). NPs can also be sterically protected by using capping agents such as silanes[77] or dendrimers[78] or by incorporating nanoparticles into polymer matrices. For instance, Jonnalaagadda and co-workers developed PdNPs stabilised with amine functionalised graphene oxide (GO) sheets which were found to be exceptional catalysts for Suzuki coupling reactions.[79] The advantage of this approach was that the graphene support prevented the PdNPs from sintering and accelerated the oxidative addition of aromatic halides to Pd(0). Similarly, Tsubaki and co-workers synthesised CuNPs stabilised with carbon nanotubes (CNTs) with different tube diameters. The systems with smaller diameter CNTs were exceptional catalysts for the hydrogenation of methyl acetate while those with larger diameter CNTs catalysts were shown to be less active.[80]

iii) Electrosteric stabilisation

Large molecules can be functionalised with polar ionic head groups which provides both steric and electrostatic stabilisation (Figure 1.10). This is often achieved by using polyacrylate dispersions,[81] amphiphilic polymers[82] and designer ILs with long alkyl chains that can encase the NPs. This type of stabilisation consists of a sterically hydrophobic outer layer and an electrostatic protective layer at the particles surface. Chaudret and co-workers reported a notable ligand effect of the RuNP-catalysed arene hydrogenation.[83] RuNPs stabilised with a range of phosphines were formed by the decomposition of [Ru(COD)(COT)] in tetrahydrofuran. Comparative catalyst testing showed that trialkylphosphine-based catalysts were highly active, whilst, triarylphosphine-stabilised catalysts were inactive for the hydrogenation of o-methylanisole due to high surface coverage from the ligands which hindered the coordination of the arene to the surface.

New materials with novel properties can be produced by chemically grafting ILs on the surface which acts as a stabilising media for NP dispersion whilst retaining the beneficial features of both the NP and the IL. These materials are referred to as "nanoparticle ionic liquid hybrids" and are of growing interest due to the potential to optimise the bulk material properties.[86a] Additionally, NP:IL hybrids can be designed so that the nanoparticles are chemically attached into an optimised preformed IL-based structure for a specific application, therefore improving the efficiency and flexibility of the overall system. For example, Li *et al.* synthesised a series of Ru-based catalysts for CO_2 methanation by the dispersion of RuNPs in various 1-butyl-3-methylimidazolium-based ILs on a silica support. The ILs were used as a protectant to prevent NP aggregation and oxidation by space resistance and electrostatic protection. In addition, they can be strongly adsorbed onto the RuNP's surface to control the NP's size and maintain high dispersion which significantly affected the catalysts activity.[84] Similarly, Cui *et al.* synthesised carboxylic acid- and amino functionalised Au and PtNPs. The larger gold nanospheres were synthesised using different quantities of reductant. The authors proposed that the stabilisation was a result of the interactions between the functional groups in the ILs and the metal atoms. Furthermore, the metal NPs were easily assembled onto the multiwalled carbon nanotubes. In this instance, the ILs served as a linker to connect the metal NPs with the carbon nanotubes.[85]

Multiple reviews have shown ILs being used to protect nanoparticles in NP:IL systems.[86b] Although, there is a wide acceptance of the DLVO theory as a reasonable model for the interaction between the ions and the nanoparticle surface, the theory does not explain ILs or other complex systems that are composed of sterically demanding ionic aggregates. Therefore, research into IL-stabilised nanoparticles has attracted great attention over the past decade. The advantages of using ILs as stabilisers is the unique microenvironment enables the physicochemical properties of the nanoparticles to be modified to enhance the catalyst performance and recyclability. In terms of a green perspective, the facile fine-tuning of the IL allows for a ligand-free synthesis of the active catalysts. In addition, the mass transport issues are prevented by the homogeneous dispersions formed by the NP:IL. The active site consists of metal surfaces as opposed to single sites which places these NP:IL at the interface of heterogenous and homogenous catalysis.

The complex interactions within ILs can prompt the formation of sophisticated structural networks. Usually the properties of ILs are due to their extensive networks as opposed to the isolated ions. For instance, the formation of exclusive polar regions enables the selective capture of the solutes in a predetermined domain.[112] This is particularly important for the dispersions of IL-NP as the use of a suitable metal precursor can allow for the NPs shape and size to be modified by altering the volume of the nanoregion. Albeit with the many examples of IL-stabilised nanoparticles it is challenging to clarify the fundamental aspects that control the shape and size of a nanoparticle. At the same time, there seems to be a synergy between the concentration and the nature of the metal precursor as the potential by-products can form aggregates on the metal surface.

In summary, NPs have various possible applications in many areas of science. For catalysis, NPs are a potential green alternative to both heterogeneous and homogeneous catalysts as they have high activities and combine the beneficial features of both types of catalysis. By modifying the surface, there is a potential to optimise the NPs catalytic performance for an array of transformations. ILs can form protective layers which prevent aggregation while assisting the recycling and determining the shape, solubility and reactivity of the NPs. Moreover, the material's properties can be further enhanced by fine-tuning several interactions for the novel application of NP-IL hybrids.

1.4 Supported Ionic Liquid Phase Catalysis

The main challenge that appears when ILs are used in homogeneous catalysis is product isolation in addition to the huge quantities of IL that are required, in particular when a process is conducted on a large scale. This is unfavourable, predominately due to the increase in the total cost of the overall process together with the potential toxicological issues derived from the insufficient understanding of the ILs long-term stability. For this reason, there has been a huge drive to develop more robust systems that can efficiently recycle and that use less IL while at the same time maintaining the positive aspects of homogeneous catalysis. One such approach is the Supported Ionic Liquid Phase (SILP) concept.

A SILP is usually present as a monolayer of covalently attached IL fragments on a surface of a support material.[87] Usually, the SILP materials are made up of three different components, (i) the porous support (silica, active carbon or alumina), (ii) the catalyst (metal complexes or nanoparticle) and (iii) the IL (a thin layer on the surface of the support). In a standard SILP system, a small amount of IL disperses over or impregnates the surface of a porous solid support with a high surface area to form a thin IL layer (10-50 Å) over a large surface area which considerably improves the mass transfer. The catalyst is then dissolved in the IL layer to deliver what is in essence a homogeneous catalyst by delivering an insoluble, reusable solid material which on a molecular scale can achieve homogeneous-type activity.

Moreover, the IL allows for a more efficient use as it exists as a thin layer at the surface of the support which results in less ionic content and therefore lower catalyst loadings are required to obtain higher activities and lower levels of leaching than in a biphasic system.[87] Hence, the dissolved catalyst within the IL layer is in close proximity to the reaction interface which considerably reduces the diffusion pathways and negates the potential issues which can arise from the high viscosity when using biphasic or bulk IL systems. Furthermore, the material's robust nature means that SILP technology enables more efficient catalyst recovery through straightforward filtration; which allows for easier scale-up and makes the process amenable for continuous flow operation e.g. in a fixed-bed reactor.[88]

The potential of immobilising the catalyst in the IL offers the advantages of both homogeneous and heterogeneous catalysis serving as both a solid, by immobilising the catalyst and as a liquid enabling the catalyst to circulate freely. The reactants and products can be IL immiscible allowing for facile separation. Similar to their IL counterparts, SILP materials have become more popular and therefore increasingly diverse in recent years with the incorporation of various ILs, support materials and catalyst. In this sense, there are four main synthetic approaches for the preparation of SILP catalysts (Figure 1.12).
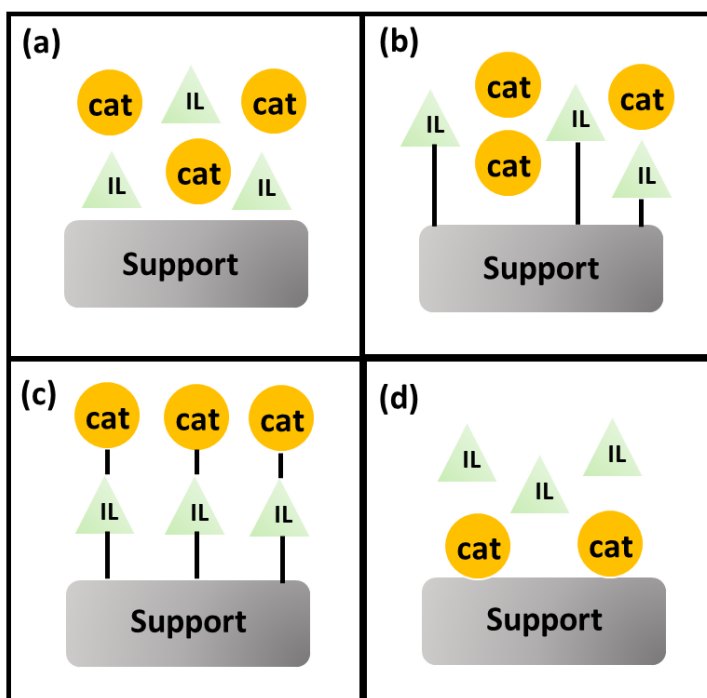
Figure 1.12: Schematic representation of different types of SILP-based materials: a) immersion method; b) covalent anchoring method; c) covalently bound catalyst or IL using anchored method; d) solid catalyst with ionic liquid layer (SCILL method).

The immersion method (Figure 1.12a) is perhaps the simplest method to generate a SILP catalyst and is therefore the most often used, in particular for the immobilisation of a homogenous metal complex. Preparation arises from the simple wet impregnation of the support material with a pre-formed solution of the pre-catalyst or a catalyst in an IL in a suitable organic solvent. After the impregnation, the ILs non-volatile nature allows the organic solvent to be removed *in vacuo* to give the desired SILP catalyst. The most common support is a highly porous silica gel (c.a. 300-500 m^2g^{-1} surface area),[89] however mesoporous silica and zeolites have also been used.[90] Alumina is far less often used, as a result of its smaller pore volume, although its great pH tolerance may favour its use under the appropriate conditions.[91] Materials prepared by the immersion method have been well-documented in their applications across a broad range of catalytic transformations which includes, hydroformylation, carbonylation, olefin metathesis, hydroamination and metal-catalysed carbon-carbon coupling.[92] The implementation of SILP materials provides advantages over bulk biphasic systems regarding enhanced reaction rates, simple catalyst isolation and

reuse, this is due to the thickness of the ILs layer and the close proximity of the layer to the reaction interface which reduces the diffusion pathway. In addition, unexpected effects can also occur upon confinement of a catalyst to the support material.

As such, earlier work with regards to Rh-catalysed hydroformylations with silica-based SILP materials demonstrated that the organometallic complex generated in solution was also formed inside the IL layer, resulting in a significantly reduced IL and metal complex mobility which led to remarkable properties in the supported complex.[93] SILP catalysts are the most successful when they are implemented in a fixed-bed reactor for continuous gaseous phase reactions. These systems can improve catalyst space-time yields, reusability and increase turnover frequencies which makes them extremely attractive for industrial processes. SILP catalysts prepared by the immersion method have been successfully implemented in gas phase fixed-bed reactors such as silica-immobilised Friedel-Crafts alkylation[94] and hydroformylation.[95] Regardless of their successful implementation in continuous processes, examples are limited to gas phase processes as the use of the liquid phase leads to problems such as IL and catalyst leaching. Alternative transport vectors have been used for example $scCO_2$, in addition covalent attachment of the ILs to the support material has overcome leaching of the IL when they are used in liquid phase systems.[96] Nevertheless, several limitations still exist include very high cost investment and operation and the limited solvating ability of $scCO_2$ which can hamper the associated advantages with its use.

In the interest of addressing the common leaching issues in SILP materials, the covalent anchoring method was established (Figure 1.12b). In this approach, the support surface is modified by the covalent attachment of either a FIL monolayer or by sol-gel synthesis.[97] The desired material can be immobilised with an additional 'free' IL through wet impregnation. In this method, a support such as graphene oxide, silica, alumina or activated carbon is modified by attaching an IL which is subsequently impregnated with a solution of homogeneous catalyst to enable catalyst adsorption onto the thin layer of IL film; the solvent is then removed to afford the desired SILP.[98] However, this approach can be synthetically challenging and therefore less economically viable which limits its use in large-scale applications. Nevertheless, the anchoring method is extensively used throughout the literature as it delivers a convenient method to stabilise and support NPs for recycling.[99] For example, Dupont *et al.* prepared hybrid organosilicas by sol–gel processing with an 1-n-butyl-3-(3-

trimethoxysilylpropyl)imidazolium cation associated with hydrophobic anions (Scheme 1.5), which were decorated with PdNPs.[100] They applied these catalysts for the selective hydrogenation of 1,3-cyclohexadiene. The activities that were achieved by the catalysts indicated that the IL layer on the supports surface had a marked influence on their catalytic performance as all the PdNPs were similar in size. Higher activities were achieved with catalysts that contained ILs with hydrophobic anions, PF_6^- and NTf_2^-, 3.03 and 2.82 s^{-1}, respectively than the catalyst without an IL (1.75 s^{-1}).
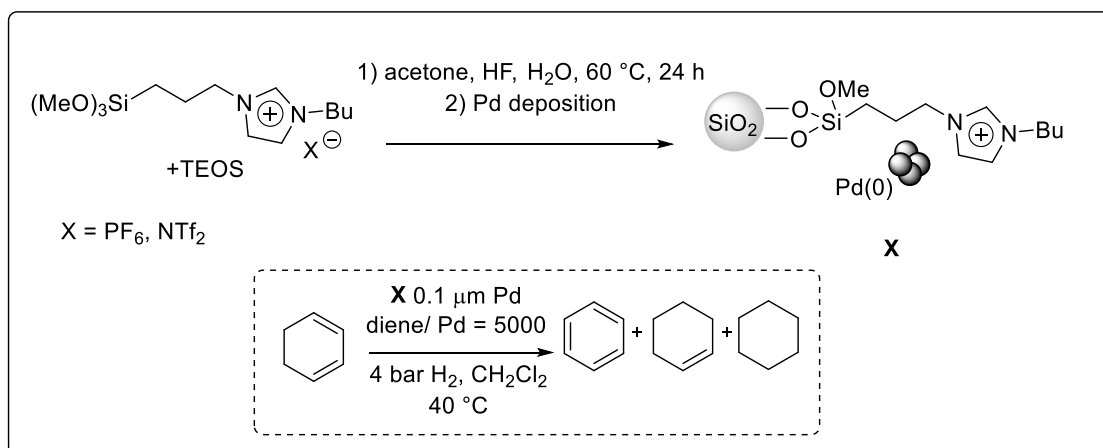
Scheme 1.5: Dupont SILP catalyst used in the hydrogenation of 1,3-cyclohexadiene.

IL monolayer functionalisation of the support's surface has also been investigated which include other materials such as carbon nanotubes (CNT), as a result of their high surface area-to-volume ratio, good mechanical strength and high chemical stability.[102] For example, co-impregnation of Ru/Fe bimetallic complexes with CNTs afforded a structurally robust material highly active for the selective hydrogenolysis of glycerol to produce glycols which exhibited excellent reusability.[103]

The covalent anchoring method used for SILP materials is not confined to IL tethering. The ligand or catalyst can be covalently bound to the IL units (Figure 1.12c). For example, Corma and Garcia functionalised the surface of Al/MCM-41 aluminosilicate with an imidazolium palladium complex and the resulting immobilised IL materials were highly active catalysts for the Suzuki-Miyaura cross-coupling of halobenzenes with phenylboronic acids.[104]

Kernchen *et al.* reported a new concept of a solid catalyst with an ionic liquid layer (SCILL) (Figure 1.12d) as a novel method to improve the selectivity in

heterogeneous catalysis. The sequential hydrogenation of cyclooctadiene (COD) to cyclooctene (COE) and cyclooctane was tested with a Ni catalyst coated with [BMIM][n-$C_8H_{16}OSO_3$]. In comparison to the original catalyst, the IL coating of the internal surface strongly enhanced the maximum intrinsic COE yield from 40 to 70 %. The robust IL layer showed no detectable leaching into the organic phase.[105] Similar results were obtained when Friedrich *et al.* investigated the influence of [BMIM][NTf$_2$] on Cu/γ-Al$_2$O$_3$ for the selective continuous flow hydrogenation of octanal in the presence of octene. The Cu SCILL catalyst showed an enhanced catalytic performance compared to the uncoated catalyst. The ILs presence improved the selectivity towards the desired product, 1-octanol, from 93.5% for the uncoated catalyst to 99.8% over the SCILL catalyst. Surface studies revealed that the IL was adsorbed onto the catalyst's surface which induced the surface acidity changes in the SCILL catalysts. It was found that the ILs polar nature favours octanol diffusion over octene within the IL layer which was proposed to be the origin of the selective hydrogenation of the C=O.[106]

The use of this methodology has been widely reported, for example Menhert *et al.* demonstrated a SILP HRh(CO)(TPPTS) immobilised with an IL phase of [bmim][PF$_6$] system that improved the activity with comparable selectivties to those of the biphasic analogue in the batch hydroformylation of 1-hexene,[107] and in the batch hydrogenation of 1-hexene, cyclohexene and 2,3-dimethyl-2-butene with [Rh(C$_7$H$_8$)(PPh$_3$)$_2$]PF$_6$.[108] In addition, the hydrogenation catalyst recycled up to 18 times without any significant loss in the activity and with no considerable catalyst leaching. Hagiwara *et al.* synthesised a catalyst with palladium acetate supported on amorphous silica aided by [bmim][PF$_6$].[109] The immobilised catalyst promoted the Mizoroki−Heck reaction with remarkable efficacy in *n*-dodecane and could be reused at least six times giving yields between 90-98%. Kirchner prepared a base-tolerant SILP system containing a hydride Fe(II) PNP pincer complex used as a catalyst in the hydrogenation of aldehydes to alcohols.[110] The highly active SILP catalyst under mild conditions gave TONs and TOFs of up to 1000 and 4000 h^{-1}, respectively, without any significant leaching of the IL or the complex and these were all conducted as batch reactions. However, for practical applications in industry the ideal process would include a continuous flow system where the reactor is continuously fed with the substrates where they react with the catalyst to afford product which is collected from

the other end. Nowadays, the use of SILP systems enables the desired homogeneous catalysts to be employed in continuous flow.

Riisager *et al.* reported the first SILP-catalysed continuous flow hydroformylation of 1-octene[111] in the liquid phase and propene in the gas phase.[112] These systems presented no leaching of the catalyst and the only issue they observed was the poor solubility of CO/H_2 in the IL which resulted in mass transfer limitations. SILP catalysts were also employed in the continuous flow hydrogenation,[113] ring opening of epoxides[114] and hydroaminations.[115] Fehrmann *et al.* prepared novel SILP catalysts for the continuous flow gas-phase hydroformylation of propene.[116] The catalysts contained immobilised Rh complexes of the bisphosphine sulfoxantphos in either 1-*n*-butyl-3-methylimidazolium hexafluorophosphate or 1-*n*-butyl-3-methylimidazolium *n*-octylsulfate on a silica support. The resulting Rh–sulfoxantphos SILP catalyst was more regioselective than the catalyst without the ligand as well as the analogous IL-free catalysts and gave up to 96% of the linear product. Moreover, the catalyst composition greatly influenced the catalysts performance.

To conclude, great strides have been accomplished in the SILP catalysis field, nevertheless it has certain limitations. For example leaching of the IL or catalyst, irreproducibility and blocking of the pores of the inorganic support can lead to catalyst deactivation. Therefore, there is a clear need to develop an understanding of the effects of the catalyst-support interactions on the performance.[117] The complex relationship between the IL-support-catalyst in SILP materials has led to only a basic understanding of various aspects of these systems rendering it harder to make general broader remarks about SILP materials. Rather, a thorough understanding for each catalytic process will require extensive mechanistic studies in addition to in-depth investigations on the fundamental reaction kinetics. The confinement of the catalytic species in an IL layer has been demonstrated to have a positive effect to overcome mass transport limitations, although it is not possible to assume that this will be the case for each IL-support-catalyst combination as confinement can also often impose geometric constraints on the organometallic complexes. Further issues arise regarding the chemical stability of the support material under harsh reaction conditions.[118]

1.5 Polymer Immobilised Ionic Liquid Phase Catalysis

As previously discussed, the SILP catalysis concept has been applied to a wide range of different materials which are generally inorganic matrices with high surface areas. Building on SILP, the concept of polymer immobilised ionic liquids (PIIL) was developed as an alternative versatile approach to immobilising molecular and nanoparticle-based catalysts. The work described in this thesis stems from the recent research conducted by the Doherty/Knight research group to develop and investigate the concept of polymer immobilised ionic liquid phase (PIILP) catalysis in an endeavour to resolve IL limitations in biphasic/homogeneous catalysis. The term PIILP was coined by the Doherty/Knight research group, however PIIL catalysts are well-documented and are often metal NPs incorporated into polymer matrices due to their convenient straightforward synthesis.[121] Polymers are often used as stabilisers for NPs because they offer good stabilisation while enabling the substrates to access the catalytically active metal surface.[120] A large number of polymers have limited solubility in ILs therefore in an attempt to overcome this problem some research groups have developed IL-like copolymers.[121]

There are several approaches used to prepare PIIL-stabilised nanoparticles (Scheme 1.6), through the rational design of IL-like monomers with neutral comonomers combined through polymerisation.[122] Following the preparation of an appropriate support material, the desired catalyst can then be immobilised by impregnation methods.
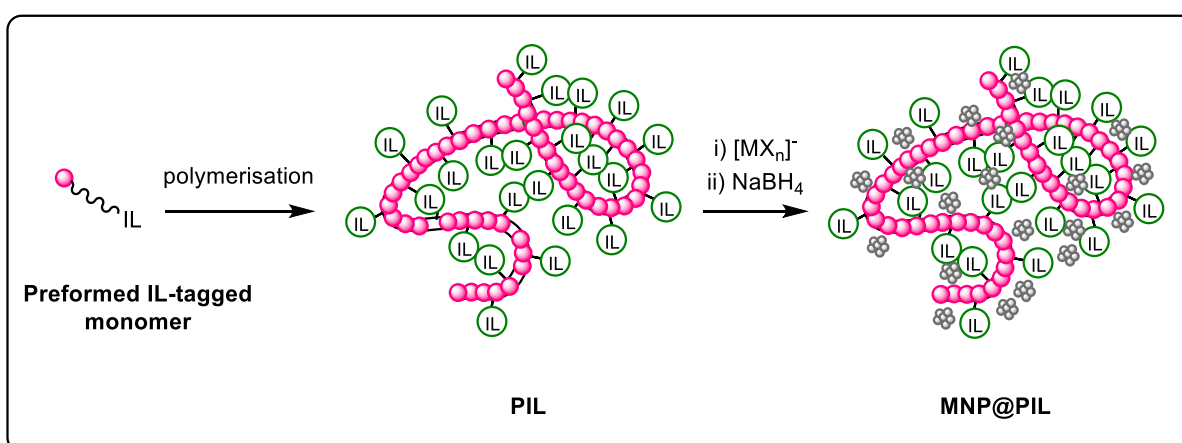
Scheme 1.6: General synthetic protocol for the preparation of PIIL-stabilised nanoparticles (NP@PIILs).

In this approach, the PIIL can offer steric protection by the large polymer backbone as well as electrosteric protection of the NPs towards aggregation through the weak interactions between the surface of the NP and the IL. The nature of the interactions at the polymer-catalyst interface can be controlled by manipulating the composition of the polymer which has been reported to result in an enhancement in the rate as well as improvements in the selectivity through multiple interactions with the substrate.[123] Immobilisation of a pre-fabricated homogeneous catalyst or their precursors in this fashion could combine the positive features of heterogeneous catalysis and the high activity and selectivity associated with homogeneous catalysts.[124] In this respect, an appropriate functionalised polymer can be tagged with an IL fragment allowing for post polymerisation or increasingly commonly an IL moiety can be functionalised as a monomer and then subsequently polymerised (*via* co-polymerisation). Using a pre-made IL-tagged monomer allows for greater control over the final PIIL material with regards to its purity, as post-polymerisation modifications are usually non-quantitative and challenging. Even though there is a potential for post polymer modification of imidazolium-functionalised polymers this approach usually presents product purification issues.

The fine-tuning effect can be seen over several different polymer systems through rational choice of the cation and anion and by modifying the morphology and the ionic loadings the materials properties including their hydrophilicity or hydrophobicity, functionality, swelling, thermal stability and ionic microstructure can all be tuned in a logical fashion which highlights the advantages of using a polymer support over other inorganic supports.[125] One advantage of using PIIL based catalysts over their SILP counterparts is their swelling properties in solution. Therefore, PIILs can be used as a support to traditional heterogeneous inorganic materials. Substrates can easily access the non-surface catalytically active sites due to the swelling of the polymer which is not feasible in rigid SILP systems.[126] Moreover, the PIIL's ionic microenvironment and its function can be controlled by incorporating various IL-tagged monomers and TSIL monomers. Therefore, the polymer's physical properties such as its thermal stability, flexibility with the degree of crosslinking and solvent compatibility can be optimised for their application over several chemical disciplines such as biotechnology,[127] energy materials,[128] fuel cell applications[129] and drug delivery.[130] Polystyrene- and vinylimidazolium-based polymers dominate the PILs used in catalysis

due to their straightforward synthesis. Such systems, have been implemented in numerous areas of catalysis although the scope of application again seems to be somewhat limited with the vast majority of the examples addressing the stabilisation of transition metal nanoparticles.[131] For example, palladium immobilised on PyOx-ligand cross-linked polystyrene has been shown to be an enantioselective and active catalyst for the asymmetric 1,4-addition of arylboronic acids to cyclic 3-substituted five- and six-membered enones. The catalyst could be reused for 6 cycles with no loss of enantioselectivity.[132] Polystyrene-stabilised PdO NPs were prepared in water by the thermal decomposition of Pd(OAc)$_2$ with polystyrene. The catalysts showed high activity for the Suzuki-Miyaura cross coupling and copper-free Sonogashira coupling reactions in water and recycled without any loss in activity.[133] In a similar manner, polymer stabilised Pd nanoparticles (PdNP@PS) are highly active catalysts for α-alkylation of aliphatic, cyclic and acyclic ketones with long chain alkyl and benzyl alcohols under mild conditions. The negligible Pd leaching and recyclability of the catalyst demonstrated the overall efficiency of the method and the catalyst.[134] Such systems highlight the synergistic effect concerning the material's physical properties which can be achieved between the polymer species and the well-defined catalysts.
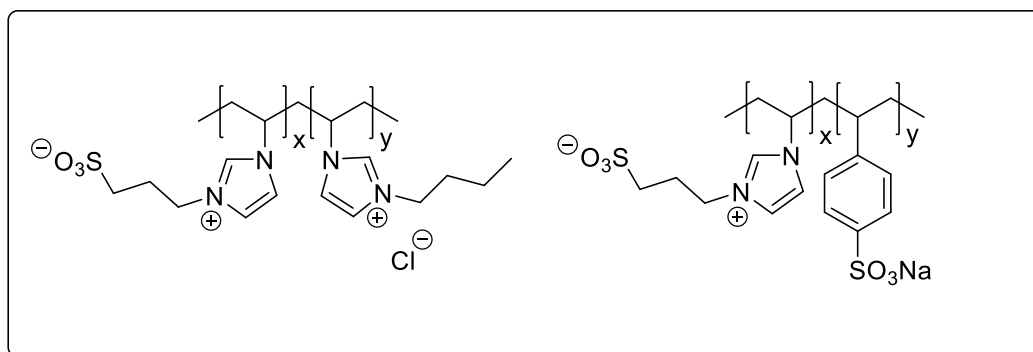
Figure 1.13: Examples taken from the literature of different functionalised polymers that are used as catalyst supports.[133-134]

Other examples which use polymer supports in SILP-type systems includes a catalyst system comprised of RuNPs stabilised by a Lewis acid-functionalised SILP.[135] The resulting system was shown to be an effective, stable and selective catalyst for the hydrogenation of benzofuran derivatives to generate biologically relevant dihydrobenzofuran motifs under continuous flow conditions. These results support the

possibility of using this approach for the preparation of finely-tuned multifunctional catalysts which are highly selective in challenging hydrogenations..

IL-tagged polymers used to support catalysts have been extended to commercially available materials. In this regard, ion exchange resins are commonly used for metal recovery or separation, water purification and in particular as supports for catalytic applications.[136] The large majority of ion exchange resins, including the quaternary ammonium-functionalised Amberlite® and the sulfonic acid-functionalised Amberlyst® are composed of a cross-linked polystyrene network bearing various ionic moieties (Figure 1.14).
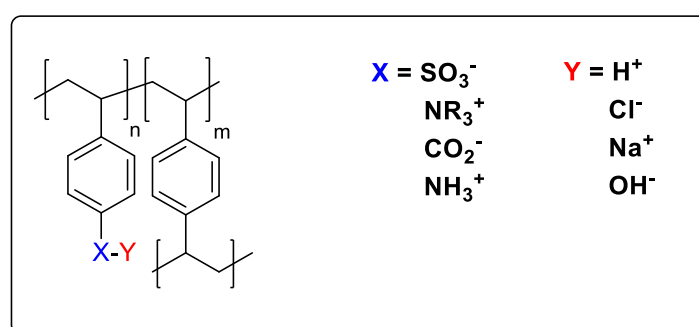
Figure 1.14: Common commercially available ion exchange resins.

As easily accessible insoluble materials, ion exchange resins can be an attractive prospect when preparing heterogeneous catalysts as they can mimic the IL's influence on a catalyst centre. These heterogeneous catalysts can be prepared by ion exchange of an appropriately charged precatalyst with the resin's counterion avoiding the requirement for any prior material synthesis. The ionic sites on the resin can be functionalised and manipulated to afford suitable IL moieties which will have enhanced ionic affinity to the desired catalyst or even covalently bind to it.[137] To this regard, ion exchange resins have been employed to immobilise a wide range of organometallic complexes which have been successfully applied to a variety of reactions such as hydroformylation,[138] carbonylation,[139] oxidation[140] and hydrogenation[141] often exhibiting good stability profiles and efficient recyclability. Although challenging, detailed studies will need to be conducted in order to develop an understanding of the nature of the catalyst-support interactions and how this influences performance if the concept of PIILP catalysis is to be fully utilised. This will ultimately allow for the

judicious modification of the support material through operationally straightforward, controlled polymer chemistry to generate efficient heterogeneous catalysts.

For example, Yuan *et al.* reported a simple template-free synthetic route for PIL complexes (PILCs) by the in situ ionic complexation between poly(acrylic acid) and imidazolium-based PILs in alkaline organic solvents, which exhibited a very stable micro-/mesoporous structure. These PILC were extremely effective for the aerobic oxidation of activated hydrocarbons under mild conditions.[142] Pourjavadi *et al.* synthesised a vinylimidazolium functionalised-PIL coated magnetic NP (Fe_3O_4@PIL) catalyst. The resulting catalysts were shown to be efficient acid catalysts for the synthesis of 1,1-diacetyl from aldehydes in high yields under solvent-free conditions. The catalyst was simply recovered after the reaction by an external magnet and recycled without any significant loss in activity. In addition, the catalyst had good thermal stability and recyclability as the polymer coated the magnetic NPs surface. Zhang *et al.* reported the synthesis of an efficient novel PIL catalyst for esterifications and their results showed that the catalysts were highly acidic and thermally stable. Under the optimised conditions, the ester yield was 97% which was a marked improvement on that obtained with commercial Amberlyst 15 resins and other catalysts. The ester yield did not decrease and the PILs structure remained stable after eight reuses.[143]

The PIL's modular synthesis enables IL-like and task specific monomers to be incorporated into the polymer backbone along with the facile incorporation of cross-linking which can alter the porosity and improve the integrity of the system. The appropriate catalyst precursor or homogeneous catalyst is impregnated into the polymer and heterogenized to improve the application facilitating catalyst recovery and product separation. By exploring polymer chemistry, it is possible to create materials that possess different chemical and physical properties by allowing the reasonable and methodical fine-tuning of the polymer's properties such as the ionic microenvironment and microstructure, porosity, durability, stability and structural integrity through a rational choice of monomer, co-monomer and cross-linker, therefore, allowing the catalyst activity and selectivity across many different transformations to be optimised.

To this end, the Doherty/Knight research group first used Ring Opening Metathesis Polymerisation (ROMP) to prepare pyrrolidinium-based PIILPs to

immobilise a peroxophosphotungstate (Figure 1.15), the resulting system was a highly efficient catalyst for the epoxidation of alkenes and allylic alcohols.[144] The role of the polymer support was confirmed during the comparative catalyst testing and showed that the PIILP systems outperformed the parent $[PO_4\{WO(O_2)_2\}_4][NEt_4]$. The PIILP catalyst recycled four times with only a minor drop in the activity and ICP analysis of the filtered solvent after the catalyst recovery showed no evidence of metal leaching. The versatility of this method was later demonstrated as similar catalyst systems were found to be extremely efficient for the oxidation of sulfides in batch and continuous flow under mild conditions.[145] The PIILP system's robust nature allowed for a stable activity-selectivity profile over eight hours under continuous flow conditions.
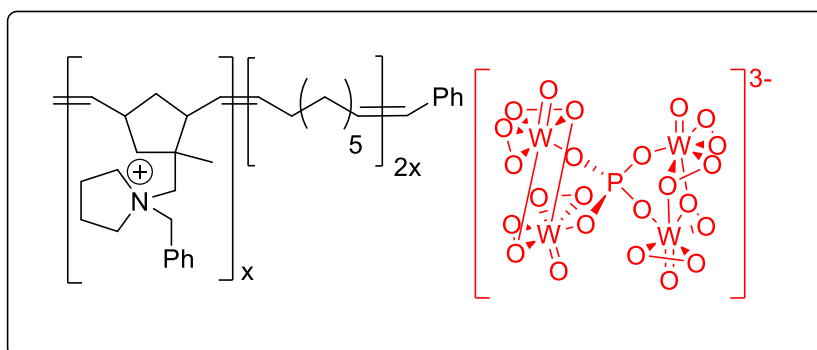
Figure 1.15: POM@PIILP catalyst developed by Doherty/Knight for the epoxidation of alkenes and allylic alcohols and for the oxidation of sulfides.[145]

The research group also prepared PIILP catalysts *via* azobisisobutyronitrile (AIBN) initiated radical copolymerisation of styryl functionalised pyrrolidinium-based ionic liquids with styrene and divinyl benzene as cross-linker for the immobilisation of chiral copper-bis(oxazoline) complexes.[146] The incorporation of chirality into the polymer structure afforded highly efficient and selective catalysts for the Diels-Alder reaction between cyclopentadiene and N-acryloyloxazolidinone. To evaluate the relative merits of PILs, the active catalyst was also immobilised onto inorganic SILP supports. The comparative catalyst testing showed that the PIILP supports gave higher ee's and activities. Furthermore, the PIILP systems revealed significant improvements in recyclability due to the enhanced binding affinity of the catalyst within the polymer network. It was postulated that the differences in the activities was due to the unique ionic microenvironment offered by the polymer support surrounding the metal triflate.

More recently the group have been exploring the use of polymer immobilised ionic liquids for the stabilisation of noble metal NPs. PdNPs stabilised by heteroatom donor-modified polymer immobilised ILs (PdNP@HAD-PIILP) were shown to be highly efficient catalysts, in particular the PPh$_2$PEG-PIILP-based catalyst, for the Suzuki-Miyaura cross-coupling in aqueous media under mild conditions (Scheme 1.7), with a TOF of 16,300 h^{-1}, which was one of the highest reported in the literature. Each of the heteroatom modified catalysts was more active than their corresponding unmodified imidazolium-based polystyrene benchmarks in addition to commercial Pd/C.[147] Furthermore, they showed that the selective removal of the ionic liquid, diphenylphosphine or PEG led to dramatic drops in the TOFs.
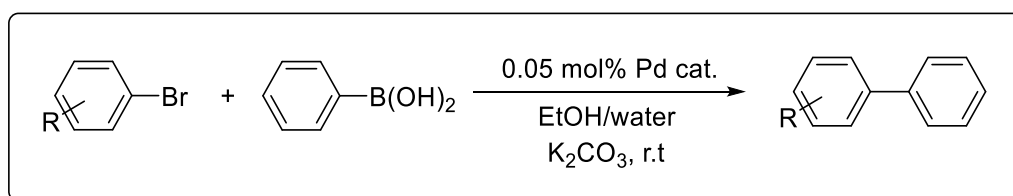
Scheme 1.7: PdNP-catalysed Suzuki-Miyaura cross-coupling by Doherty/Knight.

Moreover, the group also recently published highly efficient AuNPs stabilised by phosphine- and PEG-decorated polymer immobilised ILs (AuNP@PPh$_2$-PIILP). These catalysts were reported as multi-product selective AuNP-based systems which showed good activity in the sodium borohydride-mediated reduction of nitroarenes under mild conditions and with a very low catalyst loading of 0.005 mol% (Scheme 1.8).[148] Three different products could be obtained either by partial or full reduction of the nitroarenes in high selectivities >99%. Under the optimum conditions, in water, *N*-phenylhydroxylamine could be obtained as the sole product (TOF of 73,000 h^{-1}) whereas in ethanol the selectivity switched to afford azoxybenzene (TOF of 37,000 h^{-1}). Aniline could also be selectively produced at 60 °C with a TOF of 62,500 h^{-1}.
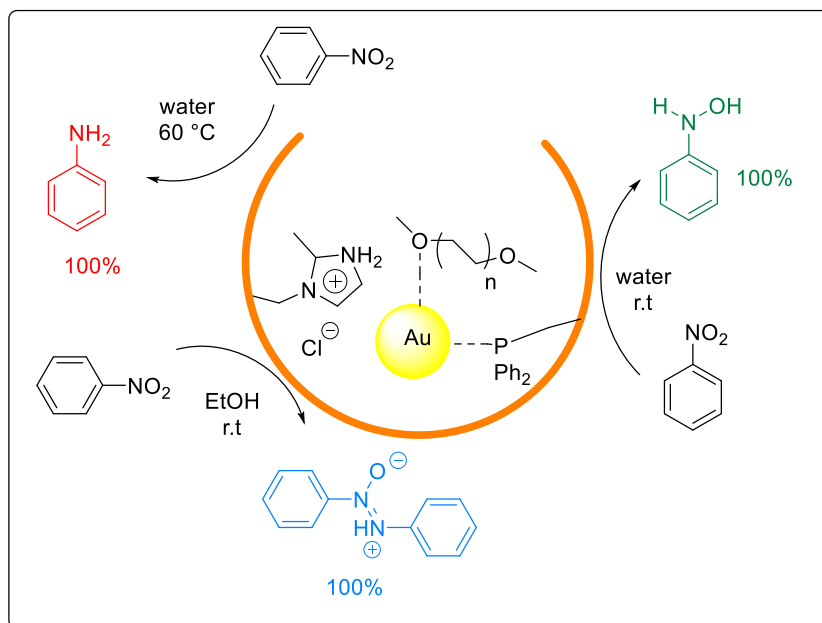
Scheme 1.8: AuNP-catalysed selective reduction of nitroarenes by Doherty/Knight.[148]

1.6   Project aims

The main objective of this project was to develop novel and sustainable catalyst technologies with regards to efficient conversion of biomass-derived and nitroaromatic substrates into high-value platform chemicals, fuels and aromatic amine intermediates, respectively. This work used the PIILP concept previously developed by the Doherty/Knight research group and will primarily focus on styrene-based heteroatom donor modified PILs for the stabilisation of metal NP or functionalised PILs for the immobilisation of polyoxometalates. The practical advantages associated with the modular synthesis of styrene-based imidazolium monomers presents a more appealing approach to PIL synthesis compared to other methods.

Innovation in this project stems from the introduction of additional functionality in the PIL support which leads to modifications in the catalyst-support interactions. This in turn should improve the catalyst activity-selectivity profile, longevity and recyclability for a range of industrially relevant transformations. Introducing phosphine donors into the polymer backbone should enable control over the NP morphological growth and activity resulting from the ligand effect previously described as well as modulating the surface electronic properties and regulating the ionic microenvironment by changing the charge density. Hence, it was necessary to conduct thorough investigations to determine the optimum property-performance profiles of the PIIL supported NP catalysts for the hydrogenation of a range of α,β-unsaturated carbonyls and bio-derived substrates. In addition, the same catalysts will be examined for the selective reduction of nitroarenes (Scheme 1.9).
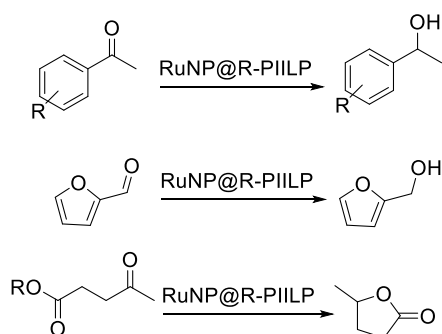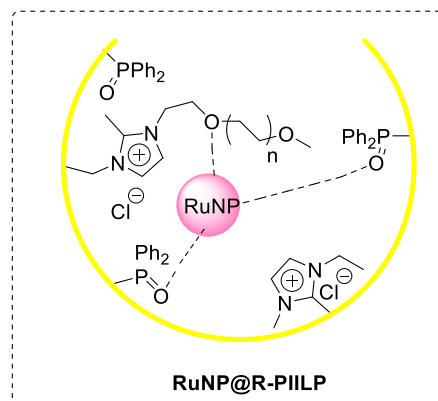
Scheme 1.9: RuNP-catalysed hydrogenation of α,β-unsaturated carbonyls, bio-derived substrates and nitroaromatic compounds.

In addition to studying PIILP stabilised RuNPs this project also aims to demonstrate the scope of PIILP materials in catalysis. Sulfonic acid-functionalised Brønsted acid IL monomers (BAILs) have also been incorporated into the polymer backbone for the immobilisation of polyoxometalates *via* simple anion exchange. Property-performance profiles were conducted on the POM@PIILP catalysts for the butanolysis of furfuryl alcohol (Scheme 1.10) with the goal to integrate the optimum system into a continuous flow reactor which is discussed in Chapter 4.
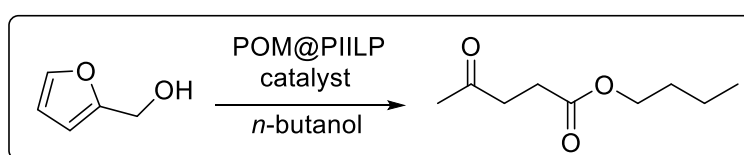
Scheme 1.10: Butanolysis of furfuryl alcohol with POM@PIILP catalyst.

1.7 References

1. P. T. Anastas and J. C. Warner, *Green Chemistry: Theory and Practice*. Oxford University Press: New York, 1998, p. 30.

2. R. A. Sheldon, *Green Chem.*, 2007, **9**, 1273-1283.

3. a) R. L. Vekariya, *J. Mol. Liq.*, 2017, **227**, 44-60; b) J. C. Védrine, *Appl. Catal. A: Gen.*, 2014, 40-50.

4. F. Chemat, M. A. Vian, A.-S. Fabiano-Tixier, M. Nutrizio, A. R. Jambrak, P. E. S. Munekata, J. M. Lorenzo, F. J. Barba, A. Binello and G. Cravotto, *Green Chem.*, 2020, **22**, 2325-2353.

5. P. Knochel, in Top. Curr. Chem., Springer Berlin Heidelberg, 1999, vol. 206, pp. 1-152.

6. E. Perperi, Y. Huang, P. Angeli, G. Manos, C. R. Mathison, D. J. Cole-Hamilton, D. A. Adams and E. G. Hope, *Chem. Eng. Sci.*, 2004, **59**, 4983-4989.

7. P. Wasserscheid, T. Welton, Ionic Liquids in Synthesis, Wiley-VCH Verleg, Stuttgart, Germany, 2002.

8. P. Walden, Acad. Sci. St. Petersbury, 1914, 405-422.

9. F.N. Hurley, T. P Wier, *J. Electrochem. Soc.*, 1951, **98**, 207–212.

10. H. L. Chum, V. R. Koch, L. L. Miller and R. A. Osteryoung, *J. Am. Chem. Soc.*, 1975, **97**, 3264-3265.

11. C. L. Hussey and T. M. Laher, *Inorg. Chem.*, 1981, **20**, 4201-4206.

12. J. S. Wilkes, J. A. Levisky, R. A. Wilson and C. L. Hussey, *Inorg. Chem.*, 1982, **21**, 1263-1264.

13. P. B. Hitchcock, T. J. Mohammed, K. R. Seddon, J. A. Zora, C. L. Hussey and E. H. Ward, *Inorg. Chim. Acta*, 1986, **113**, L25-L26.

14. S. E. Fry and N. J. Pienta, *J. Am. Chem. Soc.*, 1985, **107**, 6399-6400.

15. J. A. Boon, J. A. Levisky, J. L. Pflug and J. S. Wilkes, *J. Org. Chem.*, 1986, **51**, 480-483.

16. Y. Chauvin, B. Gilbert and I. Guibard, *J. Am. Chem. Soc. Chem. Comm.*, 1990, 1715-1716.

17. R. T. Carlin and J. S. Wilkes, *J. Mol. Catal.*, 1990, **63**, 125-129.

18. J. S. Wilkes and M. J. Zaworotko, *Chem. Comm.*, 1992, **13**, 965-967.

19. A. A. Egjarbawy, F. A. Riyadi, M. Z. Alam and M. Moniruzzaman, *J. Mol. Liq.*, 2018, **251**, 150-166.

20. A. P. M. Tavares, O. Rodríguez, E. A. Macedo, New generations of ionic liquids applied to enzymatic biocatalysis, IntechOpen; London, 2013, pp. 537–556.

21. P. Bonhôte, A.-P. Dias, N. Papgeorgiou, K. Kalyanasuundaram and M. Grätzel, *Inorg. Chem.*, 1996, **35**, 1168-1178.

22. S.-G. Lee, *Chem. Commun.*, 2006, 1049-1063.

23. M. J. Earle and K. R. Seddon, *Pure App. Chem.*, 2000, **72**, 1391-1398.

24. T. Welton, *Coord. Chem. Rev.*, 2004, **248**, 2459-2477.

25. a) A. Samanta, *J. Phys. Chem. B*, 2006, **110**, 13704-13716; b) R. K. Blundell and P. Licence, *Chem. Commun.*, 2014, **50**, 12080-12083.

26. S. Lentini, P. Galloni, I. Garcia-Bosch, M. Costas and V. Conte, *Inorgan. Chim. Acta.*, 2014, **410**, 60-64.

27. A. T. Karunanithi and R. Farahipour, *Comput. Aided Chem. Eng.*, 2016, **39**, 239-268.

28. F. Endres and S. Z. E. Abedin, *Phys. Chem. Chem. Phys.*, 2006, **8**, 2101-2116.

29. A. S. Shaplov, P. S. Vlasov, M. Armand, E. I. Lozinskaya, D. O. Ponkratov, I. A. Malyshkina, F. Vidal, O. V. Okatova, G. M. Pavlo, C. Wandrey, I. A. Godovikov and Y. S. Vygodskii, *Polym. Chem.*, 2011, **2**, 2609-2618.

30. a) M. Rueping, R. M. Koenigs and I. Atodiresei, *Chem. Eur. J.*, 2010, **16**, 9350-9365; b) J. H. Davis Jr., *Chem. Lett.*, 2004, 33, 1072-1077

31. V. Gallo, P. Mastrorilli, C. F. Nobile, G. Romanazzi and G. P. Suranna, *J. Chem. Soc., Dalton Trans.*, 2002, 4339-4342.

32. M. T. Clough, C. R. Crick, J. Gräsvik, P. A. Hunt, H. Niedermeyer, T. Welton and O. P. Whitaker, *Chem. Sci.*, 2015, **6**, 1101-1114.

33. N. Plylahan, M. Kerner, D.-H. Lim, A. Matic and P. Johansson, *Electrochimica Acta*, 2016, **216**, 24-34.

34. Y. Tao, R. Dong, I. V. Pavlidis, B. Chen and T. Tan, *Green Chem.*, 2016, **18**, 1240-1248.

35. A. Z. Fadhel, P. Pollet, C. L. Liotta and C. A. Eckert, *Molecules*, 2010, **15**, 8400-8424.

36. D. Nair, S. S. Luthra, J. T. Scarpello, L. S. White, L. M. F. dos Santos and A. G. Livingston, *Desalination*, 2002, **147**, 301-306.

37. B. Pugin, M. Studer, E. Kuesters, G. Sedelmeier and X. Feng, *Adv. Synth. Catal.*, 2004, **346**, 1481-1486.

38. J. van den Broeke, F. Winter, B.-J. Deelman and G. van Koten, *Org. Lett.*, 2002, **4**, 3851-3854.

39. N. V. Plechkova and K. R. Seddon, *Chem. Soc. Rev.*, 2008, **37**, 123-150.

40. J. Fitt, K. Prasad, O. Repic and T. J. Blacklock, *Tetrahedron Lett.*, 1998, **39**, 6991-6992.

41. W. Kunz and K Häckl, *Chem. Phys. Lett.*, 2016, **661**, 6-12.

42. S. Zhu, J. Wang and W. Fan, *Catal. Sci. Technol.*, 2015, **5**, 3845-3858.

43. C. H. Zhou, X. Xian, C. X. Lin, D. S. Tong and J. Beltramini, *Chem. Soc. Rev.*, 2011, **40**, 5588-5617.

44. S. Van de Vyver, J. Geboers, P. A. Jacobs and B. F. Sels, *ChemCatChem*, 2011, **3**, 82-94.

45. J. Julis, M. Holscher and W. Leitner, *Green Chemistry*, 2010, **12**, 1634-1639.

46. Y. Wu, Y. Zhao, H. Wang, B. Yu, X. Yu, H. Zhang and Z. Liu, *Ind. Eng. Chem. Res.*, 2019, **58**, 6333-6339.

47. U. Kernchen, B. Etzold, W. Korth and A. Jess, *Chem. Eng. Technol.*, 2007, **30**, 985-994.

48. N. Yan, Y. Yuan, R. Dykeman, Y. Kou, P. J. Dyson, *Angew. Chem. Int. Ed.*, 2010, **49**, 5549-5553.

49. S. Zhu, C. Chen, Y. Xue, J. Wu, J. Wang and W. Fan, *ChemCatChem*, 2014, **6**, 3080-3083.

50. J.-P. Lange, W. D. van de Graaf and R. J. Haan, *ChemSusChem*, 2009, **2**, 437-441; J. P. Hallett and T. Welton, *Chem. Rev.*, 2011, **111**, 3508-3576.

51. Y. Cai and Y. Liu, *Catal. Commun.*, 2009, **10**, 1390-1393.

52. Y. Hu, Y. Yu, Z. Hou, H. Yang, B. Feng, H. Li, Y. Qiao, X. Wang, L. Hua, Z. Pan and X. Zhao, *Chem. Asian J.*, 2010, **5**, 1178-1184.

53. K. L. Luska, K. Z. Denmmans, S. A. Stratton and A. Moores, *Dalton Trans.*, 2012, **41**, 13533-13540.

54. A. B. Bourlinos, K. Raman, R. Herrera, Q. Zhang, L. A. Archer and E. P. Giannelis, *J. Am. Chem. Soc.*, 2004, **126**, 15358-15359.

55. P. G. Rickert, M. A. Antonio, M. A. Firestone, K.-A. Kubatko, T. Szreder, J. F. Wishart and M. L. Dietz, *Dalton Trans.*, 2007, 529-531.

56. a) L. Liu, C. Chen, X. Hu, T. Mohamood, W. Ma, J. Lin and J. Zhao, *New J. Chem.*, 2008, **32**, 283-289; b) Y. Qiao, Z. Hou, H. Li, Y. Hu, B. Feng, X. Wang, L. Hua, Q. Huang, *Green Chem.*, 2009, **11**, 1955-1960.

57. N. S. R. Satyavolu, K. Y. Loh, L. H. Tan and Y. Li, *Small*, 2019, **15**, 1900975.

58. A. Bagheri, H. Arandiyan, C. Boyer and M. Lim, *Adv. Sci.*, 2016, **3**, 1500437.

59. N. S. Nia, D. Hauser, L. Schlicker, A. Gili, A. Doran, A. Gurlo, S. Penner and J. Kunze-Liebhäuser, *ChemPhysChem*, 2019, **20**, 3067-3073.

60. D. Siegmund, N. Blanc, M. Smailkowski, K. Tschulik and U.-P. Apfel, *ChemElectroChem*, 2020, **7**, 1514-1527.

61. K. Larson-Smith and D. C. Pozzo, *Langmuir*, 2012, **28**, 11725-11732.

62. B. J. Borah, K. Saikia, P. P. Saikia, N. C. Barua and D. K. Dutta, *Catal.S Today*, 2012, **198**, 174-183.

63. J. Dupont and M. R. Meneghetti, *Curr. Opin. Colloid Interface Sci.*, 2013, **18**, 54-60.

64. L. Hendraningrat and O. Torsaeter, *Appl. Nanosci.*, 2015, **5**, 181-199.

65. K. L. Luska and A. Moores, *ChemCatChem.*, 2012, **4**, 1534-1546.

66. B. Van Eerdenbrugh, G. van der Mooter and P. Augustijns, *Int. J. Pharm.*, 2008, **364**, 65-75.

67. F. P. de Silva, J. L. Fiorio and L. M. Rossi, *ACS Omega*, 2017, **2**, 6014-6022.

68. K. Schmid and M. Riediker, *Environ. Sci. Technol.*, 2008, **42**, 2253-2260.

69. H. Zhang and H. Cui, *Langmuir*, 2009, **25**, 2604-2612.

70. M. Zahmakiran, *Dalton Trans.*, 2012, **41**, 12690-12696.

71. Y. Wang and I. A. Weinstock, *Chem. Soc. Rev.*, 2012, **41**, 7479-7496.

72. J. S. Wang, H.-B. Pan and C. M. Wai, *J. Nanosci. Nanotechnol.*, 2006, **6**, 2025- 2030.

73. M. I. Gibson, M. Danial and H.-A. Klok, *ACS Comb. Sci.*, 2011, **13**, 286-297.

74. L. Brunet, D. Y. Lyon, E. M. Hotze, P. J. J. Alvarez and M. R. Wiesner, *Environ. Sci. Technol.*, 2009, 43, **12**, 4355-4360.

75. M.-A. Neouze, *J. Mater. Sci.*, 2013, **48**, 7321-7349.

76. A. Ferry, K. Schaepe, P. Tegeder, C. Richter, K. M. Chepiga, B. J. Ravoo and F. Glorius, *ACS Catal.*, 2015, **5**, 5414-5420.

77. X. Huang, A. Schmucker, J. Dyke, S. M. Hall, J. Retrum, B. Stein, N. Remmes, D. V. Baxter, B. Dragnea and L. M. Bronstein, *J. Mater. Chem.*, 2009, **19**, 4231-4239.

78. M. Zhao, L. Sun and R. M. Crooks, *J. Am. Chem. Soc.*, 1998, **120**, 4877-4878.

79. S. Rana, S. Maddila, K. Yalagala, S. B. Jonnalagadda, *Appl. Catal. A: Gen.*, 2015, **505**, 539-547.

80. D. Wang, G. Yang, Q. Ma, M. Wu, Y. Tan, Y. Yoneyama and N. Tsubaki, *ACS Catal.*, 2012, **2**, 1958-1966.

81. J. Hang, L. Shi, X. Feng and L. Xiao, *Powder Technol.*, 2009, **192**, 166-170.

82. M. Save, M. Manguian, C. Chassenieux and B. Charleux, *Macromolecules*, 2005, **38**, 280-289.

83. D. González-Gálvez, P. Nolis, K. Philippot, B. Chaudret and P. W. N. M. van Leeuwen, *ACS Catal.*, 2012, **2**, 317-321.

84. X. Guo, Z. Peng, A. Traitangwong, G. Wang, H. Xu, V. Meeyoo, C. Li and S. Zhang, *Green Chem.*, 2018, **20**, 4932-4945.

85. H. Zhang and H. Cui, *Langmuir*, 2009, **25**, 2604-2612.

86. a) Z. He and P. Alexandridis, *Adv. Colloid Interface Sci.*, 2017, **244**, 54-70; b) C. Verma, E. E. Ebenso and M. A. Quraishi, *J. Mol. Liq.*, 2019, **276**, 826-849; c) M. H. G. Prechtl and P. S. Campbell, *Nanotechnol. Rev.*, 2013, **2**, 577-595; d) J. D. Scholten, B. C. Leal and J. Dupont, *ACS Catal.*, 2012, **2**, 184-200.

87. C. P. Mehnert, R. A. Cook, N. C. Dispenziere and M. Afeworki, *J. Am. Chem. Soc.*, 2002, **124**, 12932-12933.

88. A. Riisager, R. Fehrmann, M. Haumann and P. Wassershceid, *Eur. J. Inorg. Chem.*, 2006, 695-706.

89. A. A. Christy, *Colloids Surf. A Physiochem. Eng. Asp.*, 2008, **322**, 248-252.

90. S. E. Lehman and S. C. Larsen, *Environ. Sci.: Nano*, 2014, **1**, 200-213.

91. N. Raza, W. Raza, S. Madeddu, R. V. Kumar and K.-H. Kim, *RSC Adv.*, 2018, **8**, 32651-32658.

92. a) A. Riisager, B. Jørgensen, P. Wasserscheid and R. Fehrmann, *Chem. Commun.*, 2006, 994-996; b) S. Breitenlechner, M. Fleck, T. E. Müller and A. Suppan, *J. Mol. Catal. A: Gen.*, 2004, **214**, 175-179; c) G. M. Ziarani, S. Rohani, A. Ziarati and A. Badiei, *RSC Adv.*, 2018, **8**, 41048-41100.

93. M. Jakuttis, A. Schönweiz, S. Werner, R. Franke, K.-D. Wiese, M. Haumann and P. Wasserscheid, *Angew. Chem. Int. Ed.*, 2011, **50**, 4492-4495.

94. J. Joni, M. Haumann and P. Wasserscheid, *Appl. Catal. A: Gen.*, 2010, **372**, 8-15.

95. M. Haumann, M. Jakuttis, S. Werner and P. Wasserscheid, *J. Catal.*, 2009, **263**, 321-327.

96. H. Yu, D. Xu and Q. Xu, *Chem. Commun.*, 2015, **51**, 13197-13200.

97. Y. Dong and C. Shannon, *Anal. Chem.*, 2000, **72**, 2371-2376.

98. J. Zhu, F. Xin, J. Huang, X. Dong and H. Liu, *Chem. Eng. J.*, 2014, **246**, 79-87.

99. J. M. González-Domínguez, M. Gonzálaz, A. Ansón-Casaos, A. M. Díez-Pascual, M. A. Gómez and M. T. Martínez, *J. Phys. Chem. C*, 2011, **115**, 7238-7248.

100. L. Luza, A. Gual, C. P. Rambor, D. Eberhardt, S. R. Teixeira, F. Bernardi, D. L. Baptita and J. Dupont, *Phys. Chem. Chem. Phys.*, 2014, **16**, 18088-18091.

101. B. Yin, Q. Wang, T. Liu and G. Gao, *New J. Chem.*, 2018, **42**, 20001-20006.

102. J. G. Park, J.-G. Kim, K. P. So, J. Y. Hwang, E. S. Kim, J. Li, D. Suh and Y. H. Lee, *Carbon*, 2019, **153**, 513-524.

103. B. Li, J. Wang, Y. Yuan, H. Ariga, S. Takakusagi and K. Asakura, *ACS Catal.*, 2011, **11**, 1521-1528.

104. A. Corma, H. Garcia and A. Leyva, *Tetrahedron*, 2004, **60**, 8553-8560.

105. U. Kernchen, B. Etzold, W. Korth and A. Jess, *Chem. Eng. Tech.*, 2007, **30**, 985-994.

106. L. Naicker, H. B. Friedrich, A. Govender and P. Mohlala, *Appl. Catal. A, Gen.*, 2018, **562**, 37-48.

107. C. P. Menhert, R. A. Cook, N. C. Dispenziere and M. Afeworki, *J. Am. Chem. Soc.*, 2002, **124**, 12932-12933.

108. C. P. Mehnert, E. J. Mozeleski and R. A. Cook, *Chem. Comm.*, 2002, 3010-3011.

109. H. Hagiwara, Y. Sugawara, K. Isobe, T. Hoshi and T. Suzuki, *Org. Lett.*, 2004, **6**, 2325-2328.

110. J. Brünig, Z. Csendes, S. Weber, N. Gorgas, R. W. Bittner, A. Limbeck, K. Bica, H. Hoffmann and K. Kirchner, *ACS Catal.*, 2018, **8**, 1048-1051.

111. A. Riisager, K. M. Eriksen, P. Wasserscheid and R. Fehrmann, *Catal. Lett.*, 2003, **90**, 149-153.

112. J. N. C. Lopes, M. F. C. Gomes and A. A. H. Pádua, *J. Phys. Chem. B*, 2006, 110, 16816-16818.

113. M. Ruta, I. Yuranov, P. J. Dyson, G. Laurenczy and L. Kiwi-Minsker, *J. Catal.*, 2007, **247**, 269-276.

114. B. M. L. Dioos and P. A. Jacobs, *J. Catal.*, 2006, **243**, 217-219.

115. C. Sievers, O. Jimenez, R. Knapp, X. Lin, T. E. Muller, A. Turler, B. Wierczinski and J. A. Lercher, *J. Mol. Catal. A: Chemical*, 2008, **279**, 187-199.

116. A. Riisager, P. Wassercheid, R. van Hal and R. Fehrmann, *J. Catal.*, 2003, **219**, 452-455.

117. D. R. Ou, T. Mori, H. Togasaki, F. Ye and J. Drennan, *Langmuir*, 2011, **27**, 3859-3866.

118. S. Shylesh, D. Hanna, S. Werner and A. T. Bell, *ACS Catal.*, 2012, **2**, 487-493.

119. B. G. Rao, D. Mukherjee and B. M. Reddy, *Nanostruc. Novel Therapy*, 2017, 1-36.

120. X. D. Mu, J. Q. Meng, Z. C. Li, Y. Kou, *J. Am. Chem. Soc.*, 2005, **127**, 9694– 9695.

121. X. Yang, Z. F. Fei, D. B. Zhao, W. H. Ang, Y. D. Li, P. J. Dyson, *Inorg. Chem.*, 2008, **47**, 3292–3297.

122. J. P. Rao and K. E. Geckeler, *Prog. Polym. Sci.*, 2011, **36**, 887-913.

123. Z. Wenwen, Y. Yinyin, Y. Hanmin, H. Li, Q. Yunxiang, Z. Xiuge and H. Zhenshan, *Chem. Eur. J.*, 2013, **19**, 2059-2066.

124. P. McMorn and G. J. Hutchings, *Chem. Soc. Rev.*, 2004, **33**, 108-122.

125. X. Wang, Z. Li, X. Han, Z. Han and Y. Bai, *Appl. Surf. Sci.*, 2017, **420**, 496-503.

126. Y. Zhang, B. Wang, E. H. M. Elageed, L. Qin, B. Ni, X. Liu and G. Gao, *ACS Macro Lett.*, 2016, **5**, 435-438.

127. J. Claus, F. O. Sommer and U. Kragl, *Solid State Ion.*, 2018, **314**, 119-128.

128. T. N. P. Truong, H. Randriamahazaka and J. Ghilane, *ACS Catal.*, 2018, **8**, 869-875.

129. G. Shorikova, D. Rauber, D. Aili, S. Martin, Q. Li, D. Henkensmeier and R. Hempelmann, *J. Membr. Sci.*, 2020, **608**, 118188.

130. J. Chen, F. Xie, X. Li and L. Chen, *Green Chem.*, 2018, **20**, 4169-4200.

131. a) S. M.-Chergui, M. Guerrouache, B. Carbonnier and M. M. Chehimi, *Colloids Surf. A Physicochem. Eng. Asp.*, 2013, **439**, 43-68; b) R. Mangaiyarkarasi, M. Priyanga, N. Santhiya and S. Umadevi, *J. Mol. Liq.*, 2020, **310**, 113241.

132. J. Bartáček, J. Váňa, P. Drabina, J. Svoboda, M. Kocúrik and M. SedláK, *React. Funct. Polym.*, 2020, **153**, 104615.

133. A. Ohtaka, T. Teratani, R. Fujii, K. Ikeshita, T. Kawashima, K. Tatsumi, O. Shimomura and R. Nomura, *J. Org. Chem.*, 2011, **76**, 4052-4060.

134. C. B. Reddy, R. Bharti, S. Kumar and P. Das, *ACS Sustainable Chem. Eng.*, 2017, **5**, 9683-9691.

135. S. E. Sayed, A. Bordet, C. Weidenthaler, W. Hetana, K. L. Luska and W. Leitner, *ACS Catal.*, 2020, **10**, 2124-2130.

136. H.-J. Cho, S.-M. Lee, S. Jung, T.-K. Lee, H.-J. Yoon and Y.-S. Lee, *Tetrahedron*, 2011, **52**, 1459-1461.

137. J. T. M. Amphlett, M. D Ogden, R. I. Foster N. Syna, K. Soldenhoff and C. A. Sharrad, *Chem. Eng. J.*, 2018, **334**, 1361-1370.

138. J. Balué and J. C. Bayón, *J. Mol. Catal. A: Chem.*, 1999, **137**, 193-203.

139. C. Carlini, M. Di Girolamo, M. Marchionna, A. M. R. Galletti and G. Sbrana, *Stud. Surf. Sci. Catal.*, 1998, **119**, 491-496.

140. M. Lakouraj, M. Tajbakhsh and H. Tashakkorian, *Monatsh. Chem.*, 2007, **138,** 83–88.

141. T. Osako, K. Torii, S. Hirata and Y. Uozumi, *ACS Catal.,* 2017, **7**, 7371-7377.

142. Q. Zhao, P. Zhang, M. Antonietti and J. Yuan, *J. Am. Chem. Soc.*, 2012, **134**, 11852-11855.

143. Y. Bian, J. Zhang, S. Zhang, C. Liu and D. Zhao, *ACS Sustainable Chem. Eng.*, 2019, **7**, 17220-17226.

144. S. Doherty, J. G. Knight, J. R. Ellison, D. Weekes, R. W. Harrington, C. Hardacre and H. Manyar, *Green Chemistry*, 2012, **14**, 925-929.

145. S. Doherty, J. G. Knight, M. A. Carroll, A. R. Clemmet, J. R. Ellison, T. Backhouse, N. Holmes, L. A. Thompson and R. A. Bourne, *RSC Advances*, 2016, **6**, 73118-73131.

146. S. Doherty, J. G. Knight, J. R. Ellison, P. Goodrich, L. Hall, C. Hardacre, M. J. Muldoon, S. Park, A. Ribeiro, C. A. N. de Castro, M. J. Lourenço and P. Davey, *Green Chem.*, 2014, **16**, 1470-1479.

147. S. Doherty, J. G. Knight, T. Backhouse, E. Abood, H. Al-shaikh, A. R. Clemmet, J. R. Ellison, R. A. Bourne, T. W. Chamberlein, R. Stones, N. J. Warren, I. A. J. Fairlamb and K. R. J. Lovelock, *Adv. Synth. Catal.*, 2018, **360**, 3716-3731.

148. S. Doherty, J. G. Knight, T. Backhouse, R. J. Summers, E. Abood, W. Simpson, W. Paget, R. A. Bourne, T. W. Chamberlein, R. Stones, K. R. J. Lovelock, J. M. Seymour, M. A. Isaacs, C. Hardacre, H. Daly and N . H. Rees, *ACS Catal.*, 2019, **9**, 4777-4791.

Chapter 2

RuNP-Catalysed Selective Hydrogenation of Aryl Ketones, Aldehydes and Biomass-Derived Substrates

Chapter 2 Ruthenium Nanoparticle Catalysed Hydrogenation of Aryl Ketones, Aldehydes and Biomass-Derived Substrates

2.1 Introduction

A global attempt to reduce carbon dioxide emissions along with the severe depletion of fossil fuel reservoirs, has increased the interest in the development of "environmentally-friendly" catalysts using renewable feedstock for the production of fine chemicals and renewable fuels.[1] To this end, the valorisation of lignocellulosic-based biomass has attracted considerable attention as it is readily available and a cheap source of carbon.[2] Furthermore, the bioderived substances that are produced afford a wide range of organic sugars and acids with various functionalities which can act as a green source of building blocks for fine chemicals and fuels (Figure 2.1).[3]
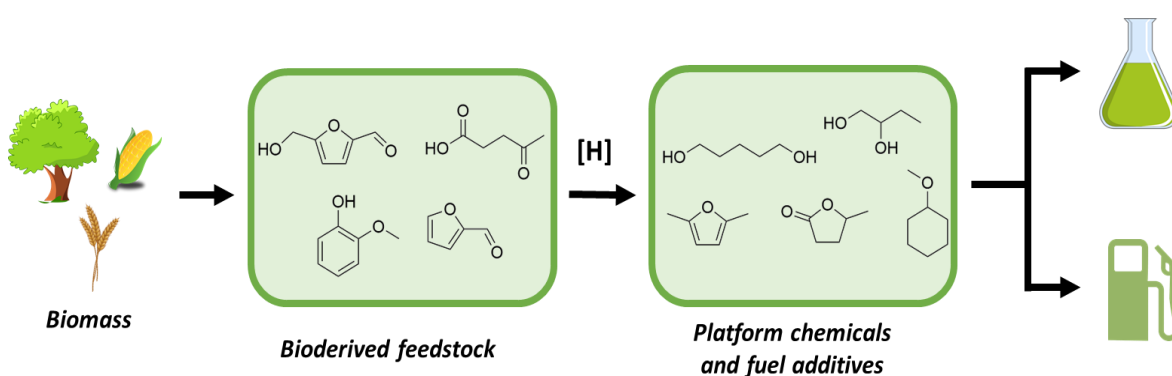
Figure 2.1: Schematic representation for production of fuel and platform chemicals from biomass.

The highly oxygenated characteristics and intrinsic combustion properties of such feedstocks limit their immediate use as a fuel additive which makes them mediocre compared to conventional fuel sources.[4] Therefore, new catalyst technologies need to be developed and strategically optimised to efficiently afford fuel-like materials with more suitable physical properties. Moreover, the products must also be able to be safely stored on a large scale.[5] A potential biofuel, 2,4-dimethyl furan can be generated from glucose, a product that is directly obtained during the processing of lignocellulose-based biomass through multiple acid- and metal-catalysed deoxygenation steps (Scheme 2.1).
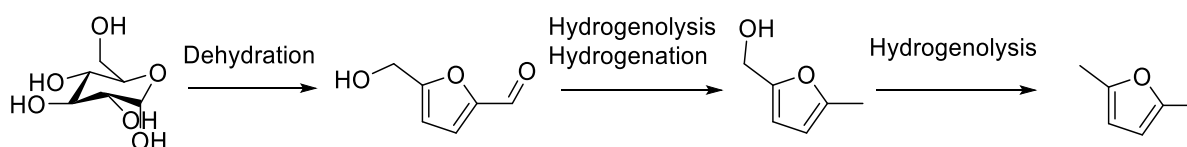
Scheme 2.1: Glucose deoxygenation to afford the potential biofuel 2,4-dimethyl furan.

Metal nanoparticle catalysed hydrogenation is an effective and facilitating technology. It is particularly important to develop catalysts that enable the selective reduction of unsaturated moieties that bear other reactive groups. The efficient use of such metal NP catalysts allows for the development of a better performing, scale-up and sustainable approach. For example, Moores *et al.* synthesised Ru-coated FeNPs which demonstrated pronounced selectivity for the hydrogenation of ketones over nitro and aldehyde groups.[7a] In addition, Zhang *et al.* developed highly active and selective RuNPs for the synthesis of γ-valerolactone from methyl levulinate (selective to ketone hydrogenation) under ambient conditions in water.[7b]

The widely accepted mechanism for the hydrogenation of an α,β-unsaturated carbonyl compound over a heterogeneous catalyst involves the absorption and dissociation of gaseous hydrogen across the metal surface to form chemisorbed surface hydrogen atoms (Scheme 2.2). This is followed by a stepwise addition of hydrogen *via* migratory insertion across the adsorbed unsaturated substrate, initially forming a surface-coordinated alkyl fragment, which is then released as the hydrogenated product.
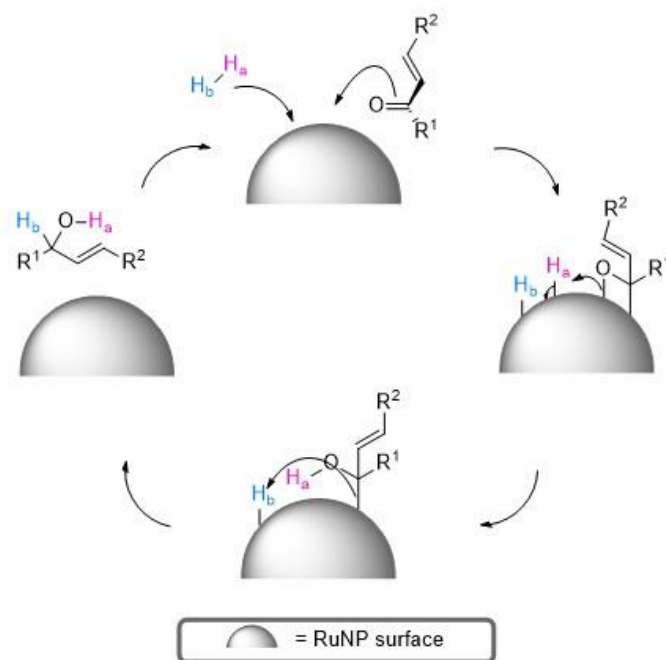
Scheme 2.2: General mechanism for the hydrogenation of an α,β-unsaturated carbonyl compound over a heterogeneous RuNP catalyst.

Furthermore, it has been proposed that altering the NP's size can change the substrate's initial absorption mode, which can impact the selectivity of a reaction.[6] In addition, the interactions between the catalyst and the support can modify the performance of the catalyst and allow for the optimisation of the catalyst by changing the functionality of the support. Several reports document the highly active catalysis and tuneable selectivity of supported homogeneous catalysts and NP-based systems.[7] Systems on a large scale can improve the overall product turnover and at the same time lower the production of waste of a process. However, in practice, industrial scale hydrogenative transformations are typically conducted in the vapour phase with heterogeneous catalysts.[9]

The application of vapour phase technology offers several practical advantages from an engineering point of view in terms of increased hydrogen solubility, better reactor design, increased mass transfer in addition to facile product extraction and catalyst reuse, which at present, exceeds the advantages of large-scale homogeneous approaches. However, the required operating conditions of high temperatures (usually above 300 °C) and pressures, impose high costs on such processes and over a

prolonged time these conditions can result in coking or deactivation of a susceptible catalyst.[10] Therefore, there is a significant drive to develop heterogeneous catalysts that operate under mild conditions in the aqueous phase, as water is a cheap, environmentally benign and non-toxic substitute to conventional organic solvents. Moreover, catalyst recycling is facilitated by the facile organic reactant/product extraction from the aqueous phase which contains the catalyst by using a two phase system.[11] However, new separation strategies and technologies need to be developed for aqueous phase catalysis if the advantages of this approach are to be fully exploited. Although, the advantages associated with the low temperature aqueous phase catalysis would considerably improve the sustainability of this process.

Such sustainable processes are developed using catalytic technologies and it is becoming increasingly more important to achieve the fundamental chemical transformations through more energy efficient and 'greener' processes. Currently, green chemistry principles conceptualise a sustainable process as one that reduces the waste production, uses renewable starting materials and avoids the production or the use of hazardous substances.[12] Even though homogeneous catalysts give high activities and selectivties the protocols for catalyst recovery are onerous and metal leaching into the product stream has prevented their use on an industrial scale.

Transition metal nanoparticle (TMNP) heterogeneous catalytic hydrogenations are generally accepted as a scalable, sustainable technology, owing to their ease of separation, high efficiency, atom economy and reusability.[13] Various TMNP catalysts have been reported for similar operations, for example, Cu[14], Ni[15], Pt[16], Rh[17] and Pd.[18] Ru seems to be the metal of choice for the hydrogenation of α, β-unsaturated carbonyl compounds as experimental and computational studies have shown that ruthenium nanoparticles (RuNPs) are highly selective for the hydrogenation of the carbonyl functionality into an alcohol in the close proximity of other reducible fragments,[19] which is one of the key chemical transformations for the valorisation of lignin-derived monomers.[20]

Whilst platinum and palladium catalysts have typically been shown to be superior to ruthenium catalysts for vapour phase hydrogenations,[21] the activity of Ru catalysts appears to be sensitive to its nearby environment, in particular under liquid phase conditions, which enables the system to be optimised and selectively tuned for

a given reaction.[18] For instance, Huber *et al.* found that monometallic RuNPs supported on alumina exhibited higher activities for the aqueous phase hydrogenation of propanal, acetone, xylose and acetaldehyde than Co, Pd, Pt or Rh.[24]

Generally, aqueous phase catalysis is favoured over catalysis in an organic solvent as it provides multiple advantages from a sustainable and engineering point of view. The highly soluble starting materials and the immiscible products in the aqueous solution enhances the catalyst-substrate interactions and reduces the overall processing cost *via* facile recovery of the reagent, product and catalyst. Furthermore, the overall process is streamlined, as the small molecules formed by the depolymerisation of lignocellulosic-based biomass are generally obtained in the aqueous solution, which eliminates the need for further processing. Water is generally deemed as an environmentally benign solvent as a result of its low toxicity, low volatility and wide availability. Thus, water compatibility is an essential feature to consider when designing a catalyst. Sustainability aside, there is also a significant amount of data that supports water, serving as an additive or as the bulk solvent, which is directly accountable for the improvement in the activity of RuNP-based catalysts for hydrogenations.[25] In most instances, the role of the solvent is to dissolve the reactants and alter the distribution of products by altering the reaction kinetics and/or the mass transfer rates. For example, Michel and Ruppert employed DFT calculations to explore the role of water on the hydrogenation of ketones over Ru(0001) surfaces.[26] They reported that the addition of the chemisorbed water to the DFT calculation allowed the reaction to operate through a lower energy pathway which was mediated by a hydrogen bond interaction between the hydroxy intermediate and the solvent.

The selective reduction of α,β-unsaturated carbonyl compounds is a widely studied fundamental transformation as well as the hydrogenative transformation of biomass-derived substrates, such as, furfural, 2-hydroxymethylfurfuraldehyde and levulinic acid (LA) and its esters, as the resulting products are key platform molecules for the production of value-added chemicals and renewable fuels.[27] There is now a large amount of literature precedent that demonstrates that the solvent of choice for the Ru-catalysed hydrogenation of α,β-unsaturated carbonyl compounds is water, specifically for carbonyl-rich biomass-derived platform molecules.[28] To this end, there have been several recent examples of systems with promising activity and selectivity

profiles based upon ultrasmall RuNPs stabilised by ionic liquids,[29] polymers,[30] β-cyclodextrins[31] and carbon materials.[32]

Other systems with encouraging performance profiles for the hydrogenation of carbonyl-based bioderived substrates such as levulinic acid or its esters into γ-valerolactone include RuNPs immobilised on either acid-functionalised mesoporous carbon,[33] acidic zirconium-containing spherical mesoporous silica,[34] commercial sulfonic acid ion exchange resin,[35] mesoporous TiO_2,[36] RuNP supported on sulfonic acid functionalised UiO-16[37] as well as chromium-based MOF MIL-101,[38] These systems can act as bifunctional catalysts with the RuNPs assisting the hydrogenation step whilst the acid catalyses the dehydration of the γ-hydroxyvaleric acid intermediate into γ-valerolactone.

In addition to favourable solvent effects, it is now well-documented that tuning the interactions between the functionalities on the ligand and/or the support can also lead to significant improvements in activity and selectivity by modifying the morphology of the particle and/or the electronic structure of the surface.[39] Recent studies have showed that heteroatom-doped materials can promote favourable electronic catalyst-support interactions which improve the catalyst performance without using expensive ligand additives that are challenging to reuse and involve multi-step syntheses.[40] Much like ligand-assisted homogenous catalysis, the electronic properties of the metal in a heterogeneous catalyst are well-known to exert a strong influence on the activity and selectivity of a reaction.[41] Especially for the hydrogenation of carbonyl functionalities, electron rich metal-centres have been shown to improve the activity of the catalyst. Enhanced carbonyl activation occurs as a result of the increase in electron density at the metal which is available for π-backbonding into the π^* orbital of the carbonyl, thereby promoting strong adsorption of the carbonyl group onto the surface of the catalyst. This has been achieved by incorporating electron donating functionality such as amines, carbenes and phosphines into the architecture of the support.

2.2 Results and Discussion

The research presented in this chapter is intended to expand the application of PIILP-stabilised NP catalysts to include RuNPs. Previous work conducted by the research group has already shown that polyethylene glycol (PEG)-modified phosphine-

decorated PIIL-stabilised PdNPs are highly selective catalysts for the aqueous phase hydrogenation of nitroarenes[42] and α,β-unsaturated carbonyl compounds.[43] The aim of this project was to explore the efficacy of PEG-modified phosphine-decorated PIIL-stabilised RuNPs for the hydrogenation of aryl ketones, aryl aldehydes and biomass-derived carbonyl compounds, in order to investigate whether the incorporation of the heteroatom donor alters the activity and/or selectivity.

2.3 Catalyst Synthesis and Characterisation

2.3.1 Monomer synthesis

The initial design was based on the use of PEG-modified phosphine-decorated PIIL, rationalising that the incorporation of imidazolium-based (**2.1**) and phosphine-based (**2.9**) IL monomers would both stabilise the RuNPs, whilst the PEG-based (**2.8**) monomer would improve the dispersibility of the catalyst in water and thus facilitate aqueous phase hydrogenation (Figure 2.2).
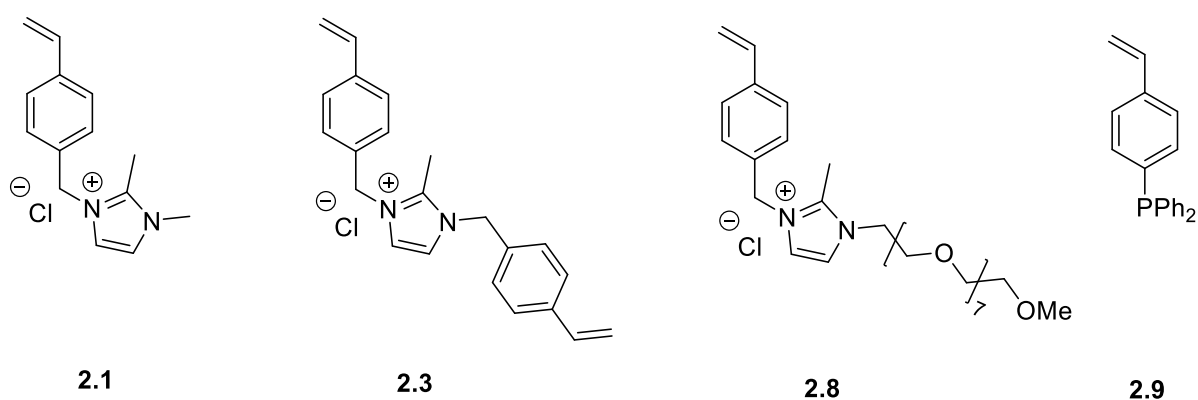
Figure 2.2: Target monomers; dimethyl imidazolium-based monomer (**2.1**), dibenzyl imidazolium-based crosslinker (**2.3**), PEGylated imidazolium monomer (**2.8**) and phosphine modified monomer (**2.9**).

Monomer **2.1** was obtained in near quantitative yield from the quaternisation of 1,2-dimethylimidazole with 4-chloromethylstyrene in chloroform at 50 °C (Scheme 2.3). Crosslinker **2.3** was prepared in a two-step protocol (Scheme 2.3). In the first step 2-

methylimidazole was deprotonated by NaH to afford the corresponding 2-methyl imidazolide anion which was reacted with 4-chloromethylstyrene to afford 2-methyl-1-(4-vinylbenzyl)-imidazole (**2.2**) as a pale-yellow oil after an acid/base workup. A subsequent quaternisation of monomer **2.2** with 4-chloromethylstyrene afforded the desired crosslinker (**2.3**) as a white powder in a 91% yield.
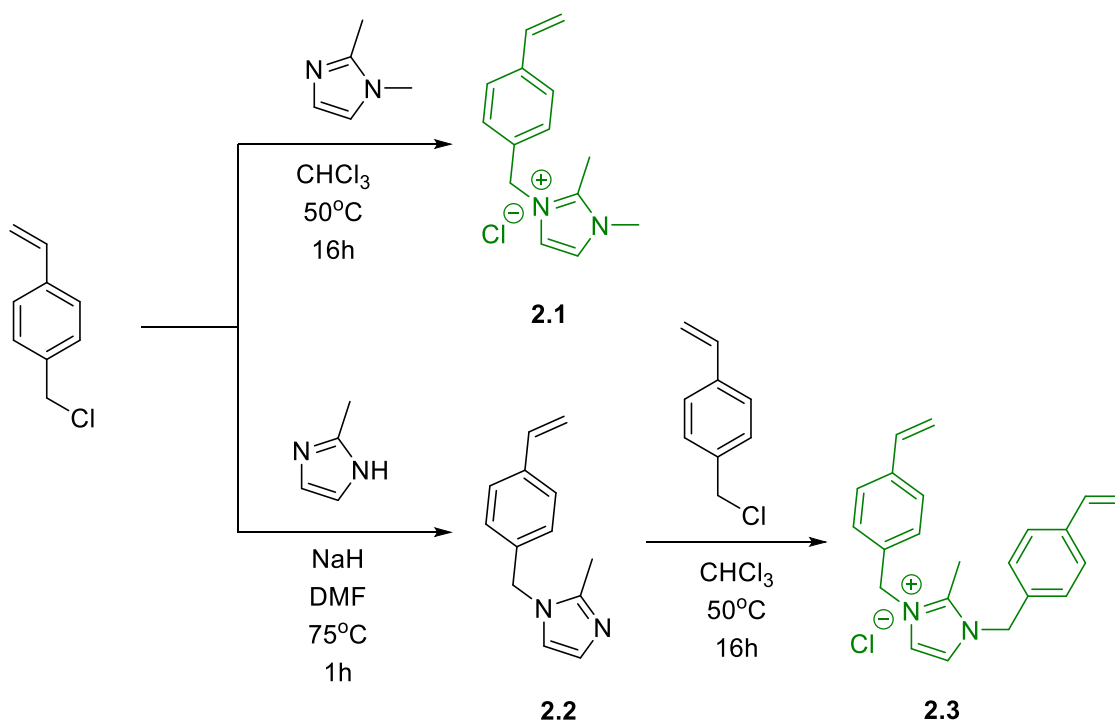
Scheme 2.3: Synthesis of the IL monomer **2.1** and the crosslinker **2.3**.

Monomer **2.8** was synthesised *via* the 4-step convergent procedure shown in Scheme 2.4. Treatment of poly(ethyleneglycol)monomethyl-350 ether (**2.4**) with pyridine and thionyl chloride in refluxing toluene for 2 days resulted in chlorination to afford **2.5** in 92% yield. Reaction of **2.5** with sodium 2-methylimidazolide in DMF resulted in substitution to afford **2.6** as a viscous yellow oil. Finally, 4-chloromethylstyrene was converted into 4-bromomethylstyrene **2.7** *via* a Finkelstein reaction with an excess of sodium bromide in acetonitrile and reacted with **2.6** to afford the PEGylated 4-(vinylbenzyl)-imidazolium monomer **2.8** as a pale-yellow oil in a 90% yield.
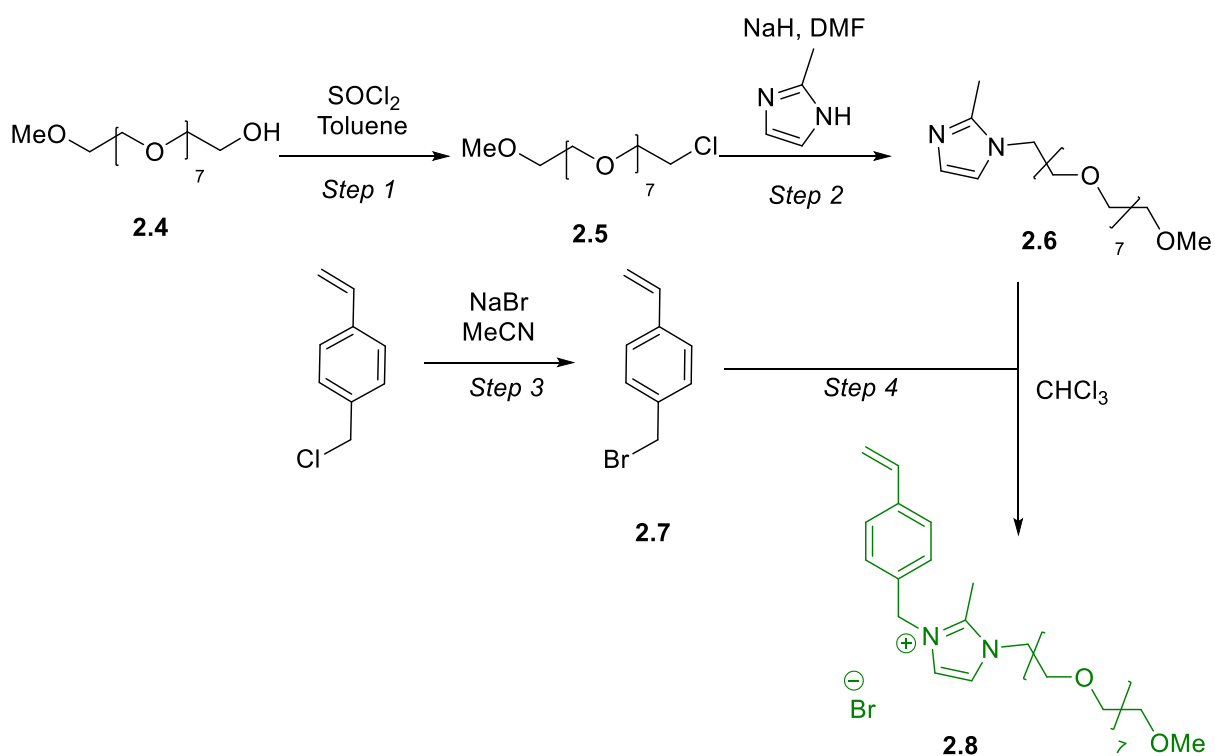
Scheme 2.4: Synthesis of the PEGylated imidazolium-based monomer **2.8**.

The Grignard reaction used to synthesise 4-diphenylphosphinostyrene (**2.9**) was adapted from the reported synthesis by Marcus and Rabinowitz (Scheme 2.5).[44] As the phosphine is very air- and moisture-sensitive, the aqueous workup was performed under a nitrogen atmosphere using degassed solvents. This method produced a white crystalline solid in 62% yield, which showed a single peak in the ^{31}P NMR spectrum at δ −5.82 ppm (spectrum in Appendix A) indicating that the product was successfully isolated and was spectroscopically pure.
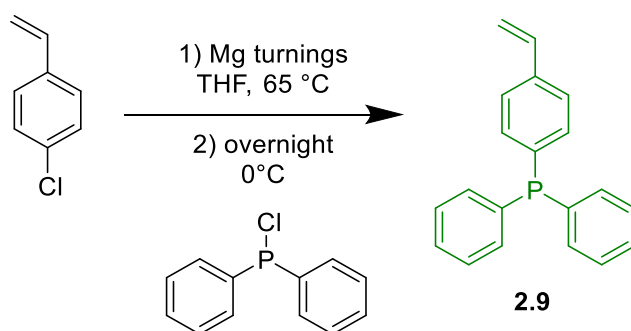
Scheme 2.5: Synthesis of the phosphine-functionalised monomer **2.9**.

2.3.2 Synthesis and characterisation of PIILs

Two phosphino-decorated polystyrene PIIL supports **2.10** and **2.11** were synthesised *via* AIBN-initiated free radical co-polymerisation of **2.3**, **2.8** and **2.9** (PPh$_2$-PEGPIIL) and **2.1**, **2.3** and **2.9** (PPh$_2$-PIIL) (Scheme 2.6). With the aim of exploring the effect of phosphine and PEG components, polymers **2.12** and **2.13** were also prepared to undertake comparative catalyst testing as supports that do not contain either a phosphine or PEG functionality. The ratio of 1.86:1:0.14 for imidazolium-IL, either a phosphine-functionalised monomer or styrene, and crosslinker, respectively, was chosen to allow for an overall 2:1 ratio of the repeating unit of cationic IL-like monomer to neutral phosphine or styrene to ensure consistency with our previous studies.

The monomers were dissolved in a 1:1 mixture of anhydrous ethanol/THF and 5 mol% AIBN initiator was added. The resulting solution was degassed using the freeze-thaw method to provide an oxygen-free system and the mixture heated at reflux for 4 days. To prevent using arduous purification methods, a further 5 mol% AIBN was added and the resulting mixture was stirred for 16 hours to guarantee full monomer consumption.

X = Br, R = $\sim$$\left[O \right]_7$ OMe

X = Cl, R = Me

PPh$_2$-PEGPIIL (**2.10**)

PPh$_2$-PIIL (**2.11**)

X = Br, R = $\sim$$\left[O \right]_7$ OMe

X = Cl, R = Me

PEGPIIL (**2.12**)

PIIL (**2.13**)
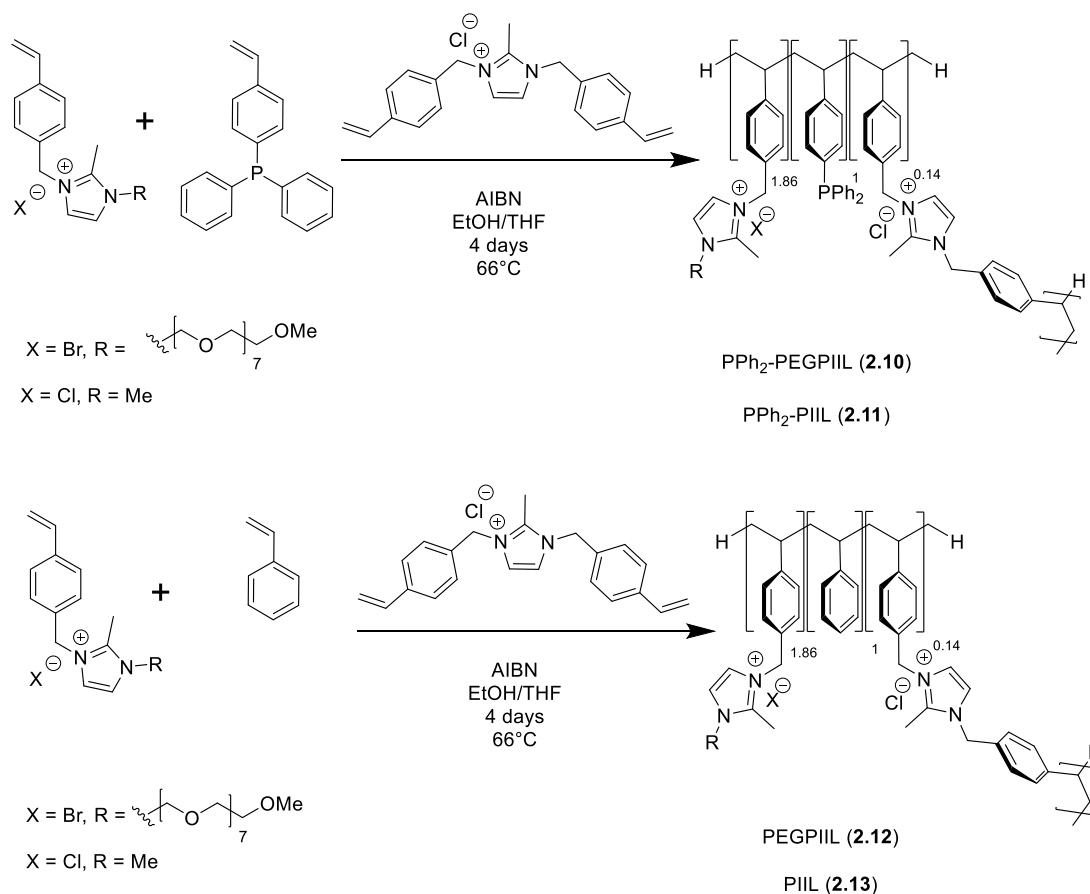
Scheme 2.6: Synthesis of PIIL support *via* AIBN-initiated free radical polymerisation.

The crude post-reaction mixture was sampled and analysed by ^{1}H NMR spectroscopy and the absence of any vinylic signals was an indication that the polymerisation was complete. As a result of the random nature of the polymer and the tumbling effects that are associated with the polymer molecules in solution, the ^{1}H signals were broadened which further indicated that the polymerisation had gone to completion (Figure 2.3). Both phosphino-functionalised PILs **2.10** and **2.11** were obtained in >90% yield as white powders after the concentration of the ethanolic reaction mixtures *in vacuo* followed by the precipitation into diethyl ether. Unfortunately, the removal of all of the residual solvent proved challenging, owing to the complexity of the cross-linked polymer networks.

2.10
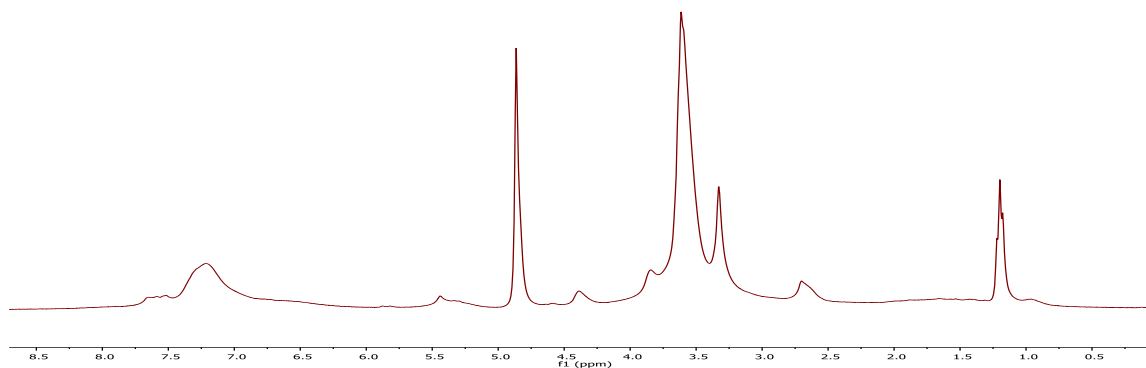
2.11
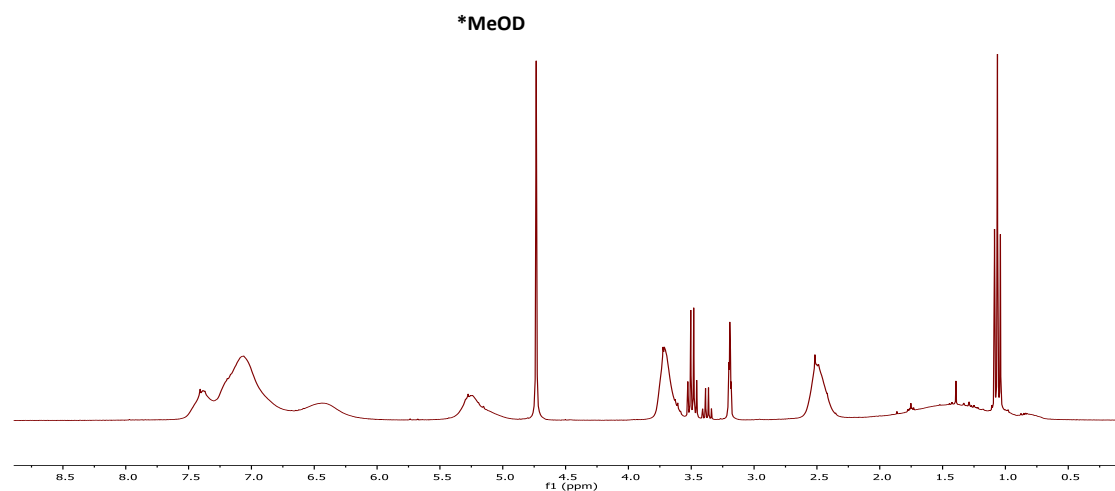
Figure 2.3: Solution ^{1}H NMR spectra of PPh$_2$-PEGPIIL (**2.10**) in CDCl$_3$ (top) and PPh$_2$-PIIL (**2.11**) in MeOD (bottom).

The inherent porosity and hydrophilicity of these PIIL materials caused a high degree of solvent trapping therefore elemental analysis was considered unreliable for the determination of the polymer composition. SEM analysis was carried out to examine the morphology of the polymer surfaces (Figure 2.4), polymer **2.10** appeared more porous due to the hydrophilic PEG group, whilst polymer **2.11** was smoother in appearance.
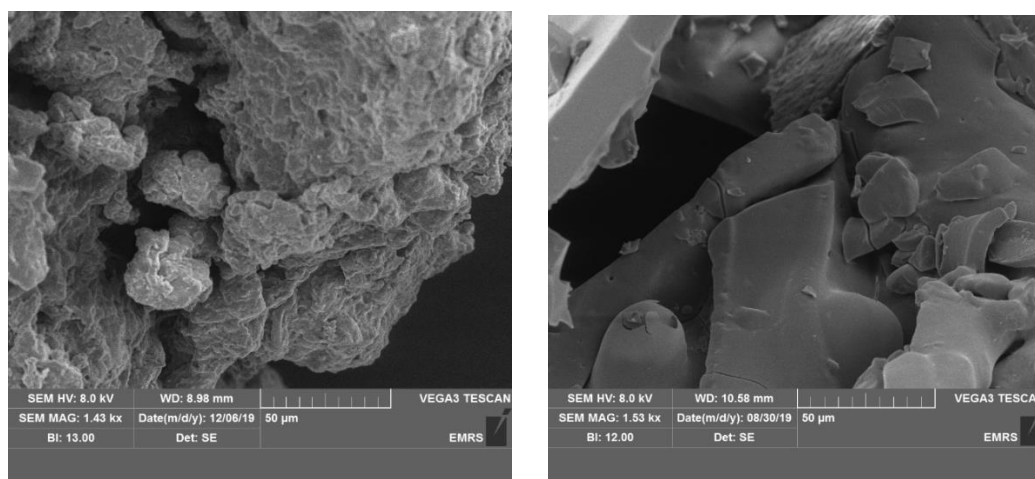
Figure 2.4: SEM images of the freshly prepared PPh$_2$-PEGPIL (**2.10**) (left) and PPh$_2$-PIL (**2.11**) (right).

Figure 2.5 shows the solid-state ^{31}P NMR spectrum of PPh$_2$-PEGPIIL (**2.10**) and PPh$_2$-PIL (**2.11**). Both spectra display a phosphorous containing species at -10.4 and –6.9 ppm, respectively. The **2.10** spectra displays a minor broad peak at 22 ppm which accounts for small amounts of phosphine oxide.

2.10

2.11
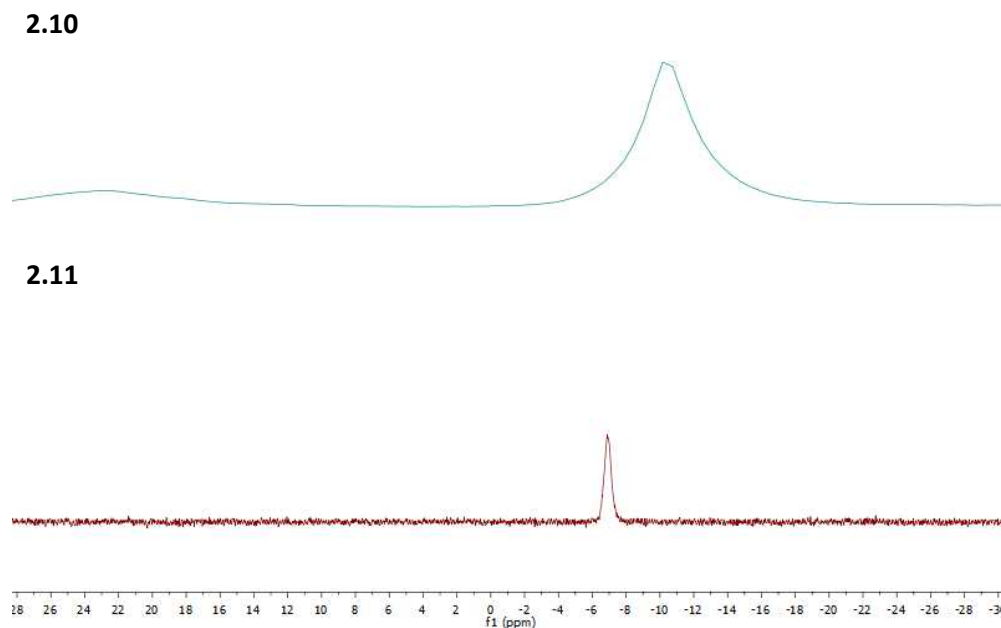
Figure 2.5: Solid state ^{31}P NMR of PPh$_2$-PEGPIIL (**2.10**) (top) and PPh$_2$-PIIL (**2.11**) in (bottom).

As these polymers will be used as supports to immobilise RuNPs for their use in catalysis their thermal stability was investigated using thermogravimetric analysis (TGA). The minor initial degradation at around 100 ℃ is a result of the loss of the physiosorbed water from the polymer, suggesting a small degree of solvent adsorption. Both polymers go through three similar degradation periods after removal of the residual solvent (Figure 2.6). The polystyrene backbone is known to degrade at approximately 500 ℃,[45] which is visible in both spectra. Therefore, the first and second pathways are most likely associated with the imidazolium, phosphine and PEG groups. As the degradation of the PIIL materials does not start until ~250 ℃, which is substantially higher than the temperatures required for liquid phase catalysis, both polymers have suitable stability for use as catalyst supports.
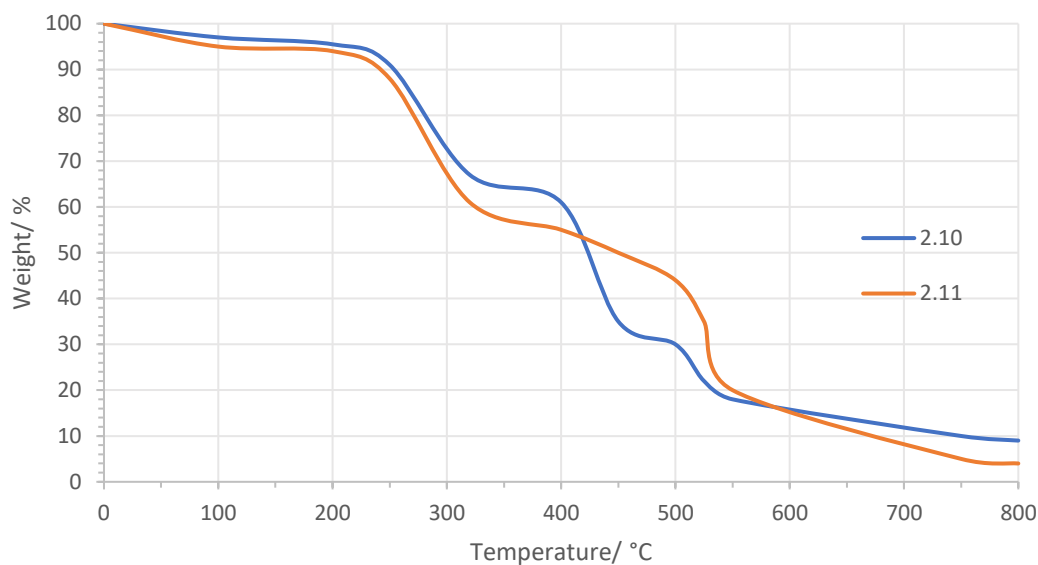
Figure 2.6: TGA curves for PPh_2-PEGPIIL (**2.10**) and PPh_2-PIIL (**2.11**).

2.3.3 Synthesis and characterisation of PIIL supported Ruthenium Nanoparticles (RuNP@R-PIILP)

Based on the literature precedent for the ion exchange method, RuNPs were integrated within the polymer network following a straightforward protocol (Scheme 2.7). Ruthenium (III) trichloride was selected as the precursor to impregnate the polymer as its reduction to RuNPs is well-documented.[46] When $RuCl_3$ is impregnated into the polymer the association with chloride affords the $RuCl_4$ anion which would provide an electrostatic driving force (for non-phosphine containing polymers), in addition the covalent association of the $RuCl_3$ with the phosphine would also provide a driving force to facilitate efficient immobilisation.

In a standard procedure, an ethanolic polymer solution was treated with commercially available $RuCl_3$ and the resulting mixture stirred for 5 hours at room temperature to guarantee complete impregnation of the metal halide. Subsequently, under a nitrogen atmosphere, the *in-situ* reduction of the Ru^{3+}-impregnated materials, *via* the dropwise addition of an aqueous solution of sodium borohydride. Following 2 hours of stirring, the resultant mixture was then concentrated, washed with acetone, water, to remove the excess borohydrate salts, ethanol and finally with diethyl ether. The collected solids were then dried under a reduced pressure to obtain the corresponding PIIL-stabilised RuNPs as black powders in near-quantitative yields.

66
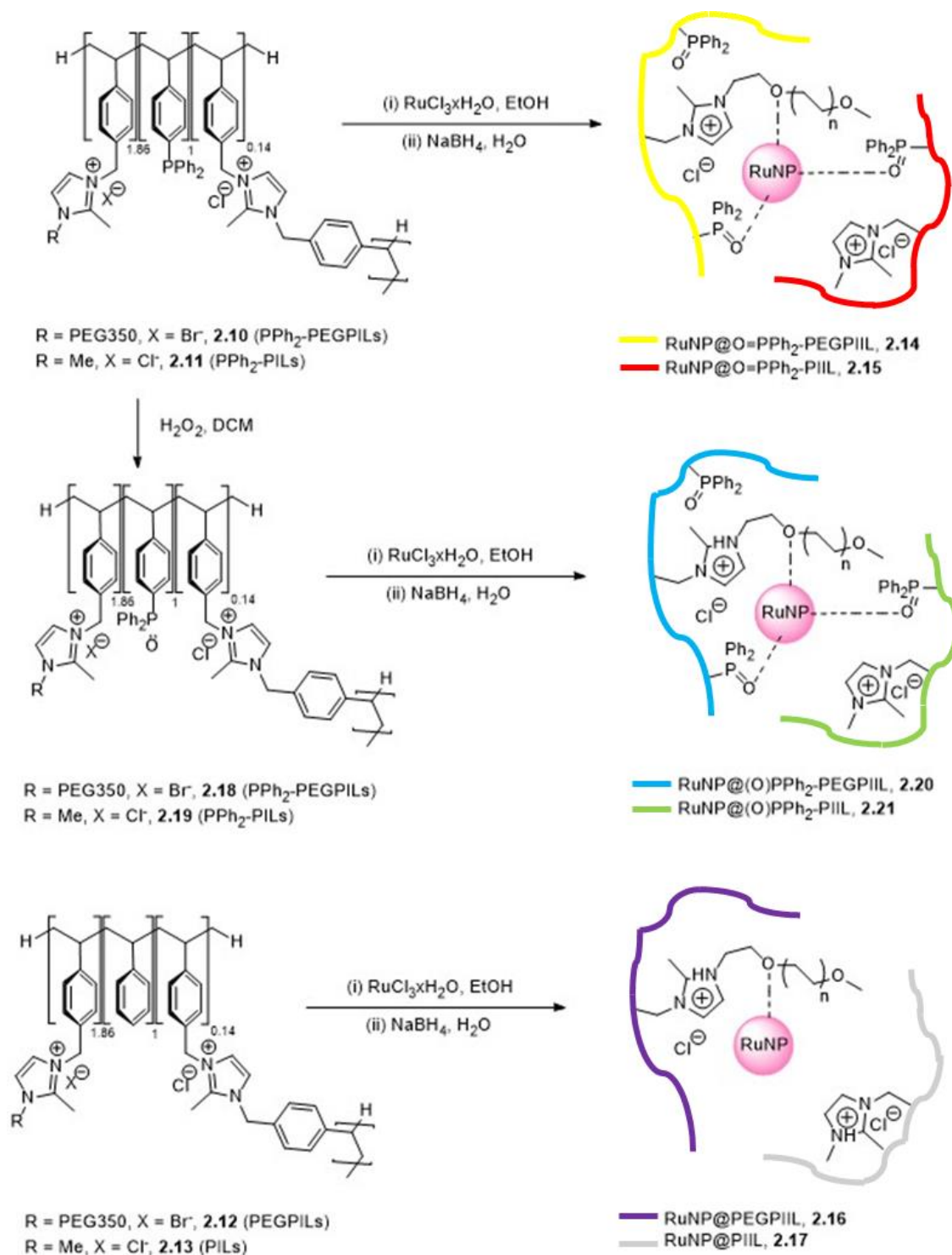
Scheme 2.7: Synthetic route used for the impregnation of the PIL materials with RuCl$_3$ followed by the NaBH$_4$ reduction to give the corresponding PIILP-stabilised RuNPs.

Not surprisingly, all of the catalysts demonstrated low solubility in common deuterated solvents, hence, solid state NMR spectroscopy was used to characterise

the product and explore potential interactions between the metal surface and the PIIL supports. The solid state ^{31}P NMR spectra of **2.14** and **2.15** both contained a single broad signal at ca. δ 25 ppm (Figure 2.7), which is characteristic of the phosphine oxide-based PIIL-stabilised RuNPs, in addition, there was no sign of a free phosphine at δ -6.8 ppm in the spectrum.
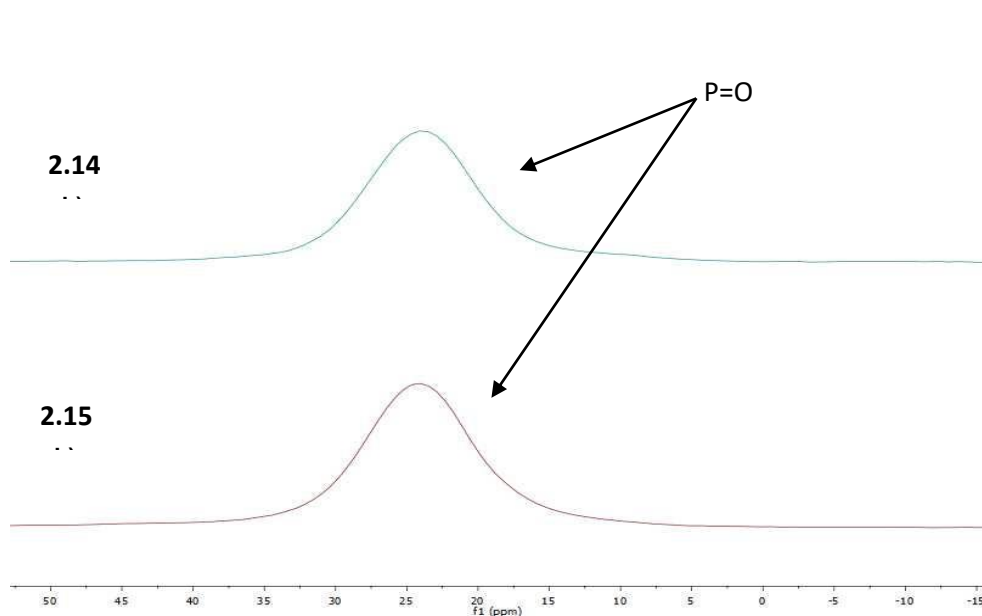
Figure 2.7: Solid state ^{31}P NMR spectra of RuNP@PPh$_2$-PEGPIILP (**2.14**) (top) and RuNP@PPh$_2$-PIILP (**2.15**) (bottom).

Whilst the initial proposal was to demonstrate whether a phosphine-based PIIL influences the RuNPs efficacy for the hydrogenation of α,β-unsaturated ketones and aldehydes, we inadvertently discovered from the XPS spectrum that impregnation of the phosphine-decorated PIILs with RuCl$_3$ resulted in the rapid reduction of the Ru(III) to afford a Ru(II) species and the resulting phosphine oxide; the RuNPs were then generated by sodium borohydride reduction. In retrospect, it is completely reasonable that the impregnation with RuCl$_3$ of either, PPh$_2$-PEGPIL (**2.10**) or PPh$_2$-PIL (**2.11**), would result in the facile phosphine oxidation with concomitant reduction to a Ru(II) species; as RuCl$_2$(PPh$_3$)$_3$ is prepared by the reaction between RuCl$_3$ and an excess of triphenylphosphine, which produces triphenylphosphine oxide as the by-product.[47] A solid state ^{31}P NMR spectrum of an authentic sample of O=PPh$_2$-PIL (**2.19**) and the corresponding RuNP@(O)PPh$_2$-PIIL (**2.21**), supports this interpretation, as both

samples contained a single broad resonance at δ 23 ppm (Figure 2.8). However, a relatively recent report revealed that a triarylphosphine-coordinated Ru cluster, (Ar$_3$P-Ru), also had a peak that appeared in this region,[48] which presented some uncertainty of this interpretation.
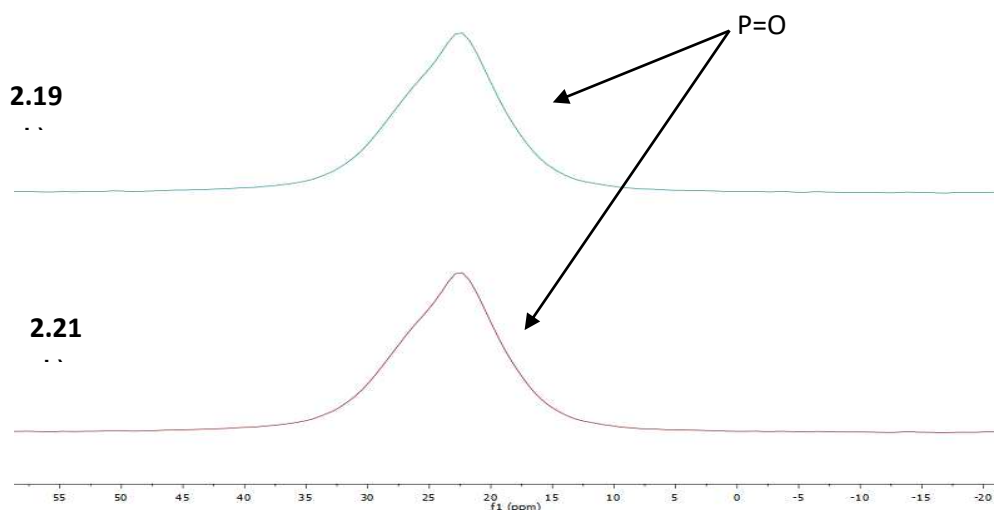
Figure 2.8: Solid state ^{31}P NMR spectra of (O)PPh$_2$-PIIL (**2.19**) (top) and RuNP@(O)PPh$_2$-PIIL (**2.21**) (bottom).

In an attempt to confirm whether the observed ^{31}P resonances for a RuNP-PAr$_3$ interaction would correspond to that of a Ar$_3$P=O, RuNP samples were prepared by the hydrogenation of a mixture of [Ru(COD)(COT)] in THF, with either PPh$_2$-PEGPIL (**2.10**) or PPh$_2$-PIL (**2.11**), following a previously well-documented literature procedure.[57] The Ru(0)-based precursor was chosen as it can form RuNPs under mild conditions and would prevent the serendipitous oxidation of the phosphine that occurs in the presence of RuCl$_3$. The solid state ^{31}P NMR spectra of both of the resulting RuNPs contained a major signal at *ca.* δ -9.5 ppm, associated with the uncoordinated phosphine, along with a minor signal at *ca.* δ 22 ppm (Figure 2.9), which we confidently attribute to the triarylphosphine-coordinated Ru interaction (Ar$_3$P-Ru), as the ^{31}P NMR spectra of **2.10** and **2.11** did not show any evidence for phosphine oxide prior to generation of the corresponding Ru(COD)(COT)-derived RuNPs.
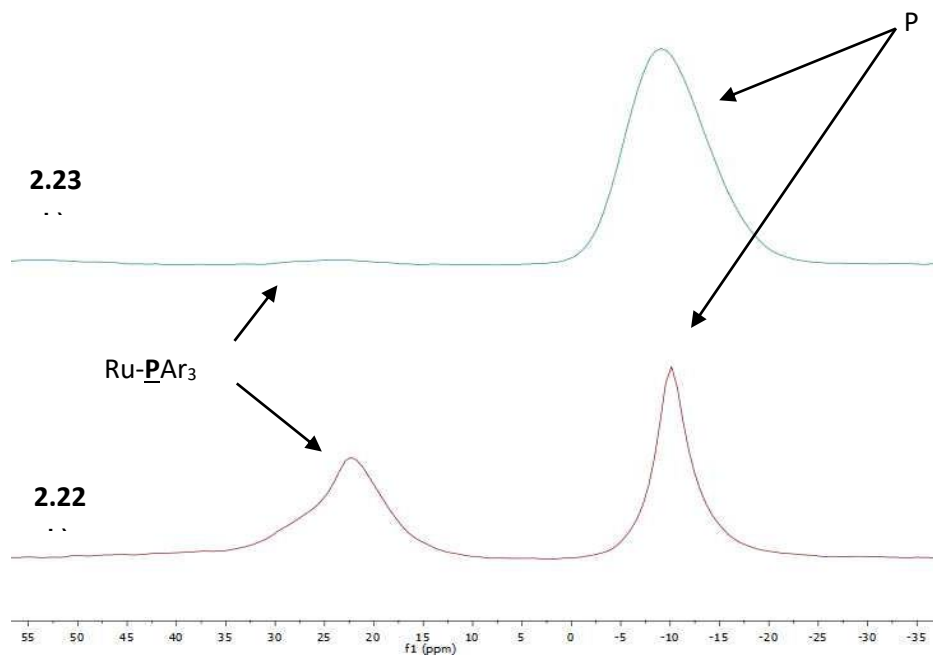
Figure 2.9: Solid state ^{31}P NMR spectra of a) RuCOD@PPh$_2$-PIILP (**2.23**) (top) and RuCOD@PPh$_2$-PEGPIILP (**2.22**) (bottom)

As a 1:1 Ru to phosphine stoichiometry was employed in the preparation of **2.14** and **2.15**, only one half of the phosphine should be oxidised and if the remaining phosphine did not form a RuNP-----PAr$_3$ interaction there should be a signal associated with uncoordinated phosphine at ca. δ -6 ppm in the ^{31}P NMR spectrum. However, complete absence of a signal in this region may imply that the signal at δ 25 ppm is actually due to a mixture of phosphine oxide-based RuNPs and the phosphine-based RuNPs, the latter comprising of a triaryl–coordinated Ru interaction (RuNP-----PAr$_3$).

Having established that, in practice, **2.14** and **2.15** were generated by coincidental oxidation of the phosphine during the impregnation of the PIIL (**2.10/2.11**) with RuCl$_3$ to give phosphine oxide-based RuNPs, the respective phosphine-oxide decorated PIILs, O=PPh$_2$-PEGPIL (**2.18**) and O=PPh$_2$PIL (**2.19**), were prepared, impregnated with RuCl$_3$ and the resulting Ru(III)/phosphine oxide-based precursors were then reduced *in-situ* to obtain phosphine oxide-based RuNPs, RuNP@(O)PPh$_2$-PEGPIIL (**2.20**) and RuNP@(O)PPh$_2$-PIIL (**2.21**) (Scheme 2.7).

The solid state ^{13}C NMR spectra of **2.20** and **2.21** (Figure 2.10) both contain characteristic resonances between δ 129 and 145 ppm which are associated with the

aromatic carbon atoms and the imidazolium ring, in addition to higher field signals which correspond to the aliphatic carbon atoms of the polystyrene backbone and the methyl group attached to the imidazolium ring; for **2.20**, the terminal methoxy unit of the PEG fragment appears at δ 57 ppm and the methylene groups appear ca. 69 ppm.
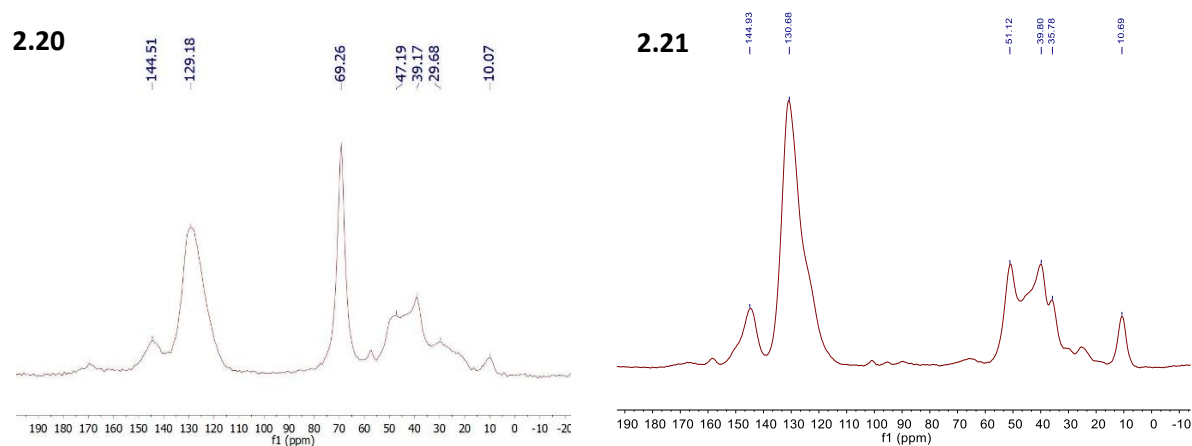
Figure 2.10: Solid state ^{13}C {^{1}H} NMR spectrum of RuNP@(O)PPh$_2$-PEGPIILP **2.20** (left) and RuNP@(O)PPh$_2$-PIILP **2.21** (right).

As anticipated, the IR, ^{13}C {^{1}H} and ^{31}P {^{1}H} NMR spectroscopic data for **2.20** and **2.21** were comparable to those for **2.14** and **2.15**, as both samples contained the phosphine oxide-decorated PIIL. The IR spectra of **2.21** showed a strong P=O band at 1112 cm^{-1} which confirms the presence of the phosphine oxide (Figure 2.11), this band was red-shifted compared to 1181 cm^{-1} for the authentic sample of phosphine oxide-decorated polymer O=PPh$_2$-PIL (**2.19**) which may well indicate the presence of a RuNP----O=PAr$_3$ interaction.[58]
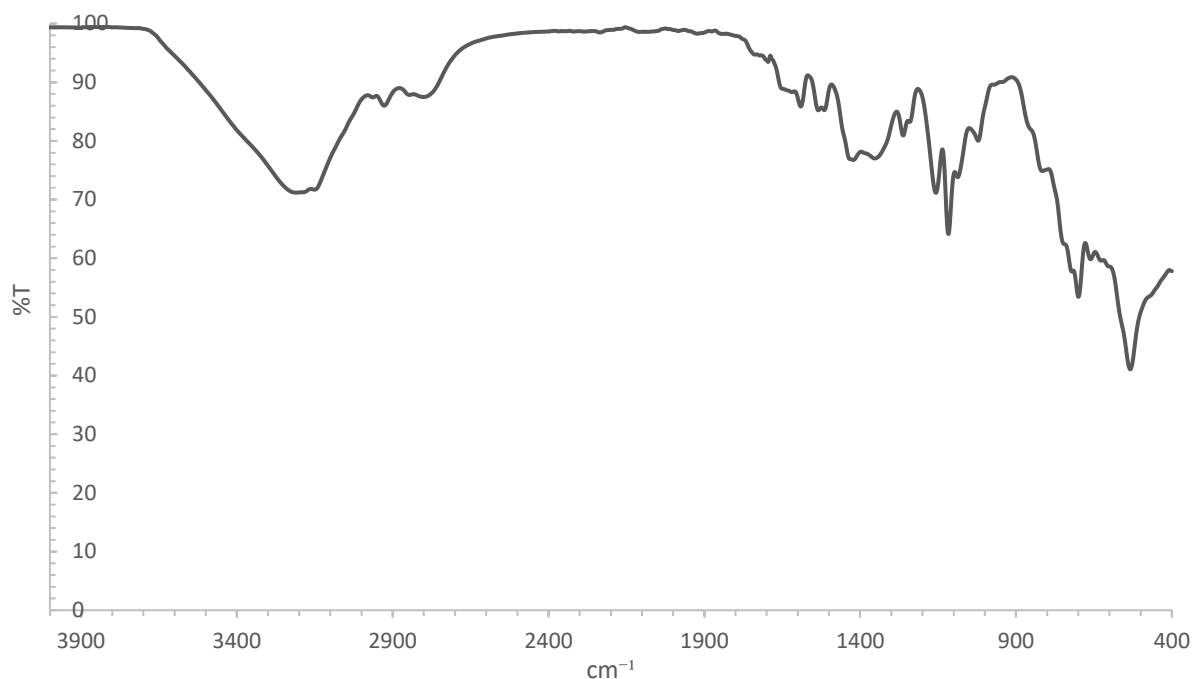
Figure 2.11: IR spectrum of RuNP@(O)PPh$_2$-PIILP (**2.21**).

SEM analysis of the freshly prepared RuNPs exhibited a notable difference in the surface morphology against the parent polymers (Figure 2.12). In this instance, the RuNP materials have a more granular texture, which is potentially due to the additional processing steps during the impregnation and reduction of RuCl$_3$ with the polymer materials.
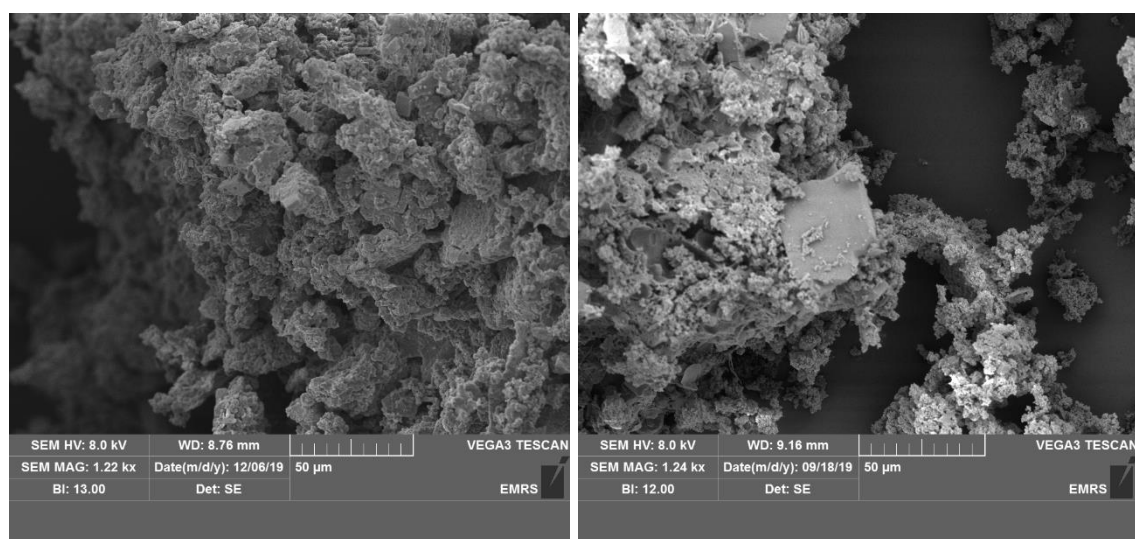
Figure 2.12: SEM images of RuNP@(O)PPh$_2$-PEGPIIL (**2.20**) (left) and RuNP@(O)PPh$_2$-PIIL (**2.21**) (right).

The ruthenium content of the catalyst was determined using ICP-OES analysis and the values are listed in Table 2.1. Surprisingly, the PIILP-support was more efficient (4.7 Ru wt%) at up-taking Ru than all of the other PIIL-based supports (entry 4).

Table 2.1: Ruthenium content of PIILP catalysts **2.14**-**2.23** determined by ICP-OES.

Entry	Catalyst	mmol Ru/ g PIILP	Ru wt%
1	RuNP@PPh$_2$PEGPIILP (2.14)	0.44	4.48
2	RuNP@PPh$_2$PIILP (2.15)	0.28	2.88
3	RuNP@PEGPIILP (2.16)	0.28	2.82
4	RuNP@PIILP (2.17)	0.47	4.70
5	RuNP@(O)PPh$_2$PEGPIILP (2.20)	0.39	3.97
6	RuNP@(O)PPh$_2$PIILP (2.21)	0.36	3.61
7	RuCOD@PPh$_2$PEGPIILP (2.22)	0.44	4.70
8	RuCOD@PPh$_2$PIILP (2.23)	0.28	2.88

XPS analysis of the isolated RuNPs was carried out by Professor Chris Hardacre (Manchester University) in an attempt to elucidate the nature of the NP's stabilising layer. XPS analysis of RuNP@(O)PPh$_2$PEGPIILP (**2.20**) revealed the presence of Ru, phosphorus, carbon and nitrogen, which indicated the presence of the IL in the RuNPs ligand sphere (Figure 2.13). Deconvolution of the Ru 3d XPS spectra for **2.14** and **2.20** showed the presence of an overlapping 3d$_{5/2}$ band with binding energies of 280 eV and 281.5 eV, in agreement with reduced Ru, in the form of a Ru(0)[77a] and a Ru(II) species,[77b] respectively (Figure 2.13). The Ru 3p region contained a doublet with binding energies of 462 eV and 485 eV, for Ru 3p$_{3/2}$ and Ru 3p$_{1/2}$, respectively, which is also in keeping with a mixture of Ru(0) and Ru(II) (Figure 2.13).[77c] Moreover, the P 2p region of **2.15** and **2.14** showed the presence of P(V), as the major species, in addition to a minor amount of a P(III) component; the former appeared in the spectrum as a broad peak at 132 eV as a result of overlapping 3p$_{3/2}$ and 3p$_{1/2}$ bands corresponding to the phosphine oxide while the latter peak appeared at 128 eV which corresponds to the phosphine (Appendix F).[77d] As anticipated, the band at 128 eV was not present in the XPS spectra for **2.20** and **2.21** as these catalysts were formed from

the pre-oxidised polymers **2.18** and **2.19**, respectively. The O 1s XPS region of the spectrum of **2.15** contained a peak at 528 eV which is characteristic of the PEG-based oxygen atoms in addition to a lower energy peak at 532 eV which was due to the O^{2-} in the phosphine oxide;[77e] this latter peak was not present in the XPS spectrum of **2.16** as it does not contain any phosphine (Appendix F).
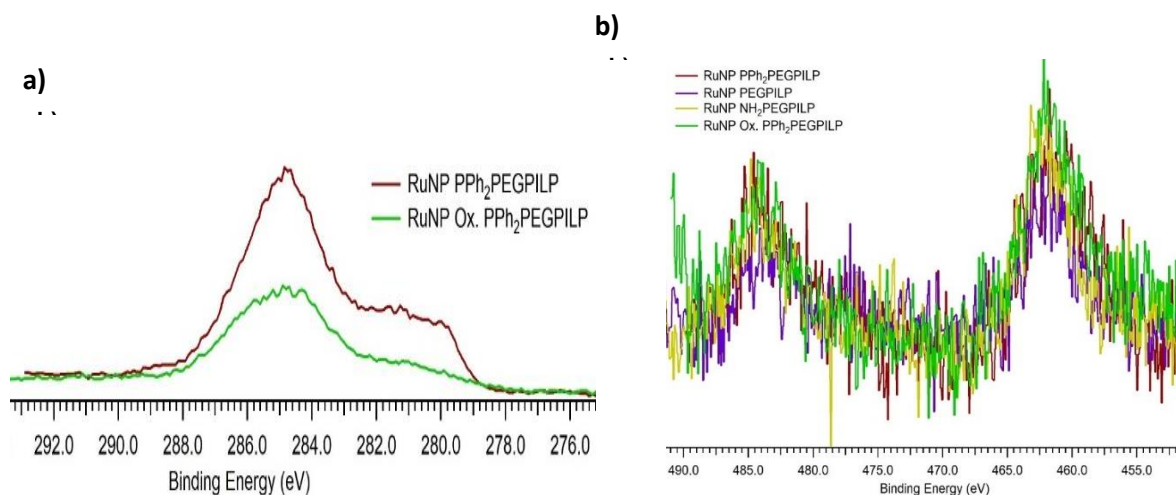
Figure 2.13: XPS spectra of a) Ru 3d of **2.14** and **2.20**, and b) Ru 3p of **2.14**, **2.16** and **2.20**.

TEM analysis was carried out by Dr Tom Chamberlain (Leeds University) to characterise the isolated RuNPs and to determine their mean diameters. TEM micrographs of **2.20** and **2.21** revealed that the RuNPs are near monodisperse with average diameters of 1.32 ± 0.30 nm and 1.54 ± 0.37 nm, respectively. The representative micrographs and their associated distribution histograms based on >100 particles are shown in Figure 2.14. In comparison, RuNPs stabilised by phosphine-functionalised IL systems generated by the hydrogenation of RuO_2 have slightly bigger average mean diameters of 2.2 nm.[49] In a similar fashion, IL-stabilised RuNPs generated by the hydrogenation of Ru(COD)(COT) or Ru(allyl)$_2$(COD) also have larger average diameters of 3.5 nm and 2.7 ± 0.2 nm, respectively.[59]
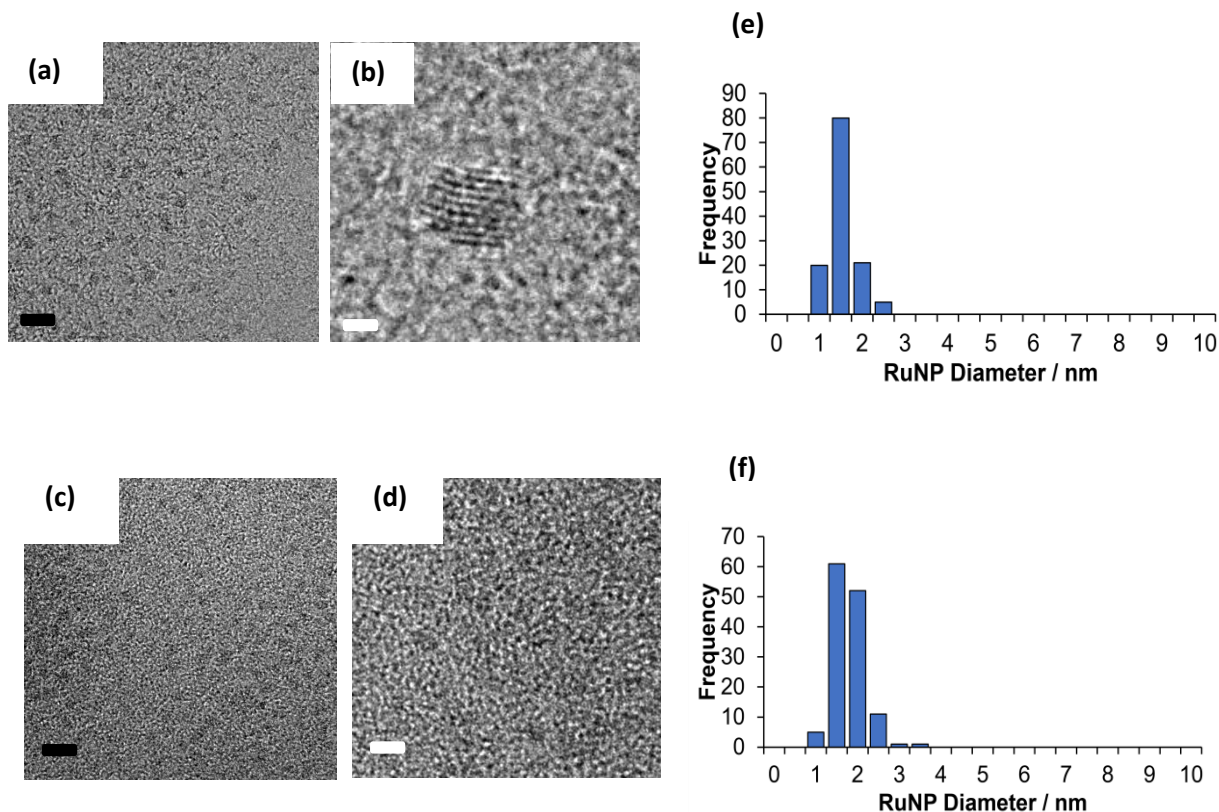
Figure 2.14: HRTEM images of (a-b) **2.20**, (c-d) **2.21**, (e-f) corresponding to the size distributions determined by counting >100 particles. Mean particle diameters are 1.32 ± 0.30 nm (**2.20**) and 1.54 ± 0.37 nm (**2.21**). Black and white scale bars are 25 and 1 nm, respectively.

2.3.4 Comparative catalyst testing

For biomass valorisation, two chemical transformations of biomass need to be considered; selective hydrogenation of the aromatic and the carbonyl functionalities, hence the aqueous phase hydrogenation of acetophenone was deemed to be an appropriate benchmark reaction for our preliminary catalyst optimisation studies. As such, there have been numerous reports of the RuNP catalysed selective hydrogenation of model ketones. In one example, Chaudret and co-workers presented a significant ligand effect of amine- and thiol-stabilised RuNPs with a relationship between the catalyst activity and the basicity of the ligand stabiliser.[50] Their experimental findings showed that the hydrogenation of the isolated ketone was evidently more thermodynamically accessible than the reduction of the aryl ring. Despite that, in the case of acetophenone, where the arene and the ketone are directly bonded, the selectivity for C=O hydrogenation was significantly lower, owing to the

increased likelihood of both the phenyl ring and the ketone simultaneously coordinating to the RuNPs surface.

The possible products from the hydrogenation of acetophenone are shown in Scheme 2.8. Selective hydrogenation of the carbonyl group of acetophenone (**A**) forms 1-phenylethanol (**B**) whilst the selective hydrogenation of the aryl ring generates 1-cyclohexylethan-1-one (**C**). Lastly, these two intermediates can be hydrogenated further, which results in the fully reduced product, cyclohexylethanol (**D**). Preliminary catalyst screening will focus on the selective hydrogenation of the carbonyl group to produce 1-phenylethanol (**B**).
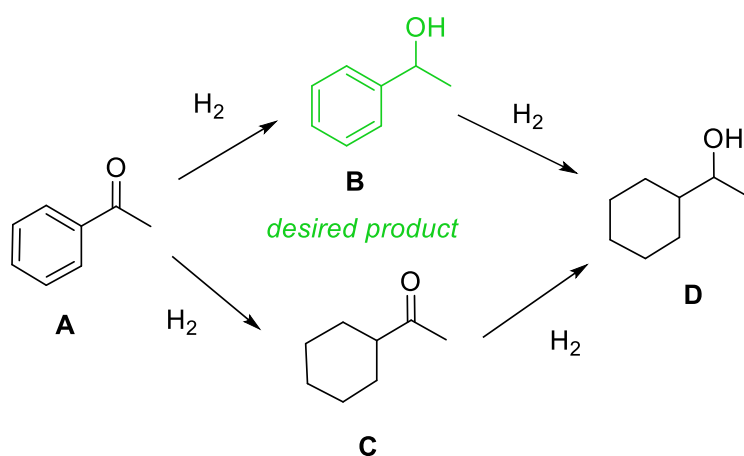
Scheme 2.8: Schematic representation of the hydrogenation of acetophenone and the possible products.

2.4 Reaction optimisation

The screening of the catalysts was carried out in a 50 mL temperature-controlled Parr benchtop reactor. In a standard procedure, a glass insert was charged with 0.1 mol% catalyst (based on the Ru content calculated from ICP-OES analysis), 1 mmol of acetophenone and 12 mL of the stated solvent. The reactor was then pressurised with 70 psi of hydrogen, the gas released and the process repeated six times to ensure complete removal of air. The reactor was finally pressurised to the desired pressure and heated at the stated temperature for the allotted time. The degree of conversion and selectivity was determined by analysing the resultant reaction mixture by ^{1}H NMR spectroscopy using 1,3-dinitrobenzene as an internal standard.

2.4.1 Solvent screen

A range of solvents was screened to establish the optimum performance of the system which ideally would also exhibit green credentials. **2.20** (RuNP@(O)PPh$_2$-PEGPIILP) was chosen as the catalyst to be optimised due to the promising findings that were previously found from the research group for the PPh$_2$-PEGPIILP supported nanoparticles.[42,43] Preliminary solvent screening revealed **2.20** to be the most efficient in a 1:1 ethanol/water mixture as 66% conversion with 95% selectivity for 1-phenyl ethanol (**B**) was obtained after 3 h at 50 °C. This may well be due to the promotional effect of the water as it is well documented in the literature that mixed alcohol/water systems can significantly enhance the selectivity of a reaction.[78] The solubility of H$_2$ in organic solvents is much higher than in water. Across all of the tested solvents (Figure 2.15), **B** remained the major product and only a minor amount of **D** was observed as the only other product. Reactions performed in neat ethanol, 2-methyl THF and toluene resulted in a minor increase in the selectivity to **B**, although, this is probably due to the low availability of **B**, to further hydrogenate, as the conversions were substantially lower in all of these cases.
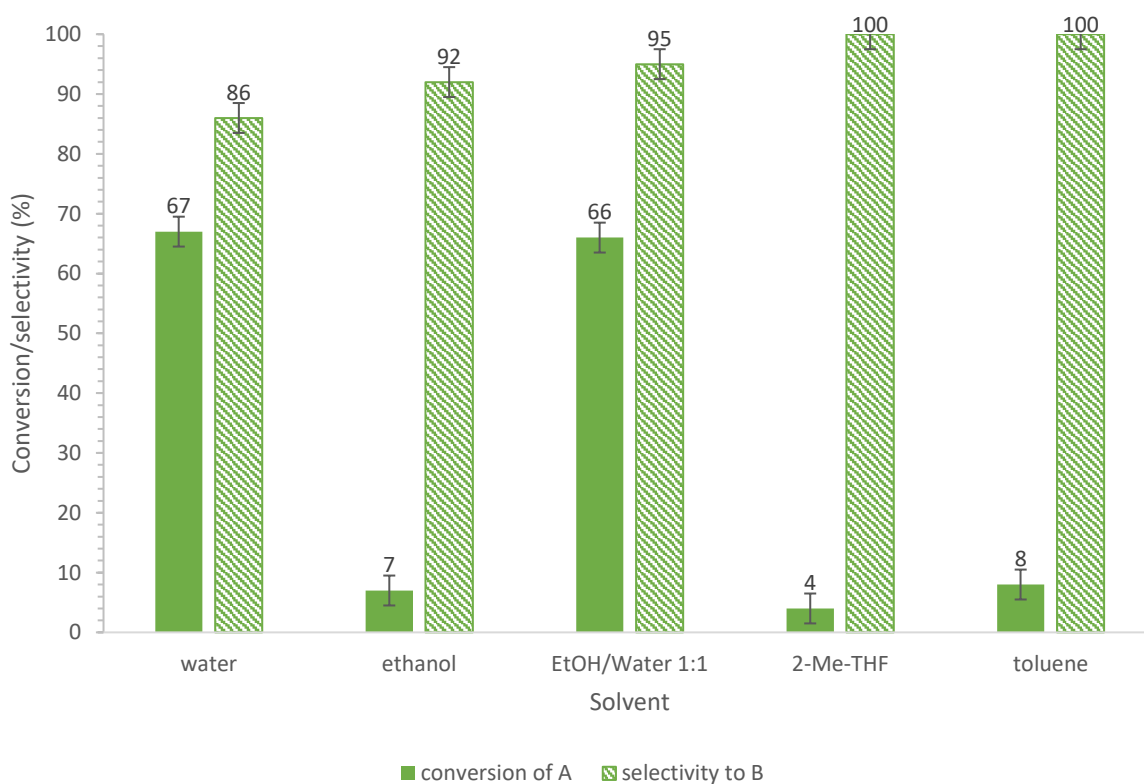
Figure 2.15: Conversion and selectivity for the hydrogenation of acetophenone (**A**) as a function of solvent. Reaction conditions: 1 mmol acetophenone, 0.1 mol%

RuNP@(O)PPh$_2$PEGPIILP (**2.20**), 70 psi H$_2$, 50 °C, 12 mL solvent, reaction time = 3 hours. Conversion and selectivity determined by ^{1}H NMR spectroscopy with 1,3-dinitrobenzene as the internal standard. Selectivity for 1-phenylethanol (**B**) = [% 1-phenylethanol / (% 1-phenylethanol + % cyclohexylethanol)].

A further ethanol: water composition study on the catalyst's performance revealed the optimum composition to be 1:1, as the conversion of **A** dramatically dropped with increasing amounts of ethanol content (Table 2.2).

Table 2.2: Optimisation of the solvent's water content for the hydrogenation of acetophenone (**A**).

Entry[a]	EtOH: H$_2$O	Conversion (%)[b]	Selectivity to B (%)[b]
1	100: 0	7	92
2	75: 25	23	93
3	50: 50	66	95
4	25: 75	66	92
5	0: 100	67	86

[a]Reaction conditions: 1 mmol acetophenone, 0.1 mol% RuNP@(O)PPh$_2$PEGPIILP (**2.20**), 70 psi H$_2$, 50 °C, 12 mL solvent, reaction time = 3 hours. [b]Conversion and selectivity determined by ^{1}H NMR spectroscopy with 1,3-dinitrobenzene as the internal standard. Selectivity for 1-phenylethanol (**B**) = [% 1-phenylethanol / (% 1-phenylethanol + % cyclohexylethanol)].

Although a purely ethanol system resulted in an extremely poor conversion of **A** (entry 1) it is clear that the presence of ethanol in the mixed solvent systems had a positive effect on the catalyst performance (entry 3-4). Even though reactions conducted in pure water resulted in a good conversion of **A** of 67%, the selectivity was lower at 86% (entry 5). With a 25:75 ratio of EtOH: H$_2$O, an increase in the selectivity to **B** to 92% was achieved (entry 4). A further increase in the selectivity to **B** to 95% was achieved in the 1:1 mixture (entry 3), hence a 1:1 EtOH: H$_2$O mixture was considered to be the optimum ratio for further catalyst optimisation studies.

2.4.2 Base additive optimisation

Previous literature reports on RuNP catalysed hydrogenation of ketones have shown strong evidence that the addition of a base can enhance the selectivity.[51] For instance, a low conversion for the hydrogenation of acetophenone was obtained with RuNPs embedded in a siloxane matrix without any base, whilst the PFIL stabilised RuNPs were completely inactive without a base, however, a 77% conversion of acetophenone with 99% selectivity to 1-phenylethanol was achieved with 1-butyl-2,3-dimethylimidazolium hydroxide.[60] In this regard, the effect on selectivity of the hydrogenation of acetophenone as a function of various inorganic bases was examined (Figure 2.16).
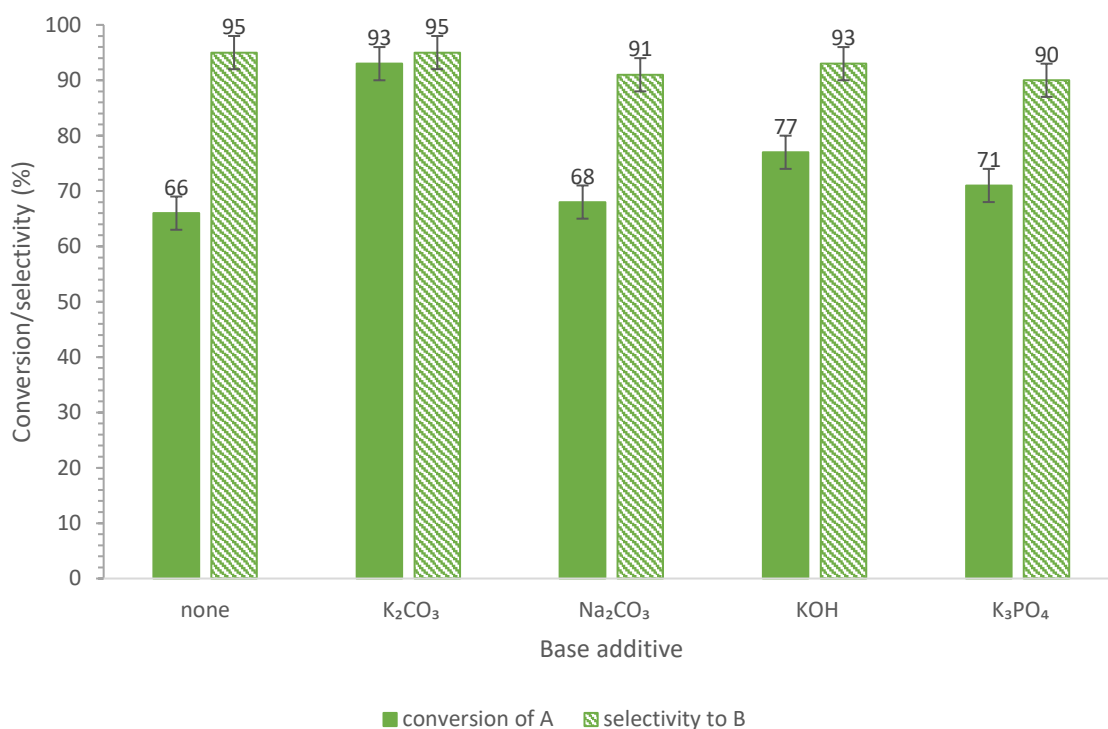
Figure 2.16: Conversion and selectivity for the hydrogenation of acetophenone (**A**) as a function of base. Reaction conditions: 1 mmol acetophenone, 0.1 mol% RuNP@(O)PPh$_2$PEGPIILP (**2.20**), 10 mol% specified base, 70 psi H$_2$, 50 ℃, 12 mL 1:1 EtOH: water, reaction time = 3 hours. Conversion and selectivity determined by ^{1}H NMR spectroscopy with 1,3-dinitrobenzene as the internal standard. Selectivity for 1-phenylethanol (**B**) = [% 1-phenylethanol / (% 1-phenylethanol + % cyclohexylethanol)].

Introducing different bases to the reaction led to a marked improvement in the performance of **2.20** as a catalyst for the selective hydrogenation of the carbonyl in

acetophenone. The highest conversion of **A** was obtained with potassium carbonate, which gave a 95% conversion with 96% selectivity for **B**, compared with 66% conversion and the same selectivity without base. Similarly, an improvement in the conversion of **A** was also obtained with other bases such as sodium carbonate, potassium hydroxide and tripotassium phosphate, however these were all less than that obtained with potassium carbonate.

Consequently, the base serves as an electronic promoter and allows a different mechanism for the activation and/or adsorption of hydrogen onto the Ru surface.[8] K_2CO_3 was deemed the best base for further studies as it is cheap, environmentally benign and readily available. To determine the optimum substrate: base ratio, several parallel reactions were performed as a function of the mole equivalents of K_2CO_3, the result of which is shown in Figure 2.17.
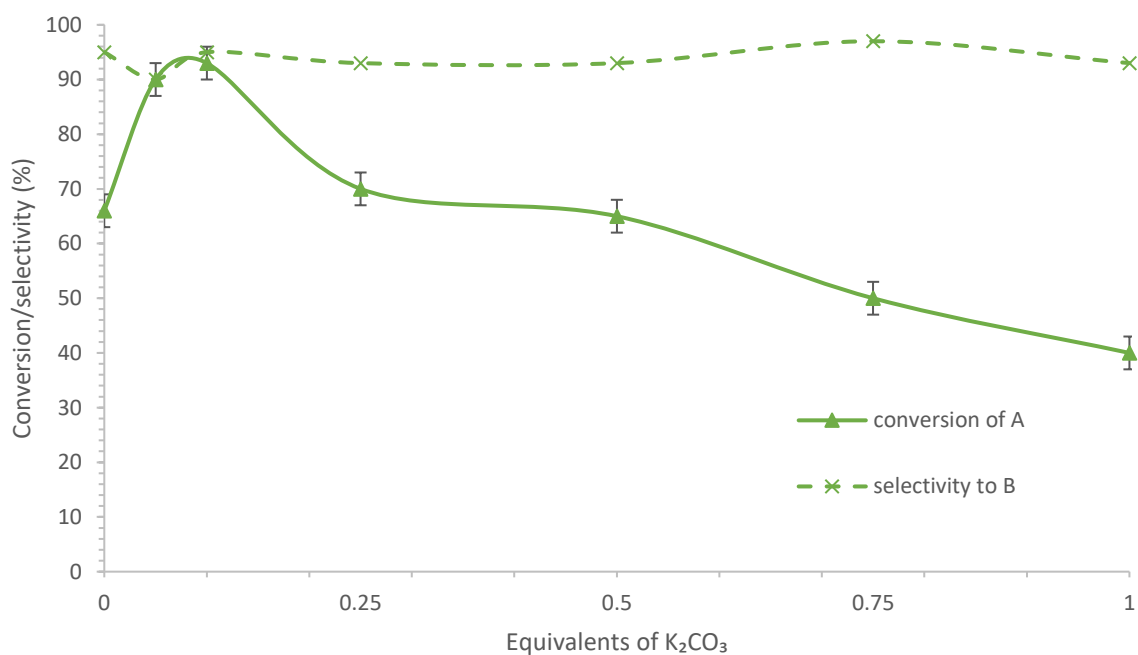
Figure 2.17: Conversion and selectivity for the hydrogenation of acetophenone catalysed by **2.20** in the presence of varying amounts of K_2CO_3. Reaction conditions: 1 mmol acetophenone, 0.1 mol% RuNP@(O)PPh2PEGPIILP (**2.20**), K_2CO_3 (specified amount), 70 psi H_2, 50 ℃, 12 mL 1:1 EtOH: water, reaction time = 3 hours. Conversion and selectivity determined by ^{1}H NMR spectroscopy with 1,3-dinitrobenzene as the internal standard. Selectivity for 1-phenylethanol (**B**) = [% 1-phenylethanol / (% 1-phenylethanol + % cyclohexylethanol)].

The profile in Figure 2.17 clearly reveals that only catalytic amounts of base are required to obtain the optimum performance. The addition of 5 mol% (0.05 equiv.) K_2CO_3 led to a significant increase in activity by 26%, however, this was accompanied by a slight drop in the selectivity of 6%. The conversion of **A** peaked in the presence of 10 mol% K_2CO_3, which resulted in a 29% increase in the conversion with 95% selectivity to **B**. Despite the high selectivities, a sharp drop in conversion occurred when the amount of K_2CO_3 was greater than 10 mol%, suggesting that high base concentrations are detrimental to catalysis. The equivalents of base additive-composition profile proved that the optimum conversion of **A** and selectivity to **B** was obtained with only 10 mol% K_2CO_3 and this amount was used for all further optimisation studies.

2.4.3 Effect of pressure

The consumption of acetophenone was then monitored as a function of pressure (Figure 2.18). To avoid the full conversion of the acetophenone at high pressures, the reaction time was reduced to 1 hour.
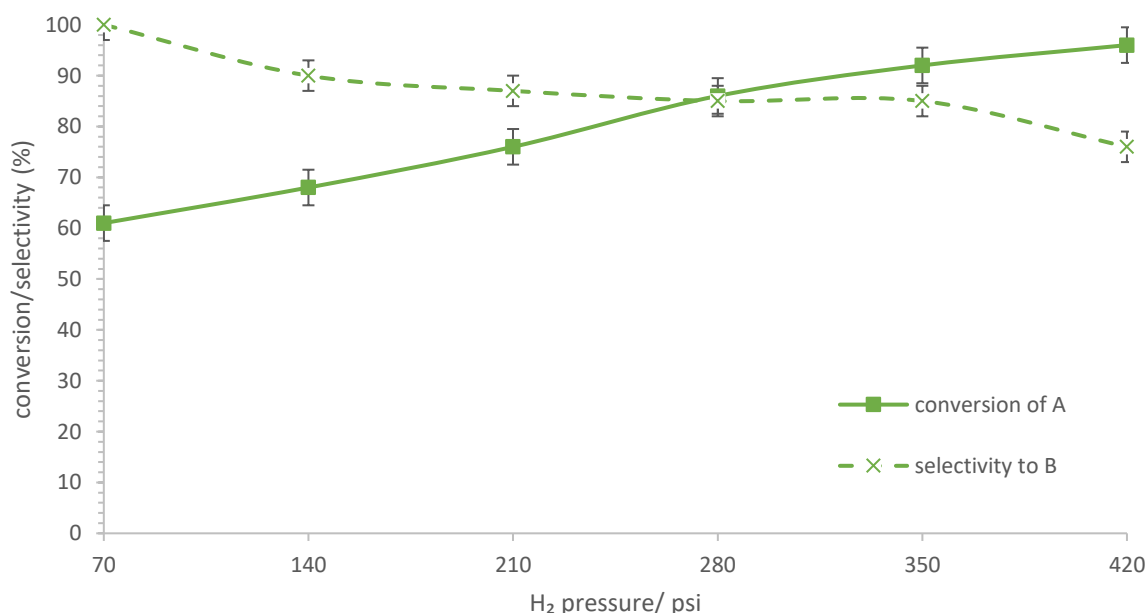
Figure 2.18: Conversion and selectivity for the hydrogenation of acetophenone as a function of hydrogen pressure. Reaction conditions: 1 mmol acetophenone, 0.1 mol% RuNP@(O)PPh$_2$PEGPIILP (**2.20**), 0.1 mmol K_2CO_3, H_2 (specified amount), 50 ℃, 12

mL 1:1 EtOH: water, reaction time = 1 hour. Conversion and selectivity determined by ^{1}H NMR spectroscopy with 1,3-dinitrobenzene as the internal standard. Selectivity for 1-phenylethanol (**B**) = [% 1-phenylethanol / (% 1-phenylethanol + % cyclohexylethanol)].

The pressure-composition profile suggests that mass transfer limited hydrogen dissolution occurred in the 1:1 ethanol/water system as the conversion of **A** gradually increased with an increase in the hydrogen pressure eventually reaching a plateau at 400 psi. However, the observed increase in the conversion of **A** occurred with a decrease in the selectivity for **B** due to hydrogenation of the aromatic ring to form **D**. Thus, although the catalyst activity peaked at higher hydrogen pressures, this is at the cost of the selectivity to **B**, which gradually dropped as the pressure increased. To examine whether the high selectivity to **B** at low pressures was achieved because of the low conversion of **A**, a set of batch reactions catalysed by **2.20** were carried out to compare the selectivities at similar conversions of **A** (85-94%) (Table 2.3).

Table 2.3: Effect of the hydrogen pressure on the selectivity for the **2.20** catalysed hydrogenation of acetophenone to 1-phenylethanol at high conversions of acetophenone.

Entry [a]	Pressure (psi)	Time (hours)	Conversion (%) [b]	Selectivity (%) [b]	TOF (h^{-1}) [c]
1	35	3.5	88	98	251
2	70	3	85	98	283
3	105	3	94	86	313
4	140	2.5	85	78	340
5	175	2.5	93	76	372
6	210	2	85	77	425

[a]Reaction conditions: 1 mmol acetophenone, 0.1 mol% RuNP@(O)PPh$_2$PEGPIILP (**2.20**), 0.1 mmol K$_2$CO$_3$, H$_2$ (specified amount), 50 ℃, 12 mL 1:1 EtOH: water. [b]Conversion and selectivity determined by ^{1}H NMR spectroscopy with 1,3-dinitrobenzene as the internal standard. Selectivity for 1-phenylethanol (**B**) = [% 1-

phenylethanol / (% 1-phenylethanol + % cyclohexylethanol)]. [c]TOF = moles of product per mole catalyst per hour based on total Ru content.

The results in Table 2.3 clearly showed that higher selectivities for **B** were achieved at the lower hydrogen pressures of 35, 70 and 105 psi (entries 1-3) which indicates that the hydrogenation of the aryl ring imposes a higher activation barrier than the ketone, rather than, as a result from the low conversion of **A**. As good conversions of **A** could be achieved at 50 ℃ under a hydrogen pressure as low as 70 psi after only 1 hour (Figure 2.18), all further studies were conducted at 70 psi and where necessary the reaction time was extended.

2.4.4 Temperature studies

The consumption of acetophenone was then monitored as a function of reaction temperature (Figure 2.19). To avoid the full conversion of **A** at high temperatures the reaction time was again reduced to 1 hour.
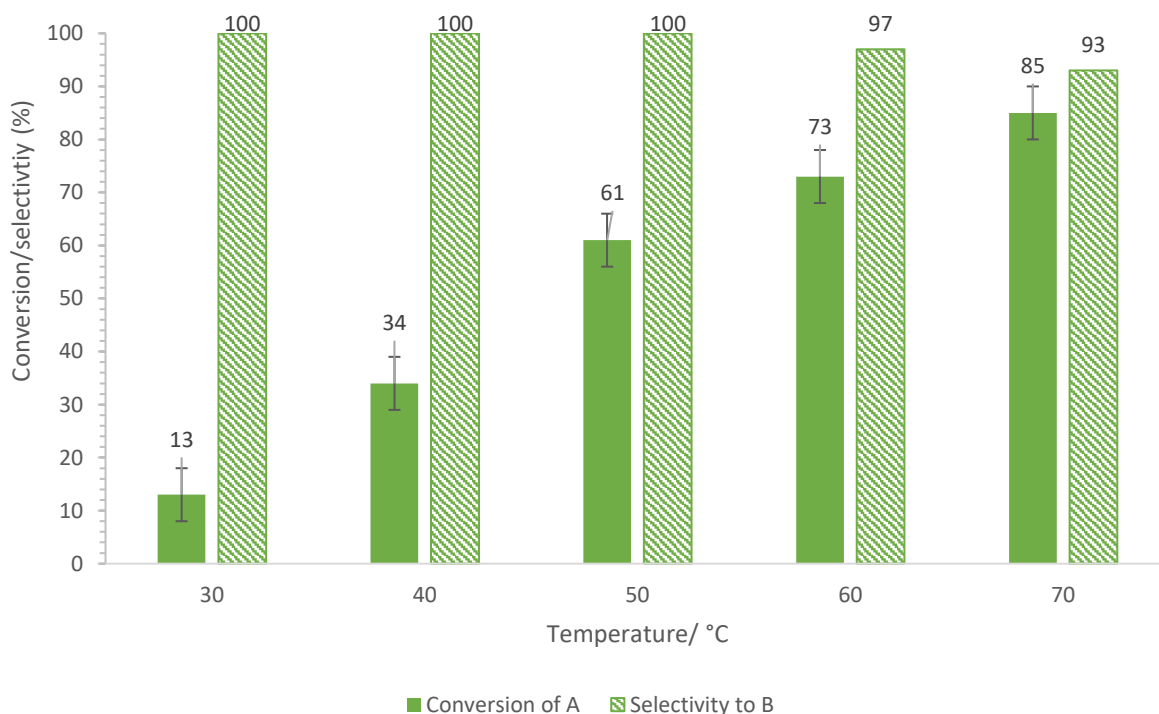
Figure 2.19: Conversion and selectivity for the hydrogenation of acetophenone as a function of temperature. Reaction conditions: 1 mmol substrate, 0.1 mol% RuNP@OPPh$_2$PEGPIILP (**2.20**), 0.1 mmol K$_2$CO$_3$, 70 psi H$_2$, temperature (specified),

12 mL 1:1 EtOH/water, reaction time = 1 hour. Conversion and selectivity determined by ^{1}H NMR spectroscopy with 1,3-dinitrobenzene as the internal standard. Selectivity for 1-phenylethanol (**B**) = [% 1-phenylethanol / (% 1-phenylethanol + % cyclohexylethanol)].

Low conversions of **A** were obtained at 30 and 40 ℃, respectively. Reactions carried out above 50 ℃, resulted in an increase in the conversion of **A**, however, the selectivity towards **B** dropped, which further indicates that hydrogenation of the aryl ring has a higher activation barrier than that of the ketone. At higher temperatures, the molecules possess enough energy to overcome this energy barrier and are subsequently transformed into **D**, and therefore, the selectivity to **B** decreased. As a reaction temperature of 50 ℃ exhibited the best balance between the conversion of **A** and the selectivity to **B** after 1 hour, this was taken as the optimum temperature for the remaining studies for the selective hydrogenation of aryl ketones.

2.4.5 Catalyst loading studies

The consumption of acetophenone was then monitored as a function of the catalyst loading (Figure 2.20). To avoid the full conversion of **A** at high catalyst loadings, the reaction time was again reduced to 1 hour.
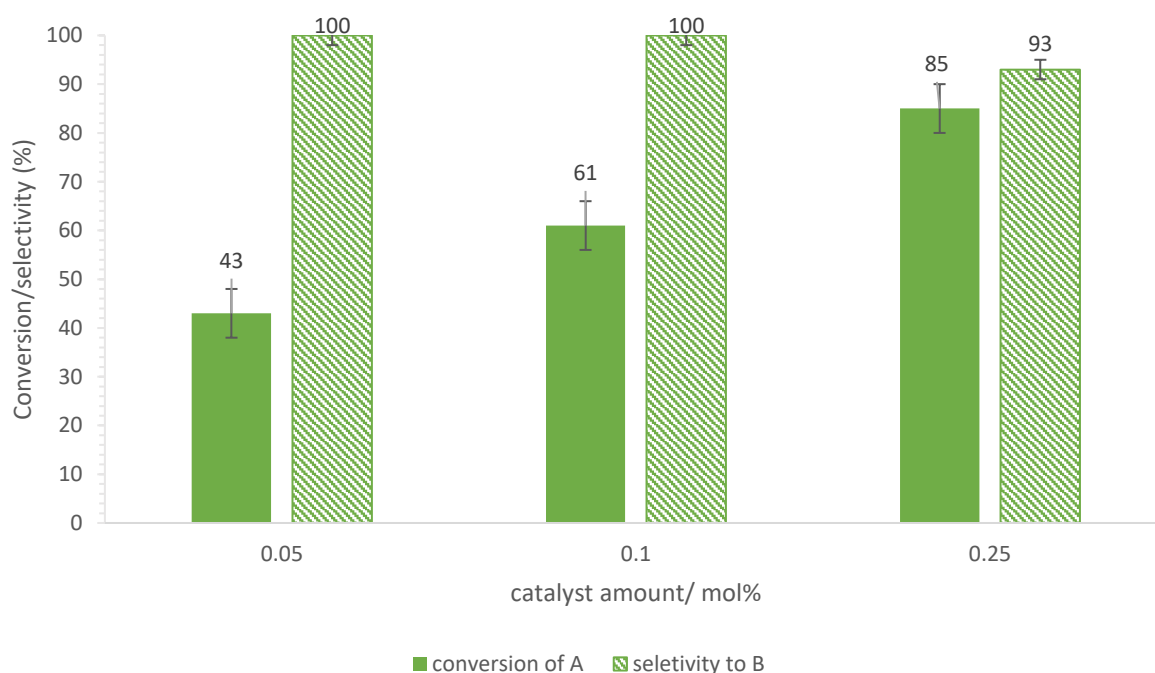
Figure 2.20: Conversion and selectivity for the hydrogenation of acetophenone as a function of the catalyst loading. Reaction conditions: 1 mmol substrate, RuNP@OPPh$_2$PEGPIILP (**2.20**) (specified amount), 0.1 mmol K$_2$CO$_3$, 50 ℃, 70 psi H$_2$, 12 mL 1:1 EtOH/water, reaction time = 1 hour. Conversion and selectivity determined by ^{1}H NMR spectroscopy with 1,3-dinitrobenzene as the internal standard. Selectivity for 1-phenylethanol (**B**) = [% 1-phenylethanol / (% 1-phenylethanol + % cyclohexylethanol)].

An increase in the catalyst loading from 0.1 mol% to 0.25 mol% resulted in an increase in the conversion of **A** from 61% to 85% however the selectivity towards **B** dropped from 100% to 93%, respectively. The catalyst activity improved with a reduction in the catalyst loading to 0.05 mol%, such that, a 43% conversion of **A** and 100% selectivity for **B** was achieved after only an hour which corresponded to a TOF of 860 h^{-1} (moles of product per mole of catalyst per hour). The catalyst loading was then reduced to 0.005 mol% to further test the efficacy of **2.20** which gave 47% conversion of **A** and 100% selectivity for **B** after 4 hours; this corresponds to a TOF of 2350 h^{-1} which is a more reasonable potential intrinsic turnover rate of the catalyst. Full conversion was achieved with 96% selectivity for **B** by extending the reaction time to 15 hours using a catalyst loading of 0.01 mol%. A catalyst loading of 0.1 mol% was used for further catalyst and substrate screening to achieve high conversions and selectivities within reasonable timescales.

2.4.6 Composition-time profile

To gain a more in-depth insight into the hydrogenation of acetophenone, the consumption of acetophenone was monitored as a function time by sampling under the reaction conditions (Figure 2.21). Each time-composition reading was conducted in a new batch reaction.
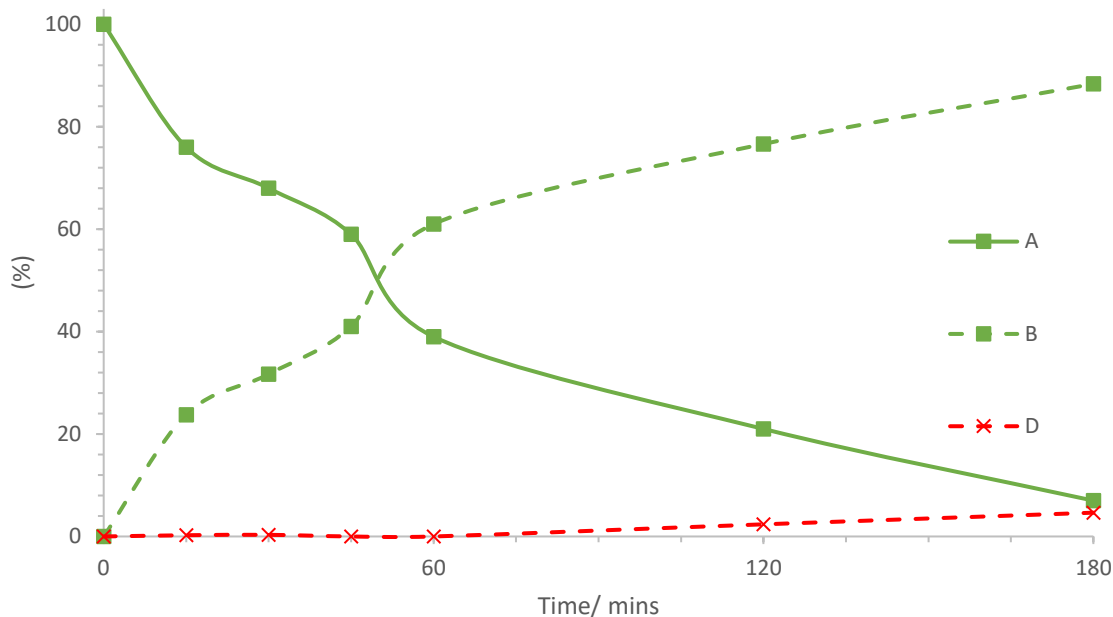
Figure 2.21: Monitoring of the catalytic hydrogenation of acetophenone as a function of time. Reaction conditions: 1 mmol acetophenone, 0.1 mol% RuNP@OPPh$_2$PEGPIILP (**2.20**), 0.1 mmol K$_2$CO$_3$, 70 psi H$_2$, 50 ℃, 12 mL 1:1 EtOH/water, reaction time = 3 hour. Conversion and selectivity determined by ^{1}H NMR spectroscopy with 1,3-dinitrobenzene as the internal standard. Selectivity for 1-phenylethanol (**B**) = [% 1-phenylethanol / (% 1-phenylethanol + % cyclohexylethanol)].

The differentiation of the functional groups reactivity was observed in the hydrogenation of **A**. **B** was formed at a faster rate than **D**, indicating that the reactivity of the carbonyl group is higher than that of the aromatic ring. This was consistent with the observations made by Arai *et al.*, who observed a similar reactivity mechanism when they monitored the hydrogenation of acetophenone.[75] At first, the C=O double bond of acetophenone was hydrogenated, followed by the very slow hydrogenation of the aromatic ring. This distinct chemoselectivity of **2.20** in the hydrogenation of the carbonyl group allows **B** to be selectivity obtained as the main product of the reaction.

2.4.7 Catalyst comparison

A series of batch reactions were then carried out under the conditions established above to compare the performance of phosphine-based, PEG-based and unmodified PIILP support catalysts and commercially available Ru/C.
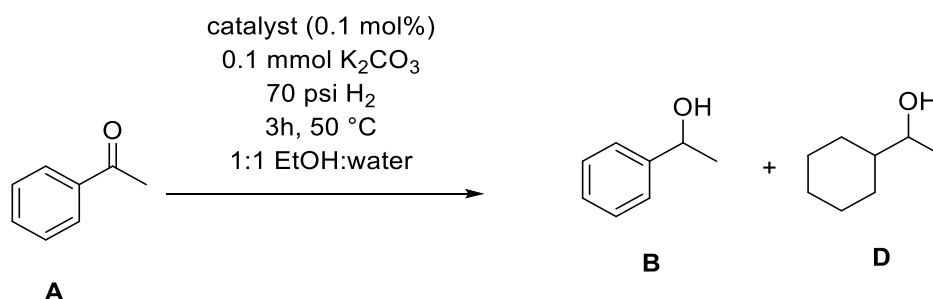
Table 2.4: Comparison of the catalytic performance for the Ru catalysed hydrogenation of acetophenone to 1-phenylethanol.

Entry [a]	Catalyst	Conversion (%) [b]	Selectivity (%) [b]
1	Ru/C	65	81
2	RuNP@PPh$_2$-PEGPIILP (2.14)	89	92
3	RuNP@PPh$_2$PIILP (2.15)	81	90
4	RuNP@PEGPIILP (2.16)	90	83
5	RuNP@PIILP (2.17)	91	84
6	RuNP@O=PPh$_2$-PEGPIILP (2.20)	93	95
7	RuNP@O=PPh$_2$-PIILP (2.21)	91	93
8	RuCOD@PPh$_2$-PEGPIILP (2.22)	85	93
9	RuCOD@PPh$_2$-PIILP (2.23)	75	91

[a]Reaction conditions: 1 mmol acetophenone, 0.1 mol% catalyst, 0.1 mmol K$_2$CO$_3$, 12 mL 1:1 EtOH: water, 50 ℃, 70 psi H$_2$, reaction time = 3 hours. [b]Conversion and selectivity determined by ^{1}H NMR spectroscopy. Selectivity for 1-phenylethanol (**B**) = [% 1-phenylethanol / (% 1-phenylethanol + % cyclohexylethanol)].
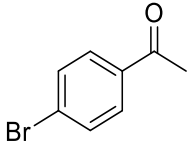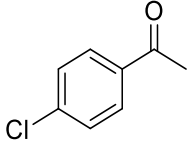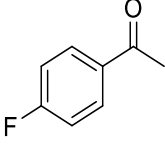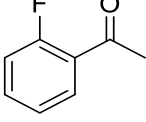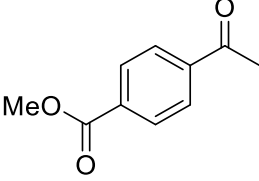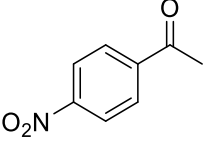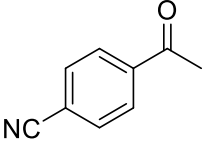
An improvement in the catalyst performance was observed for all of the PIILP-based catalysts against the commercially available Ru/C (Table 2.4, entry 1). Since the nature of the metal precursor strongly influences the particle size and dispersion
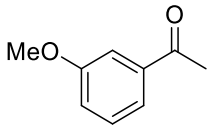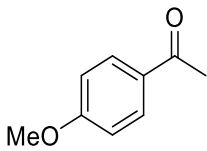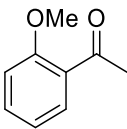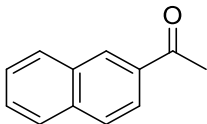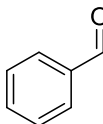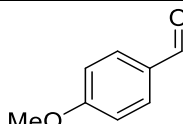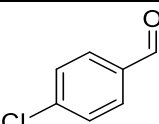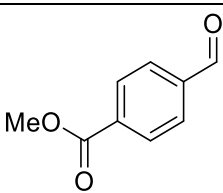
of the NP, catalysts generated from RuCl$_3$•xH$_2$O and [Ru(COD)(COT)], were tested. In general, the RuNPs **2.20** and **2.21**, prepared from RuCl$_3$•xH$_2$O, exhibited higher activities than **2.22** and **2.23**, which were prepared from [Ru(COD)(COT)] (entries 6-7 *versus* 8-9). The results presented in Table 2.4 demonstrated that PIILs can significantly enhance the catalyst performance by up to 28% and even **2.17** gave a 26% improvement in the conversion of **A** compared to Ru/C. The phosphine oxide-modified PIIL supports (entries 2, 3 and 6-9) provided both an improvement in the catalyst activity and the selectivity to **B**, this indicates that the heteroatom donor appears to be necessary in order to obtain a high selectivity to the hydrogenation of the ketone. The best chemoselectivity for the hydrogenation of **A** to **B** was achieved using RuNP **2.20** as the catalyst. Previous literature reports on metal NP catalysed hydrogenation of α,β-unsaturated ketones have shown substantial evidence that phosphine-functionalised ILs (PFILs) compared to unfunctionalised ILs can enhance the selectivity of this reaction. For example, a marked enhancement in chemoselectivity for the hydrogenation of the carbonyl in α,β-unsaturated aldehydes was obtained with AuNPs stabilised by a secondary phosphine oxide[61] and PtNPs stabilised on triphenylphosphine-modified silica revealed a significantly higher chemoselectivity in the hydrogenation of acetophenone than its unmodified counterpart; this was attributed to the σ-donor phosphine which increased the NP's surface electron density.[62]
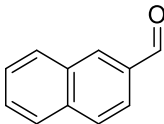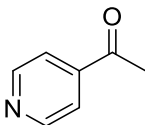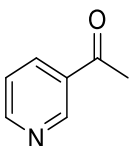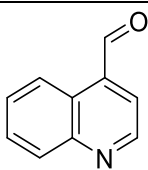
2.4.8 Substrate scope

After the optimum reaction conditions were established and a promising conversion profile for the benchmark hydrogenation of acetophenone obtained (Figure 2.21), a series of comparative catalyst testing was extended and carried out to include a wide range of substituted aromatic ketones and aldehydes to examine the efficacy and the scope of catalyst **2.20** (Table 2.5).

Table 2.5: Selective C=O hydrogenation of aromatic and heteroaromatic ketones and aldehydes catalysed by PIILP-supported RuNPs.

Entry[a]	Substrate	Catalyst (RuNP@X)	Time (hours)	Conversion (%)[b]	Selectivity (%)[b]
1	4-Br-acetophenone	2.16	4	27	33
		2.17	4	16	29
		2.20	4	63	37
		2.21	4	51	31
2	4-Cl-acetophenone	2.16	4	43	73
		2.17	4	36	70
		2.20	4	73	79
		2.21	4	51	77
3	4-F-acetophenone	2.16	4	49	97
		2.17	4	42	95
		2.20	4	95	100
		2.21	4	55	97
4	2-F-acetophenone	2.16	4	66	94
		2.17	4	40	93
		2.20	4	99	98
		2.21	4	70	94
5	methyl 4-acetylbenzoate	2.16	4	18	90
		2.17	4	18	88
		2.20	4	70	98
		2.21	4	42	94
6	4-NO2-acetophenone	2.16	3	43	98 [c]
		2.17	3	31	97 [c]
		2.20	3	65	100 [c]
		2.21	3	52	98 [c]
7	4-NC-acetophenone	2.16	4	0	0
		2.17	4	0	0
		2.20	4	0	0
		2.21	4	0	0

8		2.16	4	36	97
		2.17	4	30	88
		2.20	4	94	100
		2.21	4	68	98
9		2.16	4	39	97
		2.17	4	32	98
		2.20	4	97	88
		2.21	4	72	97
10		2.16	4	30	95
		2.17	4	30	94
		2.20	4	82	100
		2.21	4	63	97
11		2.16	24	85	100
		2.17	24	71	100
		2.20	24	95	100
		2.21	24	91	100
12		2.16	2	84	100
		2.17	2	74	100
		2.20	2	97	100
		2.21	2	96	100
13		2.16	6	61	100
		2.17	6	62	100
		2.20	6	90	100
		2.21	6	62	100
14		2.16	2	11	100
		2.17	2	15	100
		2.20	2	80	100
		2.21	2	59	100
15		2.16	3	60	100
		2.17	3	51	100
		2.20	3	73	100
		2.21	3	66	100

		Catalyst	Time (h)	Conversion	Selectivity
16		**2.16**	8	82	100
		2.17	8	75	100
		2.20	8	89	100
		2.21	8	86	100
17		**2.16**	4	35	100
		2.17	4	16	100
		2.20	4	97	100
		2.21	4	68	100
18		**2.16**	4	41	100
		2.17	4	29	100
		2.20	4	95	100
		2.21	4	70	100
19		**2.16**	8	69	100
		2.17	8	55	100
		2.20	8	89	100
		2.21	8	77	100

[a]Reaction conditions: 1 mmol substrate, 0.1 mol% catalyst, 0.1 mmol K_2CO_3, 12 mL 1:1 EtOH: water, 50 °C, 70 psi H_2, reaction time (specified). [b]Conversion and selectivity determined by ^{1}H NMR spectroscopy with 1,3-dinitrobenzene as the internal standard. [c]Selectivity for 4-aminoacetophenone. Selectivity for corresponding aromatic alcohol = [% corresponding aromatic alcohol / (% corresponding aromatic alcohol + % cyclohexylethanol)].

For all catalysts tested, poor selectivity to the aromatic alcohol was observed for the hydrogenation of 4-bromoacetophenone as a result of hydrodehalogenation to give acetophenone. The reaction catalysed by **2.20** after 4 hours occurred with 63% conversion to give a mixture of 1-(4-bromophenyl)ethan-1-ol, acetophenone and 1-phenylethanol. Similarly, all of the other tested catalysts gave comparable product distributions. At present, it is suggested that the hydrogenation to 1-phenylethanol is formed by the hydrogenation of acetophenone generated by the hydrodehalogenation of 4-bromoacetophenone as well as hydrodehalogenation of 1-(4-bromophenyl)ethan-1-ol, based on the hydrogenation of a commercial sample, which gave a 69%

conversion to 1-phenylethanol under the same reaction conditions. The hydrogenation of 4-chloroacetophenone catalysed by **2.20** (entry 2) gave the corresponding aromatic alcohol with 79% selectivity due to competing hydrodechlorination. The degree of dehalogenation was notably less than that for 4-bromoacetophenone, as the C-Cl is stronger than the C-Br bond, due to the better overlap of the atomic orbitals. Surprisingly, no dehalogenation products were observed for the hydrogenation of 4-fluoroacetophenone (entry 3), due to the stronger carbon-halogen bond, and 100 % selectivity for 1-(4-fluorophenyl)ethanol was obtained with **2.20**. Similarly, the hydrogenation of 2-fluoroacetophenone catalysed by **2.20** under the same reaction conditions (entry 4) gave near-quantitative conversion and 98% selectivity to the corresponding aromatic alcohol, which implies that *ortho*-substitution does not deactivate the carbonyl group. O*rtho-* substitution can be detrimental to catalysis as a result of the steric effects, however, no negative effect was caused by the fluorine atom, possibly due to its small size.

Hydrogenation of more challenging methyl 4-acetylbenzoate (entry 5) only achieved a conversion of 70% using **2.20** with 98% selectivity to methyl 4-(1-hydroxyethyl)benzoate and trace amounts of the corresponding substituted cyclohexylethanol. The high selectivity is associated with the low concentration of the partially reduced product. Interestingly, the hydrogenation of 4-nitroacetophenone (entry 6) proceeded with chemoselective reduction of the nitro group after 3 hours with 65% conversion to 4-aminoacetophenone as the sole product. However, when the reaction time was extended to 4 hours, complete conversion of 4-nitroacetophenone was achieved but the selectivity dropped to 86% as a result of the hydrogenation of the ketone in 4-aminoacetophenone to afford the corresponding 1-(4-aminophenyl)ethan-1-ol. Interestingly, under the same conditions, 4-acetylbenzonitrile (entry 7) exhibited no evidence for reduction, even after an extended reaction time of 10 hours, which is probably due to poisoning or deactivation of the catalyst. It appears that the surface-active Ru atoms becomes saturated by the 1000-fold excess of the nitrile donor-based substrate which prevents substrate access to the active sites.

A methoxy group at the *para-* position (entry 9) increased the conversion from 93% for the benchmark reaction of **A** to 97% for the reaction catalysed by **2.20**, with an observed drop in the selectivity from 95% to 88% which implies that the electron donating group's electronic effect modifies the reactivity of the aromatic ring and the

carbonyl group. Under the same reaction conditions, **2.16**, **2.17** and **2.21** were less active than **2.20** and gave conversions of 39%, 32% and 72%, respectively. Electron-rich substrates such as 3- and 4-methoxyacetophenone gave good conversions and high selectivities (entries 8-9), whilst the conversion of 2-methoxyacetophenone (entry 10) was slightly lower as a result of the increased steric hindrance from the proximal carbonyl; however, extending the reaction time to 6 hours improved the yield to 96%. The hydrogenation of sterically demanding naphthyl-based substrates afforded the corresponding alcohol as a single product in high yields for both the ketone and the aldehyde (entries 11 and 16), despite much longer reaction times of 24 and 8 hours, respectively.

In addition, high conversions were obtained for the hydrogenation of a range of substituted aromatic aldehydes with 100% selectivity to the corresponding aromatic alcohol, i.e., no aromatic ring reduction in reasonably short reaction times (entries 12-15). The origin of this selective conversion is most likely due to the improved reactivity of the more sterically accessible aldehydes than the corresponding ketones.
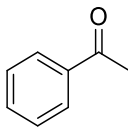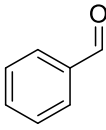
The hydrogenation of 4-acetylpyridine was investigated as a model heteroaromatic substrate and near quantitative conversion and 100% selectivity for 1-(4-pyridyl)ethanol was obtained after 4 hours using **2.20** as the catalyst (entry 17). However, in comparison the other catalysts were sluggish but did demonstrate some activity. Under the same conditions 3-acetylpyridine (entry 18) reached 95% conversion with 100% selectively to the corresponding alcohol after 4 hours and quinoline-4-carboxaldehyde (entry 19) achieved 90% conversion after 8 hours with 100% selectivity to the aromatic alcohol.

2.20 proved to be a highly active and selective catalyst for the hydrogenation of all of the substrates that were tested. Essentially chemoselectivity of C=O over C=C was observed in all cases except for 4-bromo and 4-chloroacetophenone (entry 1 and 2), which demonstrates that the system is also highly tolerant to a wide range of functional groups. In every case **2.21** was the second-best catalyst, therefore the PEG-PPh$_2$ combination appears to synergistically enhance the catalyst's selectivity towards hydrogenation of the carbonyl.

2.4.9 Catalyst poisoning

Prompted by the poor activity obtained for the hydrogenation of 4-acetylbenzonitrile, a series of batch reactions were carried out to establish whether 4-acetylbenzonitrile poisons the catalyst or if the substrate was simply inactive under the reaction conditions. To explore this possibility the hydrogenation of 1 mmol of acetophenone or benzaldehyde was catalysed with **2.20** in the presence of benzonitrile acting as a poison.

Table 2.6: Results of the catalyst poisoning studies for the hydrogenation of acetophenone and benzaldehyde in the presence of benzonitrile.

Entry [a]	Substrate	Catalyst	Time (hours)	Conversion (%) [b]	Selectivity (%) [b]
1		**2.20**	4	98	98
		2.20 [c]	4	0	0
2		**2.20**	2	97	100
		2.20 [c]	2	29	100

[a]Reaction conditions: 1 mmol acetophenone, 0.1 mol% **2.20**, 0.1 mmol K_2CO_3, 12 mL water, 50 °C, 70 psi H_2. [b]Conversion and selectivity determined by ^1H NMR spectroscopy with 1,3-dinitrobenzene as the internal standard. Selectivity = [% desired product / (% desired product + % other products)]. [c]Reaction conducted in the presence of 1 mmol benzonitrile.

The results in Table 2.6 showed that the pre-treatment of **2.20** with benzonitrile (entry 1) resulted in no hydrogenation of acetophenone, whilst in the absence of benzonitrile a 98% conversion of acetophenone was obtained under the same reaction conditions, which gives a strong indication that some kind of poisoning does occur. The activity was also significantly diminished for the hydrogenation of benzaldehyde (entry 2), although a 29% conversion of benzaldehyde was obtained compared to the 97% in the absence of benzonitrile. This could be associated with the less challenging reduction of aldehydes which have a lower energetic barrier compared to ketones. The

poisoning could also potentially be due to the binding of the nitrogen atom of the substrate onto the catalyst surface, therefore eventually all of the available active sites become saturated. Alternatively, the difference in the activity could be due to the surface's reactivity being changed by coordination of the N donor-based substrate, which may prevent the substrate from binding.

2.4.10 Recycling

As good conversions and high selectivities were obtained for the selective hydrogenation of aromatic ketones and aldehydes in a 1:1 ethanol/water mixture, as well as in water. A series of recycle experiments were carried out in water on the basis that aqueous phase catalysis would facilitate catalyst and product separation and recovery *via* a facile extraction protocol. Benzaldehyde was used as the test substrate for the recycle experiments as the short reaction times were considered to be more practical to perform multiple recycles. Each cycle was performed for 90 minutes after which the products and the unreacted benzaldehyde were extracted with ethyl acetate and ^{1}H NMR spectroscopy was used to quantify the extent of conversion and the selectivity. After extraction the reaction vessel was further charged with one equivalent of benzaldehyde and the reactor was re-pressurised with H_2.
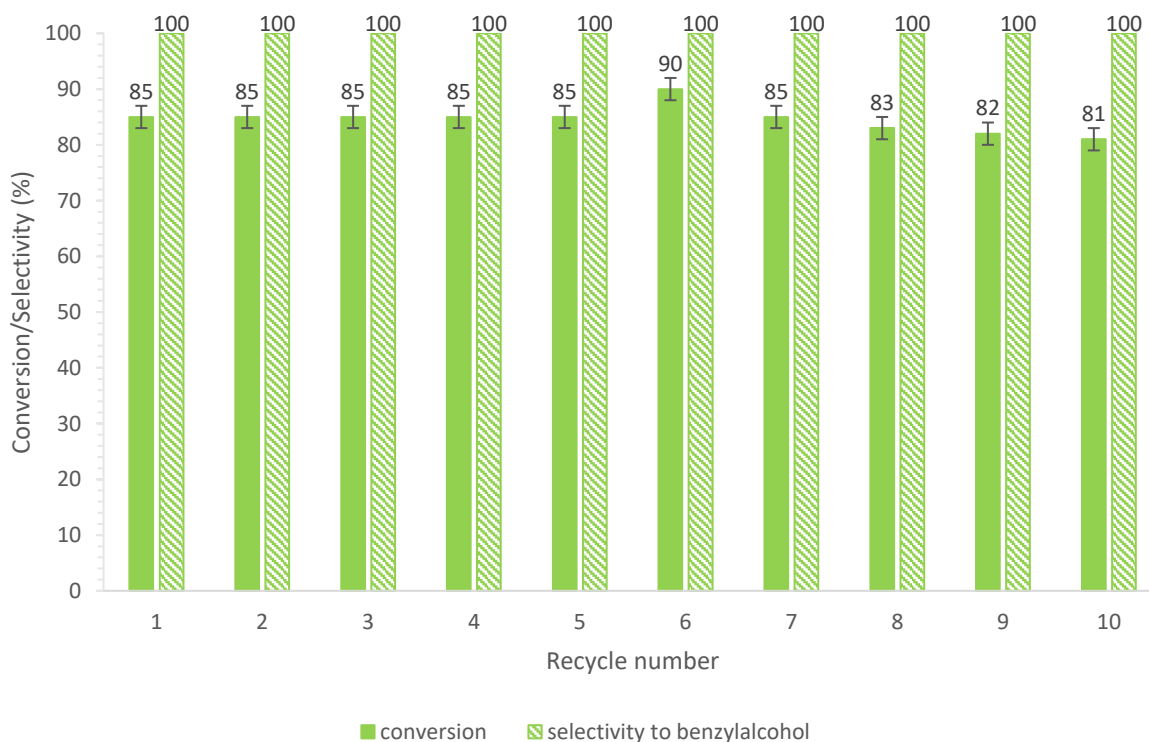
Figure 2.22: Recycling profile for the hydrogenation of benzaldehyde catalysed by **2.20**. Reaction conditions: 1 mmol benzaldehyde, 0.1 mol% RuNP@(O)PPh$_2$PEGPIILP (**2.20**), 70 psi H$_2$, 50 ℃, 12 mL water, reaction time = 90 mins. Conversion and selectivity determined by ^{1}H NMR spectroscopy with 1,3-dinitrobenzene as the internal standard. Selectivity for benzyl alcohol = [% benzyl alcohol / (% benzyl alcohol + % other products)].

The recycling profile using **2.20** (Figure 2.22) was promising and reached a steady state between runs 2-5. Interestingly, the 4% increase in the conversion of benzaldehyde to 90% between the 5th and 6th recycle was probably due to storage of the spent catalyst under 70 psi of hydrogen overnight which may well have activated the surface as a result of the successive reduction of any residual surface ruthenium oxide in the presence of hydrogen, therefore increasing the number of available active Ru sites for catalysis.[52] Nevertheless, further studies on the catalysts surface before and after the reaction using a combination of XPS, TEM and X-ray absorption fine structure analysis will need to be carried out to monitor the composition and morphology and establish the origin of this enhancement. Afterwards there was a slight drop in the conversion of benzaldehyde up to run 10 by this point the conversion (81%) was comparable to the first run. Encouragingly, complete selectivity for hydrogenation of the carbonyl group was maintained across the entire study.

TEM analysis of the catalyst recovered after the 10th run revealed that the RuNPs remained monodisperse with a mean diameter of 1.31 ± 0.42 nm, in comparison to, 1.32 ± 0.30 nm, for a freshly prepared sample of **2.20** (Figure 2.23). These results demonstrated the high stability and reusability of the catalyst. All of the results above firmly support the proposal that the reaction proceeded under heterogeneous catalysis as opposed to under homogeneous catalysis. Although further studies are clearly needed, the stable profile obtained for the reuse of **2.20** indicates that this system could be sufficiently robust for incorporation into a scale-up continuous flow process.
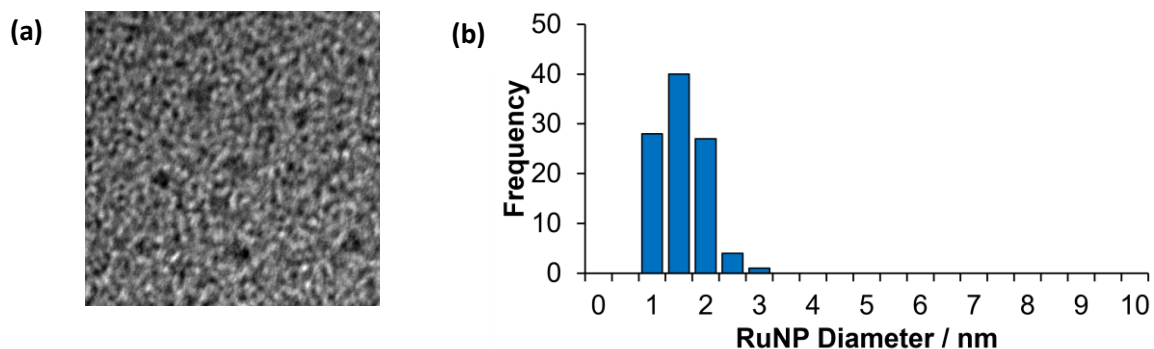
(a)   **(b)**

Figure 2.23: (a) HRTEM image of the catalyst after the 10th recycle for the hydrogenation of benzaldehyde in water catalysed by **2.20** and (b) particle size distribution for RuNP@O=PPh$_2$-PEGPIILP (**2.20**) after 10 recycles showing an average NP diameter of 1.31 ± 0.42 nm. Scale bars are 5 nm (white).

2.4.11 Complete Hydrogenation

During the optimisation of **2.20**, most of the reactions consistently showed trace amounts of 1-cyclohexylethanol (**D**) and together with several recent reports that RuNP-based systems are efficient catalysts for the hydrogenation of aromatic compounds,[53] it was then explored whether it was possible to obtain **D** simply by modifying the reaction conditions.

Considering the stability of the aryl ring against hydrogenation under the previous optimum conditions, to achieve the complete reduction of acetophenone would require harsh conditions such as an increase in the temperature, hydrogen pressure and reaction time. Having demonstrated that the reaction is mass transfer limited by the solubility of hydrogen, reactions were conducted under 400 psi of hydrogen at 70 °C. Under these conditions, Figure 2.24 showed that acetophenone was rapidly consumed using 0.1 mol% **2.20** to give **B** as the major species (62%) together with a significant amount of **D** (26%) after only 10 minutes. Longer reaction times resulted in further hydrogenation of **B**, to give quantitative conversion to **D** after only 70 minutes.
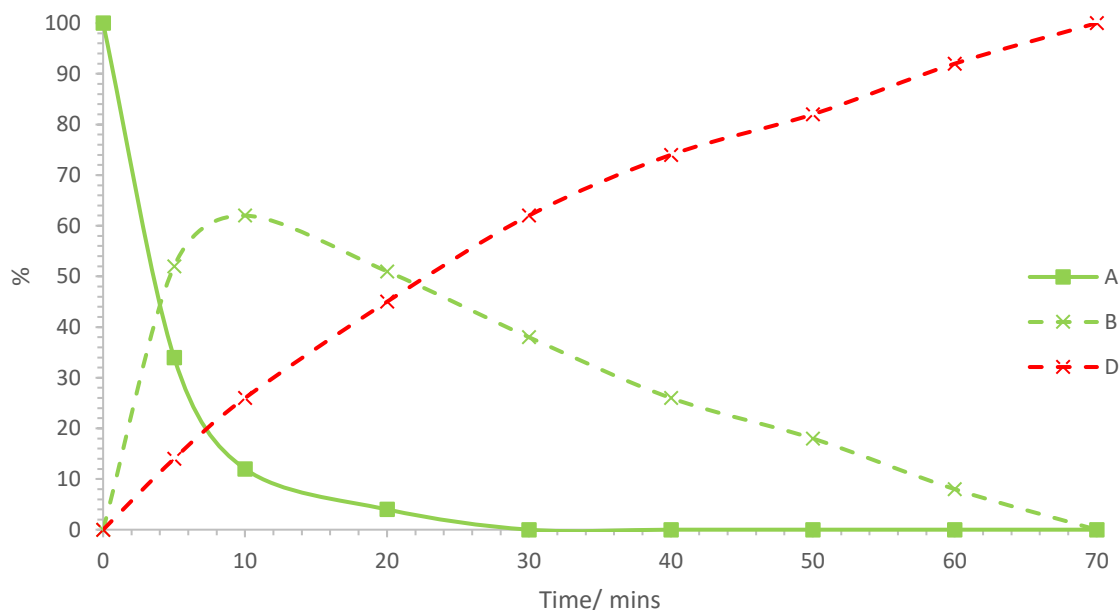
Figure 2.24: Monitoring of the complete catalytic hydrogenation of acetophenone as a function of time. Reaction conditions: 1 mmol acetophenone, 0.1 mol% RuNP@OPPh$_2$PEGPIILP (**2.20**), 0.1 mmol K$_2$CO$_3$, 12 mL 1:1 EtOH/water, 70 ℃, 400 psi H$_2$, reaction time = 70 minutes. Conversion and selectivity determined by ^{1}H NMR spectroscopy with 1,3-dinitrobenzene as the internal standard. Selectivity for 1-cyclohexylethanol (**D**) = [% 1-cyclohexylethanol / (% 1-phenylethanol + % cyclohexylethanol)].

A reduction in the catalyst loading to 0.005 mol% gave 84% conversion of **A** with 80% selectivity for **D** after 4 hours, which corresponds to an initial TOF of 3,400 h^{-1} (where TOF is moles of **D** formed per mole of catalyst per hour). A parallel study conducted with 0.1 mol% Ru/C (5 wt%) as the benchmark, under otherwise identical conditions gave a 100% conversion of **A** but only 31% selectivity for **D** after 3 hours which highlights the advantages of the PIIL cation-decorated supports. Although, a meaningful or reliable comparison with the existing systems was difficult to achieve due to the vastly disparate conditions reported in the literature, it appears that catalyst **2.20** either competes with or outperforms most of the reported RuNP-based catalysts. For example, the initial TOF of 3,400 h^{-1} obtained with **2.20** in 1:1 ethanol/water at 70 °C, under 400 psi hydrogen, is a marked improvement on that of 60 h^{-1} obtained with RuNP@[C$_{12}$MIM][BTA] (120 °C, 1,740 psi H$_2$)[63] and 2,600 h^{-1} achieved with poly-N-vinylpyrrolidone-stabilised RuNPs in cyclohexane (80 °C, 580 psi H$_2$).[64]
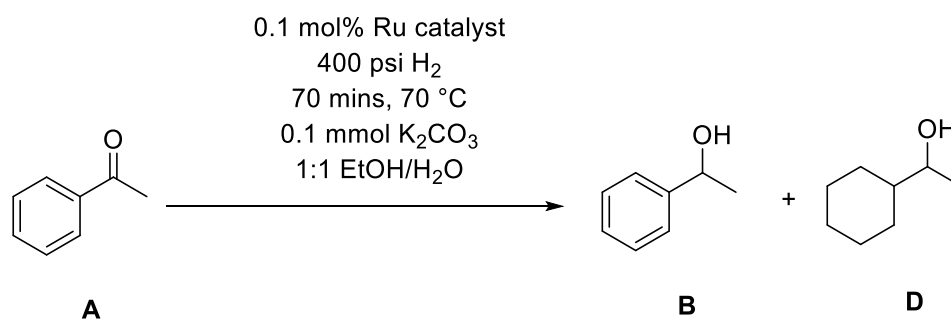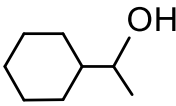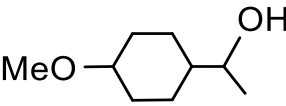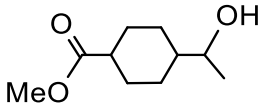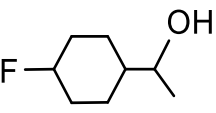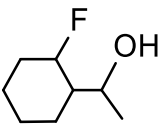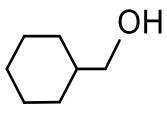
Table 2.7: Comparison of the Ru catalysts for the complete hydrogenation of acetophenone (A) to produce 1-cyclohexyl ethanol (D).

Entry [a]	Catalyst	Conversion (%) [b]	Yield of D (%) [b]
1	Ru/C	100	39
2	RuNP@PPh$_2$PEGPIILP (2.14)	100	100
3	RuNP@PPh$_2$-PIILP (2.15)	100	94
4	RuNP@PEGPIILP (2.16)	100	54
5	RuNP@PIILP (2.17)	100	48
6	RuNP@O=PPh$_2$PEGPIILP (2.20)	100	100
7	RuNP@O=PPh$_2$PIILP (2.21)	100	100

[a] Reaction conditions: 1 mmol acetophenone, 0.1 mol% catalyst, 0.1 mmol K$_2$CO$_3$, 12 mL 1:1 EtOH: water, 70 ℃, 400 psi H$_2$, reaction time = 70 mins. [b] Conversion and selectivity determined by ^{1}H NMR spectroscopy with 1,3-dinitrobenzene as the internal standard. Selectivity for 1- cyclohexylethanol (D) = [% 1-cyclohexylethanol / (% 1-phenylethanol + % cyclohexylethanol)].

The same protocol was then extended to the reduction of electron-rich and electron-poor substrates; 4-methoxyacetophenone, methyl 4-acetylbenzoate, 4- and 2-fluoroacetophenone and 4-hydroxyacetophenone; gratifyingly, each substrate gave the corresponding substituted 1-cyclohexylethanol with high selectivity in relatively short reaction times (Table 2.8).

Table 2.8: Complete hydrogenation of the substituted acetophenones catalysed by **2.20** to their corresponding substituted cylohexylethanol.[a]

Product			
	(cyclohexyl ethanol)	(MeO-cyclohexyl ethanol)	(MeO-C(=O)-cyclohexyl ethanol)
Conversion[b]	100% (70 min)	99% (70 min)	100% (70 min)
Selectivity[d]	100%	79%	62%
Product			
	(F-cyclohexyl ethanol)	(F-cyclohexyl ethanol)	(cyclohexyl methanol)
Conversion[b]	100% (70 min)	100% (70 min)	100% (70 min)
Selectivity[d]	84%	57%	100%

[a] Reaction conditions: 1 mmol of substrate, 0.1 mol% RuNP@(O)PPh$_2$PEGPIILP **2.20**, 12 mL 1:1 EtOH/water, 0.1 mmol K$_2$CO$_3$, conversion followed by the time in parenthesis, 70 °C, 400 psi H$_2$. [b] Conversions determined by ^{1}H NMR spectroscopy using 1,3-dinitrobenzene as internal standard. Average of three runs. [c] Selectivity for the cyclohexyl ethanol product [% cyclohexylethanol / (% arylethanol) + (% cyclohexylethanol) + (% cyclohexylethanone)] x 100%.

2.5 Application of RuNP@R-PIILP Catalysts for the Hydrogenation of Bioderived Substrates

In accordance with the eventual aims of this project, an investigation of the efficacy of the PIIL-based catalysts for the selective hydrogenation of C=O containing renewable feedstock was carried out. However, the challenging hydrogenative transformation for the selective formation of the target products often demands more harsh reaction conditions. Furthermore, these conditions typically result in extensive reaction networks, including the formation of ring-opened products and polyols, as a result of the unstable intermediates and products. A number of the products can still form under such conditions even with clean feeds and catalyst poisoning often occurs. Most of the reaction pathways proceed *via* two fundamental steps, including the metal-catalysed hydrogenation/hydrogenolysis and various simultaneous ring-opening/closing or decarbonylation-based transformations. The acidity or basicity of the particle's surface

or support sites can sometimes accelerate these steps and therefore it is necessary to systematically optimise these reactions.

2.5.1 PIILP-Supported RuNP-Catalysed Hydrogenation of Furfural

Having shown that **2.20** is a highly efficient catalyst for selective hydrogenation of the C=O in aromatic ketones and aldehydes, the range of substrates was extended to include important sustainable biomass-derived substrates, including furfural which is a product produced through the processing of the lignocellulosic-based biomass[54] and levulinic acid and its ethyl ester as the products formed are key bio-derived platform chemicals. Furfural is identified as a renewable source for the formation of oxygen-containing value-added chemicals in the biorefinery field.[55] Selective hydrogenation of the carbonyl in furfural (**E**) (Scheme 2.9) affords furfuryl alcohol (**F**), a possible sustainable source for the production of resins and a key intermediate in the acid-catalysed alcoholysis to form alkyl levulinates. Further hydrogenation of the heteroaromatic ring yields tetrahydrofurfuryl alcohol (**G**).
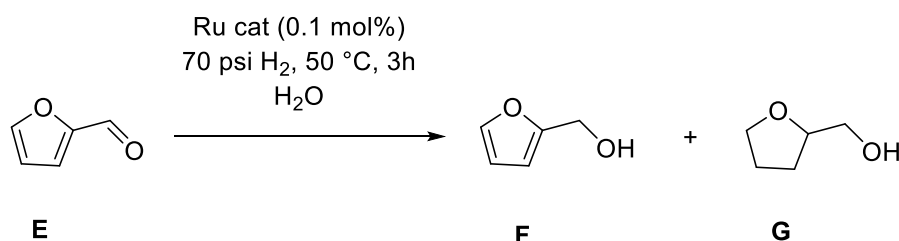
Scheme 2.9: The products of the Ru-catalysed hydrogenation of furfural (**E**).

As the formation of **F** is a straightforward one-step transformation it was chosen as the ideal benchmark reaction to assess the performance of **2.20**. Since furfural is similar to the previously optimised model ketones, the same reaction parameters were used as a lead to optimise the hydrogenation of furfural (**E**).

Table 2.9: Optimisation of the reaction parameters for the selective C=O hydrogenation of furfural (**E**) to furfuryl alcohol (**F**) catalysed by RuNPs.[a]

Entry[a]	Catalyst	Solvent	Additive	Conversion (%)[b]	Selectivity to F (%)[b]
1	**2.20**	Water	None	83	100
2	**2.20**	1:1 Ethanol/water	None	78	100
3	**2.20**	Ethanol	None	69	100
4	**2.20**	2-Me THF	None	36	100
5	**2.20**	toluene	None	43	100
6	**2.20**	Water	0.1 eq. K_2CO_3	81	100
7	**2.20**	Water	0.25 eq. K_2CO_3	81	100
8	**2.20**	Water	0.5 eq. K_2CO_3	81	100
9	**2.20**	Water	1 eq. K_2CO_3	80	100
10	**2.21**	Water	None	77	100
11	**2.16**	Water	None	61	100
12	**2.17**	Water	None	59	100
13	**Ru/C**	Water	None	21	100

[a]Reaction conditions: 1 mmol furfural, 0.1 mol% catalyst, 12 mL solvent, 50 °C, 70 psi H_2, reaction time = 3 hours. [b]Conversion and selectivity determined by ^{1}H NMR spectroscopy with 1,3-dinitrobenzene as the internal standard. Selectivity for furfuryl alcohol (**F**) = [% furfuryl alcohol / (% furfuryl alcohol + % tetrahydrofurfuryl alcohol)].

A solvent screen based on the optimum conditions established above as a lead revealed that 0.1 mol% of **2.20** gave the highest conversions in water and a 1:1 ethanol-water mixture (83% and 78%, respectively), both with 100% selectivity for furfuryl alcohol (**F**), after 3 hours at 50 ⁰C under 70 psi of hydrogen (entry 1 and 2). The solvent's ability to hydrogen bond and its highly polar nature appear to be essential for improving the activity of the catalyst as high conversions of **E** were also achieved in neat ethanol (entry 3). In contrast to the catalyst testing on acetophenone, moderate

conversions of **E** were also obtained in the organic solvents; 2-methyl THF and toluene (entry 4 and 5), however these conversions were below the optimum obtained in water.

Interestingly in comparison to the hydrogenation of aromatic ketones and aldehydes there was no evident effect observed on the addition of potassium carbonate as a base (entries 6-9). The results in Table 2.9 indicate that the heteroaromatic ring was significantly less susceptible to hydrogenation than the aldehyde group as there was no evidence for the fully reduced tetrahydrofurfuryl alcohol (**G**) in any of the reactions. Comparative catalyst testing showed that good conversions of **E** were obtained with **2.21**, while the activity dropped when the phosphine oxide was removed from the catalyst support as **2.16** and **2.17** gave conversion of 59% and 61%, respectively (entries 10-12). Catalyst **2.20** was significantly more active than commercially available Ru/C (5 wt%) which only reached 21% conversion after 3 hours with 100% selectivity for **F** (entry 13), confirming the advantage of the PIIL-modified supports. The catalyst loading was then reduced to 0.005 mol%, to further test the efficacy of **2.20** and after 5 hours a conversion of 79% with 100% selectivity for **F** was obtained; this corresponds to a TON of 15,800 and a TOF of 3,160 h^{-1}. Several recent reports of RuNP-catalysed hydrogenation of furfural are consistent with the high selectivity for furfuryl alcohol which include RuNP-coated polyethersulfone membrane,[65] RuNPs supported on reduced graphene oxide,[66] ultra-small RuNPs on porous supports,[67] and RuNPs stabilised on silica.[68] Apart from the RuNP-polyethersulfone membrane catalyst, which gave a TOF of 48,000 h^{-1}, catalyst **2.20** outperforms each of these catalyst systems. For instance, the initial TOF of 3,160 h^{-1} achieved with **2.20** in water is substantially higher than 137 h^{-1} for graphene-modified RuNPs at 20 ºC,[66] 30 h^{-1} for RuNPs on porous supports at 40 ºC,[67] and 237 h^{-1} for silica-supported RuNPs at 100 ºC.[68]

As there was no evidence for hydrogenation of the furan ring, the conversion of **E** was monitored as a function of pressure to examine whether an improvement in the catalyst activity could be achieved while maintaining 100% selectivity for **F**. The reaction time was reduced to 45 minutes to allow room for the improvement in the conversion of **E**.

Figure 2.25: Conversion and selectivity for the hydrogenation of furfural as a function of hydrogen pressure. Reaction conditions: 1 mmol furfural, 0.1 mol% RuNP@(O)PPh$_2$PEGPIILP (**2.20**), H$_2$ (specified), 50 ℃, 12 mL water, reaction time = 45 mins. Conversion and selectivity determined by ^{1}H NMR spectroscopy with 1,3-dinitrobenzene as the internal standard. Selectivity for furfuryl alcohol (**F**) = [% furfuryl alcohol / (% furfuryl alcohol + % tetrahydrofurfuryl alcohol)].

The pressure-composition profile in figure 2.25 revealed that the aqueous phase hydrogenation of furfural mirrored that for the hydrogenation of acetophenone, in that an increase in hydrogen pressure results in an increase in the conversion of **E**, reaching a plateau above 400 psi, which is indicative of a mass transfer limited solubility of hydrogen. In contrast to the pressure study carried out during the optimisation of acetophenone (Figure 2.18), **F** remained the sole product suggesting that hydrogenation of the aromatic furan ring is significantly more challenging than the phenyl ring in acetophenone. Under the optimum conditions earlier obtained, and using

350 psi H₂, **E** was quantitatively converted to **F** when the reaction time was extended to 90 minutes.

2.5.2 Hydrogenation of levulinic acid and its ethyl ester into γ-valerolactone

Ruthenium appears to be the choice of metal for the selective hydrogenation of levulinic acid (LA) and its esters to γ-valerolactone (GVL), on the basis of its remarkable selectivity for hydrogenation of the keto functionality in the presence of other unsaturated functional groups.[19] This specific transformation has been recognised as one of the most challenging in the emerging field of green chemistry; any successful approaches would offer a new, sustainable route to γ-valerolactone, which serves as a renewable feedstock with various applications in the fuel and fine chemical industry.[56] To this end, there are several reports of RuNP-based systems with promising reaction credentials for the hydrogenation of LA to GVL. For example, cyclodextrin-based polymer-stabilised RuNPs,[69] RuNPs on mixed magnesium lanthanum oxide,[70] and RuNPs supported on TiO₂.[71]

The main pathway for this transformation involves the selective hydrogenation of the terminal ketone in levulinic acid (**H**) by the heterolytic H₂ cleavage to give 4-hydroxypentanoic acid (**I**), which readily undergoes intramolecular lactonisation to form the cyclic ester γ-valerolactone (**J**) (Scheme 2.10).
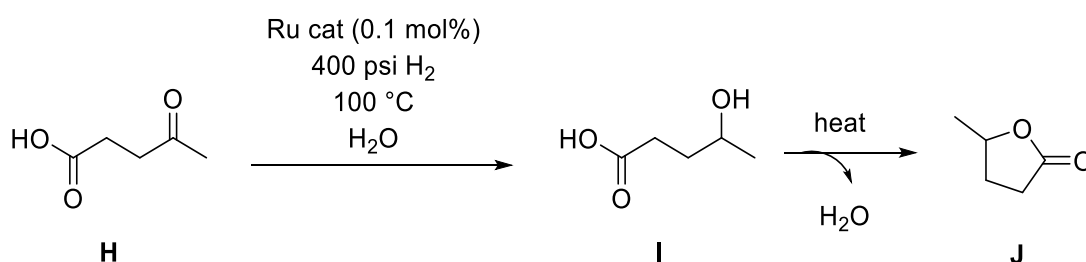
Scheme 2.10: Products of the Ru catalysed hydrogenation of levulinic acid (**H**).

As molar amounts of water are produced during the reaction, it is essential that the catalyst has good hydrothermal stability. The nature of this reaction will require high temperatures in order to force the cyclisation to go to completion. On the other

hand, the cyclisation reaction can also be enhanced by using a bifunctional catalyst including Lewis acids or Brønsted acidic sites.[23] Although this approach can be advantageous under the appropriate reaction conditions, the substrate scope is often limited as some hydrogenation products and/or reaction intermediates are susceptible to undesired acid-catalysed transformations which then later poison the catalyst. Consequently, this would increase the overall process cost as the catalyst lifetime decreases and the reactor would then require more frequent recharging.

The significance of water to carry out the catalytic hydrogenation of LA has been well-documented due to: (i) water being involved as a by-product; (ii) highly polar nature renders water as an excellent medium to convert polar, hydrophilic substrates for example LA; (iii) the presence of the aqueous solvent has a positive influence and enormously improves hydrogenation rates, whilst the use of various organic solvents leads to a dramatic reduction in the catalytic activities. (iv) water is a green/sustainable, non-toxic, safe, readily available, non-flammable and cheap solvent; and (v) the high heat capacity of water makes it an ideal medium to conduct large scale exothermic hydrogenations more selectively and securely. Therefore, the hydrogenation of LA in water would require a highly active metal catalyst because of the low solubility of H_2 in water. Participation of the water in the hydrogenation has been confirmed by mechanistic isotope labelling studies carried out by Michel *et al*.[76]

Preliminary reactions were conducted using 0.1 mol% **2.20** in water at 100 °C under 400 psi of hydrogen (Scheme 2.10), the hydrogen pressure was increased to 400 psi as an increase in the temperature would promote the cyclisation and the rate of hydrogenation. To guarantee mass balance, after workup the residual aqueous layer was concentrated to dryness and analysed by ^{1}H NMR spectroscopy adding 1,3-nitrobenzene as an internal standard to quantify any unextracted reactants.

Table 2.10: Results of the Ru catalysed hydrogenation of levulinic acid (**H**).

Entry[a]	Catalyst	Time / hours	Conversion / %[b]	Yield of I / %[b]	Yield of J / %[b]
1	**2.20**	4	100	22	78

2	**2.20**	8	100	0	100
3	**2.20**	8[c]	55	13	42
4	**2.16**	8	66	3	63
5	**2.17**	8	68	6	62
6	**2.21**	8	75	3	72
7	**Ru/C**	8	41	2	43

[a]Reaction conditions: 1 mmol levulinic acid, 0.1 mol % catalyst, 12 mL water, 100 ℃, 400 psi H_2, reaction time (specified). [b]Conversion and selectivity determined by ^{1}H NMR spectroscopy with 1,3-dinitrobenzene as the internal standard. [c] Reaction performed in the presence of 0.1 mmol K_2CO_3. Selectivity for γ-valerolactone (**J**) = [% γ-valerolactone / (% 4-hydroxypentanoic acid + % γ-valerolactone)].

The results in Table 2.10 show that under these conditions, **I** is the only detectable intermediate identified by analysis of the reaction mixture using ^{1}H NMR spectroscopy. Moreover, under these conditions the rate determining step is clearly the intramolecular cyclisation since 4 hours was required to obtain complete consumption of **H** with 78% conversion to **J** and 22% conversion to **I** (entry 1). Complete conversion of **H** to **J** as the sole product was achieved after 8 hours (entry 2). Interestingly, the addition of 10 mol% K_2CO_3 as an additive resulted in a significant reduction in catalyst activity as the conversion of **H** only reached 55% to afford a mixture of **J** (42%) and **I** (13%), which was somewhat surprising considering the positive effect of the addition of K_2CO_3 on the hydrogenation of model ketones in section 2.3.1 (entry 3). Comparative catalyst testing demonstrated that all PIILP-based catalysts under otherwise identical reaction conditions outperformed the commercial Ru/C (5 wt%), which only achieved 41% conversion (entries 2 and 4-6). Reduction of the catalyst loading to 0.005 mol% gave 61% conversion to a mixture of **J** (56%) and **I** (5%) after 5 hours, corresponding to an initial TOF of 2,440 h^{-1}. Complete conversion of **H** to **J** was achieved by extending the reaction time to 20 hours.

Unfortunately, reliable kinetic modelling is challenging as the system is mass transfer limited under these conditions. With the goal of comparing the efficacy of catalyst **2.20** against already existing systems, a series of reactions were carried out

to obtain time-composition profiles to provide a more detailed understanding of the relative reaction rates.
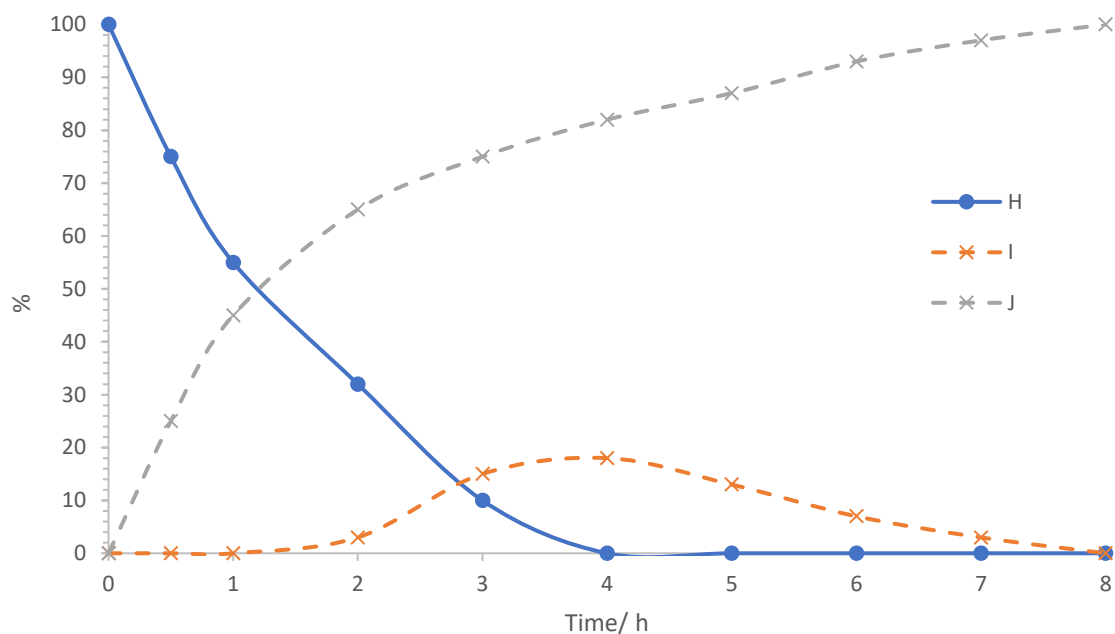
Figure 2.26: Product distribution for the catalytic hydrogenation of levulinic acid (**H**) as a function of time. Reaction conditions: 1 mmol levulinic acid, 0.1 mol % RuNP@(O)PPh$_2$PEGPIILP **2.20**, 12 mL water, 100 ℃, 400 psi H$_2$. Conversion and selectivity determined by ^{1}H NMR spectroscopy with 1,3-dinitrobenzene as the internal standard. Selectivity for γ-valerolactone (**J**) = [% γ-valerolactone / (% 4-hydroxypentanoic acid + % γ-valerolactone)].

The resulting time-composition profile in figure 2.26 revealed complete conversion of **H** occurred after 4 hours to give an 18:82 mixture of **I** and **J**, and 8 hours was required to obtain **J** as the sole product. Notably, at low **H** concentration below 30% there was no intermediate **I**, suggesting a similar rate for both the hydrogenation and the cyclisation. However, as the reaction proceeded the cyclisation rate began to drop, resulting in an increase in the relative concentration of **I**. A consistent increase was seen until **H** had been fully consumed, at which point, **I** gradually cyclised to afford **J**. As cyclisation can be acid-catalysed, **H** may well act as a catalyst for the

intramolecular lactonisation at low conversions, however as it becomes consumed and the concertation drops cyclisation would become rate limiting.

A series of reactions were conducted under the same reaction conditions but with the addition of one equivalent of commercial sulfonated-cation exchange resin (dry Amberlyst H15, 4.7 meq/g). There was no evidence for the build-up of **I** and **J** was obtained as the sole product in quantitative yield after 4 hours, in accordance with the rapid lactonisation throughout the reaction.

To explore the effect of the base on the reaction, the hydrogenation of **H** was conducted under the same conditions with the addition of 10 mol% K_2CO_3.
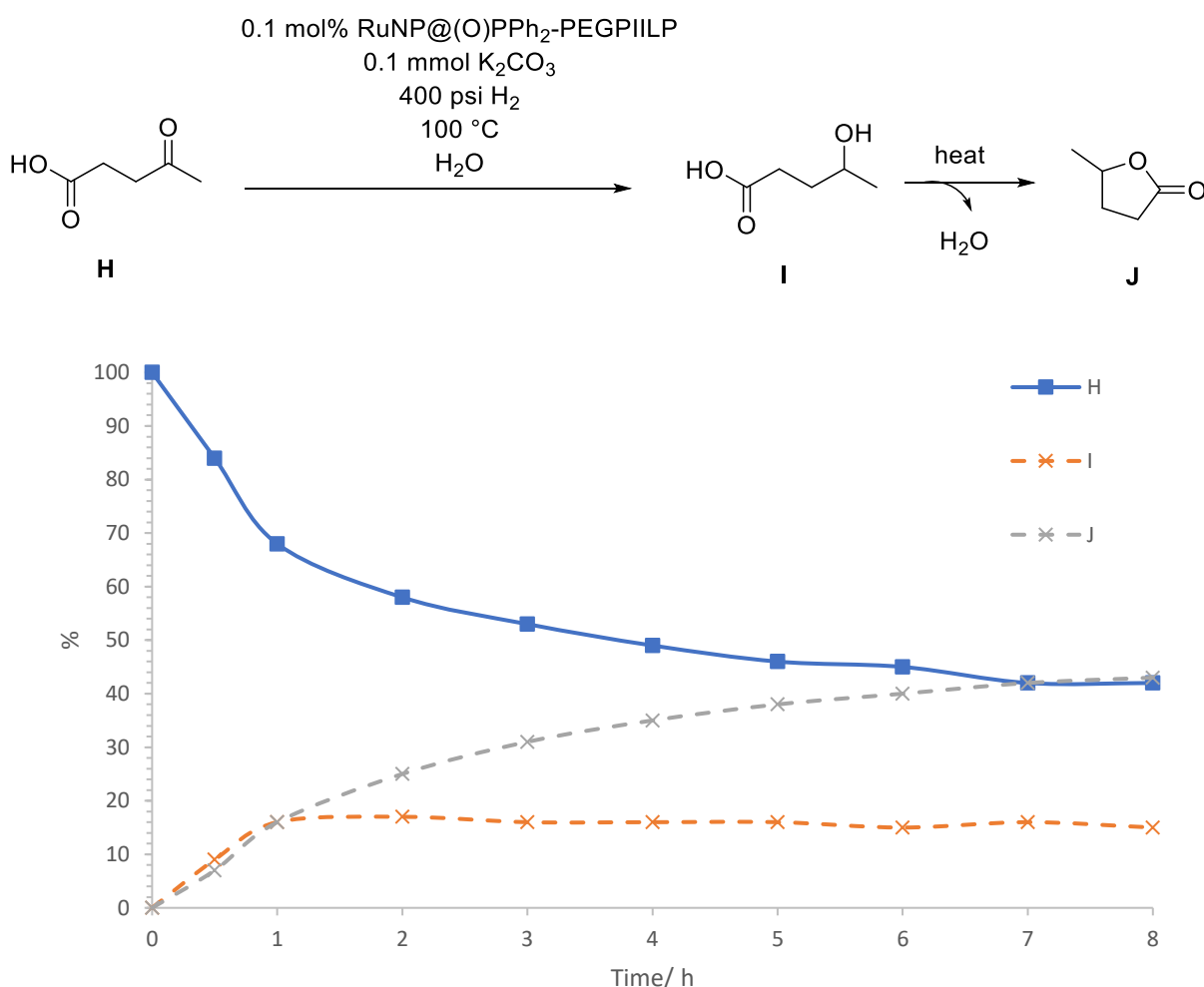
Figure 2.27: Product distribution for the hydrogenation of levulinic acid catalysed by **2.20** with a base additive as a function of time. Reaction conditions: 1 mmol levulinic acid, 0.1 mol % RuNP@(O)PPh₂PEGPIILP **2.20**, 0.1 mmol K_2CO_3, 12 mL water, 100

℃, 400 psi H_2. Conversion and selectivity determined by ^1H NMR spectroscopy with 1,3-dinitrobenzene as the internal standard. Selectivity for γ-valerolactone (**J**) = [% γ-valerolactone / (% 4-hydroxypentanoic acid + % γ-valerolactone)].

The composition-time plot in figure 2.27 demonstrated a marked contrast to the plot without a base in figure 2.26. The addition of a base appeared to have a considerable effect on the conversion-selectivity profile, as both the hydrogenation and the lactonisation steps appear to be inhibited. Under these reaction conditions the conversion of **H** only reached 55% after 8 hours, with a product distribution of 42% **J** and 13% **I**; in contrast 100% conversion of **H** was achieved in the absence of a base in figure 2.25. The increase in the pH, as a result of the base addition, may slow down the acid-catalysed ring closure due to neutralisation of the acid. Furthermore, the base may also poison the catalyst, by partially inhibiting it and thereby impeding the initial hydrogenation step. However, the influence of the bases on the hydrogenation step is more difficult to justify, particularly given that the base enhances the hydrogenation of aryl ketones.

A literature survey revealed that catalyst **2.20** either competed with or outperformed several existing RuNP-based systems. For example, the initial TOF of 2,440 h^{-1} obtained with **2.20** in water at 100 ºC under 400 psi of hydrogen is a substantial improvement on 210 h^{-1} for cyclodextrin-based polymer-assisted RuNPs,[69] and 374 h^{-1} obtained with Ru-NHC derived RuNPs at 130 °C.[72] There have also been reports of more efficient systems such as RuNP@TiO$_2$, which gave a TOF of 7,676 h^{-1}.[71] The efficacy of this system was attributed to the highly dispersed nature of the electron rich ruthenium centres and the promoting effect of water, which was involved in the C=O hydrogenation. The system's composition allows for the modular design of more active NP-based PIIL-supported catalysts since the system is amenable to functionalisation and modification.

An initial reusability study was conducted for the hydrogenation of **H** to **J** to evaluate the longevity and robustness of **2.20**. However, the practical issues involved with the recovery of the small amount of catalyst (0.5 mol%, 2.1 mg) by filtration prevented a conventional recycle experiment. Consequently, a reuse experiment was carried out by using ethyl acetate to extract the product and unreacted starting material before recharging the aqueous phase with an additional portion of levulinic acid and

Amberlyst resin. Under these conditions, **2.20** could be recycled ten times over three days with only a slight drop in the conversion of **H** from 86% to 84% and no detectable loss in selectivity for **J** (Figure 2.28). The successful reuse of catalyst **2.20** was highly encouraging and implied that this class of catalyst may well be amenable to scale-up studies using continuous flow.
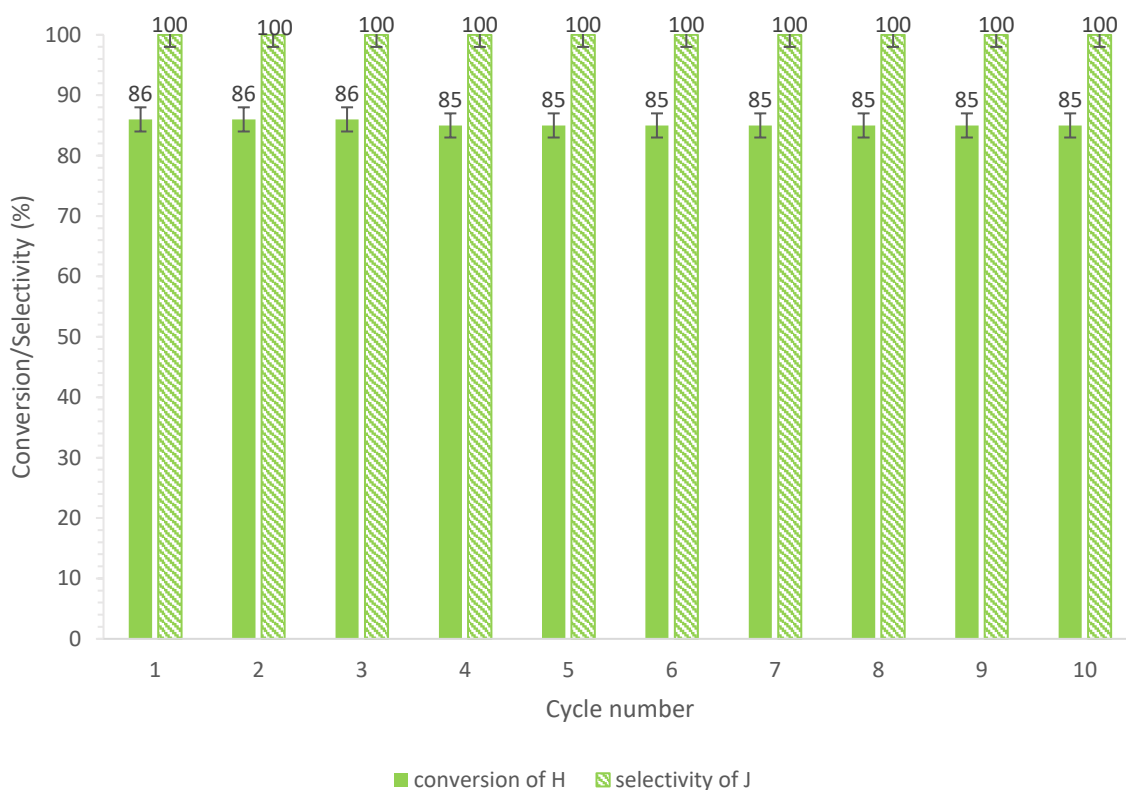
Figure 2.28: Reuse study for the hydrogenation of levulinic acid (**H**) catalysed by **2.20**. Reaction conditions: 1 mmol levulinic acid, 0.1 mol % RuNP@(O)PPh$_2$PEGPIILP **2.20**, 1 mmol Amberlyst-15, 12 mL water, 100 ℃, 400 psi H$_2$, 4h. Conversion and selectivity determined by ^{1}H NMR spectroscopy with 1,3-dinitrobenzene as the internal standard. Selectivity for γ-valerolactone (**J**) = [% γ-valerolactone / (% 4-hydroxypentanoic acid + % γ-valerolactone)].

Alternatively, γ-valerolactone can be obtained by the hydrogenation of levulinate esters, a direct cellulosic product obtained *via* acid-catalysed esterification of levulinic acid in alcoholic solvents.[54] The benefits of obtaining γ-valerolactone *via* this approach is that it would be less challenging to separate the ester from the oxygenated water-soluble compounds in the aqueous depolymerisation streams.

Hence, a versatile catalyst which does not discriminate between levulinic acids and its esters would for that reason enhance the economic benefit of this step on a larger scale and at the same time broaden the applications of the catalyst.

As alkyl levulinates (AL) can also be obtained by the acid-catalysed esterification of cellulose feed,[54] a parallel study was also conducted to test the efficacy of **2.20** for the hydrogenation of ethyl levulinate (**K**) (Scheme 2.11) to compare with levulinic acid, the results of which are summarised in Table 2.11.
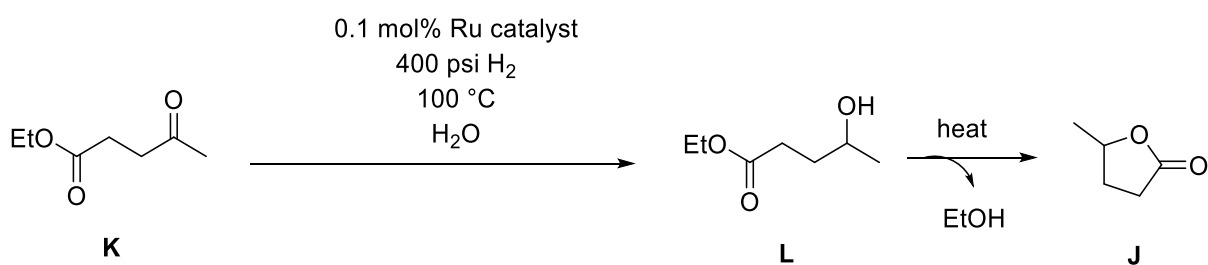
Scheme 2.11: Products of the Ru-catalysed hydrogenation of ethyl levulinate (**K**).

Table 2.11: Results of the Ru catalysed hydrogenation of ethyl levulinate (**K**).

Entry[a]	Catalyst	Time / hours	Base[b]	Conversion / (%)	Yield of L/ (%)[c]	Yield of J / (%)[c]
1	**2.20**	4	0	86	47	38
2	**2.20**	8	0	100	32	68
3	**2.20**	8	K_2CO_3	100	0	100
4	**2.16**	8	K_2CO_3	56	47	9
5	**2.17**	8	K_2CO_3	46	39	7
6	**2.21**	8	K_2CO_3	91	7	84
7	**Ru/C**	8	K_2CO_3	41	39	2

[a]Reaction conditions: 1 mmol ethyl levulinate (**K**), 0.1 mol % catalyst, 12 mL water, 100 °C, 400 psi H_2, reaction time (specified). [b]0.1 mmol of K_2CO_3 added. [c]Conversion and selectivity determined by ^{1}H NMR spectroscopy with 1,3-dinitrobenzene as the internal standard. Selectivity for γ-valerolactone (**J**) = [% γ-valerolactone / (% 4-hydroxypentanoic acid ethyl ester + % γ-valerolactone)].

Under optimum reaction conditions, 0.1 mol% **2.20** gave full conversion of **K** to a 32:68 mixture of **L:J** after 8 hours (entry 2), whereas in the same time levulinic acid gave quantitative conversion to γ-valerolactone as the sole product (Table 2.10, entry 2). However, a significant improvement in the catalyst efficacy was achieved by the addition of 10 mol% base and as complete conversion to **J** was achieved in the same time (entry 3). Comparative catalyst testing revealed that **2.20** was considerably more efficient compared to all of the other tested catalysts (entries 4-7).

The composition-time plot in Figure 2.29 showed that the initial hydrogenation of **K** was the rate determining step, as only small quantities of intermediate **L** were observed during the reaction. This case is different from that of levulinic acid, given that consumption of the levulinate ester is unlikely to significantly alter the pH of the reaction, this allowed the base-catalysed lactonisation to yield **J** as the sole product after 8 hours. To further examine and directly optimise the catalyst it would be practical to improve the hydrogenation step.

Figure 2.29: Product distribution for the hydrogenation of ethyl levulinate (**K**) catalysed by **2.20** with a base additive as a function of time. Reaction conditions: 1 mmol ethyl levulinate, 0.1 mol % RuNP@(O)PPh$_2$-PEGPIILP **2.20**, 0.1 mmol K$_2$CO$_3$, 12 mL water, 100 ℃, 400 psi H$_2$. Conversion and selectivity determined by ^{1}H NMR spectroscopy with 1,3-dinitrobenzene as the internal standard. Selectivity for γ-valerolactone = [% γ-valerolactone / (% 4-hydroxypentanoic acid ethyl ester + % γ-valerolactone)].

In the absence of a base (Figure 2.30), the concentration of **L** increased to 55% during the initial 3 hours of the reaction, which indicated that the hydrogenation of **K** also occurred *via* a two-step hydrogenation-lactonisation process. Consistent with the results obtained in Table 2.11, catalyst efficacy is markedly reduced in the absence of a base as only 68% of **J** was obtained after 8 hours. Furthermore, in agreement with the levulinic acid studies, faster rates of hydrogenation were obtained in the absence of base, indicating that hydrogenation of **L** may be inhibited by the base; although, contrary to levulinic acid, the improvement was only negligible.

Figure 2.30: Product distribution for the hydrogenation of ethyl levulinate (**K**) catalysed by **2.20** in the absence of a base additive as a function of time. Reaction conditions: 1 mmol ethyl levulinate, 0.1 mol % RuNP@(O)PPh$_2$PEGPIILP **2.20** catalyst, 12 mL water, 100 °C, 400 psi H$_2$. Conversion and selectivity determined by ^{1}H NMR spectroscopy with 1,3-dinitrobenzene as the internal standard. Selectivity for γ-valerolactone (**J**) = [% γ-valerolactone / (% 4-hydroxypentanoic acid ethyl ester + % γ-valerolactone)].

Enhancements in the RuNP-catalysed production of GVL by assisting the lactonisation step with either acid-functionalisation of the NP support or by the addition of a base has been reported. For example, a substantial improvement in the yield of GVL was obtained with ruthenium hydroxide supported on anatase in the presence of a heterogeneous base such as MgO and hydrocalcite, which acted as co-catalysts.[73] Furthermore, dual bifunctional catalysts made from RuNPs supported in a sulfonic acid-modified MOF (UiO-66 and MIL-101) gave much higher yields of GVL compared to the corresponding systems without acid which gave 4-hydroxypentanoic acid methyl ester as the major product.[74]

The encouraging results presented so far suggest that the PIIL-stabilised NPs have the potential to be a tool to generate platform chemicals and fuels in a more sustainable manner. Furthermore, the outcomes from this chapter will act as a platform for further optimisation of these systems through variation of the substrate: catalyst ratio, in addition to screening an array of additives with cautious pH modulation. As regards the latter, a continuous flow reactor could enable the optimisation of the chemical transformations, along with improving the reaction scalability and increase the feasibility for industrial use.

2.6 Conclusion

Impregnation of the phosphine-decorated PIILs with ruthenium trichloride during the preparation of RuNPs resulted in the serendipitous reduction to give a Ru(II) species and a phosphine oxide. Surface XPS studies point to the presence of Ru----O=PPh$_2$ interactions. The resulting ultra-small, monodisperse phosphine oxide-decorated PIIL-stabilised RuNPs are highly active and selective catalysts for the aqueous phase

hydrogenation of a wide array of aryl and heteroaryl ketones and aldehydes to either the respective aryl-based alcohol or the cyclohexyl-based alcohol and in addition to the conversion of key biomass-derived substrates, furfural to furfuryl alcohol and levulinic acid and its ethyl ester to γ-valerolactone. Furthermore, catalysts prepared by reduction of the pre-made phosphine oxide-decorated PIILs impregnated with $RuCl_3$ were as efficient as those generated from PPh_2PIILP or its PEGylated counterpart and $RuCl_3$ which streamlined the catalyst preparation, handling and storage.

Optimisation of the reaction conditions highlighted the beneficial influence of the aqueous medium, as the catalyst performed best for the hydrogenation of acetophenone in a 1:1 water/ethanol system. The selective hydrogenation of a series of substituted acetophenone substrates with different electronic and steric profiles showed that the PPh_2 and PEG modification were essential to obtain high activity and selectivity for hydrogenation of the carbonyl. All PIILP-based catalysts tested were unable to catalyse the hydrogenation of the nitrile-bearing substrate which prompted a more in-depth examination into the likely poisoning effects of nitrogen donors. Carrying out the benchmark reaction of acetophenone and benzaldehyde in the presence of benzonitrile showed that the nitrile substrate deactivates the catalyst, most likely due to strong adsorption and/or saturation of the active sites.

Batch recycle experiments conducted on the hydrogenation of benzaldehyde were extremely promising as **2.20** showed a reasonably stable activity-selectivity profile over 10 runs, with only a slight reduction in the conversions between runs 7 and 10. The optimum system **2.20** also catalysed the hydrogenation of the aryl ring of acetophenone to give quantitative yields of cyclohexylethanol. The hydrogenation of acetophenone to 1-phenyl ethanol and furfural into furfuryl alcohol gave initial TOFs of 2,350 h^{-1} and 3,160 h^{-1}, respectively, which are amongst the highest to be reported in aqueous media for these transformations.

2.20 was also an efficient and selective catalyst for the partial hydrogenation of furfural to give furfuryl alcohol in a 100% conversion and selectivity under relatively mild conditions, with a low catalyst loading, in water and short reaction times. Furthermore, **2.20** facilitated the selective formation of the key intermediate, γ-valerolactone, in a clean and sustainable method from both levulinic acid and its ethyl ester. Time-conversion profiles showed that the hydrogenation of levulinic acid is more

rapid in the absence of a base and that the lactonisation of the 4-hydroxypentanoic acid intermediate is faster in the presence of residual acidic levulinic acid or with the addition of Amberlyst resin, which could catalyse the lactonisation step. A stable profile was also achieved over ten runs in the recycle study of the hydrogenation of levulinic acid, which indicated that these systems could be applicable for a continuous flow reactor platform.

Lastly, comparative catalyst testing against commercially available Ru/C (5 wt%), revealed that the ionic microenvironment provided by the cation-decorated polymer support was beneficial, as all four PIILP-modified catalysts outperformed Ru/C in both the activity and the selectivity for all the chemical transformations. Despite this being the first report of phosphine-oxide stabilised RuNPs, it is likely that there have been recent examples of the use of a phosphine-modified polymers to synthesise phosphine-stabilised RuNPs which were misunderstood, as these resulting catalysts were actually phosphine oxide derived from the reduction of impregnated $RuCl_3$, in the same manner as discussed in this chapter (Section 2.3.3). Further surface studies employing techniques for example *in situ* DRIFTS and XAS analysis would be needed to unequivocally establish the nature of the Ru-----$O=PPh_2$ interaction and to fully understand how these PIIL-supports effects the catalyst efficacy.

2.7   References

1. J. C. Serrano-Ruiz, R. Luque and A. Sepulveda-Escribano, *Chem. Soc. Rev.* 2011, **40**, 5266–5281.

2. D. M. Alonso, S. G. Wettstein and J. A. Dumesic, *Green Chem.*, 2013, **15**, 584-595.

3. F. A. Kucherov, L. V. Romashov, K. I. Galkin and V. P. Ananikov, *ACS Sustainable Chem. Eng.*, 2018, **6**, 8064-8092.

4. A. Demirbas, *Prog. Energy Combust, Sci.*, 2004, **30**, 219-230.

5. K. T. Tan, K. T. Lee, A. R. Mohamed and S. Bhatia, *Renew. Sust. Energy Rev.*, 2009, **13**, 420-427.

6. E. Gross, *Stud. Surf. Sci. Catal.*, 2017, **177**, 57-84.

7. a) R. Hudson, V. Chazelle, M. Bateman, R. Roy, C.-J. Li and A. Moores, *ACS Sustainable Chem. Eng.,* 2015, **3**, 814-820; b) Z. Lin, X. Cai, Y. Fu, W. Zhu and F. Zhang, *RSC Adv.*, 2017, **7**, 44082-44088; c) C. Yang, S. Bai, Y. Feng and X. Huang, *ChemCatChem*, 2019, **11**, 2265-2269; d) T. Mitsudome and K. Kaneda, *Green Chem.*, 2013, **15**, 2636-2654; e) M. S. Ide, B. Hao, M. Neurock and R. J. Davis, *ACS Catal.*, 2012, **2**, 671-683; f) S. Rösler, J. Obenauf and R. Kempe, *J. Am. Chem. Soc.*, 2015, **137**, 7998-8001.

8. K. Grubel, W. W. Brennessel, B. Q. Mercado and P. L. Holland, *J. Am. Chem. Soc.*, 2014, **136**, 16807-16816.

9. K. V. R. Chary, D. Naresh, V. Vishwanathan, M. Sadakane and W. Ueda, *Catal. Commun.*, 2007, **8**, 471-477.

10. A. N. K. Lup, F. Abnisa, W. M. A. W. Daud and M. K. Aroua, *J. Ind. Eng. Chem.*, 2017, **56**, 1-34.

11. Behr, Y. Brunsch and A. Lux, *Tetrahedron Lett.*, 2012, **53**, 2680-2683.

12. P. Anatas and N. Eghbali, *Chem. Soc. Rev.*, 2010, **39**, 301-312.

13. L. D. Pachón and G. Rothenberg, *Appl. Organomet. Chem.*, 2008, **22**, 288-299.

14. R. Mehrani, M. Barati, A. Tavasoli and A. Karimi, *Environ. Today*, 2015, **36**, 1265-1272.

15. D. Yao, Q. Hu, D. Wang, H. Yang, C. Wu, X. Wang and H. Chen, *Bioresour.*, 2016, 216, 159-164.

16. D. O. Özgür and B. Z. Uysal, *Biomass Bioenergy*, 2011, **35**, 822-826.

17. M. E. Domine, E. E. Iojoiu, T. Davidian, N. Guilhaume and C. Mirodatos, *Catal. Today*, 2008, **134**, 565-573.

18. X. Qin, H. Li, S. Xie, K. Li, T. Jiang, X.-Y. Ma, K. Jiang, Q. Zhang, O. Terasaki, Z. Wu and W.-B. Cai, *ACS Catal.*, 2020, **10**, 3921-3932.

19. C. Michel and P. Gallezot, *ACS Catal.* 2015, **5**, 4130–4132.

20. K. Wu, Y. Wu, Y. Chen, H. Chen, J. Wang and M. Yang, *ChemSusChem*, 2016, **9**, 1355-1385.

21. A. K. Talukdar, K. G. Bhattacharyya and S. Sivasanker, *Appl. Catal. A: Gen.*, 1993, **96**, 229-239.

22. R. V. Sharma, U. Das, R. Sammynaiken and A. K. Dalai, *Appl. Catal. A: Gen.*, 2013, **454**, 127-136.

23. K. Ishihara, M. Kaneeda and H. Yamamoto, *J. Am. Chem. Soc.*, 1994, **116**, 11179-11180.

24. J. Lee, Y. Xu and G. W. Huber, *Appl. Catal. B: Environ.*, 2013, **140-141**, 98-107.

25. J. A. Melero, J. Moreno, J. Iglesias, G. Morales, J. L. G. Fierro, R. Sánchez-Vázquez, A. Cubo and B. García, *Mol. Catal.*, 2020, **484**, 110802.

26. C. Michel, J. Zaffran, A. M. Ruppert, J. Matras-Michalska, M. Jędrzejczyk, J. Grams and P. Sautet, *Chem. Commun.*, 2014, **50**, 12450-12453.

27. J. J. Bozell, L. Moens, D. C. Elliott, Y. Wang, G. G. Neuenscwander, S. W. Fitzpatrick, R. J. Bilski and J. L. Jarnefeld, *Resour. Conserv. Recycl.*, 2000, **28**, 227-239.

28. A) P. Kluson and L. Cerveny, *Appl. Catal. A: Gen.*, 1995, **128**, 13-31; b) X. Jin, B. Yin, Q. Xia, T. Fang, J. Shen, L. Kuang and C. Yang, *ChemSusChem*, 2019, **12**, 71-92; c) W. Luo, U. Deka, A. M. Beale, E. R. H. van Eck, P. C. A. Bruijnincx and B. M. Weckhuysen, *J. Catal.*, 2013, **301**, 175-186.

29. J. Julis, M. Hölscher and W. Leitner, *Green Chem.*, 2010, **12**, 1634–1639.

30. a) J. Gmeiner, S. Behrens, B. Spliethoff and O. Trapp, *ChemCatChem,* 2016, **8**, 571–576; b) G. Bagnato, A. Figoli, C. Ursino, F. Galiano and A. Sanna, *J. Mater. Chem. A*, 2018, **6**, 4955–4965.

31. S. Noël, D. Bourbiaux, N. Tabary, A. Ponchel, B. Martel, E. Monflier and B. Léger, *Catal. Sci. Technol.*, 2017, **7**, 5982–5992.

32. D. Ganapathy and G. Sekar, *Catal. Commun.*, 2013, **39**, 50-54.

33. A. Villa, M. Schiavoni, C. E. Chan-Thaw, P. F. Fulvio, R. T. Mayes, S. Dai, K. L. More, G. M. Veith and L. Prati, *ChemSusChem,* 2015, **8**, 2520–2528.

34. Y. Kuwahara, Y. Magatani and H. Yamashita, *Catal. Today,* 2015, **258**, 262–269.

35. C. Moreno-Marrodan and P. Barbaro, *Green Chem.* 2014, **16**, 3434–3438.

36. U. Mandi, N. Salam, S. K. Kundu, A. Bhaumik and Sk. M. Islam, *RSC Adv.* 2016, **6**, 73440–73449.

37. Z. Lin, X. Cai, Y. Fu, W. Zhu and F. Zhang, *RSC Adv.*, 2017, **7**, 44082–44088.

38. Z. Lin, M. Luo, Y. Zhang, X. Wu, Y. Fu and F. Zhang, *Appl. Catal. A: Gen.,* 2018, **563**, 54–63.

39. S.-Y. Kim, H. W. Lee, S. J. Pai and S. S. Han, *ACS Appl. Mater. Interfaces*, 2018, **10**, 26188-26194.

40. E. Lam and J. H. T. Luong, *ACS Catal.*, 2014, **4**, 3393-3410.

41. J. A. Rodriguez, J.-Y. Kim, J. C. Hanson, S. J. Sawhill and M. E. Bussell, *J. Phys. Chem. B*, 2003, **107**, 6276-6285.

42. S. Doherty, J. G. Knight, T. Backhouse, A. Bradford, F. Saunders, A. R. Bourne, T. W. Chamberlain, R. Stones, A. Clayton, K. Lovelock, *Catal. Sci. Technol.,* 2018, **8**, 1454–1467.

43. S. Doherty, J. G. Knight, T. Backhouse, E. Abood, H. Al-shaikh, S. J. I. Fairlamb, A. R. Bourne, T. W. Chamberlain, R. Stones, *Green Chem.*, 2017, **19,** 1635–1641.

44. R. Rabinowitz and R. Marcus, *J. Org. Chem.*, 1961, **26**, 4157-4158.

45. Q. Yao and C. Wilkie, *Polym. Degrad. Stab.*, 1999, **66**, 379-384.

46. X. Yan, H. Liu and K. Y. Liew, *J. Mater. Chem.*, 2001, **11**, 3387-3391.

47. J. A. Osborn, F. H. Jardine, J. F. Young and G. Wilkinson, *J. Chem. Soc. A*, 1966, 1711-1732.

48. D. González-Galvez, P. Nolis, K. Philippot, B. Chaudret, P. W. N. M. van Leeuwen, *ACS Catal.,* 2012, **2**, 317–321.

49. H. Jiang, X. Zheng, *Catal. Sci. Technol.* 2015, **5**, 3728–3734.

50. C. Pan, K. Pelzer, K. Philippot, B.Chaudret, F. Dassenoy, P. Lecante and M.-J. Casanove, *J. Am. Chem. Soc.*, 2001, **123**, 7584-7593.

51. a) F. Leng, I. C. Gerber, M. R. Axet and P. Serp, *Comptes Rendus Chimie*, 2018, **21**, 346-353; b) H.-Y. Jiang and X.-X. Zheng, *Catal. Sci. Technol.*, 2015, **5**, 3728-3734; c) M. Selva, P. Tundo and A. Perosa, *J. Org. Chem.*, 1998, **63**, 3266-3271; d) T. Ohkuma, H. Ooka, S. Hashiguchi, T. Ikariya and R. Noyori, *J. Am. Chem. Soc.*, 1995, **117**, 2675-2676; e) R. L. Chowdhury and J.-E. Bäckvall, *J. Chem. Soc., Chem. Commun.*, 1991, 1063-1064.

52. C. T. Williams, K.-Y. Chen, C. G. Takoudis and M. J. Weaver, *J. Phys. Chem. B*, 1998, **102**, 4785-4794.

53. K. V. R. Chary, D. Naresh, V. Vishwanathan, M. Sadakane and W. Ueda, *Catal. Commun.*, 2007, **8**, 471-477.

54. F. H. Isikgor and C. R. Becer, *Polym. Chem.*, 2015, **6**, 4497-4559.

55. R. Mariscal, P. Maireles-Torres, M. Ojeda, I. Sádaba and M. López-Granados, *Energy Environ. Sci.*, 2016, **9**, 1144-1189.

56. A. Osatiashtiani, A. F. Lee and K. Wilson, *Chem. Technol. Biotechnol.*, 2017, **92**, 1125-1135.

57. K. Philippot, B. Chaudret, *C. R. Chim.*, 2003, **6**, 1019–1034.

58. K. M. Oliveira, R. S. Corrẻa, M. I. F. Barbosa, J. Ellena, M. R. Cominetti and A. A. Batista, *Polyhedron*, 2017, **130**, 108-114.

59. a) J. Julis, M. Hölscher, W. Leitner, *Green Chem.* 2010, **12**, 1634–1639; b) L. M. Martinez-Prieto, A. Ferry, L. Rakers, C. Richter, P. Lacante, K. Philippot, B. Chaudret, F. Glorius, *Chem. Commun.* 2016, **52**, 4768–4771.

60. H.-Y. Jiang and X.-X. Zheng, *Catal. Sci. Technol.*, 2015, **5**, 3728-3734.

61. N. Almora-Barrios, I. Cano, P. W. N. M. van Leeuwen and N. López, *ACS Catal.*, 2017, **7**, 3949-3954.

62. S. Jayakumar, A. Modak, M. Guo, H. Li, X. Hu and Q. Yang, *Chem. Eur. J.*, 2017, **23**, 7791-7797.

63. J. Julis, M. Hölscher and W. Leitner, *Green Chem.*, 2010, **12**, 1634-1639.

64. E. Bresó-Femenia, B. Chaudret and S. Castillón, *Catal. Sci. Technol.*, 2015, **5**, 2741-2751.

65. G. Bagnato, A. Figoli, C. Ursino, F. Galiano and A. Sanna, *J. Mater. Chem. A*, 2018, **6**, 4955-4965.

66. J. Tan, J. Cui, X. Cui, T. Deng, X. Li, Y. Zhu and Y. Li, *ACS Catal.*, 2015, **5**, 7379-7384.

67. Z. Zhang, J. Song, Z. Jiang, Q. Meng, P. Zhang and B. Han, *ChemCatChem*, 2017, **9**, 2448-2452.

68. L. J. Durndell, G. Zou, W. Shangguan, A. F. Lee and K. Wilson, *ChemCatChem*, 2019, **11**, 3927-3932.

69. M. Chen, Q. Dong, W. Ni, X. Zhao, Q. Gu, G. Tang, D. Li, W. Ma and Z. Hou, *ChemistrySelect*, 2017, **2**, 10537-10545.

70. V. S. Jaya, M. Sudhakar, S. N. Kumar and A. Venugopal, *RSC Adv.*, 2015, **5**, 9044-9049.

71. J. Tan, J. Cui, T.Deng, X.Cui, G. Ding, Y. Zhu and Y. Li, *ChemCatChem*, 2015, **7**, 508-512.

72. B. Y. Tay, C. Wang, P. H. Phua, L. P. Stubbs and H. V. Huynh, *Dalton Trans*. 2016, 45, 3558–3563.

73. Y. Kuwahara, W. Kaburagi and T. Fujitani, *RSC Adv.*, 2014, **4**, 45848-4855.

74. a) Z. Lin, X. Cai, Y. Fu, W. Zhu and F. Zhang, RSC Adv., 2017, 7, 44082-44088; b) Z. Lin, M. Luo, Y. Zhang, X. Wu, Y. Fu, F. Zhang and W. Zhu, *Appl. Catal. A: Gen.*, 2018, **563**, 54-63.

75. H. Yoshida, Y. Onodera, S.-I. Fujita, H. Kawamori and M. Arai, *Green Chem.*, 2015, **17**, 1877-1883.

76. a) C. Michel, J. Zaffran, A. M. Ruppert, J. Matras-Michalska, M. Jedrzejczyk, J. Grams and P. Sautet, *Chem. Commun.*, 2014, **50**, 12450-12453; (b) C. Michel and P. Gallezot, *ACS Catal.*, 2015, **5**, 4130–4132.

77. a) Y. Wang, Y. Nie, L. Wang and C. Q. Sun, *J. Phys. Chem. C*, 2010, **114**, 1226-1230; b) K. Tanaka, A. Endo, T. Hashimoto and K. Shimizu, *Surf. Sci. Spectra*, 2000, **7**, 101-113; c) L. Zeng, H. Peng, W. Liu, J. Yin, L. Xiao, J. Lu and L. Zhang, *J. Power Sources*, 2020, **461**, 228147; d) D. E. Starr and H. Bluhm, *Surf. Sci.*, 2013, **608**, 241-248; e) S. J. Kerber, J. J. Bruckner, K. Wozniak, S. Seal, S. Hardcastle and T. L. Barr, *J. Vac. Sci. Technol. A*, 1996, **14**, 1314-1320.

78. X. Jiang, Y, Wang and M. Li, *Sci. Rep.*, 2014, **4**, 6070.

Chapter 3

RuNP-Catalysed Reduction of Nitroarenes

Chapter 3 RuNP-Catalysed Reduction of Nitroarenes

3.1 Introduction

Aromatic amines (anilines) are essential intermediates in the production of additives, pharmaceuticals, agrochemicals, pigments, and dyes.[1] Even though this class of compound is available through a number of synthetic pathways, some of which include the reduction of nitriles or imines[2] and *N*-arylation[3], the reduction of nitroaromatic compounds is the most versatile and commonly used.[4] In addition, water and soils are often contaminated with nitroaromatic compounds that are toxic and are therefore detrimental to the ecosystem.[5] However there are several drawbacks to this approach which include the need for high catalyst loadings, the use of toxic reducing agents and harmful organic solvents. In addition, poor functional group tolerance, harsh reaction conditions, partial reduction of nitroaromatics to hydroxylamines, hydrazones, azoxyarenes and azoarenes and metal contamination of the product all restrict the application scope of this technology. For this reason, there is a great deal of interest in the development of selective catalysts which can operate under mild conditions in environmentally green solvents at low catalyst loadings.

In general, homogeneous metal catalysts such as Ru and Rh complexes have been employed although, the homogeneous catalytic process is commonly not accepted as the preferred route, as the recovery and reuse of the expensive metals is challenging and the majority of the reactions only proceed with the use of expensive ligands.[6-7] Heterogeneous catalysts including Pd,[8] Au,[9] and Ru[10] have several advantages over their homogeneous counterparts, such as their simple removal or recovery from the reaction mixture and recyclability. The use of metal nanoparticles stabilised by either carbon or inorganic based materials are unfolding into an efficient class of catalyst for the reduction of nitroarenes as they have demonstrated high activities and selectivities, efficient recycling and, by using continuous flow technology, they are amenable for scale-up.[11] Examples of other systems with promising reaction credentials for either hydrogenation or transfer hydrogenation of nitroaromatics include size controlled palladium nanoparticles immobilised on carbon nanospheres,[12] gold nanoparticles supported by imidazolium-based organic polymers[13] and polystyrene-stabilised ruthenium nanoparticles.[14] Other newly developed systems with promising performance profiles include ruthenium nanoparticles stabilised on nitrogen doped carbon,[15] mesoporous titanium dioxide,[16] or by phosphine functionalised ionic liquid

polymers.[17] Although some of these systems possess desirable reaction credentials, few possess all the requirements that are deemed essential for a sustainable and environmentally green process, i.e. mild conditions, short reaction times, high selectivity, low catalyst loadings, operationally straightforward procedures and efficient recyclability. Therefore, there is great opportunity and potential to develop new catalyst technologies that will address all of these issues and ultimately identify improved catalysts. An example of such a system developed by the Doherty/Knight group is based on Pd nanoparticles immobilised on a phosphine decorated PEGylated polymer which appeared to fulfil the majority of the requirements by delivering safe, environmentally sustainable and selective aqueous phase reduction of nitro groups at room temperature.[18]

Ru catalysts supported on high surface area heterogeneous supports have been recognised as promising catalysts for the reduction of nitroaromatic compounds because of their low cost and high catalytic activity.[20] However, RuNPs have a tendency to agglomerate, therefore the accessibility to their surface is often limited which can result in a poor catalytic activity and short lifetime of the catalyst.[21] This can be overcome by choosing a large surface area support material such as graphene oxide, silica or a polymer, to immobilise the RuNPs.[22] A host of highly efficient, well-dispersed RuNPs supported on a variety of supports have been reported for the selective catalytic hydrogenation of nitroarenes.[9-11, 26-31]

Scheme 3.1 shows the mechanism proposed by Haber for the reduction of nitroarenes to anilines which involves two competing pathways,[32] the direct route, (a), through the nitrosoarene and *N*-arylhydroxylamine and (b) the condensation route through the corresponding azoxyarene, azoarene, and hydrazoarene.[33]

nitro

nitroso   condensation   azoxy

$-H_2O$ H_2

$-H_2O$ $-H_2O$ H_2

hydroxylamine   azo

$-H_2O$ H_2 H_2

aniline H_2 hydrazo
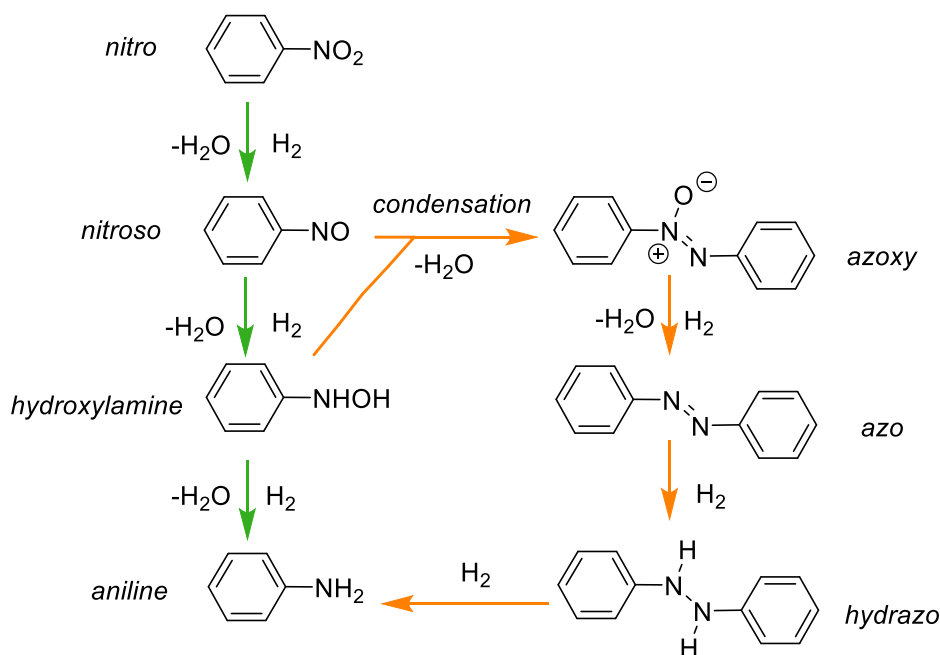
Scheme 3.1: (a) Direct (green) and (b) condensation (orange) pathways for the reduction of nitrobenzene to aniline.

The initial step involves the addition of a chemisorbed molecule of H_2 on the catalyst surface to nitrobenzene (NB) and the subsequent loss of water to afford nitrosobenzene, this rapidly accepts another H_2 equivalent to form the thermally unstable *N*-phenylhydroxylamine (*N*-PHA). In the direct pathway, the *N*-phenylhydroxylamine undergoes further hydrogenation to generate the fully reduced aniline, which is the most commonly reported pathway for Ru based catalysts.[34] However, *N*-phenylhydroxylamine can accumulate on the surface of the catalyst, which facilitates the generation of azoxybenzene (AYB) *via* a condensation between nitrosobenzene and *N*-phenylhydroxylamine. Afterwards, three further sequential hydrogenations afford azobenzene, hydrazobenzene and ultimately aniline (AN) as the final product. Overall, six possible different products can be formed under any given reaction conditions, emphasising the need to develop selective catalysts that can generate a single product in a high yield, thus avoiding challenging and financially and environmentally costly purification procedures.

Nitroarenes have been reduced using various hydrogen sources, which include sodium borohydride,[35] formic acid,[36] hydrazine,[37] molecular hydrogen[38] and pinacol.[39] Amongst them, hydrazine hydrate ($N_2H_4 \cdot H_2O$) and H_2 are recognised as the most

attractive green reducing agents,[40] Hydrogen is inexpensive, abundant and atom efficient. Hydrazine hydrate is easily handled and generates environmentally benign water and N_2 as the byproducts,[41] therefore they produce less waste in the resulting reaction mixture.[42]

There is a great incentive in industry to design more chemoselective catalysts with 'green' credentials. So far, the results presented in Chapter 2 have shown that by utilising the PIILP catalysis concept, the favourable features of ILs can be harnessed such as their functionalisation and tuneable physicochemical properties. Using ILs within a polymer immobilised ionic liquid (PIIL) enables facile catalyst separation and recovery, will minimise loss of IL and reduces the amount of IL required as the catalyst is retained in a small volume. In addition to improving the long term stability and recyclability of the NPs, incorporation of heteroatom donors into a PIIL support offers several advantages including control over nucleation of the particle and therefore control of NP size and morphology, modification of the electronic structure of the metal surface and the potential to balance the hydrophilicity of the ligand environment.[18,43] In this regard, the aim of this project was to examine the efficacy of the prepared PIIL stabilised RuNPs from Chapter 2 as catalysts for the reduction of nitroarenes.

3.2 Results and Discussion

3.2.1 Reaction Optimisation

Our initial investigation in this area demonstrated that phosphine oxide-decorated PEGylated polymer immobilised ionic liquid stabilised ruthenium nanoparticles (RuNP@(O)PPh$_2$-PEGPIIL) (See Figure 3.1) are highly active and selective catalysts for the hydrogenation of aryl ketones, aldehydes and bio-derived substrates (furfural, levulinic acid and ethyl levulinates) giving high conversions and selective reduction of the C=O double bond (see Chapter 2). It appeared to be essential to incorporate both the immobilised IL and heteroatom phosphine donor to achieve high activities and selectivities. To further explore the efficacy of RuNP@PIIL-based systems and assess whether the same properties influence their performance as catalysts in other reductions, our studies were extended to include a comparative study of the reduction of nitroarenes.
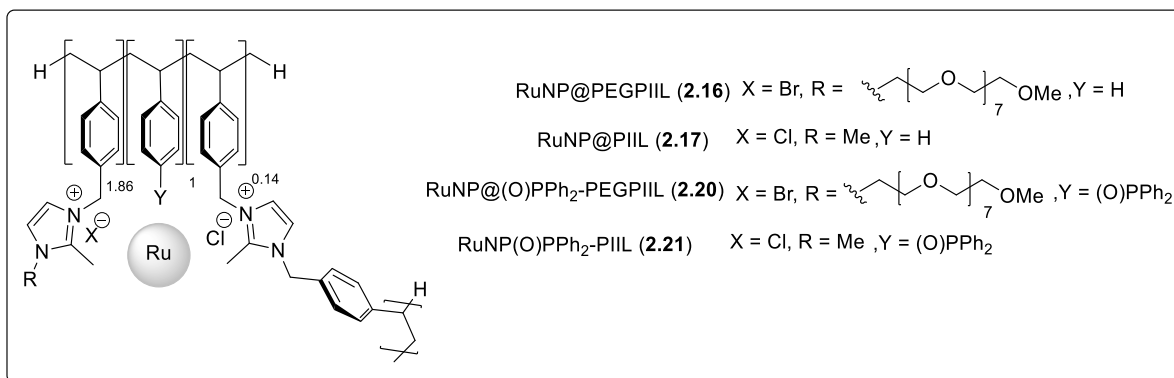
Figure 3.1: Composition of the PIIL stabilised RuNP catalysts.

A preliminary series of experiments were conducted with nitrobenzene (NB) as the benchmark substrate to examine the efficacy of **2.20** as a catalyst for the reduction of nitroarenes and undertake optimisation studies. Using literature precedent as a lead, hydrazine monohydrate was initially used as the reducing agent as it is readily available and cheap, which provided a practical scope for comparison. Firstly, to gain a more in-depth insight into the reduction of nitrobenzene, the composition of the reaction mixture was monitored as a function time based on conditions reported by Jia *et al.* (Figure 3.2).[31]
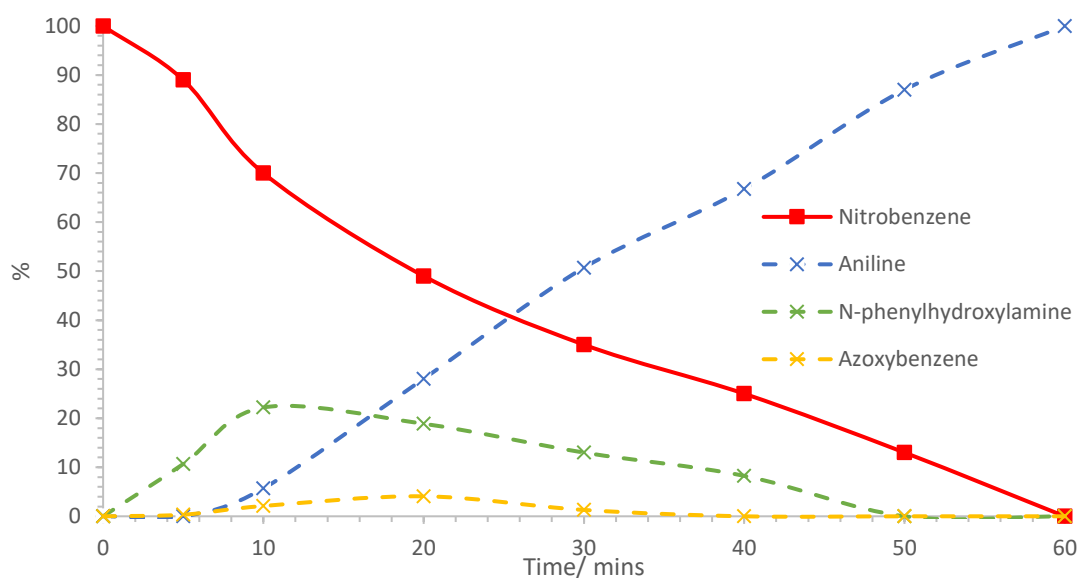
Figure 3.2: Monitoring of the catalytic hydrogenation of the reduction of nitrobenzene (NB) under N_2. Reaction conditions: 1 mmol nitrobenzene, 0.1 mol% RuNP@(O)PPh₂PEGPIILP (**2.20**), 3 mmol N_2H_4, 2 mL EtOH, RT, 5 h. Conversion and

selectivity determined by ^{1}H NMR spectroscopy with dioxane as the internal standard. Average of 3 runs. Selectivity for aniline (AN) = [% aniline / (% aniline + % *N*-phenylhydroxylamine (*N*-PHA) + % azoxybenzene (AYB))].

Figure 3.2 showed that consumption of nitrobenzene was complete after 120 minutes to give a mixture containing 70% *N*-phenylhydroxylamine, 21% aniline and 9% azoxybenzene. Longer reaction times resulted in a drop in the *N*-phenylhydroxylamine selectivity with a concomitant increase in the amount of aniline to 56%. After 5 hours, 100% conversion with 65% selectivity to aniline, 27% selectivity to *N*-phenylhydroxylamine and 8% selectivity to azoxybenzene was observed.

The consumption of nitrobenzene was then monitored as a function of reaction temperature between 0 ℃ and 40 ℃ (Figure 3.3). To avoid full conversion of nitrobenzene at higher temperatures, the reaction time was reduced to 1 hour, as 81% conversion was achieved at room temperature.
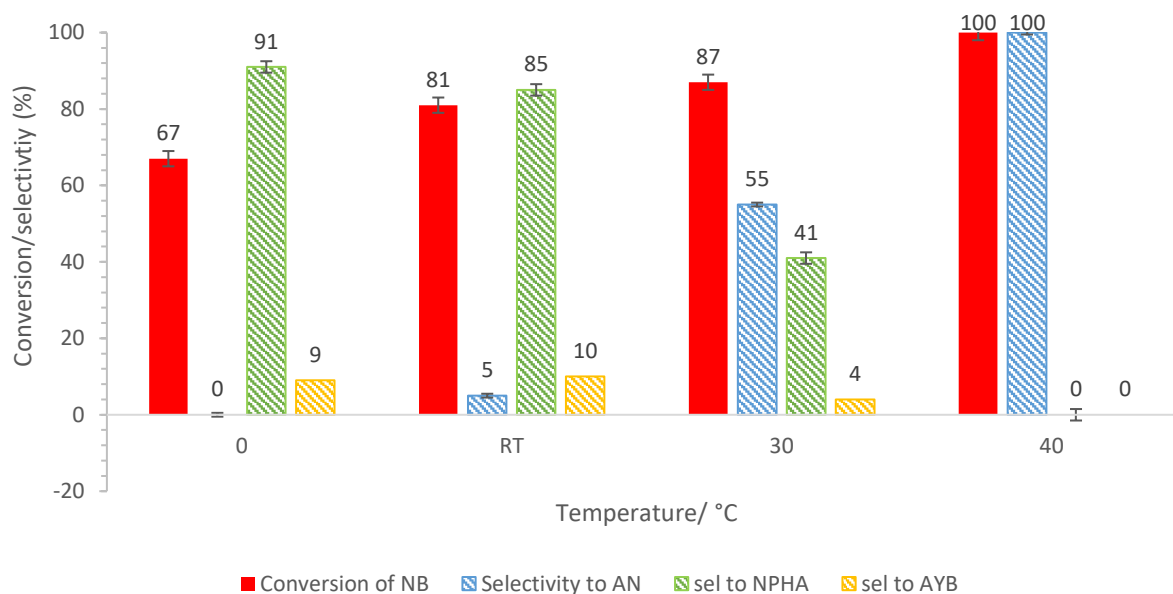
Figure 3.3: Conversion and selectivity for the reduction of nitrobenzene as a function of temperature. Reaction conditions: 1 mmol nitrobenzene, 0.1 mol% RuNP@(O)PPh$_2$PEGPIILP (**2.20**), 3 mmol N$_2$H$_4$, 2 mL EtOH, 1 h. Conversion and selectivity determined by ^{1}H NMR spectroscopy with dioxane as the internal standard. Average of 3 runs. Selectivity for aniline = [% aniline / (% aniline + % *N*-phenylhydroxylamine + % azoxybenzene)].

The conversion-selectivity profile in Figure 3.3 shows that at 0 ℃, 67% conversion of nitrobenzene and *N*-PHA with a selectivity of 91%; the only other detectable product was a minor amount of AYB. At room temperature 81% conversion was obtained to afford *N*-phenylhydroxylamine as the major product with a selectivity of 85%. When the temperature was raised to 30 ℃ reduction to aniline became dominant while at 40 ℃, the conversion of nitrobenzene was quantitative to afford aniline as the sole product after 1 hour. This indicates that enough energy is available to overcome the activation barrier for hydrogenation of *N*-phenylhydroxylamine and azoxybenzene at this temperature; these results are consistent with the literature.[34] Most of the previously reported studies operate at temperatures between room temperature and 40 °C, therefore, 40 ℃ was chosen as the optimum reaction temperature due to the short reaction time that is required to obtain a quantitative conversion to aniline.

A range of solvents were screened to establish the optimum performance of the system.
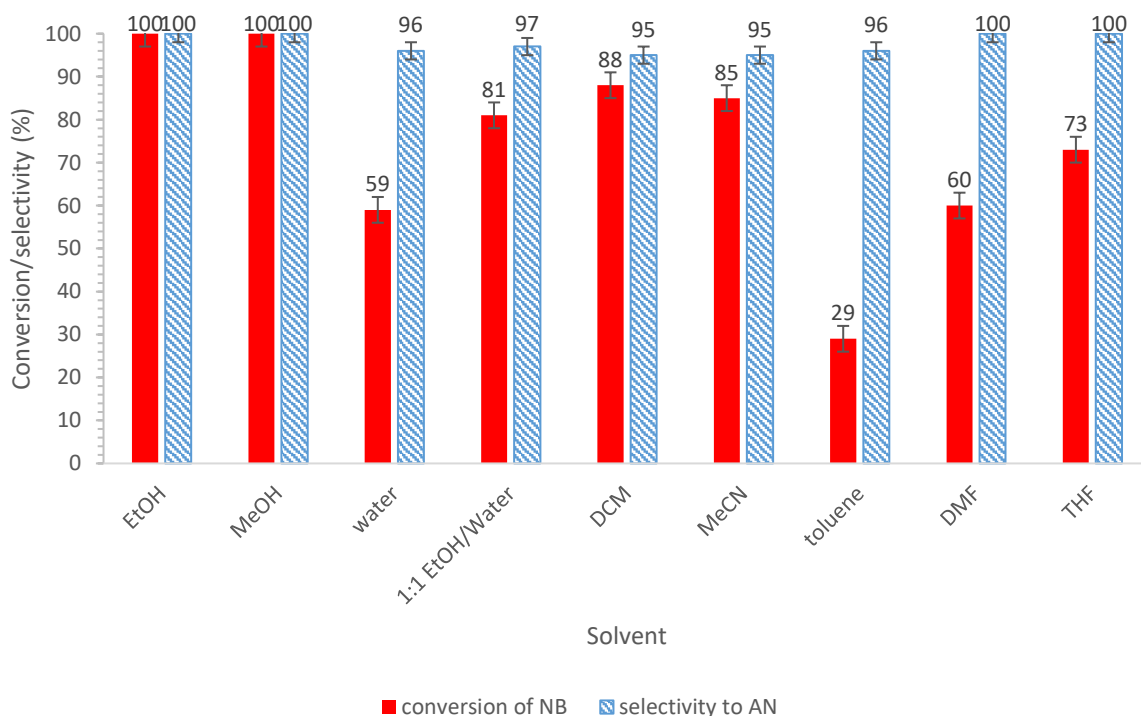
Figure 3.4: Conversion and selectivity for the reduction of nitrobenzene as a function of solvent. Reaction conditions: 1 mmol nitrobenzene, 0.1 mol%

RuNP@(O)PPh$_2$PEGPIILP (**2.20**), 3 mmol N$_2$H$_4$, 2 mL solvent, 40 ℃, 1 h. Conversion and selectivity determined by ^{1}H NMR spectroscopy with dioxane as the internal standard. Average of 3 runs. Selectivity for aniline = [% aniline / (% aniline + % *N*-phenylhydroxylamine + % azoxybenzene)].

Across all the solvents tested (Figure 3.4), aniline remained the major product and only minor amounts of *N*-phenylhydroxylamine and/or azoxybenzene (<4%) were observed as the other products. Quantitative conversion to aniline was achieved with 0.1 mol% **2.20** in protic solvents such as MeOH and EtOH at 40 ℃. The reaction in ethanol at 40 ℃ after 1 hour gave a 100% conversion and 100% selectivity for aniline. It is well-known in the literature that the use of alcohol as the solvent can significantly enhance the selectivity of this reaction.[30,31] The solubility of nitrobenzene in alcohols is much higher than that in water therefore allowing for better diffusion. Alcohols are known to interact *via* their oxygen atom to the catalyst surface, often resulting in the dissociation of the solvent molecules onto the surface which would lead to a greater coverage of the support's surface with hydrogen. A rapid rate of hydrogenation in alcohols could then be obtained through an increased hydrogen spillover effect.[44] The rich OH---N and OH---O bonding activates the polar nitro group which results in enhanced catalyst turnover and optimised selectivity due to the suppressed formation of hydroxylamine byproducts. This also activates the reaction towards the complete hydrogenation to aniline.[45] Ethanol and methanol were shown to be the optimal solvents for this catalytic system, however, the use of methanol was avoided for further applications based on its harmful effects and ethanol was preferred as it is available from biomass.

Even in water, 59% conversion with 99% selectivity for the desired aniline was achieved (after extraction of the aqueous phase with ethyl acetate); the lower conversion compared with that obtained in ethanol could be due to the poor solubility of nitrobenzene in water. However, quantitative conversion to aniline was obtained by extending the reaction time to 2 hours at 40 ℃. A reaction conducted in a 1:1 mixture of alcohol and water gave 81% conversion with 97% selectivity for aniline. Reactions performed in conventional organic solvents including dichloromethane, acetonitrile, toluene, dimethylformamide and tetrahydrofuran resulted in similar selectivities to

aniline (95-100%) although the conversions were lower in all cases. Furthermore, inert atmosphere conditions are preferred over open-air conditions as azoxyarene is usually formed *via* metal-catalysed aerobic oxidation of *N*-PHA.[46] In these reactions, high chemoselectivity for reduction of the nitro group over the benzene ring is the result of the nitro group being more reactive.

Further, the catalytic activity of **2.20** for the reduction of nitrobenzene was also examined in the presence of various reducing agents (Figure 3.5).

Figure 3.5: Conversion and selectivity for the reduction of nitrobenzene as a function of reducing agent. Reaction conditions: 1 mmol nitrobenzene, 0.1 mol% RuNP@(O)PPh$_2$PEGPIILP (**2.20**), 3 mmol reducing agent, 2 mL EtOH, 40 ℃, 1 h. Conversion and selectivity determined by ^{1}H NMR spectroscopy with dioxane as the internal standard. Average of 3 runs. Selectivity for aniline = [% aniline / (% aniline + % *N*-phenylhydroxylamine + % azoxybenzene)].

In a control experiment using 0.1 mol% **2.20** without any reductant there was no reaction, confirming that the reducing agent is the primary source of hydrogen rather than ethanol. Quantative conversion of nitrobenzene to aniline was obtained when hydrazine hydrate was used as the reducing agent in ethanol at 40 ℃. None of the other reducing agents reached complete conversion or 100% selectivity for aniline as *N*-PHA was consistently formed as a minor component. For example, using sodium borohydride in ethanol, the conversion of nitrobenzene was 80% and the selectivity to aniline was 92%. Dimethylamine borane and formic acid gave low conversions of 26% and 18% and lower aniline selectivities of 84% and 80%, respectively. A low conversion of 21% and a selectivity of 98% for aniline was obtained when the reaction was carried out in a stirred benchtop reactor under 300 psi of H_2 at 40 ℃ for 1 hour.

To determine the optimum ratio of substrate to reducing agent, several parallel reactions were performed as a function of ratio of nitrobenzene to N_2H_4 to monitor the conversion and the product distribution.
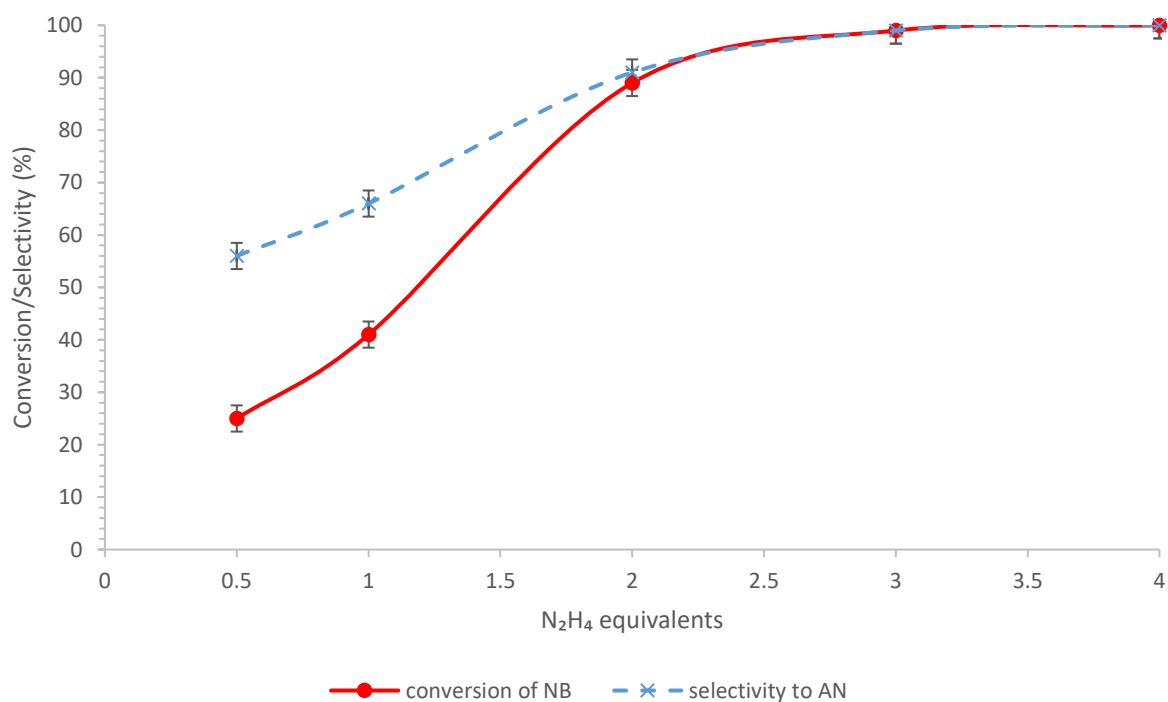
Figure 3.6: Conversion and selectivity for the reduction of nitrobenzene in the presence of varying amounts of N_2H_4. Reaction conditions: 1 mmol nitrobenzene, 0.1 mol% RuNP@(O)PPh$_2$PEGPIILP (**2.20**), 2 mL EtOH, 40 ℃, 1 h. Conversion and selectivity determined by ^1H NMR spectroscopy with dioxane as the internal standard.

Average of 3 runs. Selectivity for aniline = [% aniline / s(% aniline + % *N*-phenylhydroxylamine + % azoxybenzene)].

The profile in Figure 3.6 showed that the catalytic activity improved upon increasing the hydrazine content and reached a stable value above a hydrazine to substrate mole ratio of 3:1 to selectively make aniline.
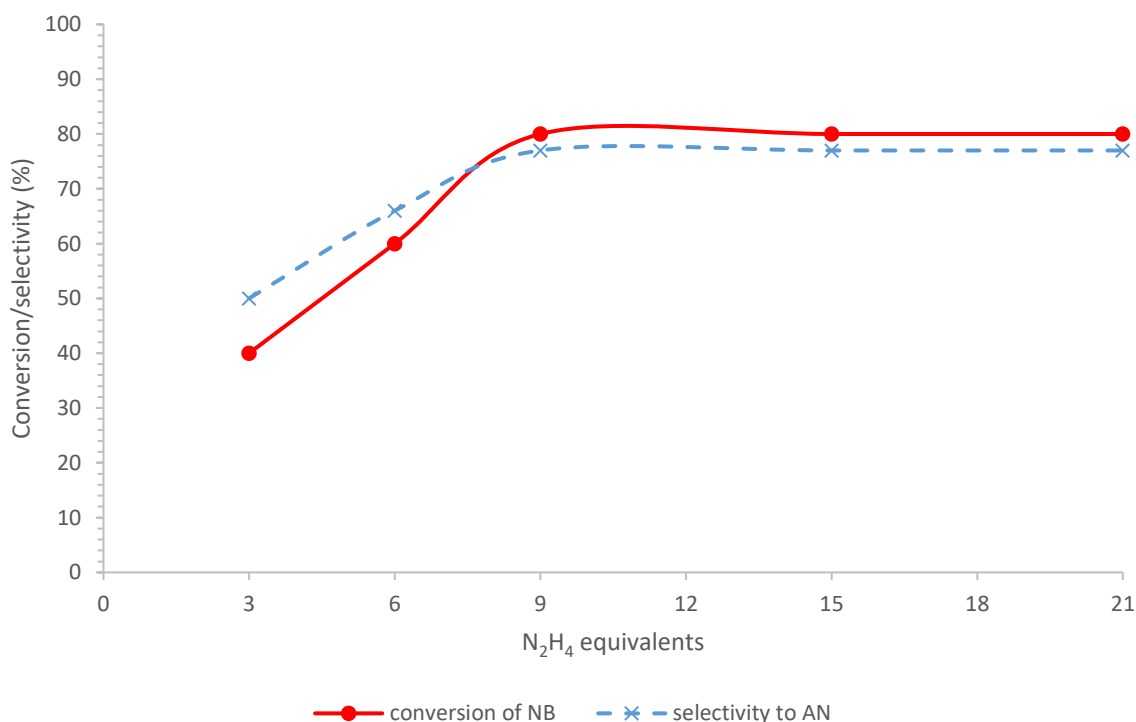
Figure 3.7: Conversion and selectivity for the reduction of nitrobenzene in the presence of varying amounts of N_2H_4. Reaction conditions: 1 mmol nitrobenzene, 0.1 mol% RuNP@(O)PPh$_2$PEGPIILP (**2.20**), 2 mL EtOH, 40 ℃, 20 mins. Conversion and selectivity determined by ^1H NMR spectroscopy with dioxane as the internal standard. Average of 3 runs. Selectivity for aniline = [% aniline / (% aniline + % *N*-phenylhydroxylamine + % azoxybenzene)].

Moreover, with an appropriate decrease in the reaction time to 20 minutes, it was shown that increasing the N_2H_4: substrate ratio from 3 to 6 resulted in an increase in conversion of 16% (Figure 3.7). The conversion continued to increase slightly above this ratio until 9 equivalents to the point where the solution is likely to be saturated with

N_2H_4. At this point, a conversion of 80% with 77% selectivity for aniline was attained after 20 minutes at 40 ℃. This profile clearly demonstrates that when the reaction uses 3 equivalents of N_2H_4 it operates under mass transfer limitations. However, given that 100% yield of aniline is achievable with 3 equivalents in 1 hour (Figure 3.6), this was carried forward for the remaining studies.

The consumption of nitrobenzene was then monitored as a function of the catalyst loading between 0.025 mol% to 0.2 mol% (Figure 3.8). To avoid the full conversion of nitrobenzene at higher catalyst loadings, the reaction time was reduced to 50 minutes as 100% conversion was achieved in 60 minutes with a catalyst loading of 0.1 mol% (Figure 3.5).

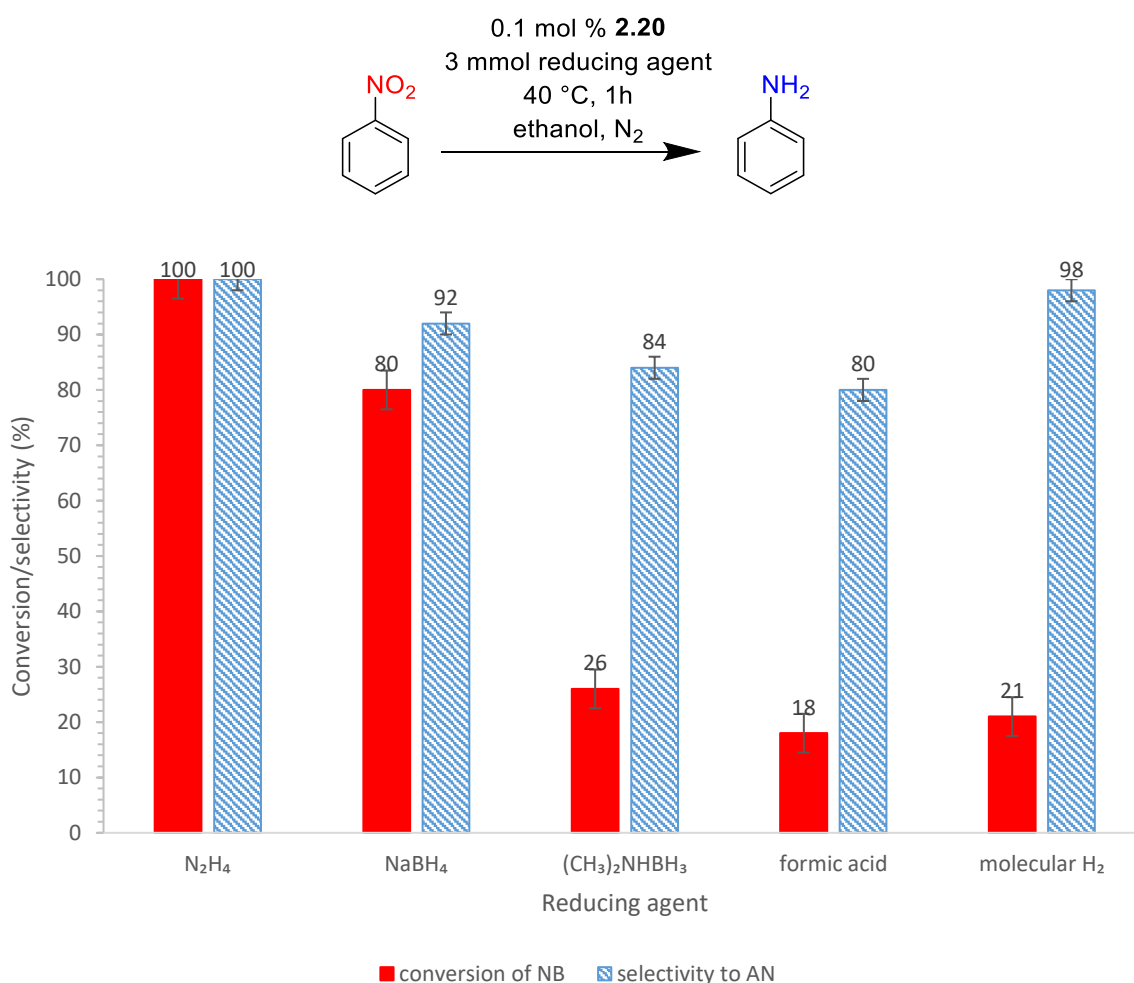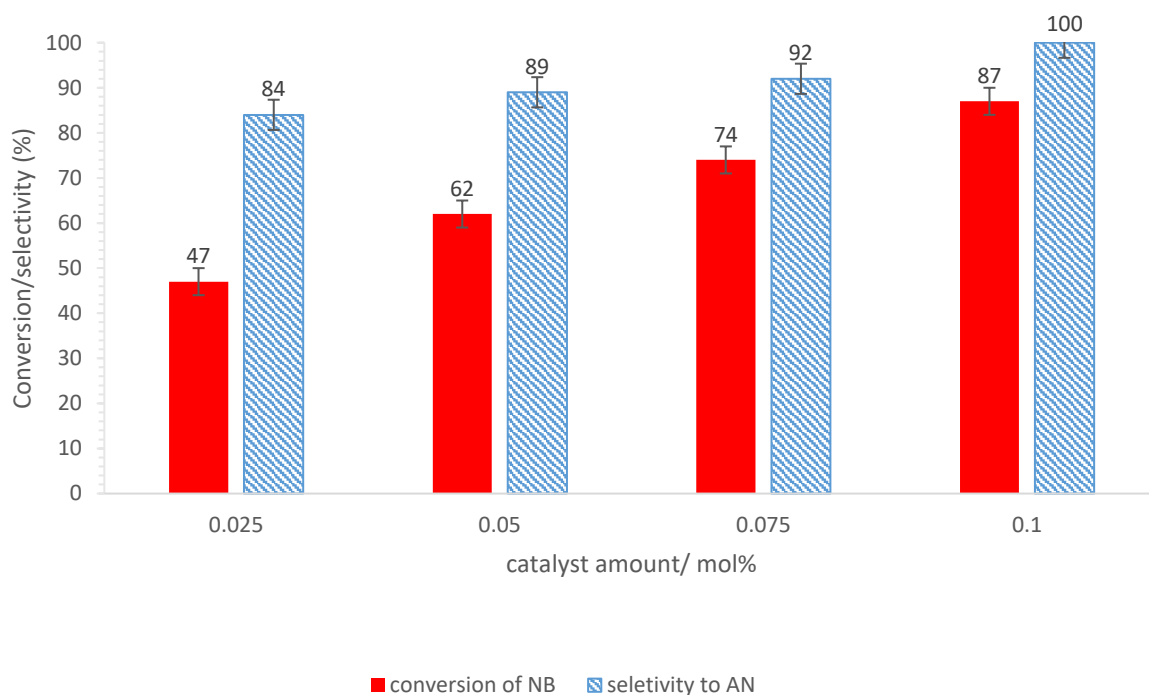**Figure 3.8:** Conversion and selectivity for the reduction of nitrobenzene as a function of temperature. Reaction conditions: 1 mmol nitrobenzene, 0.1 mol% RuNP@(O)PPh$_2$PEGPIILP (**2.20**), 3 mmol N_2H_4, 2 mL EtOH, 40 ℃, 50 mins. Conversion and selectivity determined by ^{1}H NMR spectroscopy with dioxane as the internal standard. Average of 3 runs. Selectivity for aniline = [% aniline / (% aniline + % *N*-phenylhydroxylamine + % azoxybenzene)].

In the absence of catalyst, quantitative amounts of starting material were recovered confirming the active role of the Ru catalyst. Figure 3.8 shows that a catalyst loading of 0.05 mol% gave 62% conversion and 89% selectivity to aniline after 50 minutes. When the catalyst loading was increased to 0.1 mol% the conversion increased to 87% conversion (TOF = 115 h^{-1}) with 100% selectivity for aniline, this suggests that there is enough available catalytically active sites for the complete conversion of nitrobenzene to generate aniline as the sole product. The best result for the reduction of nitrobenzene was obtained with 0.1 mol% catalyst and was taken forward as the optimum catalyst loading. Furthermore, reducing the catalyst loading to 0.01 mol % afforded aniline in 75% conversion and 89% selectivity after 16 hours, which corresponds to a TON of 6,672 and TOF of 417 h^{-1}, this is a more reasonable potential intrinsic turnover rate of the catalyst.

To gain a more in-depth insight into the reduction of nitrobenzene, the consumption was monitored as a function time at 40 ℃ (Figure 3.9).
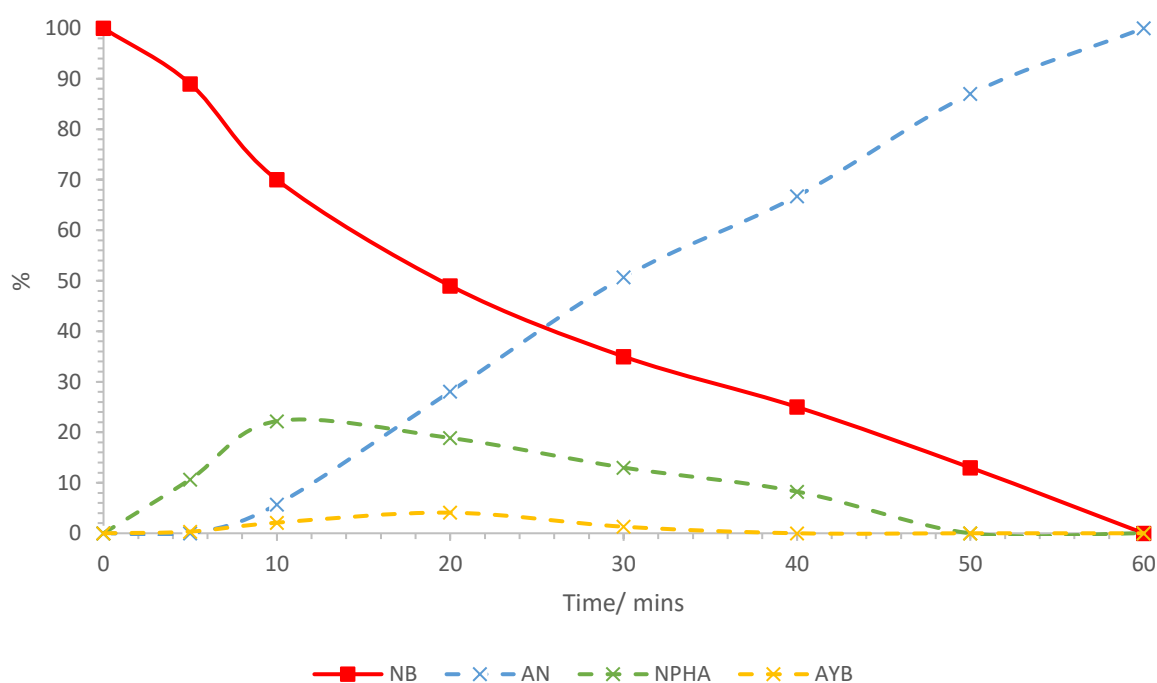
Figure 3.9: Monitoring of the catalytic hydrogenation of the reduction of nitrobenzene. Reaction conditions: 1 mmol nitrobenzene, 0.1 mol% RuNP@(O)PPh$_2$PEGPIILP (**2.20**), 3 mmol N$_2$H$_4$, 2 mL EtOH, 40 ℃, 1 h. Conversion and selectivity determined by ^{1}H NMR spectroscopy with dioxane as the internal standard. Average of 3 runs.

Selectivity for aniline = [% aniline / (% aniline + % N-phenylhydroxylamine + % azoxybenzene)].

Figure 3.9 shows the reaction profile for a reaction time of 60 minutes. Over the first 10 minutes the conversion of nitrobenzene reached 30% with high selectivity for N-PHA. After this point, complete hydrogenation to aniline dominated and it became the major component after only 20 minutes, suggesting that the rates of hydrogenation of N-PHA and nitrobenzene are comparable. The nitrobenzene present began to slowly hydrogenate and produced 19% aniline with an accumulation of N-phenylhydroxylamine; the intermediate appears to be less reactive compared to nitrobenzene. A simultaneous drop in the concentration of nitrobenzene was observed over the 50-minute period and a low level of azoxybenzene (< 5%) was also visible in the first 30 minutes of the reaction. The time study showed that complete conversion to aniline was achieved after 1 hour.

3.2.2 Catalyst Comparison

A series of batch reactions was then carried out under the optimum conditions to compare the performance of **2.20** against modifications based on RuNP@PEG-PIILP (**2.16**) , RuNP@PIILP (**2.17**), RuNP@O=PPh$_2$PIILP (**2.21**) and commercially available Ru/C in order to explore the influence of the various PIIL components.
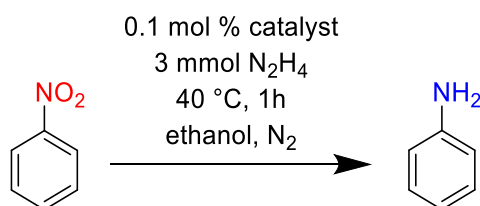
Table 3.1: Comparison of the catalytic performance for the RuNP catalysed reduction of nitrobenzene to aniline.

Entry [a]	Catalyst	Conversion (%) [b]	Selectivity (%) [b]	TOF (h^{-1})
1	Ru/C	41	66	270
2	RuNP@PEGPIILP (2.16)	90	99	891
3	RuNP@PIILP (2.17)	86	99	851
4	RuNP@(O)PPh$_2$-PEGPIIILP (2.20)	100	100	1000
5	RuNP@(O)PPh$_2$-PIIILP (2.21)	95	99	940
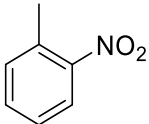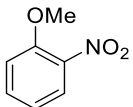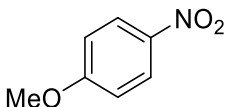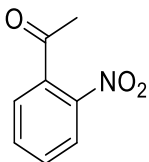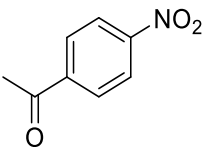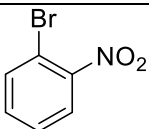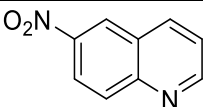
[a]Reaction conditions: 1 mmol nitrobenzene, 0.1 mol% catalyst, 3 mmol N_2H_4, 2 mL EtOH, 40 ℃, 1 h. [b]Conversion and selectivity determined by ^{1}H NMR spectroscopy with dioxane as the internal standard. Average of 3 runs. Selectivity for aniline = [% aniline / (% aniline + % *N*-phenylhydroxylamine + % azoxybenzene)].

Commercially available Ru/C only gave 41% conversion with 66% selectivity for aniline (Table 3.1, entry 1). All the PIILP systems outperformed the commercially available Ru/C (entry 2-5), with the selectivity for aniline close to 100% in all cases. As shown in Table 3.1 the best reaction outcome was obtained with **2.20** (entry 4). The selective removal of the PEG resulted in a decrease in TOF from 1,000 h^{-1} for **2.20** to 940 h^{-1} for **2.21**, which most likely indicates an improvement in dispersibility for the PEG-based system, since the mean diameters of both NP systems are similar. Interestingly, the selective removal of the PPh$_2$ also resulted in a considerable drop in catalytic activity to 891 h^{-1} for **2.16**. As PEG-based systems are expected to be alcohol and water soluble and highly dispersed, the lower activity of the catalyst could be due to the weaker metal-support interactions (SMSI). Larger metal nanoparticles have less SMSI effect compared to smaller metal nanoparticles[47] and therefore the high catalytic activity of **2.20** could be due to its smaller size (1.34 $\pm$ 0.30 nm) compared with **2.21** (2.61 $\pm$ 0.31 nm). As it is clear that each component has a direct effect on catalyst performance further studies will be required in order to determine the role of the heteroatom donor i.e. whether it controls NP size, formation and/or surface properties or alters catalyst solubility and dispersibility.

3.2.3 Substrate screening

The optimised conditions were applied to a range of substituted nitroarenes and a nitro heteroarene to examine the scope of **2.20**.

Table 3.2: Reduction of various substituted nitroarenes catalysed by **2.20**.

Entry [a]	Substrate	Time (mins)	Conversion [b] (%)	Selectivity [b] (%)
1		90	84	100
2		90	86	100
3		60	99	100
4		90	85	100
5		60	99	100
6		300	92	100
7		100	93	100

[a]Reaction conditions: 1 mmol substate, 0.1 mol% **2.20**, 3 mmol N_2H_4, 2 mL EtOH, 40 °C. [b]Conversion and selectivity calculated by ^1H NMR spectroscopy using dioxane as the internal standard, average of 3 runs.

The data presented in Table 3.2 show that **2.20** is an efficient catalyst for the reduction of a range of functionalised nitroarenes giving the corresponding amine as

the sole product in excellent yields (see Appendix H for spectra). Nitroarenes with nonreducible, electron donating groups such as –CH$_3$ (nitrotoluene) and -OCH$_3$ (nitroanisole) were converted into the corresponding aniline in excellent yields (84-99%) in 1 hour (entries 1–3). In addition, **2.20** is functional group tolerant as it catalysed the reduction of substrates substituted with reducible electron withdrawing groups and gave the corresponding aniline with complete chemoselectivity and in high yields (entries 4 and 5). Sterically demanding substrates required slightly longer reaction times to reach the same conversion as their 4-substituted counterparts (entries 2 and 3). Surprisingly, it was found that 1-bromo-2-nitrobenzene (entry 6) could be reduced to the corresponding amine in a near-quantative yield with no evidence of competing hydrodehalogenation, this is an important transformation as haloaromatic amines are important chemical intermediates that are widely used in the synthesis of dyes, herbicides, pesticides and drugs.[29] The same protocol was applied to the reduction of 6-nitroquinoline which gave quinoline-6-amine in 92% yield after only 100 minutes (entry 7). This result is usual as there are only a couple of reports for the reduction of nitro-substituted heteroaromatics catalysed by RuNP-based systems; typically requiring high catalyst loadings, reaction temperatures as high as 80 °C in addition to long reaction times.[15,25]

3.2.4 Recycling

With the aim of exploring and assessing the stability profile of **2.20** recycle studies on the selective reduction of nitrobenzene to aniline were conducted. As good conversions and high selectivties were obtained for the selective reduction in methanol, ethanol and water, initial recycle experiments were performed in water, on the basis that the use of an aqueous phase would facilitate catalyst and product separation and recovery *via* a facile extraction protocol. Each cycle was performed for 90 minutes after which the products and unreacted nitrobenzene were extracted with ethyl acetate and the reaction mixture analysed by ^{1}H NMR spectroscopy to quantify the extent of conversion and selectivity. After extraction, the flask was further charged with one equivalent of nitrobenzene and 3 equivalents of N$_2$H$_4$ and the reaction repeated.
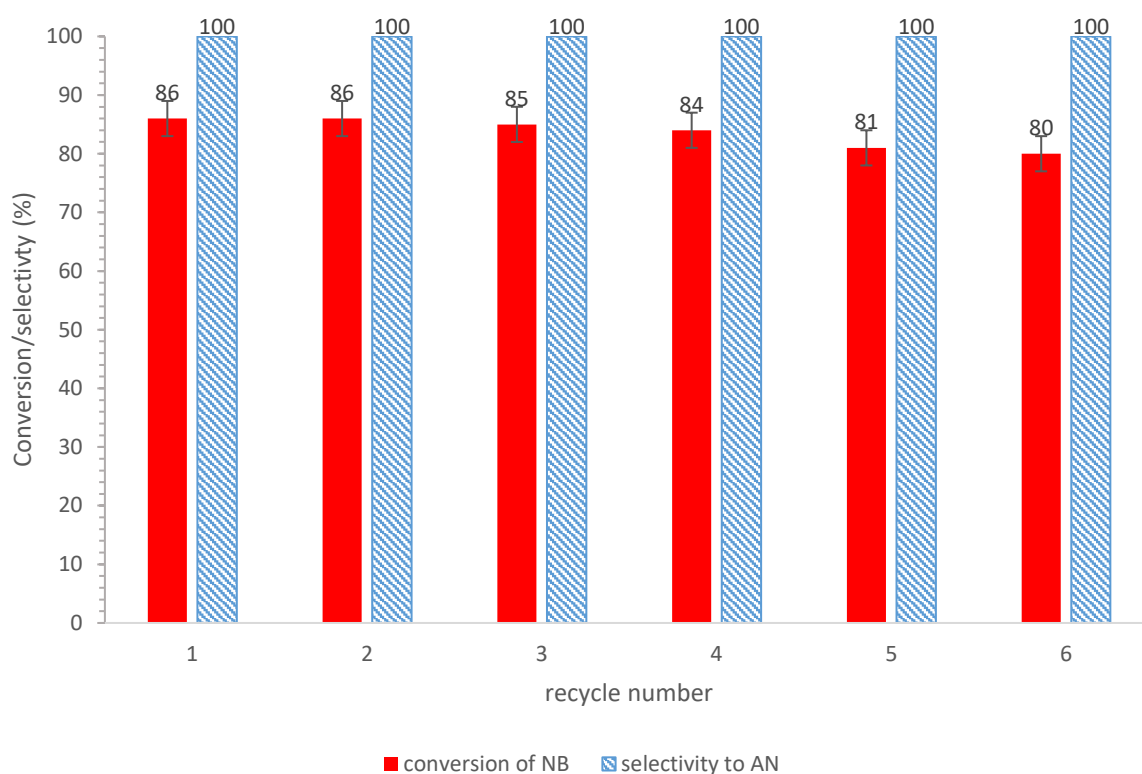
Figure 3.10: Recycling profile for the reduction of nitrobenzene catalysed by **2.20**. [a] Reaction conditions: 1 mmol nitrobenzene, 0.1 mol% RuNP@(O)PPh$_2$PEGPIILP (**2.20**), 3 mmol N$_2$H$_4$, 2 mL H$_2$O, 40 ℃, 90 mins. [b]Conversion and selectivity determined by ^{1}H NMR spectroscopy with dioxane as the internal standard. Average of 3 runs. Selectivity for aniline = [% aniline / (% aniline + % *N*-phenylhydroxylamine + % azoxybenzene)].

Figure 3.10 shows that **2.20** has a stable activity profile and that the catalyst can be efficiently recycled and reused 6 times with only minor reduction in the yield of aniline. The conversion decreased slightly from 86% in the first cycle to 80% in the sixth cycle, while the selectivity for aniline was maintained at 100 %. The activity remained constant for the first three runs and then gradually decreased during runs 3-6. ICP analysis on the combined organic extracts confirmed that leaching was negligible (<0.2 ppm). The gradual loss in catalyst activity could be due to adhesion of the catalyst to the glassware during the separation and recovery procedure as only a small amount of catalyst is used (*ca.* 5 mg) and therefore a small loss would result in a significant reduction in the Ru content. Continuous flow would allow the efficacy of **2.20** for the reduction of nitroarenes under mild conditions to be investigated and this

should allow for straightforward product separation, overcoming any catalyst loss problems and in addition allow the process to be amenable to scale-up.

3.3 Conclusion

Catalyst **2.20** is highly active for the selective reduction of nitrobenzene to generate aniline in high yields at 40 ℃ in ethanol. Sampling of the reaction demonstrated that reduction most likely occurs *via* the direct route as *N*-PHA appeared as the major intermediate. The selective reduction of a series of substituted nitroaromatic substrates with different electronic and steric properties using hydrazine hydrate as the reducing agent showed that **2.20** gave good conversions to the corresponding aniline with exclusive chemoselectivity for reduction of the nitro group. Differences in catalyst efficacy resulting from selective changes of the support have been attributed to altering the balance of hydrophobicity/ hydrophilicity which affects catalyst dispersibility and facilitates substrate access to the active site. It is not yet possible to completely deconvolute how each component influences catalyst performance, for example, solubility, dispersibility, NP size and surface modification, this study showed that both PEG and phosphine components are necessary in order to achieve optimum catalyst efficiency.

Promising batch recycle studies showed that the catalyst could be separated using a straightforward extraction procedure and reused several times with only a slight loss in activity over six runs. The catalytic process is environmentally friendly as only water and nitrogen are produced as waste and economically advantageous due to the low-cost reagents and high process efficiency. This may therefore be of significant industrial importance as a sustainable approach for the large-scale synthesis of value-added anilines, therefore the next steps would be to apply the RuNP catalyst systems under continuous flow operation.

3. 4 References

1. G. Sabbioni and E. Richter, *Toxicology*, 1999, 729-741.

2. a) N. Gandhamsetty, J. Jeong, J. Park, S. Park and S. Chang, *J. Org. Chem.*, 2015, **80**, 7281-7287; b) K. Müther, J. Mohr and M. Oestreich, *Organometallics.*, 2012, **32**, 6643-6646.

3. Y. Chi, Y.-G. Zhou and X. Zhang, *J. Org. Chem.*, 2003, **68**, 4120-4122.

4. a) Q. Xiao, S. Sarina, E. R. Waclawik, J. Jia, J. Chang, J. D. Riches, H. Wu, Z. Zheng and H. Zhu, *ACS Catal.*, 2016, **6**, 1744-1753; b) X. Chen, Q. Shen, Z. Li, W. Wan, J. Chen and J. Zhang, *ACS Appl. Mater. Interfaces*, 2020, **12**, 654-666; c) H. Yu, W. Tang, K. Li, S. Zhao, H. Yin and S. Zhou, *ACS Appl. Mater. Interfaces*, 2019, **11**, 6958-6969; d) S. M. Kelly and B. H. Lipshutz, *Org. Lett.*, 2014, **16**, 98-101; e) P. S. Rathore, R. Patidar, T. Shripathi and S. Thakore, *Catal. Sci. Technol.*, 2015, **5**, 286-295.

5. J. D. Rodgers and N. J. Bunce, *Water Res.*, 2001, **35**, 2101-2111.

6. N. Marozsán, H. Horváth, A. Erdei and F. Joó, *J. Mol. Catal. A*, 2016, **425**, 103-109.

7. P. P. Sarmah and D. K. Dutta, *Appl. Catal. A*, 2014, **470**, 355-360.

8. a) J. Tuteja, S. Nishimura and K. Ebitani, *RSC Adv.*, 2014, **4**, 38241-38249. b) D. Zhang, F. Ye, T. Xue, Y. Guan and Y. Wang, *Catal. Today*, 2014, **234**, 133-138.

9. a) N. Perret, X. Wang, T. Onfroy, C. Calers and M. A. Keane, *J. Catal.*, 2014, **309**, 333-342. b) D. Wang and D. Astruc, *Chem. Rev.*, 2015, **115**, 6621-6686.

10. a) Y. Gao, S. Jaenicke and G. Chuah*, Appl. Catal. A*, 2014, **484**, 51-58. b) R. B. N Baig and R. S. Varma, *ACS Sustainable Chem. Eng.*, 2013, **1**, 805-809.

11. a) V. Heeesel, D. Kralisch, N. Kockmann, T. Noel and Q. Wang, *ChemSusChem*, 2013, **6**, 746–789; b) T. Noel and S. L. Buchwald, *Chem. Soc. Rev.*, 2011, **40**, 5010–5029.

12. Y.-M. Lu, H.-Z. Zhu, W.-G. Li, B. Hu and S.-H. Yu, *J. Mater. Chem. A*, 2013, **1**, 3783–3788.

13. Y. Su, X. Li, Y. Wang, H. Zhong and R. Wang, *Dalton Trans.*, 2016, **45**, 16896–16903.

14. J. H. Tyler, S. H. Nazari, R. H. Patterson, V. Udumula, S. J. Smith and D. J. Michaelis, *Tetrahedron Lett.*, 2017, **58**, 82-86.

15. H. Zhong, Y. Gong, W. Liu, B. Zhang, S. Hu and R. Wang, *Dalton Trans.*, 2019, **48**, 2345-2351.

16. U. Mandi, N. Salam, S. K. Kundu, A. Bhaumik and S. M. Islam, *RSC Adv.*, 2016, **6**, 73440-73449.

17. X. Cia, J. Nie, G. Yang, F. Wang, C. Ma, C. Lu and Z. Chen, *Mater. Lett.*, 2019, **240**, 80-83.

18. S. Doherty, J. Knight, T. Backhouse, A. Bradford, F. Saunders, R. A. Bourne, T. W. Chamberlain, R. Stones, A. Clayton and K. Lovelock, *Catal. Sci. Technol.*, 2018, **8**, 1454-1467.

19. H.-U. Blaser, H. Steiner and M. Studer, *ChemCatChem*, 2009, **1**, 210-221.

20. J. Zhao, H. Yuan, J. Li, W. Bing, Y. Liu, J. Chen, C. Wei, L. Zhou and S. Fang, *ACS Omega,* 2020, **5**, 12, 7011-7017.

21. Z. Cui, Y. Guo, Z. Feng, D. Xu and J. Ma, *New J. Chem.*, 2019, **43**, 4377-4384.

22. K. X. Yao, X. Liu, Z. Li, C. C. Li, H, C. Zeng and Y. Han, *ChemCatChem*, 2012, **4**, 1938-1942.

23. K. Taniguchi, X. Jin, K. Yamaguchi and N. Mizuno, *Catal. Sci, Technol.*, 2016, **6**, 3929-3937.

24. L. Liu and A. Corma, *Chem. Rev.*, 2018, **118**, 4981-5079.

25. A. I. Carrillo, K. G. Stamplecoskie, M. L. Marin and J. C. Scaiano, *Catal. Sci. Technol.*, 2014, **4**, 1989-1996.

26. W.-G. Jia, T. Zhang, D. Xie, Q.-T. Xu, S. Ling and Q. Zhang, *Dalton Trans.*, 2016, **45**, 14230-14237.

27. N. M. Patil, T. Sasaki and B. M. Bhanage, *RSC Adv.*, 2016, **6**, 52347-52352.

28. W.-G. Jia, H. Zhang, T. Zhang, S. Ling, *Inorg. Chem. Commun.*, 2016, **66**, 15-18.

29. Q. Wei, Y.-S. Shi, K.-Q. Sun and B.-Q. Xu, *Chem. Commun.*, 2016, **52**, 3026–3029.

30. R. Nandhini, B. S. Krishnamoorthy and G. Venkatachalam, *J. Organomet. Chem.*, 2019, **903**, 120984.

31. W.-G. Jia, M.-X. Cheng, Q.-T. Xu, L.-L. Gao and G. Yuan, *Polyhedron*, 2018, **153**, 69-75.

32. a) P. Serna and A. Corma, *ACS Catal.*, 2015, **5**, 7114-7121; b) E. A. Gelder, S. D. Jackson and C. M. Lok, *Chem. Commun.*, 2005, 522-524; c) A. Mahata, R. K. Rai, I.Choudhuri, S. K. Singh and B. Pathak, *Phys. Chem. Chem. Phys.*, 2014, **16**, 26365-26374.

33. K. Gupta, R. K. Rai and S. K. Singh, *ChemCatChem*, 2018, **10**, 2326-2349.

34. S.-C. A. Lin, Y.-H. Liu, S.-M. Peng and S.-T. Liu, *Mol. Catal.*, 2019, **466**, 46-51.

35. S. P. Jr, D. M. Cedillo, C. Tamez, N. Izquierdo, J. G. Parsons and J. J. Gutierrez, *Tetrahedron Lett.*, 2014, **55**, 5468-5470.

36. K. Chaiseeda, S. Nishimura and K. Ebitani, *ACS Omega*, 2017, **2**, 7066-7070.

37. D. Cantillo, M. M. Moghaddam and C. O. Kappe, *J. Org. Chem.*, 2013, **78**, 4530-4542.

38. X. Lu, Y. Chen, Z. Zhao, H. Deng, D. Zhou, C. Wei, R. Nie and Q. Xia, *RSC Adv.*, 2016, **6**, 15354-15361.

39. N. García, P. García-García, M. A. Fernández-Rodríguez, R. Rubio, M. R. Pedrosa, F. J. Arnáiz and R. Sanz, *Adv. Synth. Catal.*, 2012, **354**, 321-327.

40. a) X. Sun, A. I. Olivos-Suarez, D. Osadchii, M. J. V. Romero, F. Kapteijn and J. Gascon, *J. Catal.*, 2018, **357**, 20-28; b) M. Tian, X. Cui, K. Liang, J. Ma and Z. Dong, *Inorg. Chem. Front.*, 2016, **3**, 1332-1340.

41. a) S. Cai, H. Duan, H. Rong, D. Wang, L. Li, W. He and Y. Li, *ACS Catal.*, 2013, **3**, 608-612; b) G. Wienhöfer, M. Baseda-Krüger, C. Ziebart, F. A. Westerhaus, W. Baumann, R. Jackstell, K. Junge and M. Beller, *Chem. Commun.*, 2013, **49**, 9089-9091.

42. N. García, P. García-García, M. A. Fernández-Rodríguez, R. Rubio, M. R. Pedrosa, F. J. Arnáiz and R. Sanz, *Adv. Synth. Catal.*, 2012, **354**, 321-327.

43. S. Doherty, J. G. Knight, T. Backhouse, R. J. Summers, E. Abood, W. Simpson, W. Paget, R. A. Bourne, T. W. Chamberlein, R. Stones, K. R. J. Lovelock, J. M. Seymour, M. A. Isaacs, C. Hardacre, H. Daly and N . H. Rees, *ACS Catal.*, 2019, **9**, 4777-4791.

44. J. Zawadzki, B. Azambre, O. Heintz, A. Krzton and J. Weber, *Carbon*, 2000, **38**, 509-515.

45. a) J. B. F. N. Engberts and M. J. Blandamer, *Chem. Commun.*, 2001, 1701-1708; b) M. Jorge, M. Natalia, D. S. Cordeiro and N. A. Seaton, *J. Phys. Chem. C.*, 2007, **111**, 17612-17626; c) X. C. Meng, H. Y. Cheng, S. Fujita, Y. C. Yu, F. Y. Zhao and M. Arai, *Green Chem.*, 2011, **13**, 570-572.

46. S. S. Acharyya, S. Ghosh and R. Bal, *ACS Sustainable Chem. Eng.*, 2014, **2**, 584-589.

47. F. Jiang, J. Cai, B. Liu, Y. Xu and X. Liu, *RSC Adv.*, 2016, **6**, 75541-75551.

Chapter 4

Brønsted Acid Ionic Liquid Catalysed Alcoholysis of Furfuryl Alcohol

Chapter 4 Brønsted Acid Ionic Liquid Catalysed Alcoholysis of Furfuryl Alcohol

4.1 Introduction

By 2030, the US government and the European Union aim to produce 20% of their fuels and 25% of their chemicals from sustainable, renewable resources in an effort to reduce the reliance on non-renewable and diminishing resources, such as fossil fuels.[1] As a result, renewable biomass as a fuel source and in the production of chemicals has become appealing to the research community.[2] Several approaches have been employed to convert renewable biomass which are abundant, cost-effective and sustainable into chemicals and transportation fuels. However, in general the conversion of biomass has common issues of low conversion rates, harsh reaction conditions and low selectivities which limits the development and implementation of such processes; there is therefore an urgent demand for these issues to be solved.[3] As a result, how to obtain the efficient conversion of biomass resources has turned into a topic of great interest in recent years. One conversion of particular interest is the acid hydrolysis of cellulose, an abundant biomass component which yields, including other products, furfural (FF), a chemical intermediate with an average annual demand of 200 kt.[4]

Furfuryl alcohol (FFA) is usually made by the reduction of furfural (FF) over copper-based catalysts[5] and can be used in the production of alkyl levulinates (AL) due to its availability from alcoholysis reactions.[6] Alkyl levulinates from biomass-derived chemicals have potential applications in the transportation fuel sector and in the fine chemical industry.[7] In 2004, ALs were identified as one of the top 10 biorefinery candidates.[8] ALs are comprised of two functional groups, an ester and a ketone group which makes them good precursors and/or building blocks for chemical synthesis. These ALs have wide-ranging applications such as, a blending agent for the flavouring and fragrance industries, plasticising agents, chemical and drug synthesis and as green solvents due to their lower vapour pressures in comparison to conventional solvents which are often volatile.[9,10]

An attractive feature of ALs is their fuel additive properties. They can be considered as second generation oxygenates, they increase the oxygen content in gasoline to burn more efficiently and minimises the release of harmful gases.[11] Ethyl,

butyl and alkyl levulinates can be added directly to diesel fuel as they are miscible, this minimises the swelling of the engine and enhances the fuel performance of cotton-seed derived biodiesel.[12-14] Among the potential ester candidates, ethyl levulinate (EL) and butyl levulinate (BL) are the most studied.[15] Although the synthesis of EL has been widely studied, the work on BL in the open literature is more scarce, even though it is a more promising fuel additive for diesel. BL improves the conductivity, lubricity, cold-flow properties and reduces the vapour pressure of diesel fuel when it is blended and produces a cleaner combustion process with significantly lower smoke and nitrogen dioxide emissions.[16-17]

The various applications of ALs have caused their synthesis to become more appealing in the recent decade. It is well-known that acid catalysts, in particular the amount and the strength of the acid, are important factors in the production of ALs.[18] ALs can be synthesised *via* direct and indirect routes shown in scheme 4.1.
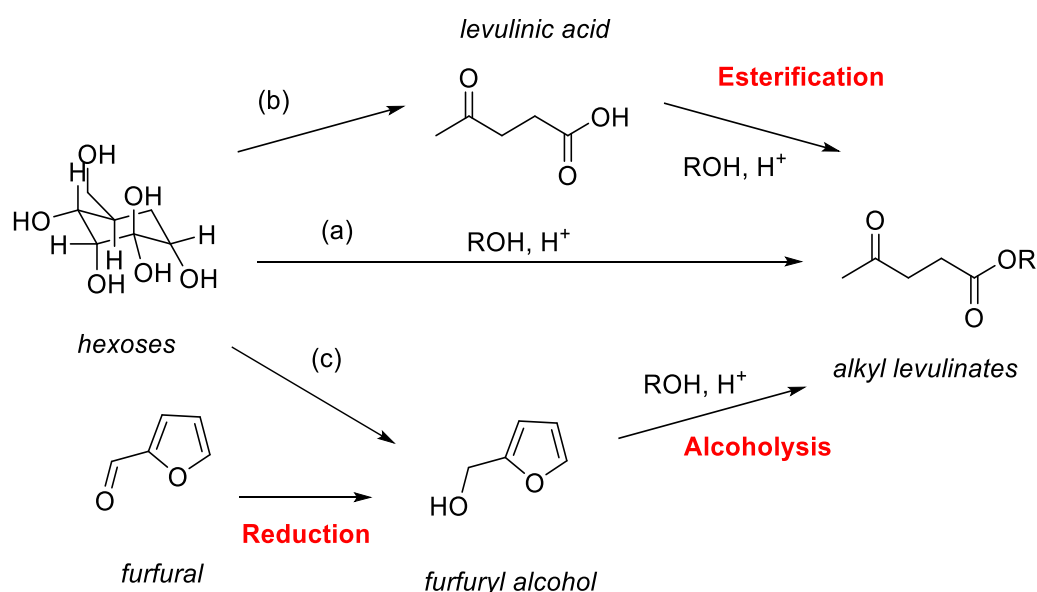
Scheme 4.1: (a) Direct and (b-c) indirect pathways for the generation of alkyl levulinates from biomass-derived compounds.

In the direct synthesise route (a), a carbohydrate for example hexose, glucose, hemicellulose or cellulose is converted into ALs in the presence of an alcohol and an acid catalyst. Even though this route is economical, time-saving and efficient for

biomass conversion, it is corrosive to reactors and potentially is harmful to the environment. To improve on these drawbacks, two alternative indirect routes (b-c) have been developed. In the industrial sector, ALs are primarily obtained by the first route, (b), *via* acid-catalysed esterification of levulinic acid (derived from cellulose) with an alcohol in the presence of an acid catalyst. Currently, increasing attention is being focused on the second route, (c), which involves the acid-catalysed alcoholysis of furfuryl alcohol with other alcohols.[19,20] The conversion of FFA to AL demonstrates good atom economy and facile product separation[21] therefore, FFA is widely accepted as the better substrate for the synthesis of ALs. In addition, regarding the chemical statistics, FFA is oversupplied and not fully exploited in the chemical market.[22,23] Hence, it is essential to develop efficient new approaches to convert low-value FFA into high-value ALs and therefore this part of the thesis will solely focus on assessing prepared acid-catalysts to be used in this capacity.

Conventionally, in the synthesis of ALs, mineral acids such as H_2SO_4, H_3PO_4, and HF are employed as inexpensive homogeneous catalysts.[24] Adversely, these homogeneous acids are extremely corrosive to the reactors and equipment, require neutralisation, are difficult to separate from the reaction mixture and are environmentally unfriendly.[25] To circumvent the use of these conventional acids a range of heterogeneous acid catalysts have been produced as a greener approach for the synthesis of ALs (Figure 4.1).
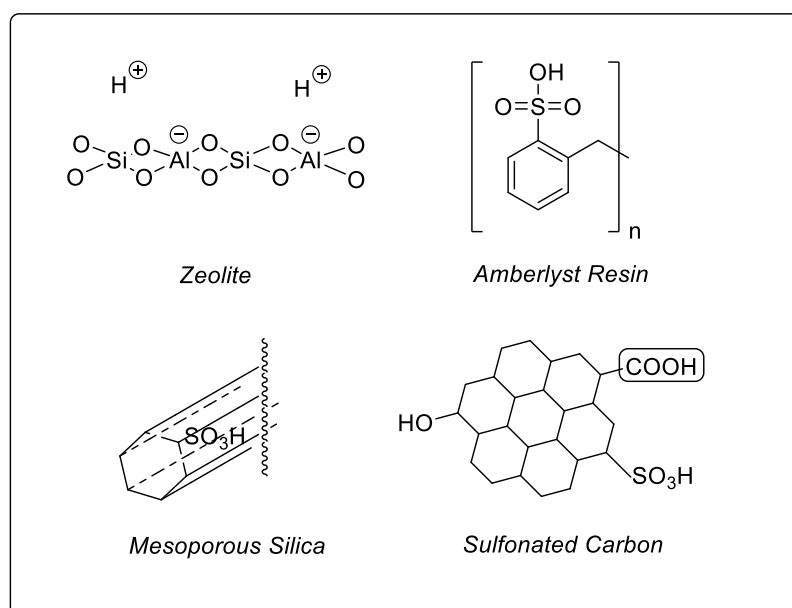
Figure 4.1: Common examples of solid acid catalysts bearing Brønsted acid sites.

For example, zirconia bifunctionalised organosilica-modified heteropoly acid (HPA),[26] organosulfuric-acid functionalised organosilica hollow nanopsheres,[27] SO_3H-functionalised ionic liquids (SFILs),[28] acidic ion exchange resin,[29] graphene oxide[30] and zeolites[31] have been designed as catalysts for the synthesis of ALs. Amongst them, HPAs have exhibited excellent catalytic performance in a wide range of acid-catalysed reactions owing to their well-defined Keggin ($XY_xM_{(12-x)}O_{40}$) or Dawson ($X_2M_{18}O_{62}$) structures, low corrosiveness, widely tuneable acidity, reusability and reproduceability.[32] In addition, HPAs in particular phosphotungstic acid which is a super acid, have Brønsted acidity and high thermal stabilities (570– 620 K).[34,35] However, reports on the HPA-catalysed alcoholysis of FFA are limited and primarily focus on the conventional phosphotungstic acid ($H_3PW_{12}O_{40}$) and its derivatives.[33] All of the above mentioned catalysts exhibited good activities, selectivities and stability in the alcoholysis of FFA. Nevertheless, many of these catalysts involve high costs, tedious multi-step preparations and difficult catalyst recoveries.

Pagilaro and co-workers examined the catalytic condensation of FFA with 1-butanol to produce butyl levulinate.[36] Propylsulfonic acid-functionalised mesoporous silica proved to be more efficient than state-of-the-art phosphotungstic acid (PTA) catalysts. The catalyst gave 96% yield with 100% selectivity to butyl levulinate after only 4 hours compared to 75% yield and 95% selectivity with the PTA system. The reaction profiles of the before and after hot filtration test confirmed that the active catalytic species did not leach into the solution.[36] Strong Brønsted acid SFILs were initially reported as the competing acid catalysts compared to the conventional acid catalysts as they are recyclable, flexible and can act as the solvent and as a catalyst.[37] As a result, the use of recoverable SFILs has great environmental and economic benefits. Song and co-workers reported that SFILs catalysed the alcoholysis of FFA to ALs and gave yields of 95% in 2 hours.[38] In a recent report Lange and co-workers obtained excellent yields of ethyl levulinate from the ethanolysis of FFA using several solid acid catalysts such as zeolites and acidic ion-exchange resins.[39]

In the last couple of years, organic-inorganic hybrid materials have attracted great attention as a result of the versatility of both their organic and their inorganic groups.[40] One example of such a hybrid material is methylimidazolebutylsulfate phosphotungstate ($[MIMBS]_3PW_{12}O_{40}$) derived from a conventional ionic liquid by replacement of a counter anion, such as BF_4^- or Cl^-, by a Keggin heteropoly anion.

Wang and co-workers developed a novel phosphotungstate-functionalised catalyst and applied this to the esterification of citric acid with *n*-butanol which displayed excellent catalyst performance.[41]

The acid-catalysed ethanolysis of FFA is widely known.[42,43] Relative to this, publications on the butanolysis of FFA are scarce. One report which outlines using a solid acid catalyst for the conversion of FFA into ALs by Zhang and co-workers showed that 5 mol% of methylimidazolebutylsulfate phosphotungstate gave 93% yield of *n*-butyl levulinate in 12 hours.[44] Kamaraju *et al.* prepared an efficient catalyst for the alcoholysis of FFA in batch and continuous process over a Al_2O_3/SBA-15 catalyst, in which 0.4 g of catalyst produced *n*-butyl levulinate in a 94% yield after 6 hours in batch at 140 °C and a 91% yield in a continuous process at 180 ℃ after 6 hours.[24] However, SBA-15 is expensive and therefore impractical, specifically in biorefineries that commonly use inexpensive feeds.

The most widely used ion-exchange resins have sulfonic acid groups attached to polymer carriers involving polystyrene cross-linked with divinylbenzene (DVB).[45] These heterogeneous ion-exchange resins in particular Amberlyst-15, have received considerable attention due to their advantageous features over homogeneous catalysts (Appendix I), as well as the elimination of side reactions, simple removal from the reaction mixture, high product purity and their non-corrosive nature.[46] However, their hydrothermal stability is not very high ,<150 °C.[47]

The work described in this chapter is based on the expansion of the Doherty/Knight research group/s application of polymer immobilised ionic liquid (PIIL) systems in the sustainable transformation of renewable resources into high-value chemicals. The goal was to prepare HPA-based PIIL systems and compare their performance as catalysts for the butanolysis of furfuryl alcohol to butyl levulinate in both batch and continuous flow to the commercially available ion exchange resin Amberlyst-15.

4.2   Polymer and Catalyst Design and Synthesis

The target was to prepare a set of heteropolyanion-based and/or hydrogen sulfate-based ionic liquid polymer catalysts bearing a functionalised imidazolium group with R (R = SO_3H, H) (Figure 4.2).
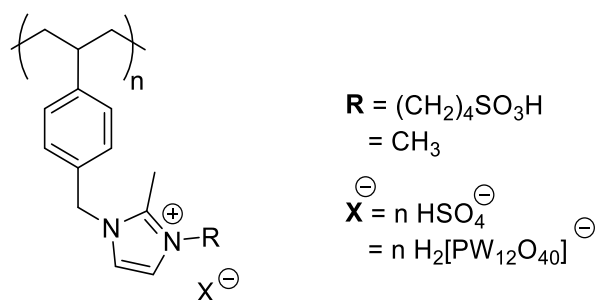
Figure 4.2: Structure of the target catalyst.

A set of imidazolium monomers **2.1** and **4.1** with varied "R" groups were prepared in order to probe the role of the sulfonate group and the polyoxometalate (POM) anion with respect to the acid-catalysed butanolysis of furfuryl alcohol (FFA) (Figure 4.3). Monomers **2.1** and **4.1** were polymerised with and without styrene to obtain a set of linear polymer supports.
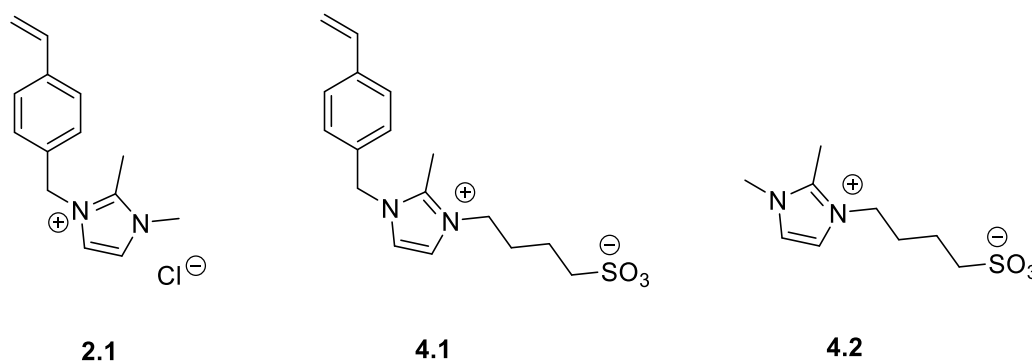
Figure 4.3: Target imidazolium-based monomers 2.1, 4.1 and 4.2.

Monomer **2.1** was prepared under the same conditions as described in Chapter 2 (Scheme 4.2). Monomer **4.2** was prepared in 85% yield by nucleophilic ring opening of 1,4-butane sulfone with 1,2-dimethylimidazole in acetonitrile. The ^{1}H and ^{13}C NMR spectra were consistent with those previously reported and showed that the product could be used without further purification. **4.2** was prepared on the basis for probing the use of non-polymeric ILs as a potential acid catalyst.
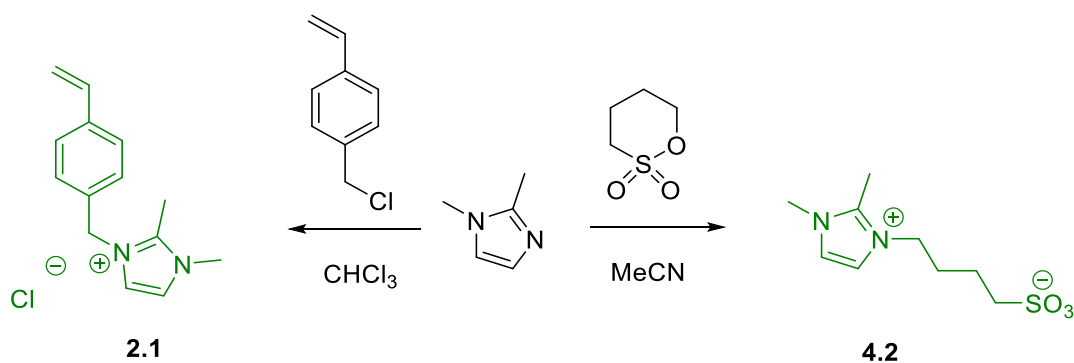
Scheme 4.2: Synthesis of monomers **2.1** and **4.2**.

The sulfonated-functionalised zwitterion **4.1** was prepared *via* scheme 4.3. The general synthesis is split into two steps. In the first step, 2-methyl imidazole was deprotonated with sodium hydride in anhydrous dimethylformamide, to afford the imidazolide anion for the nucleophile substitution with 4-chloromethylstyrene to afford **2.2** as a yellow oil. Subsequent reaction of **2.2** as the nucleophile for the ring opening of 1,4-butane sultone gave the desired monomer **4.1** in 80% yield as a spectroscopically and analytically pure white solid.
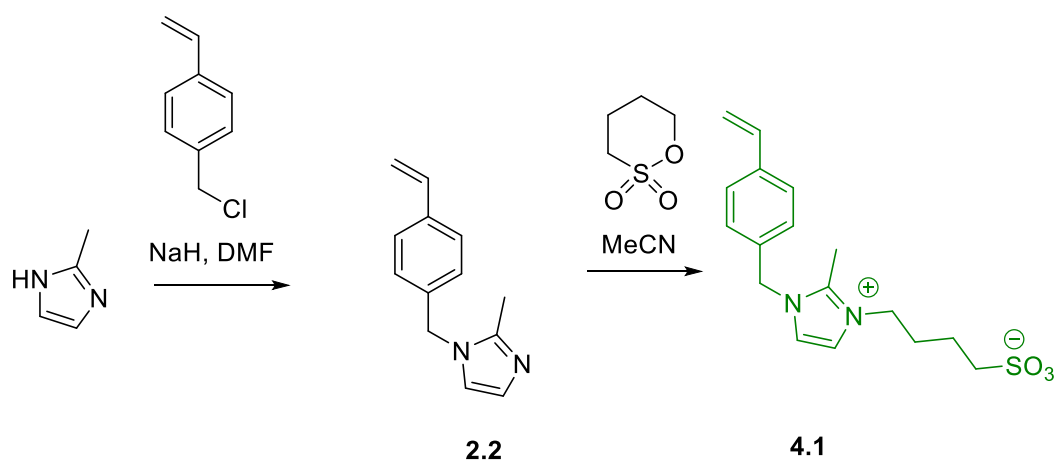
Scheme 4.3: Synthesis of monomer **4.1**.

Following the successful synthesis of the styrenic imidazolium monomers, **2.1** and **4.1** were used to prepare a series of four linear polymers **4.3**-**4.6**, with polymers **4.4** and **4.6** incorporating the desired SO_3H functionality while **4.3** and **4.5** did not

contain this group and would be used as benchmarks. Each of the polymers (see Figure 4.4) were synthesised *via* AIBN-initiated free radical polymerisation. As previously discussed in Chapter 2, radical polymerisation was identified as the optimum method to generate these linear cationic PIIL materials owing to the experimental simplicity and low-cost. The resulting pale-yellow solids were characterised by ^{1}H NMR spectroscopy, solid state ^{13}C NMR spectroscopy, SEM, TGA, IR, and elemental analysis.

The imidazolium-based IL monomers were polymerised either alone to obtain homopolymers **4.3** and **4.4** or, co-polymerised with styrene as neutral spacers to afford co-polymers **4.5** and **4.6**. A 2:1 ratio of the imidazolium monomer to styrene co-monomer was chosen so that the overall polymer had more cationic imidazolium groups to neutral styrene groups to maximise the amount of acid bearing content within the polymer support, without the support being completely cationic. Furthermore, a full exchange of chloride in polymer **4.5** would afford a 2:1 POM to imidazolium ratio. The monomers were dissolved in anhydrous ethanol and 5 mol% AIBN was added. The resulting reaction mixture was then degassed using the freeze-thaw method to remove any oxygen from the system and then refluxed for 3 days.
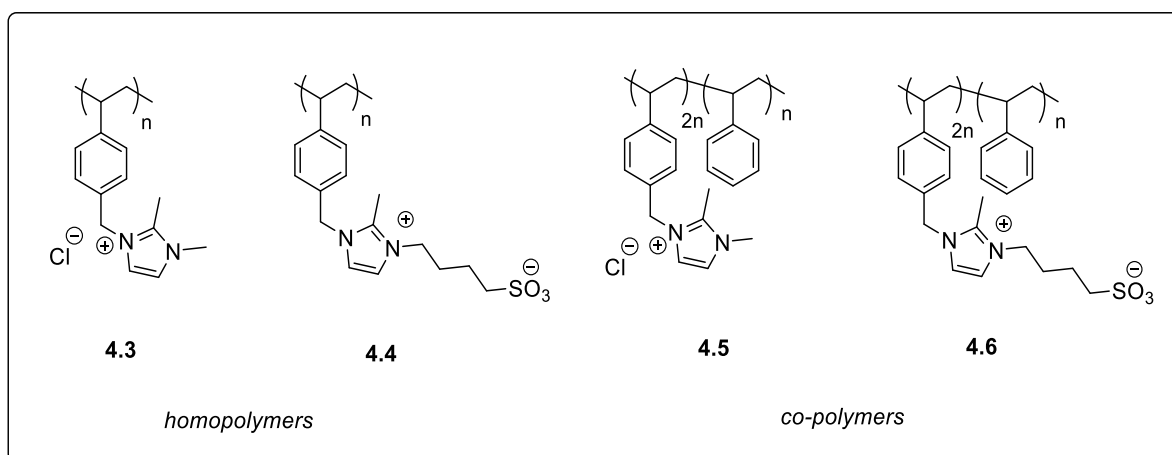
Figure 4.4: Library of imidazolium-based PIL supports (**4.3** – **4.6**) obtained *via* AIBN-initiated free radical polymerisation.

The resulting crude reaction mixtures were sampled after 3 days and analysed by ^{1}H NMR spectroscopy. The monomer's sharp distinct vinylic signals which appeared at 6.5 - 7.5 ppm had disappeared indicating that all the monomer had been consumed

(Figure 4.5a). The imidazolium-monomer: styrene monomer ratio was exactly 2:1, which was determined by the comparison of the integration of the N-CH$_2$ signals (4 H) at δ 4.50 – 6.00 ppm against the total integration of the aromatic protons at δ 6.25 – 8.25 ppm (17 H) (shown in Figure 4.5b). After concentration of the reaction mixtures *in vacuo*, PILs **4.3**, **4.4**, **4.5** and **4.6** were precipitated into diethyl ether and the product dried under reduced pressure; yields of polymer were typically in excess of 90%.
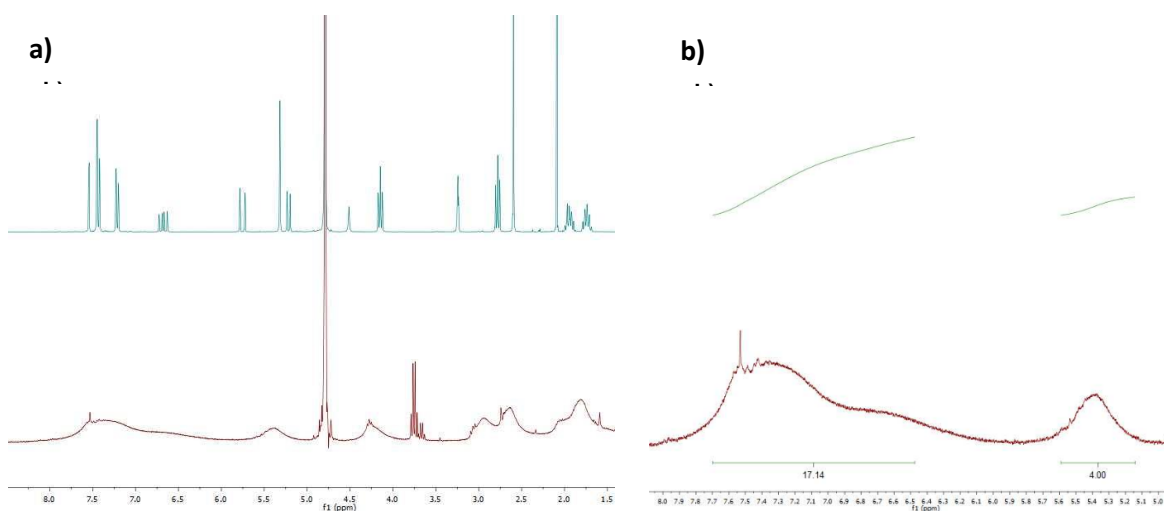
Figure 4.5: An example of a solution ^{1}H NMR spectrum of a) monomer **4.1** (top spectrum) stacked with PIIL (**4.6**) (bottom spectrum) and b) an integrated ^{1}H NMR spectrum of PIIL **4.6**, both in D$_2$O/NaCl.

Calculation of the 2:1 monomer feed ratio was also confirmed from the elemental analysis (CHN). The calculation for the dimethylimidazolium polymer **4.5** and the 2-methyl imidazolium sulfonate polymer **4.6** corresponded to an imidazolium-monomer: styrene monomer ratio of 2:1, these calculations can be found in Appendix L. SEM analysis was also carried out to probe the morphology of the polymer surfaces (Figure 4.6). All of the polymers appeared to have smooth surfaces with no visible evidence of surface deposition or pores.
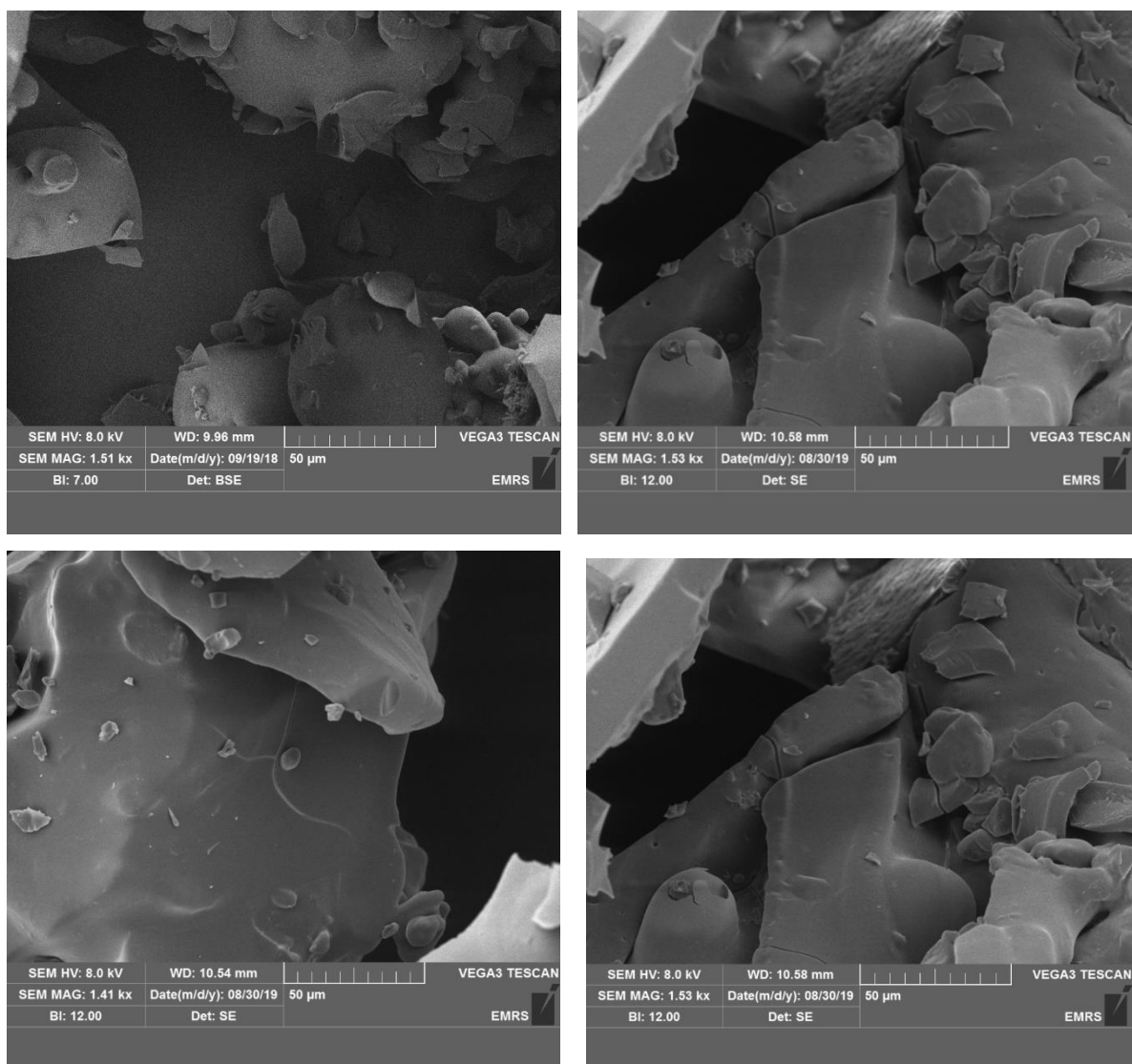
Figure 4.6: SEM images of PILs **4.3** (top left), **4.4** (top right), **4.5** (bottom left) and **4.6** (bottom right).

The thermal stability of the polymers **4.3-4.6** was investigated using TGA. All of the polymers followed a similar degradation pattern to that shown in figure 4.7 (Appendix K). The initial degradation at 100 ℃ was due to the loss of the physisorbed water from the polymer support. This was followed by 2 degradation stages; firstly at ~330 ℃, this corresponds to the decomposition of the imidazole fragment which indicates that the polymers were thermally stable, far above the reaction temperatures that are used in liquid phase catalysis. The large step degradation ~450 ℃ was attributed to the decomposition of main polymer backbone chain and less than 25 wt% of the material remains at 800 ℃.
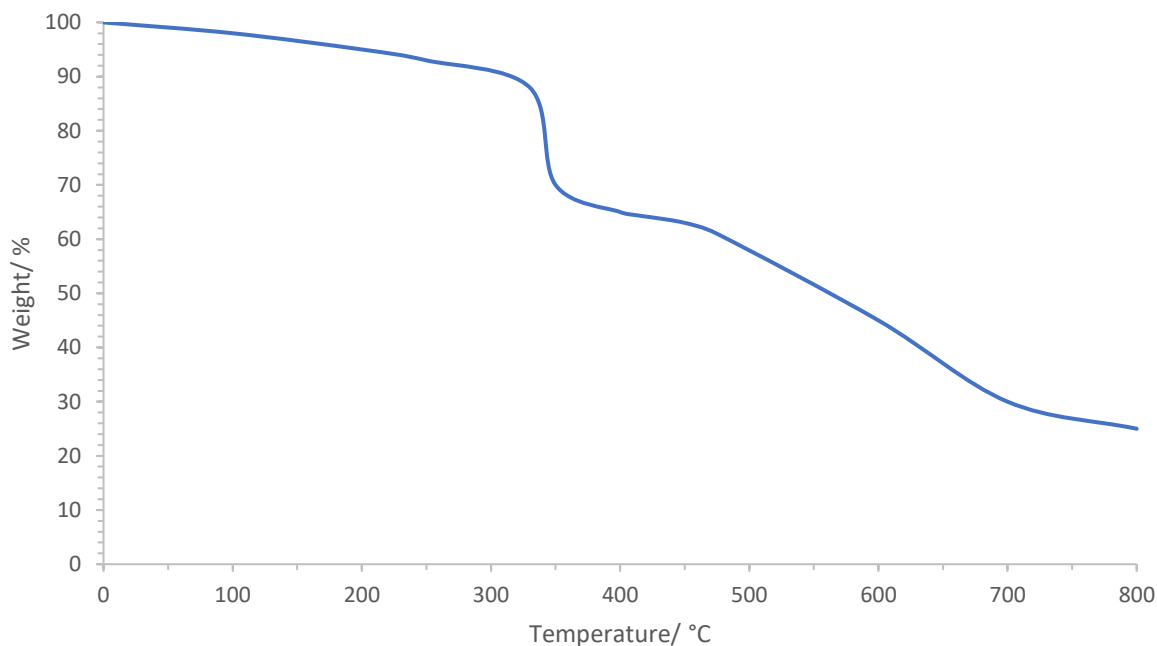
Figure 4.7: TGA analysis of polymer **4.6;** wt% versus temperature, heating rate 10 °C min^{-1} in air.

The POM impregnated PIILs **4.7**, **4.8**, **4.9**, **4.10** and monomer **4.11** (Figure 4.8) were obtained in a straightforward protocol.[48,49] This one-pot procedure produced the active POM@PIIL catalysts. In a standard procedure a methanolic solution of the polymer or monomer was added to an aqueous solution of the commercially available polyoxometalate, (either with phosphotungustic acid ($H_3PW_{12}O_{40}$) or silicotungstic acid ($H_4SiW_{12}O_{40}$) for **4.11**), in a stoichiometric amount. After stirring at room temperature for 16 hours the corresponding POM@PIILs were filtered, washed with water to remove excess POM, then ethanol and diethyl ether; the resulting solid was dried under reduced pressure to give **4.7**-**4.11** as pale-orange solids in good yield (>85%).
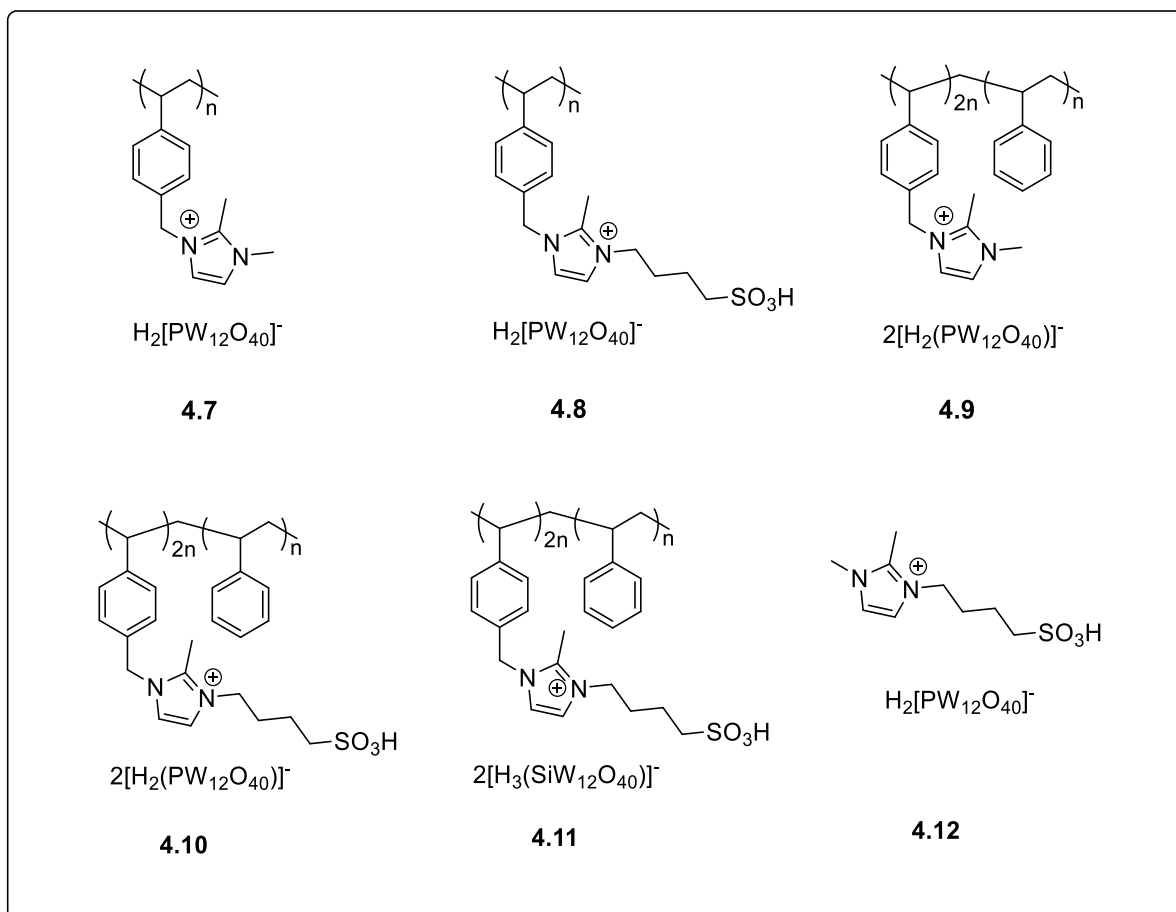
Figure 4.8: Library of the POM-loaded imidazolium-based catalysts **4.7-4.12**.
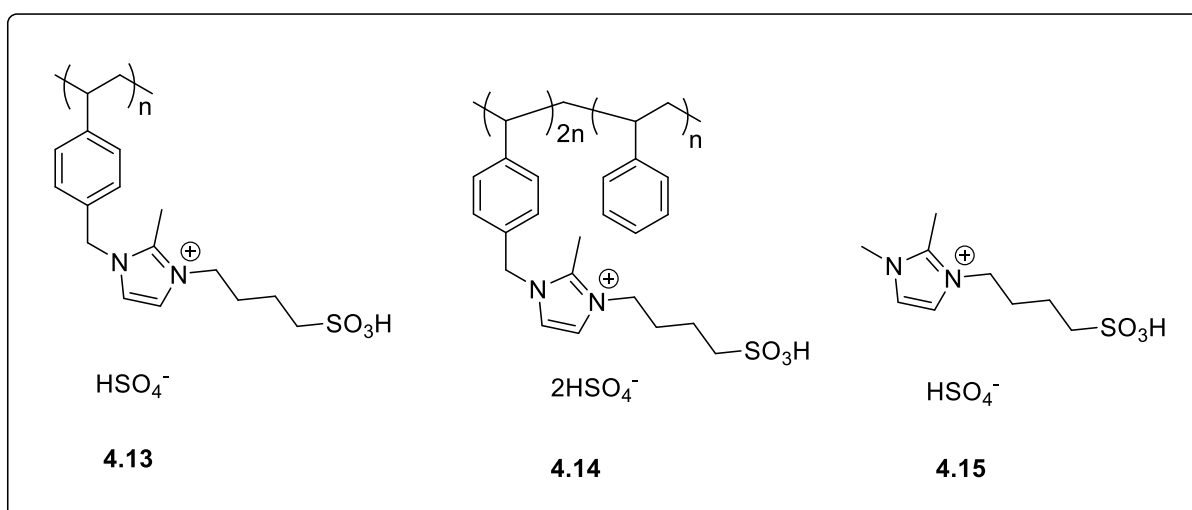
Figure 4.9: Library of the HSO$_4$@PIIL catalysts **4.13-4.15**.

The acidified PILs **4.13**, **4.14** and monomer **4.15** (Figure 4.9) were obtained by adding a methanolic solution of the polymer or monomer to a 2 M methanolic solution of sulfuric acid. After stirring at room temperature for 16 hours the acidified PIILs were filtered and washed with water, methanol and diethyl ether and dried under reduced pressure to give pale-yellow solids in good yield (>90%).

As anticipated, all of the POM@PIIL catalysts showed low solubility in common deuterated solvents therefore, solid state NMR spectroscopy was used to examine the interactions between the polyoxometalate and the PIIL support. The solid state ^{13}C NMR spectra of **4.9** and **4.10** in figure 4.10 both contained characteristic resonances between δ 115 - 155 ppm which are associated with the aromatic carbon atoms and the imidazolium ring and a resonance that appears at δ 10 ppm which is associated with the methyl group attached to the imidazolium ring. The methylene group adjacent to the SO$_3$ fragment in **4.10** appears ca. 40 ppm (Figure 10b).
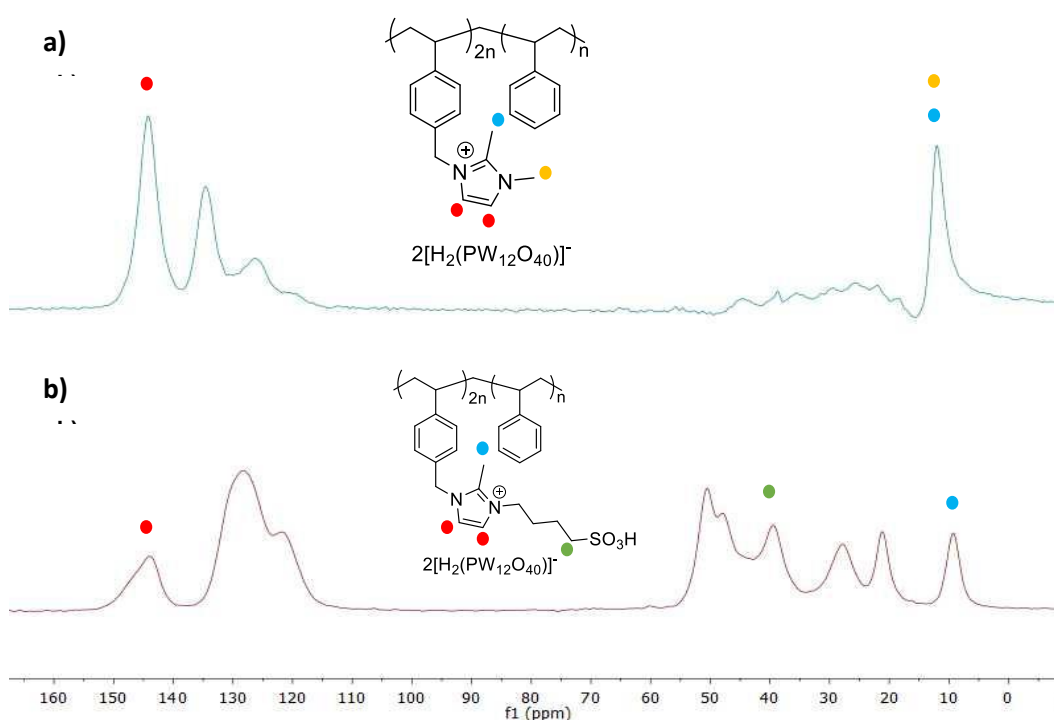
Figure 4.10: Solid state ^{13}C NMR spectra of a) **4.9** and b) **4.10**.

Solid state ^{31}P NMR spectra of the phosphotungustic acid-loaded PIILs (spectra in Appendix J) also confirmed that the polyoxometalate had been incorporated into the polymers with phosphorus chemical shifts in the range of -18 ppm to -15 ppm for **4.7**,

4.8, **4.9**, **4.10** and **4.12** (Table 4.1), which are consistent with those previously reported for supported phosphotungstic acid.[50a] The observation of only one product peak in the spectra and the disappearance of the phosphotungstic acid starting material peak (δ -15.37 ppm) indicated that there was no remaining free polyoxometalate in any of the prepared samples.

Table 4.1: ^{31}P NMR values for phosphotungustic acid and POM@PIIL catalysts **4.7-4.10** and **4.12**.

	$H_3PW_{12}O_{40}$	**4.7**	**4.8**	**4.9**	**4.10**	**4.12**
δ / ppm	-15.37	-17.94	-18.04	-17.94	-17.89	-18.00

TGA analysis was carried out to assess the thermal stability of the POM@PIIL catalysts (Figure 4.11). In contrast to the polymers which showed just two main degradation stages, these POM@PIIL materials presented three, the first at ~270 ℃ which was clearly attributed to the loss of the surface adsorbed water in the POM-based PIILs. Then ~370 ℃, 10% loss for **4.10** and 9% loss for **4.11** which corresponds to the weight percent of styrene-imidazolium-butane-1-sulfonate fragment in the POM@PIILs, respectively. Finally a loss ~ 490 ℃ which corresponds to the onset of the thermal decomposition of the polyoxometalates.[50b] Unlike the corresponding polymer materials which retained less than 25% of its weight by 500 ℃, here **4.10** and **4.11** retained around 80 % of their weight, indicating that the POM species is thermally robust.
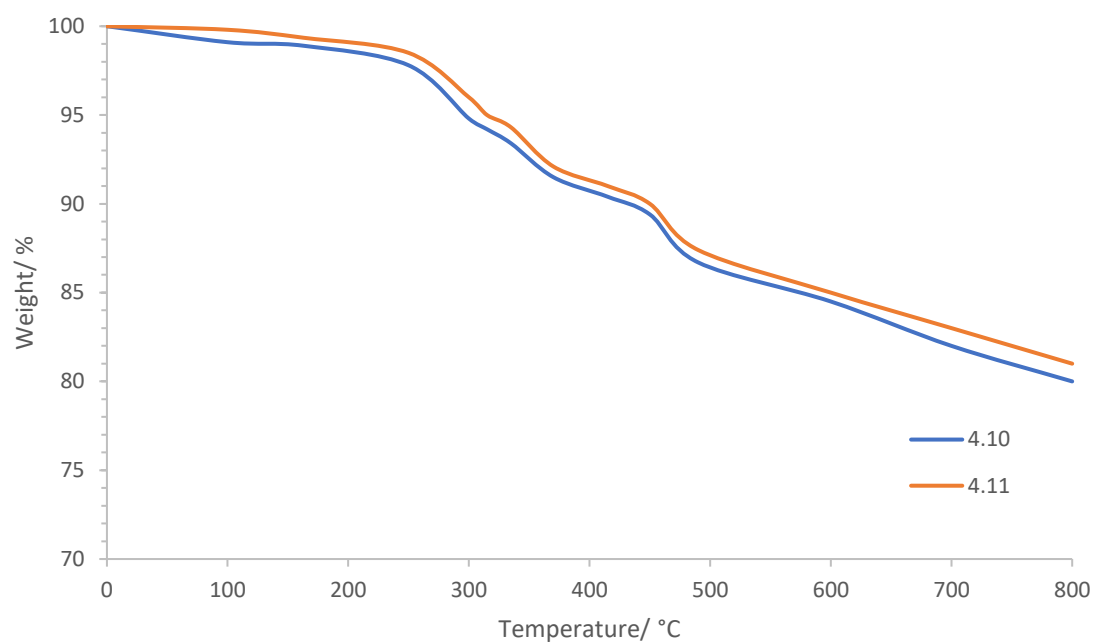
Figure 4.11: TGA curve for POM@PIILs **4.10** and **4.11**; wt% versus temperature, heating rate 10 °C min^{-1} in air.

The TGA curve for **Amberlyst-15** (Figure 4.12) includes four main degradation stages arising from the desolvation, dehydroxylation, desulfonation and decomposition of the polymer backbone. The first weight loss at ~100 °C corresponds to the desolvation of the ion exchange resin, the second weight loss at ~250 °C, the weight loss is associated with the dihydroxylation of the OH groups. The weight loss in the third degradation ~300-450 °C is due to desulfonation and finally the polymer backbones are degraded at temperatures over 480 °C. Similar to the PIILs, only 25 wt% of the resins weight was retained at 800 ℃ which indicates that the ion exchange resin is not thermally stable.
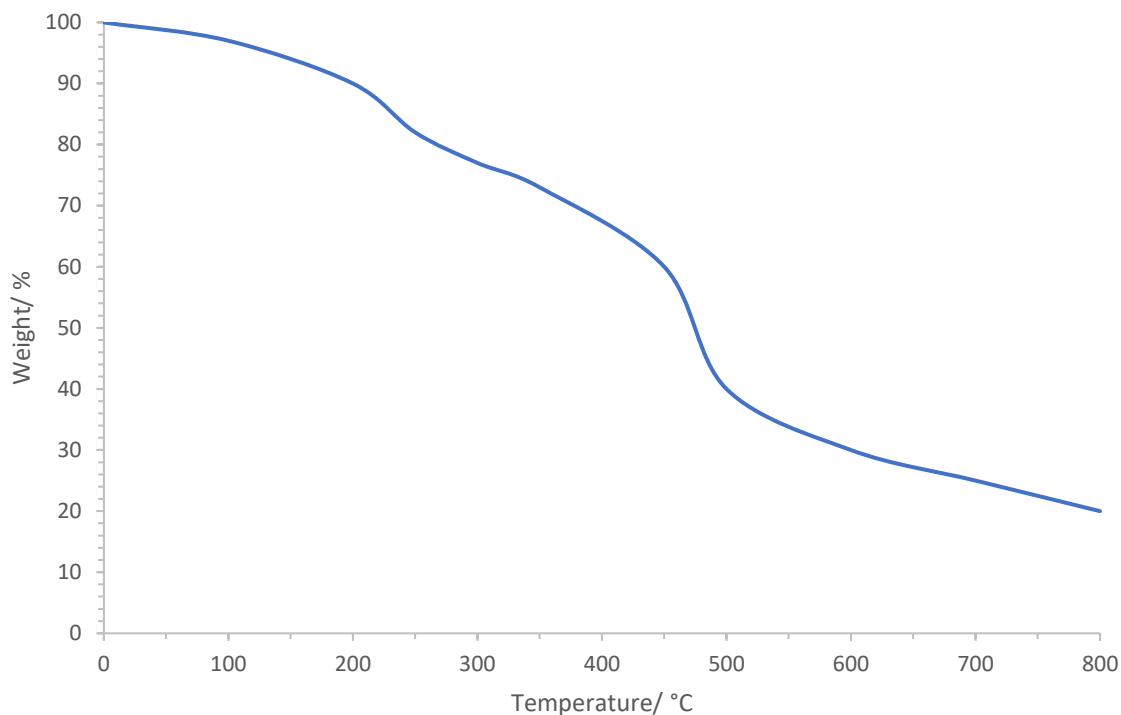
Figure 4.12: TGA analysis of the commercial ion exchange resin **Amberlyst-15**; wt% versus temperature, heating rate 10 °C min^{-1} in air.

The surface morphology of the freshly prepared POM@PIILs (Figure 4.13) displayed distinct differences in their texture to the parent polymers (Figure 4.6) in the SEMs. In this case, the samples were more granular and the surface uneven which may be due either to aggregation of the peroxotungstate which becomes visible on the surface and/or the additional processing steps involved in the polyoxometalate impregnation.
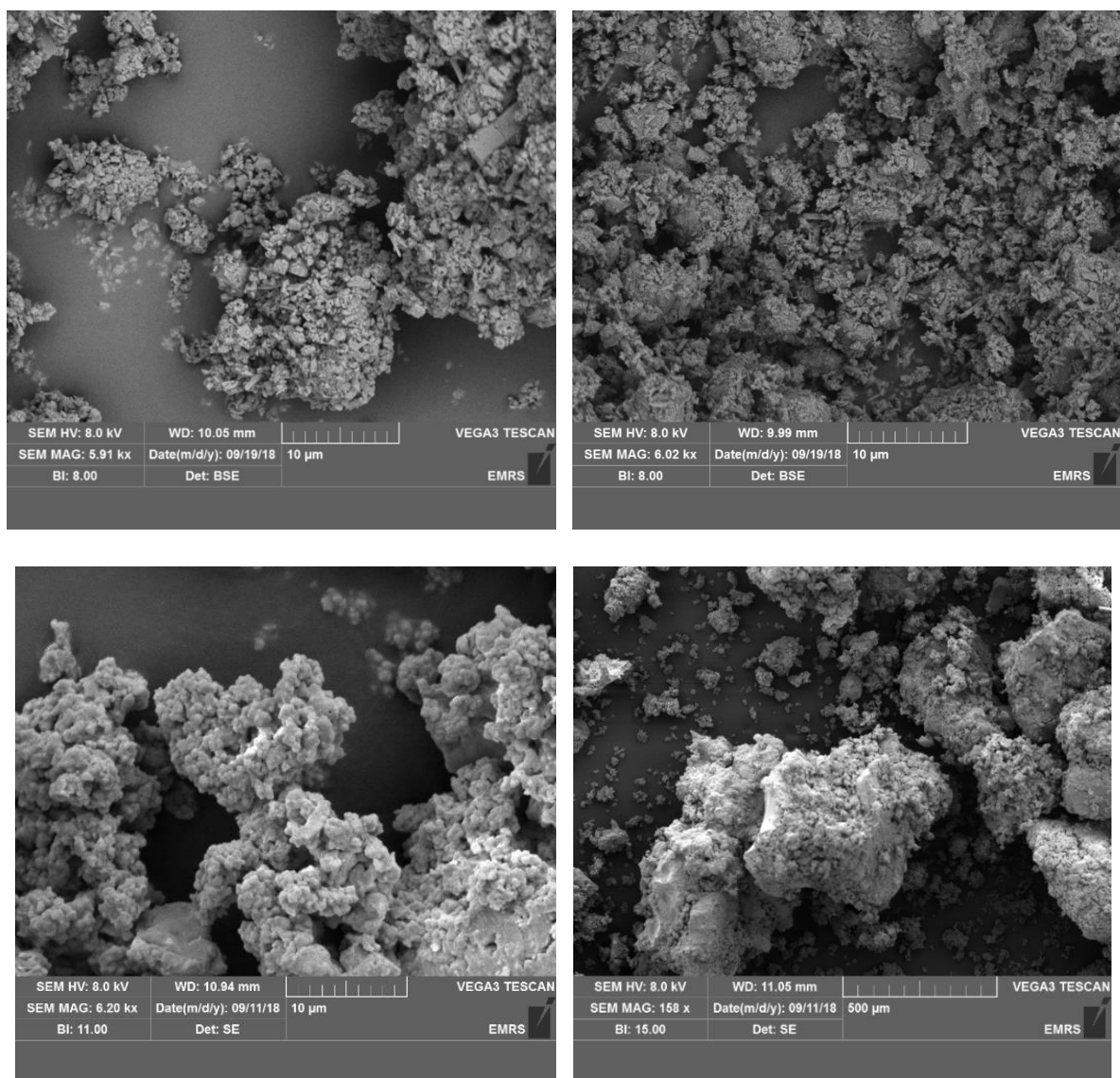
Figure 4.13: SEM images of the POM@PIILs **4.8** (top left), **4.9** (top right) **4.10** (bottom left) and **4.11** (bottom right).

Elemental analysis was used to determine the tungsten content in the POM@PIIL material. An example of the calculation to determine the tungsten loading in POM@PIIL **4.10** is shown in figure 4.14. The calculations for all other POM@PIILs can be found in Appendix L. The calculated catalyst acidity was determined by CHN analysis and confirmed by acid-base titrations which are listed in Table 4.2.

CHN Anal. Calc. for:

Polymer, $C_{43}H_{60}N_4O_6S_2$ (792 g/mol): C, 65.2 ;H, 7.63 ; N, 7.07 %
POM@PIIL, $C_{43}H_{66}N_4O_{86}P_2S_2W_{24}$ (6552.34 g/mol): C, 2.63; H, 3.37; N, 2.85.
Found:
Polymer, $C_{43}H_{60}N_4O_6S_2$ (792 g/mol): C, 59.6 ;H, 6.35 ; N, 6.95 %
POM@PIIL, $C_{43}H_{66}N_4O_{86}P_2S_2W_{24}$ (6552.34 g/mol): C, 15.81; H, 1.75; N, 1.78.

Therefore: 1 g of polymer contains 0.0695/14.0 = 4.96 x 10^{-3} moles N

1 g POM@PIIL = 0.0178/ 14 = 1.27 x 10^{-3} moles N

$\frac{moles\ of\ N\ on\ 1\ g\ polymer}{moles\ of\ N\ on\ 1g\ POM@PIIL}$ = 4.96 x 10^{-3} / 1.27 x 10^{-3} = 3.905

3.905 g of POM@PIIL contains 4.96 x 10^{-3} moles of N (see above) = 1 g polymer

Therefore 2.905 g of polymer (3.905-1g) of PIIL contain POM only

2.905 g extra mass is from POM = ((2881 $gmol^{-1}$)) = 2881 $gmol^{-1}$

2.905 g/ 2881 $gmol^{-1}$ = 1.01 x10^{-3} moles of POM = 1.01 x 10^{-3} mol x 2881 $gmol^{-1}$ (=MW of POM) = 2.905 g POM on 3.905 g PIIL

Therefore 1 g PIIL contains, 1 / 3.905 g x 2.905 g = 0.744 g POM = 2.58 x 10^{-4} moles $[PW_{12}O_{40}]^{3-}$

$\frac{moles\ of\ N\ on\ 1g\ of\ POM@PIIL}{2}$ = 1.27 x 10^{-3} moles of N/2 = 6.35 x 10^{-4} moles of SO_3H

$\frac{moles\ of\ SO3H}{moles\ of\ POM}$ = $\frac{0.000635}{0.000258}$ = 2.46 therefore 1:2.5 of POM to SO_3H polymer

Figure 4.14: Calculation of the W loading for the POM@PIIL **4.10** from the CHN analysis.

Table 4.2: Composition of the PIIL catalysts **4.7**-**4.15** and the ion exchange resin **Amberlyst 15**.

Entry	Catalyst	POM (mmol/g) [a]	HSO_4 (mmol/g) [a]	SO_3H (mmol/g) [a]
1	**4.7**	0.294	-	-
2	**4.8**	0.255	-	0.770
3	**4.9**	0.270	-	-
4	**4.10**	0.258	-	0.635
5	**4.11**	0.302	-	0.321
6	**4.12**	0.252	-	1.18
7	**4.13**	-	1.05	2.61
8	**4.15**	-	1.08	2.22
9	**Amberlyst 15 H**	-	-	4.70

[a] Determined by CHN analysis (see Appendix L for the CHN values and the calculation mmol/g)

Using the calculations shown in figure 4.14, the elemental analysis for **4.10** (C 15.81, H 1.75, N 1.78) and **4.11** (C 10.05, H 1.48, N 0.90) polyoxometalate loadings of 0.258 and 0.302 mmol g^{-1} respectively. Which was calculated from the CHN nitrogen/sulphur content data of both the POM@PIIL catalyst and its corresponding polymer. Silicotungstic acid is less acidic than phosphotungstic acid,[51] however during the preparation of the POM@PIIL catalysts, the Si-POM loaded more efficiently onto the PIL support.

The ion exchange capacity of the HSO_4@PIIL catalysts **4.13**, **4.14**, **4.15** and resin **Amberlyst 15** was determined experimentally. In a standard test, 1 g of the catalyst or resin was dispersed in 30 mL of 1M NaCl solution and sonicated for 15 minutes. The (filtrate) solution was then titrated against 0.1N NaOH using phenolphthalein as an indicator. The acid-site concentration (an average of three measurements) obtained was 0.89 ± 0.94 eq L^{-1} for **4.13**, 1.65 ± 0.05 eq L^{-1} for **4.15**,

4.75 ± 0.05 eq L^{-1} for **Amberlyst 15,** in agreement with the values as reported for similar catalysts in the literature and/or the manufacturer.[52]

A stretching vibration at ~1150 cm^{-1} in the IR spectrum of the catalysts was assigned to the S=O stretch, which proved that the sulfonic group was present. Catalysts **4.8**, **4.10** and **4.12** all showed five characteristic bands in their IR spectrum, which confirmed that both the polyoxometalate and the sulfonic acid groups were present in the catalyst (Table 4.3, spectra in the Appendix N). The Keggin structure of phosphotungstic acid has four types of oxygen atoms that can be assigned. These include the oxygen atoms attached to the heteroatom and to the three metal atoms υ (P-O), terminal oxygen atoms υ (W=O$_{ter}$) and the bridging oxygen atoms υ (W-O-W) (Figure 4.15).[44] In agreement with the previously reported literature the peaks at 1129, 1014 and 986 cm^{-1} were assigned to the SO$_4^{2-}$ vibration for HSO$_4$@PIIL catalysts (spectra in the Appendix N).[54]
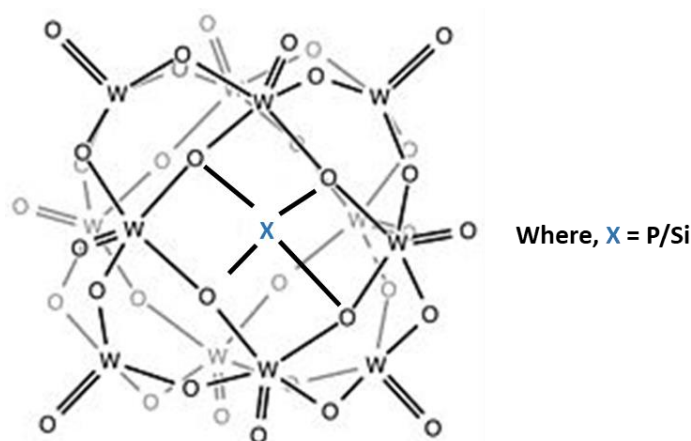
Figure 4.15: The structure of the peroxotungstate, H$_x$XW$_{12}$O$_{40}$.

Table 4.3: IR data of phosphotungustic acid, silicotungstic acid and the POM@PIIL catalysts **4.7**-**4.12**.

Entry	Catalyst	υ (P-O)	υ (W=O$_{ter}$)	υ (W-O$_c$-W)	υ (W-O$_e$-W)
1	H$_3$PW$_{12}$O$_{40}$	1075	976	903	755
2	H$_4$SiW$_{12}$O$_{40}$	-	976	907	735

3	**4.7**	1078	973	892	785
4	**4.8**	1078	974	893	790
5	**4.9**	1079	975	893	799
6	**4.10**	1075	974	892	787
7	**4.11**	-	972	909	727
8	**4.12**	1077	975	892	797

4.3 Batch Alcoholysis Optimisation

The efficacy of each of the PIIL catalysts was investigated for the butanolysis of furfuryl alcohol; a range of supported and immobilised systems including Al_2O_3/SBA,[24] double SO_3H-functionalised ILs,[38] and an organic-inorganic solid acid catalyst,[44] have recently been reported to catalyse this transformation and as such provided an informative comparison. This reaction has been shown to occur *via* initial reaction of furfuryl alcohol with *n*-butanol (Scheme 4.4) to afford the intermediate 2-butoxymethylfuran which subsequently undergoes ring opening to afford *n*-butyl levulinate.
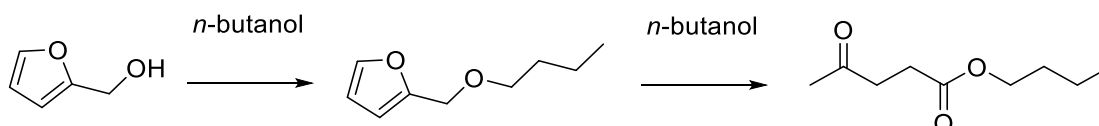
Scheme 4.4: The butanolysis of furfuryl alcohol to give 2-butoxymethyl furan and *n*-butyl levulinate.

Several studies have been published on the mechanism of this alcoholysis.[38, 44, 55] One possible mechanism involves the dehydration of FFA to α-angelica lactone following an attack by the alcohol to generate the AL.[56] The possible reaction mechanism is shown in scheme 4.5. First, the alcohol group of FFA is protonated to make it a better leaving group and/or more electrophilic. Nucleophilic substitution followed by intermolecular dehydration affords the intermediate 2-alkoxymethylfuran. In the third step, a further alcohol molecule attacks the furan ring in the presence of

the acid catalyst to form the 1,4-addition product. The 1,4-addition product is then further protonated and the furan ring opens *via* the attack of a water molecule to form the dieneol intermediate which then affords the alkyl levulinate *via* keto-enol tautomerization. The proton is then lost which regenerates the active catalyst.[57]
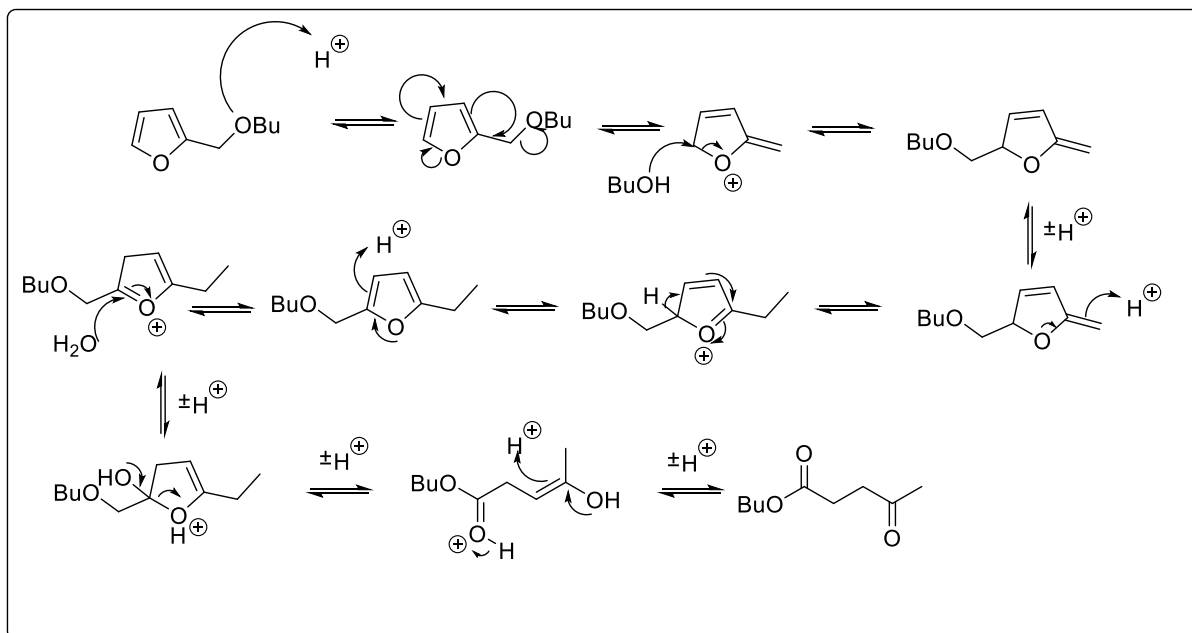
Scheme 4.5: Possible reaction mechanism for the conversion of furfuryl alcohol into butyl levulinate (AL).

4.3.1 Reaction Optimisation

Preliminary testing was conducted in a glass tube reactor using a 2.5 mol% loading of catalyst, based on the acid content calculated from the CHN analysis, in 3 mL of *n*-butanol. The mixture was heated at 110 ℃ with constant stirring (800 rpm), 1 mmol of furfuryl alcohol was then added and this was taken as t_0 and the reaction was run for 1 hour. After completion, the reaction flask was cooled to room temperature in a cold-water bath to stop any further reaction. The POM@PIIL catalyst and **Amberlyst-15** resin separated as a solid at the bottom of the flask and therefore could be easily removed by a straightforward decantation. The alkyl levulinate product along with any unconverted reactants, be it FFA or the intermediate, were in the upper liquid layer. The reaction mixtures were sampled and analysed by ^{1}H NMR spectroscopy, (using 1,4-dioxane as an internal standard) as well as gas chromatography (GC-MS) using a HP-5 capillary column in an Agilent 7820A GC with an FID detector.

The conversion of the reactant was calculated by:

$$\text{Conversion (\%)} = \frac{\text{moles of reactant converted}}{\text{moles of reactant loaded}} \times 100 \qquad (1)$$

The yield of the target products was calculated by:

$$\text{Yield (\%)} = \frac{\text{moles of product produced}}{\text{moles of reactant loaded}} \times 100 \qquad (2)$$

4.3.2 Catalyst Comparison

A series of batch reactions were first conducted to evaluate the efficiency of the POM@PIILs against HSO4@PIIL, as well as a sample of the commercially available ion exchange resin **Amberlyst-15**. The results of this screening are shown in table 4.4.
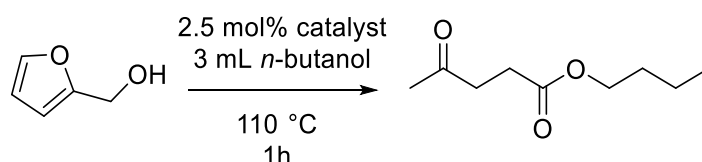
Table 4.4: Catalyst performance comparison for the acid-catalysed alcoholysis of furfuryl alcohol to *n*-butyl levulinate.

Entry [a]	Catalyst	Conversion (%) [b]	Selectivity (%) [b]	Yield (%) [c]
1	**4.6**	0	0	0
2	**4.7**	0	0	0
3	**4.8**	100	93	93
4	**4.9**	3	10	0.3
5	**4.10**	100	100	100
6	**4.11**	100	100	100
7	**4.12**	100	100	100
8	**4.13**	100	50	50
9	**4.14**	100	63	63
10	**4.15**	100	56	57
11	**Amberlyst-15**	100	100	100
12	**H₂SO₄**	100	100	100

13	$H_3PW_{12}O_{40}$	100	100	100
14	$H_4SiW_{12}O_{40}$	100	100	100

[a]Reaction conditions: 2.5 mol% catalyst, 1 mmol furfuryl alcohol, 3 mL *n*-butanol, 110 ℃, 1 h, 800 rpm. [b]Conversion and selectivity determined by ^{1}H NMR spectroscopy with 1,4-dioxane as the internal standard and gas chromatography. Selectivity for *n*-butyl levulinate = [% *n*-butyl levulinate / (% *n*-butyl levulinate + % 2-butoxymethylfuran)]. Yield of n-butyl levulinate = [% conversion of furfuryl alcohol x (% selectivity *n*-butyl levulinate / 100). Average of 3 runs.

The initial control experiment was conducted without any catalyst and showed that no conversion of FFA occurred confirming that the alcoholysis of FFA was catalytic. FFA alcoholysis was attempted with **4.6**, the precursor of **4.10**, but no conversion of FFA was detected (Table 4.4, entry 1). This was because **4.6** is a neutral salt (zwitterion) which could not catalyse this reaction. This confirmed that the catalyst needs to be acidic which can be obtained either by the reaction of the PIL support with a conventional acid or a POM. The catalysts bearing no sulfonate groups (entries 2 and 4) gave 0% and 3 % conversion of FFA which confirmed that the sulfonate groups appeared to be crucial for alcoholysis of FFA.

Good conversions of FFA and high selectivities and yields for BL were obtained for POM@PIIL catalysts **4.8**, **4.10** and **4.11** (entries 3, 5 and 6) and the commercially available **Amberlyst-15** ion exchange resin (entry 11). All of which outperformed the benchmark HSO_4@PIIL catalysts **4.13** and **4.14** (entries 8 and 9). Additionally, the 2 to 1 co-polymers **4.10** (entry 5) were slightly more selective for BL than the homopolymer **4.8** (entry 3) which gave BL with 100% and 91% selectivity, respectively. This may be due to the better dispersion of the polymer support which facilitates access of the substrates to the active sulfonated sites. The minor decrease in the conversion of FFA with the homopolymer-based catalyst supports were relatively minor and the interpretation should be treated with caution.

The corresponding HSO_4@PIIL systems **4.13** and **4.14** (entries 8 and 9) gave full conversion of FFA but gave lower selectivity for BL of 50% and 63%, respectively, due to the formation of significant amounts of 2-BMF. This further supports the conclusion that not only is the acidic butylsulfonic group essential for high conversion of FFA but that the polyoxometalate is also required which promotes the insolubility of

the catalyst, in order to achieve a high selectivity for BL. The selectivity for intermediate 2-BMF decreased whenever a polyoxometalate was present which may well be due to its high acidity.

The use of **4.12**, sulfuric acid, phosphotungstic acid ($H_3PW_{12}O_{40}$) and silicotungstic acid ($H_4[W_{12}SiO_{40}]$) catalysts (entries 7, 11-14) gave 100% conversion of FFA with 100% selectivity for BL. However, a homogeneous reaction mixture was obtained at the end of the reaction which made the catalyst extremely challenging to separate and recycle in contrast to POM@PIIL catalysts **4.10** and **4.11**. In addition, the resulting acid-leached samples could not be analysed by GC-MS due their highly acidic nature which is not compatible with the GC column. Furthermore, sulfuric acid produces highly toxic waste to the environment and its corrosive properties could render the process too costly and therefore not appropriate for industrial scale-up. Thus, the complete conversion of FFA and 100% selectivity for BL obtained with **4.10**, **4.11** and **Amberlyst-15** prompted the use of these catalysts for the remaining optimisation studies.

4.3.3 Kinetic Studies

The reaction time is a significant factor which influences the product species therefore the alcoholysis of FFA was monitored as a function of time to obtain a composition profile. This was achieved by removing a 0.1 mL sample of the reaction mixture at different times up to 1 hour and analysing the aliquot by ^{1}H NMR spectroscopy after dilution with 0.6 mL of *n*-butanol; details of which are presented in figure 4.14.
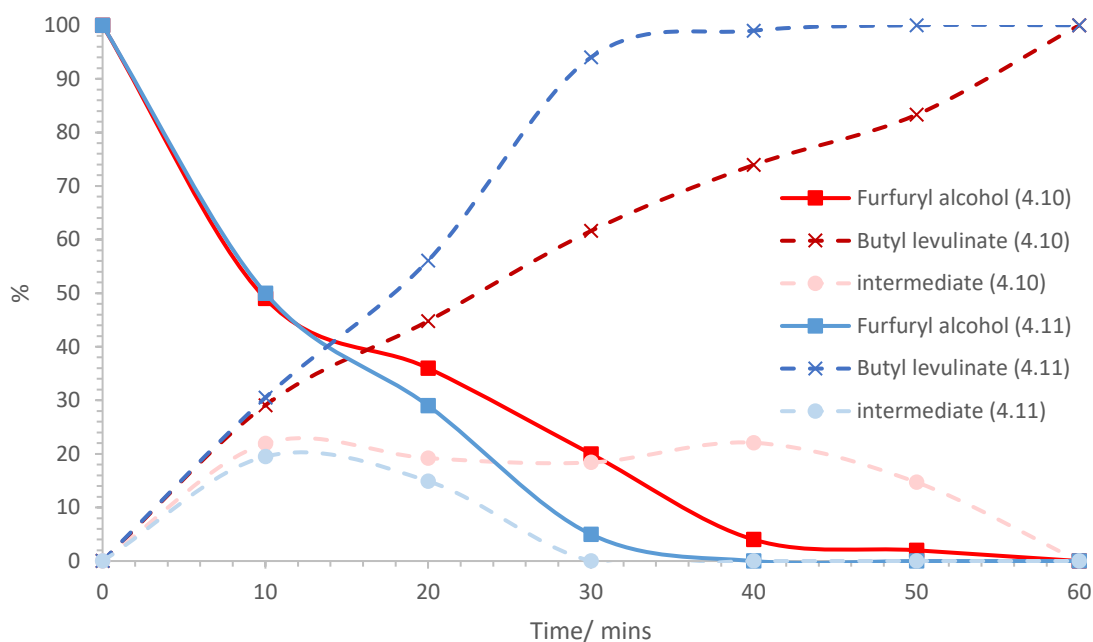
Figure 4.16: Effect of the reaction time on FFA alcoholysis. Reaction conditions: 2.5 mol% catalyst; FFA, 1 mmol; n-butanol, 3 mL; temperature, 110℃, 800 rpm. Conversion and selectivity determined by ^{1}H NMR spectroscopy with 1,4-dioxane as the internal standard. Selectivity for n-butyl levulinate = [% n-butyl levulinate / (% n-butyl levulinate + % 2-butoxymethylfuran)]. Average of 3 runs.

The time-composition profile revealed that the alcoholysis of FFA with all of the catalysts tested exhibited a rapid conversion of FFA with an increase in the selectivity for BL accompanied with a decrease in the selectivity towards intermediate 2-BMF over the 60 minutes. After 20 minutes, the selectivity towards BL was 70-80% and 20-30% towards 2-BMF for all 3 catalysts. Figure 4.16 shows **4.11** gave butyl levulinate as the exclusive product after only 35 minutes, whereas **4.10** required a reaction time of 40 minutes to reach complete conversion to C; therefore the Si-POM-based catalyst **4.11** appears slightly more active than its P-POM-based counterpart **4.10**. **Amberlyst-15** managed to achieve a 97% conversion of FFA and 92% selectivity for BL after 60 minutes. All reactions were run for 40 minutes without any sampling and similar results were obtained at 40 minutes within ± 3% error to the sampled reaction. In addition, it was observed that during the reaction the colour of the reaction mixture rapidly (> 5 minutes) turned from light-orange to dark-brown/black. This indicated that the carbonation and/or polymerisation of FFA had occurred.

All reactions were carried out at a stirring speed of 800 rpm with a magnetic stirrer plate. The high stirring speeds are used to force the substrates to be in contact with the catalyst and consequently increase the rate of conversion. In solid-liquid catalytic reactions external mass transfer resistances exist.[58] This can be decreased by increasing the disturbance of the reaction medium; this can be achieved by varying the speed of agitation. Therefore, the effect of the speed of agitation on the catalyst activity of **4.11** and **Amberlyst-15** on the butanolysis of FFA was investigated at various agitation speeds between 0 to 1200 rpm to explore the impact of the mass transfer resistance as shown in figure 4.17.
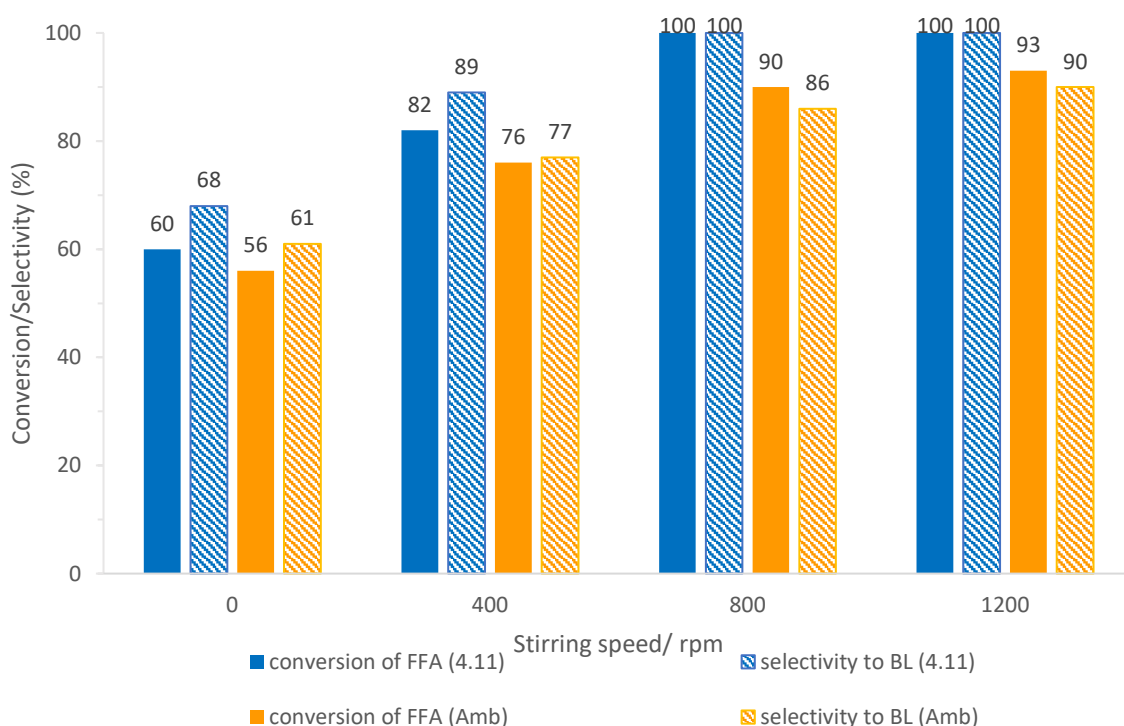
Figure 4.17: Effect of the speed of agitation on the alcoholysis of FFA catalysed by **4.11** and **Amberlyst-15**. Reaction conditions: 2.5 mol% catalyst; FFA, 1 mmol; *n*-butanol, 3 mL; temperature, 110 ℃; time, 40 mins. Conversion and selectivity determined by ^{1}H NMR spectroscopy with 1,4-dioxane as the internal standard. Selectivity for *n*-butyl levulinate = [% *n*-butyl levulinate / (% *n*-butyl levulinate + % 2-butoxymethylfuran)]. Average of 2 runs.

Figure 4.17 shows that reaction conducted with no stirring or, at a lower stirring speed of 400 rpm, gave low conversions and low selectivity which may simply be due to formation of polyfurfuryl alcohol which blocks access to the active sites. While an increase in the stirring speed to 800 rpm resulted in a marked enhancement in both

conversion and selectivity. The conversion-selectivity were very similar for reactions agitated at speeds of 800 and 1200 rpm. Therefore, all of the following experiments were conducted at a stirring speed of 800 rpm to overcome the effects of external mass transfer and to prevent catalyst breakage at a higher rpm.

4.3.4 Catalyst Loading Optimisation

A reaction time of 25 minutes was used to guarantee that the experiments were carried out at low conversions of FFA and to guarantee that the conversion of FFA was not limited by the amount of substrate that was available. From section 4.3.2, it is known that a certain amount of catalyst is necessary for the reaction to proceed and that for this mechanism an abundant concentration of H^+ ion is required to obtain the product. The catalyst and resin provide the active sites for the reaction, to protonate the furfuryl alcohol and therefore lower the activation energy of the overall reaction. The amount of catalyst strongly affects the acid concentration and therefore influences the distribution of the products in the reaction mixture. For comparison, the efficiency of **4.10**, **4.11** and **Amberlyst-15** was investigated between 0.75 – 5 mol% to determine the optimum catalyst loading, the results of which are shown in figure 4.18. Fresh catalyst and resin were used for each catalyst loading test.
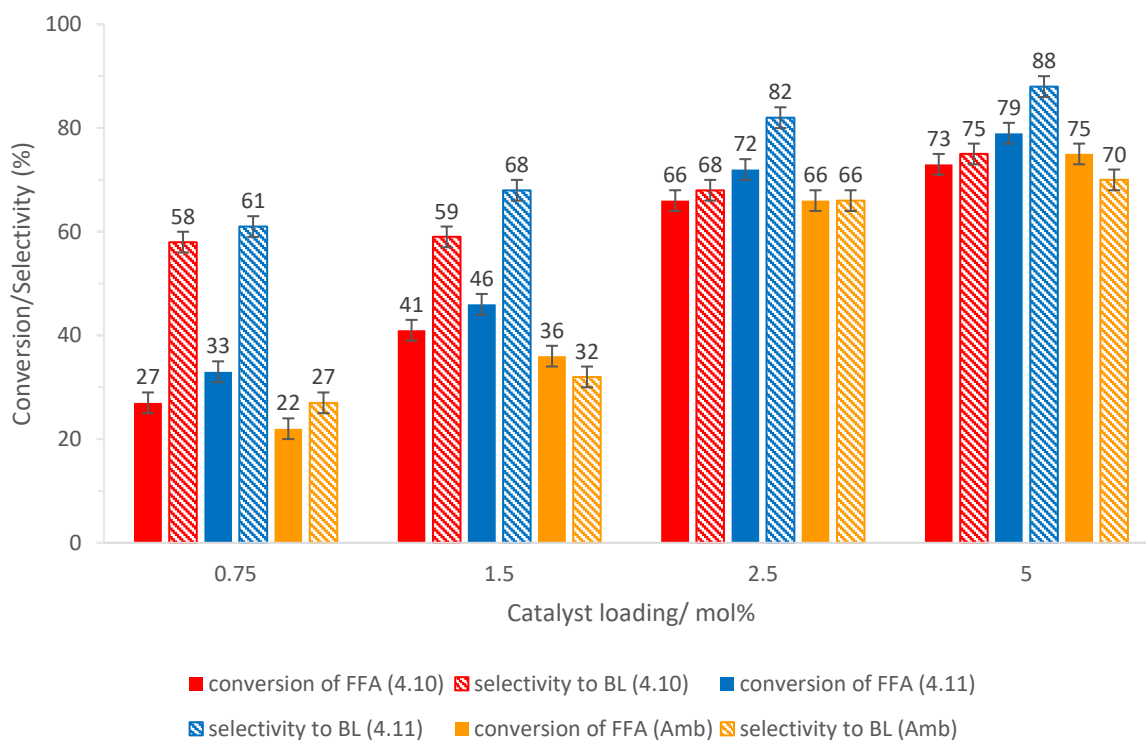
Figure 4.18: Effect of catalyst loading on FFA alcoholysis. Reaction conditions: FFA, 1 mmol; *n*-butanol, 3 mL; catalyst, (set amount); temperature, 110 ℃; time, 25 mins; agitation, 800 rpm. Conversion and selectivity determined by ^{1}H NMR spectroscopy with 1,4-dioxane as the internal standard. Selectivity for *n*-butyl levulinate = [% *n*-butyl levulinate / (% *n*-butyl levulinate + % 2-butoxymethylfuran)]. Average of 3 runs.

Figure 4.18 shows that the selectivity towards BL increased with an increase in the catalyst loading as a result of the increase in available acidic sites. 2.5 mol% of **4.10** and **4.11** gave 72% and 66% conversion of FFA, respectively. However, it was observed that as the catalyst loading increases from 0.75 to 5 mol%, the colour of the reaction mixture turned from light-orange to dark-brown/black.

At increased catalyst loading up to 5 mol% resulted in an increase in percent conversion and selectivity this suggests that an adequate amount of catalytically active acid sites was available for the reactant and the complete conversion of the intermediate 2-BMF, to produce BL as the sole product and that the reaction is mass transfer limited. When the reaction time was extended to 1 hour catalyst **4.11** gave conversions of 50, 65, 100 and 100% using 0.75, 1.5, 2.5 and 5 mol%, respectively and conversions of 40, 56, 100 and 100% for **Amberlyst-15**. Catalyst **4.11** and **Amberlyst-15** gave high conversions of FFA but with the added advantage of the ability to tailor the PIIL-based catalyst **4.11** to a specific need and therefore expanding the scope of application of PIILs. The results from the study of the sulfonic acid resin **Amberlyst-15** were similar to those obtained by Pagliaro and co-workers.[36] The initial BL selectivity was poor at lower catalyst loadings. This also suggests that when a higher catalyst loading was used the reaction started to become predominantly mass transfer limited and as it is not of practical interest to use large amounts of catalyst, 2.5 mol% catalyst was fixed as the optimum amount for the butanolysis of FFA. Regardless of the catalyst loading **4.11** always outperformed **4.10** and **Amberlyst-15**. These results were promising compared the catalyst loadings that were used by Zhang, Kamaraju and Song of 5 mol% [MIMBS]$_3$PW$_{12}$O$_{40}$, 0.4 g Al$_2$O$_3$/SBA-15 and 0.6 mmol [(HSO$_3$-p)$_2$im][HSO$_4$], respectively.

4.3.5 Amount of *n*-Butanol Optimisation

It is widely reported that FFA readily polymerises at high concentrations in the presence of strong acid catalysts.[58] Hence, the amount of *n*-butanol may well have a considerable effect on the product yield if the amount of FFA is kept constant. During the reaction, *n*-butanol was used as an excess reactant with FFA as the limiting reactant to drive the equilibrium towards the formation of *n*-butyl levulinate. The effect of the volume of *n*-butanol on FFA alcoholysis was examined between 1 mL and 5 mL the results are shown in figure 4.19. During the reaction, for all volumes, the mixture rapidly turned black within the first 5 minutes, indicating that the FFA had readily polymerised to form polyfurfuryl alcohol which is black in appearance.
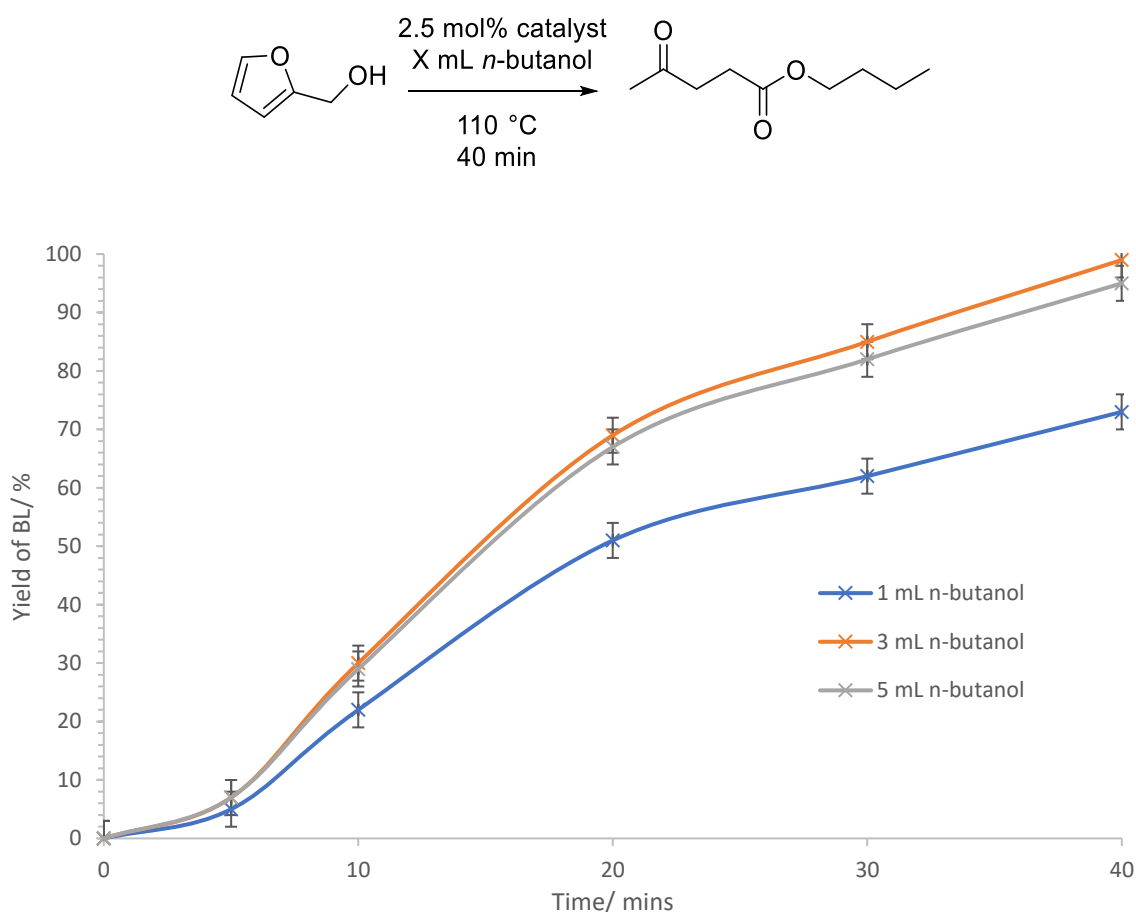
Figure 4.19: Effect of the volume of *n*-butanol on FFA alcoholysis. Reaction conditions: 2.5 mol% 4.11; FFA, 1 mmol; *n*-butanol, (set amount); temperature, 110 °C; time, 40 mins; agitation, 800 rpm. Conversion and selectivity determined by ^{1}H NMR spectroscopy with 1,4-dioxane as the internal standard. Yield for *n*-butyl levulinate = [% conversion of furfuryl alcohol x (% selectivity *n*-butyl levulinate / 100). Average of 3 runs.

When the volume of *n*-butanol was decreased from 3 to 1 mL the yield and selectivity of BL decreased from 100 to 73%, respectively. Increasing the amount of *n*-butanol is highly useful for the reaction as it increases the probability of the reactants colliding. However, excess *n*-butanol could also result in a dilution effect and is not effective for minor changes in the reaction. The maximum yield of BL was achieved with 3 mL of *n*-butanol and as there was little difference between 3 and 5 mL, 3 mL was chosen as the optimal volume for all further batch reactions to reduce wastage of solvent. The sole reaction of *n*-butanol at 110 ℃ in the absence of furfuryl alcohol after 40 minutes gave ethers such as dibutylether, dibutoxyalkanes and esters such as acetic acid butyl ester, butanoic acid butyl ester. Therefore, the unproductive *n*-butanol consumption may also be a result of self-reactions of the *n*-butanol.[31]

4.3.6 Temperature Optimisation

Temperature is recognised to have an extreme effect on both the reaction rate and the product yield. The effect of the temperature on the butanolysis of FFA was studied in the temperature range 50-110 ℃, the results of which are shown in figure 4.20. The temperatures mentioned in these studies were the temperatures recorded in the oil bath.
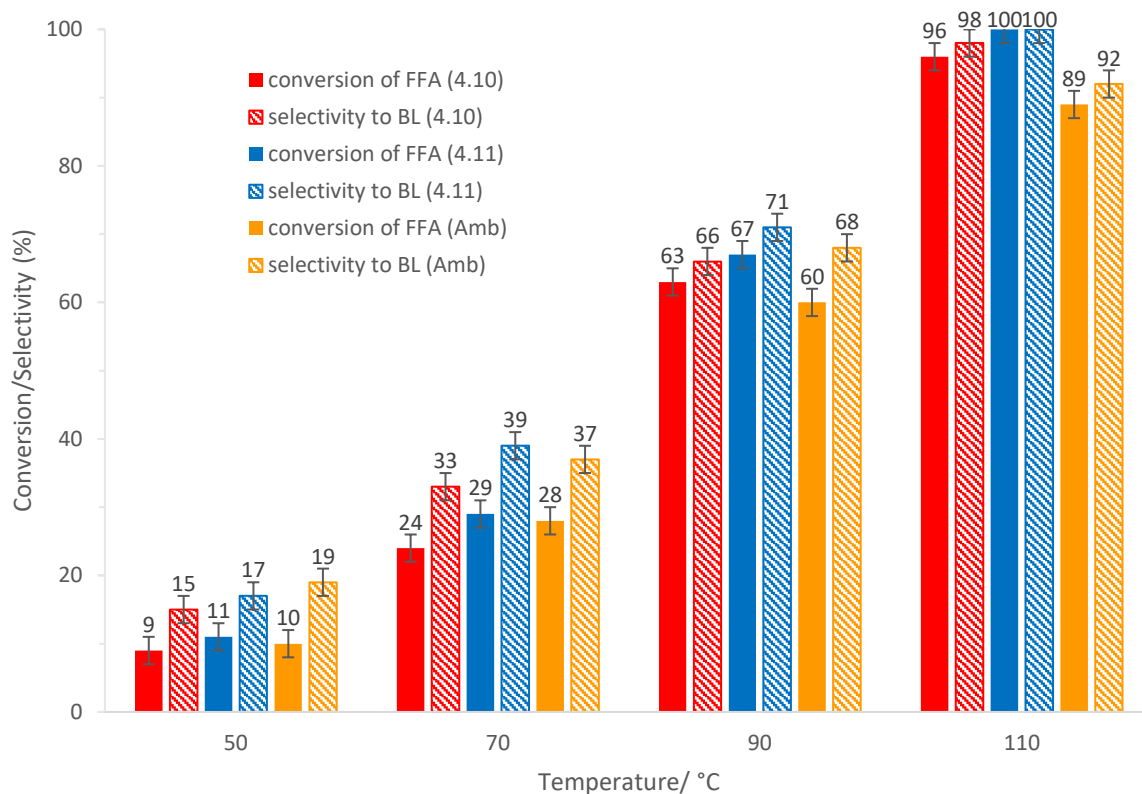
Figure 4.20: Effect of the temperature on FFA alcoholysis. Reaction conditions: 2.5 mol% catalyst; FFA, 1 mmol; *n*-butanol, 3 mL; temperature, (specified temp); time, 40 mins; agitation, 800 rpm. Conversion and selectivity determined by ^{1}H NMR spectroscopy with 1,4-dioxane as the internal standard. Selectivity for *n*-butyl levulinate = [% *n*-butyl levulinate / (% *n*-butyl levulinate + % 2-butoxymethylfuran)]. Average of 3 runs.

The conversion-selectivity profile showed that little activity was observed at 50 °C. Above 50 °C, the conversion of FFA and the amount of BL that was produced increased. The reaction at 70 ℃ also showed that a significant amount of FFA had remained unreacted, this indicated that the first reaction step to form the 2-butoxymethylfuran intermediate was demanding and the rate determining step of the reaction. The temperature of the alcoholysis of FFA has a significant impact on the rate of the reaction and thereby influences the conversion of FFA. Hence, at higher temperatures the increase in the rate of reaction may well be due to accessibility of the substrate to the active site, possibly resulting from swelling of the catalyst. This results in a higher conversion of FFA and a higher yield of BL as a result of the more frequent,

successful collisions between the reactants, which have sufficient energy to break the bonds in the reactant molecules to form the product. Therefore, it is not surprising that the selectivity for BL and the conversion of FFA increased with increasing temperature. When the temperature was increased to 90 ℃, the selectivity towards BL increased to 66-71% with a concomitant decrease in the selectivity for 2-BMF. A further increase to 110 ℃ resulted in complete conversion of FFA and selectivities for BL between 92-100%. As the temperature increased from 50 to 110 ℃, the selectivity drastically decreased towards the intermediate 2-BMF, suggesting that the conversion of 2-BMF to BL was higher at 110 and 90 ℃ in comparison to the lower temperatures of 70 and 50 ℃. These results are consistent with the literature which report that at higher temperatures there was an enhanced butanolysis of FFA which led to the increased rates of *n*-butyl levulinate production.[24, 38, 44] Most of the studies in the literature on the FFA alcoholysis were performed at temperatures between 110 and 140 °C therefore, 110 ℃ was chosen as the optimum reaction temperature for the batch butanolysis reactions due to the short reaction times required and the high *n*-butyl levulinate yields obtained.

Prompted by the poor activity obtained for the butanolysis of FFA after the formation of polyfurfuryl alcohol, a series of batch reactions were carried out to establish whether the polyfurfuryl alcohol poisons the catalyst. The butanolysis of 1 mmol of furfuryl alcohol using 2.5 mol% of either **4.11** or **Amberlyst-15** as a function of the amount of polyfurfuryl alcohol was investigated to explore the possibility of catalyst poisoning.
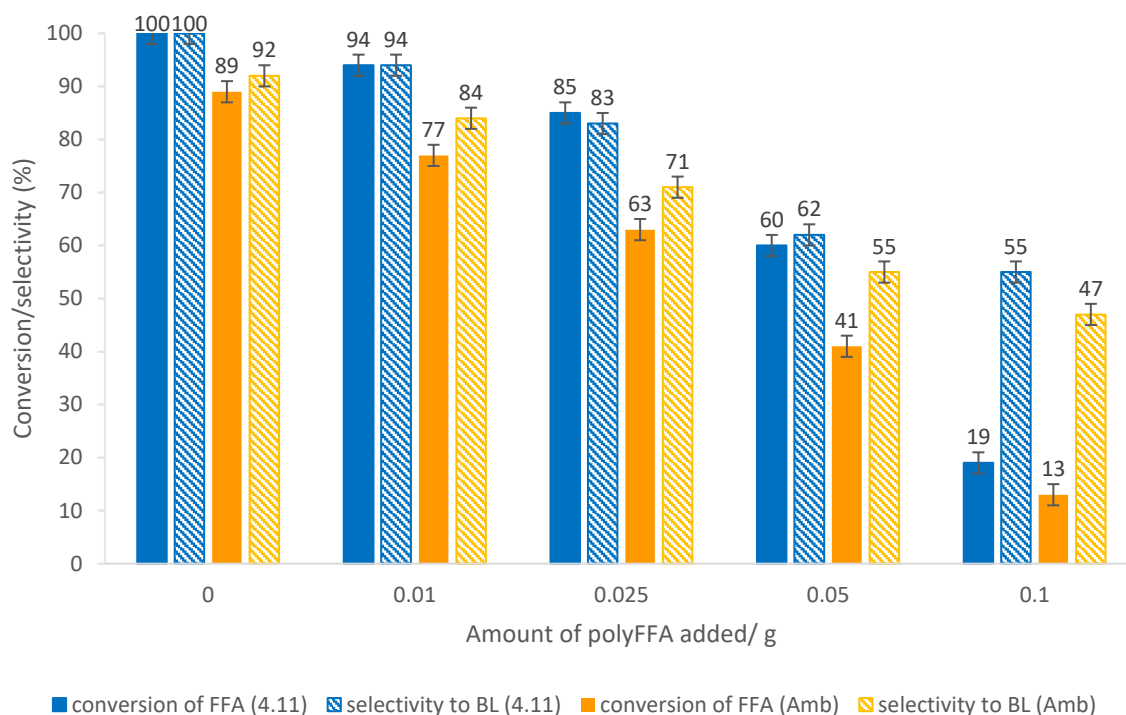
Figure 4.21: Conversion and Selectivity as a function of the amount of polyfurfuryl alcohol on the butanolysis of FFA. Reaction conditions: 2.5 mol% catalyst; FFA, 1 mmol; n-butanol, 3 mL; temperature,110 ℃; time, 40 mins; agitation, 800 rpm. Conversion and selectivity determined by ^{1}H NMR spectroscopy with 1,4-dioxane as the internal standard. Selectivity for *n*-butyl levulinate = [% *n*-butyl levulinate / (% *n*-butyl levulinate + % 2-butoxymethylfuran)]. Average of 3 runs.

The results in figure 4.21 showed that pretreatment with 0.05 g of polyfurfuryl alcohol resulted in a reduction in the butanolysis of FFA by 40%, whilst in the absence of polyfurfuryl alcohol 100% conversion of FFA was obtained under the same reaction conditions; this suggests that the polymer may well deactivate the catalyst by 'blocking' the pores and preventing access to the active sites. The activity was also significantly diminished for the butanolysis of FFA when 0.1 g of polyfurfuryl alcohol was added, although only 19% conversion was obtained compared to 100% in the absence of polyfurfuryl alcohol. The reduced conversion for BL could be associated with the polyfurfuryl alcohol binding to the catalytic active sites which eventually saturates the available sites, therefore leading to an accumulation of the intermediate 2-BMF as it impedes the substrates access to the catalyst. The formation of this

oligomeric/polymeric side product was found to be more suppressed by operating at moderate temperatures and/or reducing the reaction time.

4.3.7 Comparison with Existing catalysts

The activity of the best performing POM@PIIL catalyst **4.11**, was compared with other acid catalysts reported in the literature for the butanolysis of furfuryl alcohol to compare the catalyst performance against state-of-the-art catalysts (Table 4.5). Some of which include a tin exchanged tungstophosphoric acid (TPA) supported on montmorillonite K-10 clay catalyst, titanium incorporated mesoporous KIT-6 molecular sieve catalyst, TPA and alumina impregnated mesoporous silica, Zeolite HZSM-% (Si/Al ratio 50) and aluminium supported dendritic fibrous nanosilica bifunctional solid acid catalyst.

Table 4.5: Catalytic performance of acid catalysts reported in the literature for the butanolysis of furfuryl alcohol to *n*-butyl levulinate after 1 hour.

Entry	Mole ratio (FFA: butanol)	Catalyst	Catalyst amount (g)	FFA conv. (%)	BL yield (%)	Ref
1[a]	1:20	Sn_1TPA/K-10	0.4	100	70	[60]
2[b]	1:60	100Ti-KIT-6	0.3	75	45	[62]
3[b]	1:65	25 wt% TPA/SBA-16	0.3	100	38	[63]
4[b]	1:65	$20Al_2O_3$/SBA-15	0.4	100	35	[24]
5[b]	1:48	$[MIMBS]_3PW_{12}O_{40}$	0.2	99	25	[44]
6[b]	1:33	HZSM-5	0.05	100	22	[36]
7[b]	1:8	Amberlyst 39	1	53	21	[64]
8[a]	1:15	$40Al/DFNS/Pr-SO_3H$	0.05	87	14	[65]
9[b]	1:33	POM@PIIL **4.11**	0.1	100	100	This work

[a]Reaction was conducted at 120 ℃. [b]Reaction was conducted at 110 ℃.

This comparison is semi-quantitative as the reaction conditions applied in most of the cases are far from ideal. The catalytic activity was compared based on the yield of *n*-butyl levulinate after 1 hour. The data in table 4.5 show that **4.11** (entry 10) either rivals or outperforms previously reported catalysts in that it gives higher conversions to furfuryl alcohol with complete selectivity for *n*-butyl levulinate. In addition, all of the reported experiments in the literature on the conversion of FFA to *n*-butyl levulinate were performed in batch reactions, except for 20Al$_2$O$_3$/SBA-15 (entry 5), which is, to the best of our knowledge the only study on the continuous flow butanolysis of FFA.[24] Therefore, more research is required in the application of acid catalysts in flow for the butanolysis of FFA (see later).

4.3.8 Substrate Screening

The encouraging results obtained for the alcoholysis of FFA with **4.11** led to the catalyst testing being extended to a range of alcohols to explore the scope of this method (Scheme 4.6) and the influence of the alcohol on the efficacy of **4.11** and **Amberlyst-15** (Table 4.6).
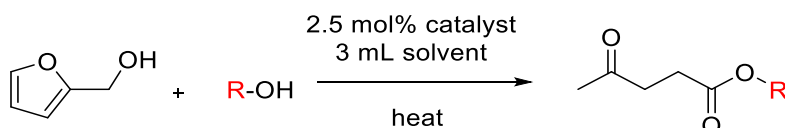
Scheme 4.6: Alcoholysis of furfuryl alcohol with different alcohols catalysed by **4.11** and **Amberlyst-15**.

Table 4.6: Substrate screening for the alcoholysis of furfuryl alcohol.

Entry[a]	Substrate	Boiling point/ °C	Catalyst	Conversion (%)[b]	Selectivity to AL (%)[b]	Yield of AL (%)
1	Ethanol	78.4	**4.11**	66	51	33
			Amberlyst 15	61	44	27
2	*n*-propanol	97.1	**4.11**	65	63	41
			Amberlyst 15	62	58	36
3	*n*-butanol	117.3	**4.11**	100	100	100
			Amberlyst 15	100	90	86

4	*n*-pentanol	137.3	**4.11**	100	100	100
			Amberlyst 15	100	90	90
5	*n*-hexanol	157	**4.11**	100	100	100
			Amberlyst 15	100	92	92

[a]Reaction conditions: 2.5 mol% **4.11** or **Amberlyst-15**; FFA, 1 mmol; alcohol, 3 mL; temperature, (reflux); time, 40 mins; agitation, 800 rpm. [b]Conversion and selectivity determined by ^{1}H NMR spectroscopy with 1, 4-dioxane as the internal standard. Selectivity for alkyl levulinate (AL) = [% alkyl levulinate / (% alkyl levulinate + % 2-alkylmethylfuran)]. Average of 3 runs.

FFA alcoholysis with ethanol and *n*-propanol gave moderate conversions (50-70%) with lower selectivity towards the alkyl levulinate (AL) of 27-40% in all of the cases (entries 1 and 2). As a result of the lower reflux temperatures of ethanol and *n*-propanol compared to the higher alcohols (*n*-butanol, *n*-pentanol and *n*-hexanol) conversion of the intermediate alkoxymethylfuran to AL was much slower. However, complete conversion with 100% selectivity for the AL was achieved in both cases by extending the reaction time to 90 minutes.

4.3.9 Recycling Studies

Reasoning that the highly ionic microenvironment of PIILs should efficiently retain the active polyoxometalate during the extraction, recycle experiments were conducted using 2.5 mol% of catalyst for the butanolysis of FFA to assess the robustness and longevity of these systems and their potential for the incorporation of these systems into a continuous flow process. The reaction time was reduced from 40 minutes to 30 minutes for this study to prevent the full consumption of FFA to enable changes in conversion to be identified. After one run the spent catalyst was recovered by centrifugation (5 min, 6000 rpm) of the resulting reaction mixture followed by filtration to recover the catalyst. This was then washed with water and ethyl acetate three times to remove unreacted FFA. The recovered catalyst was dried at 100 ℃ for 3 hours, before being reused directly for the subsequent cycles without being replenished or reconditioned, the results across 4 recycles are represented in figure 4.22.
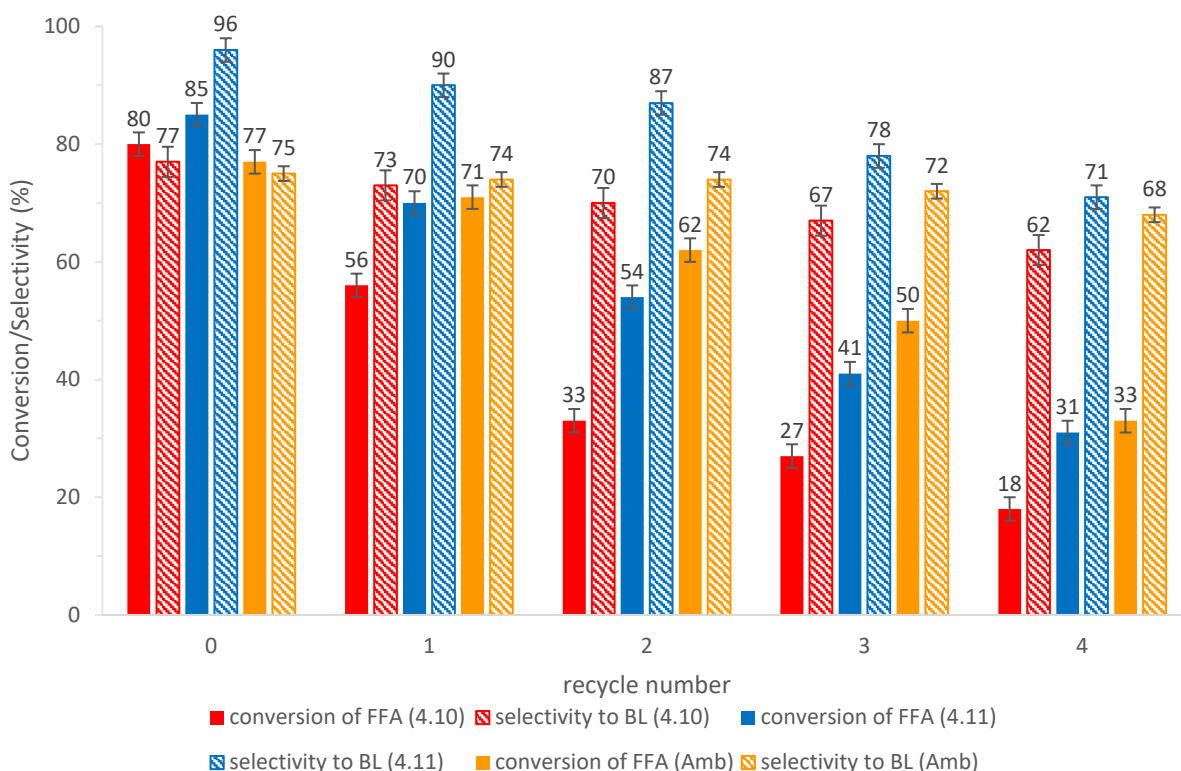
Figure 4.22: Recyclability of **4.10**, **4.11** and **Amberlyst-15** in the alcoholysis of FFA with *n*-butanol. Reaction conditions: 2.5 mol% catalyst; FFA, 1 mmol; n-butanol, 3 mL; temperature, 110 ℃; time, 30 mins; agitation, 800 rpm. Conversion and selectivity determined by ^{1}H NMR spectroscopy with 1, 4-dioxane as the internal standard. Selectivity for *n*-butyl levulinate = [% *n*-butyl levulinate / (% *n*-butyl levulinate + % 2-butoxymethylfuran)]. Average of 2 runs.

As seen in figure 4.22, there is a clear decline in both the conversion of FFA and selectivity to BL for all of the systems in the successive runs which indicated a significant deactivation of the catalysts had occurred. The drop in the conversion between the runs may be due to attrition during the filtration and the catalyst recovery procedure. After the 4th run, 0.055 g and 0.072 g of **4.10** and **4.11**, respectively was recovered which is significantly less than the initial ~0.1 g (2.5 mol%) of catalyst used in the first run; this would account for the drop in conversion with each recycle. Analysis of the catalysts recovered after each recycle showed that their IR bands were essentially superimposable with fresh catalysts (Appendix N for the spectra). This

strongly indicated that the attrition i.e. loss of supported catalyst and that the drop in the conversion of FFA was due to catalyst deactivation and/or leaching of the polyoxometalate. In addition, CHN analysis of the spent catalyst after the 4th run showed the presence of a carbonaceous species, which was not found in the fresh catalyst. Therefore, the drop in the conversion of FFA may be due to absorption of the insoluble, oligomeric by-product from FFA polymerisation onto the surface of the solid catalyst which would hinder access of the substrate to the catalytic active sites.

During the alcoholysis process it is expected that a loss of H^+ ions would occur through water dissolution from the reaction, although, such H^+ ion loss can be replenished in the acid-washing step. The reduced catalytic activity is presumably due to the saturation of water clusters that surround the active sites and by the irreversible fouling of polyfurfuryl alcohol with the support which leads to the partial blocking of the active sites. This could also be the cause for the reduction of the *n*-butyl levulinate yield. A closer inspection revealed that the colour of the surface of the recovered POM@PIIL catalysts became dark-brown after each catalytic run. This could be a result of the deposition or adsorption of the solid by-products of the furfuryl alcohol polymerisation on the catalyst surface, which resulted in the partial shielding of the active catalytic sites. This was measured by acid−base back titrations which showed that after the first cycle the total acid density of spent **Amberlyst-15** was 2.10 mmol g^{-1} which obviously declined compared to that of the fresh **Amberlyst-15** with an acid amount of 4.75 mmol g^{-1}. It further suggests that the partial shield was of the surface acid sites and/or cation exchange may have occurred during the reaction.

Consequently, the spent POM-based PIIL catalysts were calcined at 300 °C for 3 hours (PIL support is stable at this temperature from the TGA analysis) prior to each recycle run to burn away any deposited polymer impurities. As the structure of polyfurfuryl alcohol is similar to the structure of the PIIL supports, a higher temperature will be required to burn off the polymer although this would consequently degrade the PIIL support. As it was inappropriate to calcine recovered **Amberlyst-15** due to its poor thermal stability, the recovered **Amberlyst-15** resin was soaked in a 2M HCl solution for 1 hour prior to each recycle run.[67] The reuse experiments demonstrated that the regenerated **Amberlyst-15** retained high activity with only a minor reduction in the yield of *n*-butyl levulinate over 4 successive runs.

These results highlight the necessity to obtain an understanding about how the polymer's microenvironment can change under harsh conditions. For example, swelling of the polymer may render the catalyst's pore structure unsuitable for the reaction. Due to the broad industrial application of alkyl levulinates as either a fuel additive or in fine chemical production, the utilsation of a highly efficient, environmentally benign, selective catalyst is very desirable in scale-up reactions. As such, a more detailed study into the alcoholysis of FFA using POM@PIIL catalysts and cation exchange resin and their implementation into continuous flow processes was carried out.

4.4 Alcoholysis Under Flow Conditions

The successful application of the POM@PIILs **4.10** and **4.11** and the ion exchange resin **Amberlyst-15** for the butanolysis of FFA in batch prompted us to explore the potential application of these systems to segmented and continuous flow protocols to assess the robustness, longevity and relative merits of these POM@PIIL systems. To further demonstrate the efficiency of POM@PIILs, the catalysts were examined under various flow conditions by modifying the residence time (i.e. the amount of time that the reactant feed remains in contact with the reactor subject to the flow rate of the reactant solution), the reaction temperature and the related combinations. The challenging alcoholysis reaction often demands harsh reaction conditions; therefore, a number of products can still form under such conditions and catalyst poisoning usually occurs.

One of the main limitations of continuous flow operation, when optimising conditions for a new chemical reaction is attaining steady state. The steady state is when the variations in the substrate mixing, flow rate and heat transfer no longer need to be considered under continuous flow conditions. Usually, five-fold increase in the residence time, R_t is required to reach the steady state and therefore eliminate any variability in the experimental output.[66] To this end, the optimisation is usually not ideal when several reaction components must be studied such as the residence time, reagent stoichiometry and reaction temperature. Such continuous flow experiments which require sequential optimisation quickly becomes very time-consuming, while at the same time require enormous amounts of reagent and solvent. In this regard, the

use of segmented flow conditions is employed for efficient and rapid reaction screening and optimisation (Figure 4.23). Performing reactions in this way enables small volumes of the reaction mixture to be, in a rapid manner, effectively exposed to different reaction conditions while using significantly less reagent. For this reason, the initial optimisation of the reaction conditions for the newly designed flow system was carried out under segmented flow.
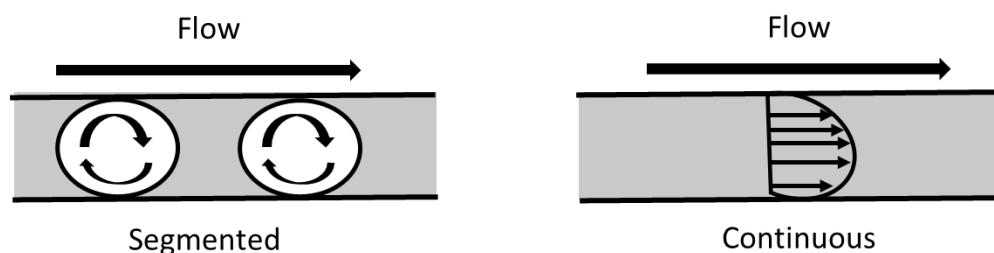
Figure 4.23: Schematic representation of the different mixing modes observed in segmented and continuous flow conditions.

Continuous flow reactions are more suitable for industrial applications as they offer several advantages over batch systems such as enhanced mass and heat transfer, time efficiency (larger throughput at a faster pace), long term production, the possibility of multistep reactions in a continuous sequence, effective mixing, facile scale-up and reaction optimisation and cheaper automation. In this regard, there have been surprisingly few reports of the continuous flow alcoholysis of furfuryl alcohol, with only one for the butanolysis;[24] and as such there is a need to explore this technology to identify systems that give high conversions of FFA and selectivities for *n*-butyl levulinate.

An operationally straightforward flow set-up was developed using a Uniqsis FlowSyn reactor with a 10 mm by 100 mm reactor cartridge (Figure 4.24).
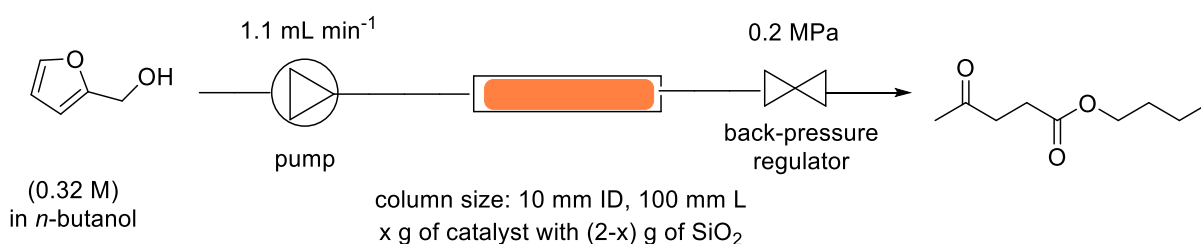
Figure 4.24: Schematic representation of the Uniqsis FlowSyn setup used for the segmented and continuous flow reactions catalysed by a cartridge of catalyst mixed with silica.

A diluted mixture of 1.0 g of the catalyst with 1.0 g of silica (Geduran Si60 0.060-0.2 mm) was packed into the cartridge reactor. This was then mounted in a heating mantle and connected to a flow reactor using Teflon tubing. The total flow-through volume (including the feed and reactor sections) was found to be 4.4 mL. First, pure *n*-BuOH was pumped through the system and then the feed was switched to the 0.32 M FFA feedstock. The flow was continued until the desired temperature and hydrodynamic pressure of 0−50 bar of the reactor module was reached. Then, in function of the flow rate, the reaction proceeded for 12 minutes before the first sample was collected (sample at time = 0 minutes). Following the reaction, the product stream passes through a backpressure regulator prior to collection. The reaction mixture was collected at the reactor's outlet and further samples were collected after regular time intervals and analysed by ^{1}H NMR spectroscopy. The aliquots were concentrated *in vacuo* and 1,4-dioxane was used as an internal standard to determine the conversion and selectivity for BL. Under the experimental conditions, highly reproducible flow patterns were observed within short equilibration times.

4.4.1 Catalyst Loading

Preliminary investigation and optimisation studies were conducted using segmented flow in which 3 mL aliquots of (0.32 M) FFA in *n*-butanol were pumped through a cartridge reactor packed with (2-x) g of silica mixed with varying amounts of catalyst (x = 0.1 − 1.5 g) at a flow rate of 1.1 mL min^{-1}; this corresponds to a residence time of 4 minutes. Based on the batch results, **4.11** outperformed **4.10** in every optimisation and therefore only **4.11** catalyst amount was optimised with the flow conditions. Reactions were monitored after one hour and the results are shown in figure 4.23.
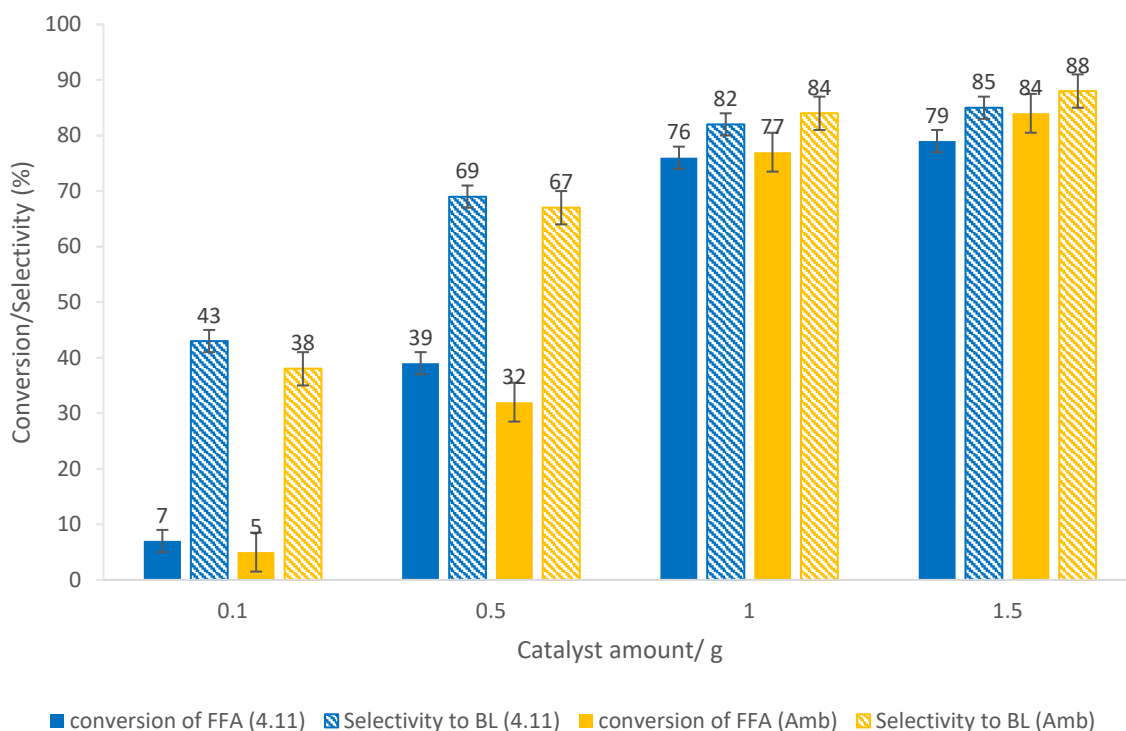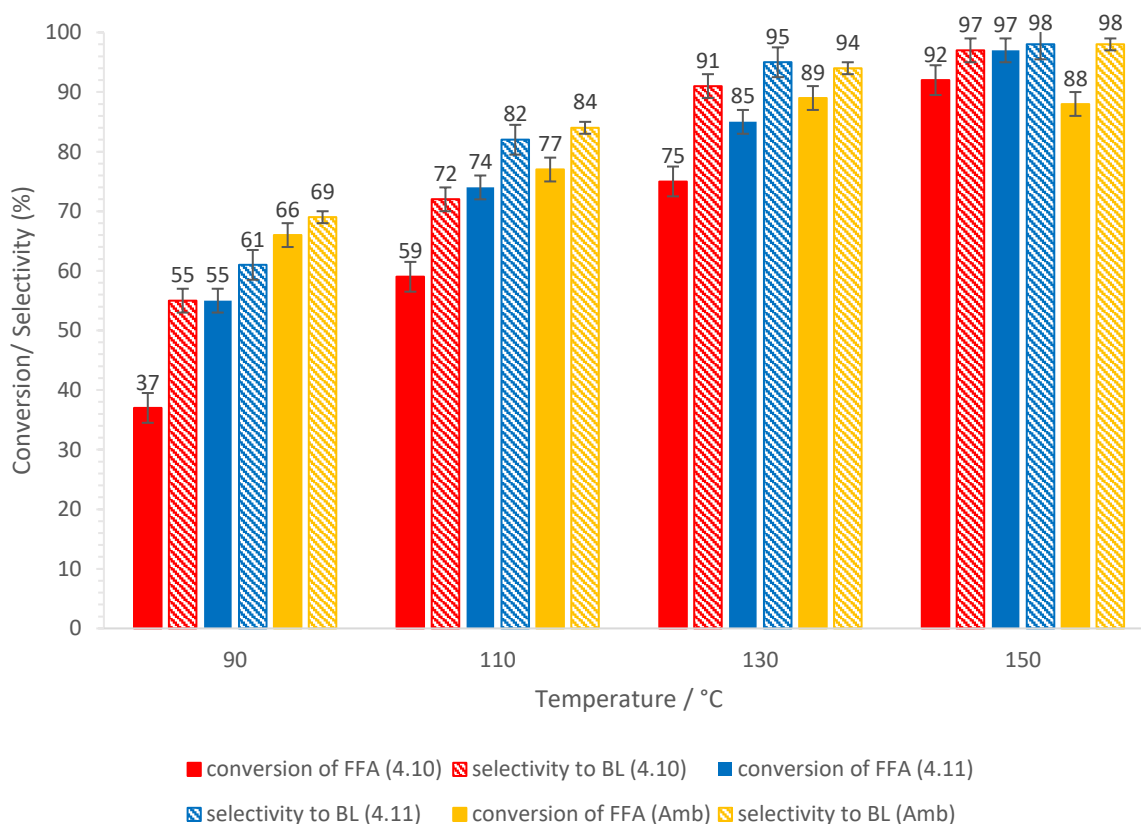
Figure 4.25: Influence of the catalyst amount on the selectivity and conversion for the segmented flow alcoholysis of FFA in *n*-butanol catalysed by **4.11**/SiO$_2$ and **Amberlyst-15**/SiO$_2$. Reaction conditions: catalyst, (specified amount, x g of POM@PIIL or resin mixed with 2-x g of silica); 0.32 M FFA in *n*-butanol; temperature, 110 ℃, flow rate, 1.1 mL min^{-1}; time, 60 mins. Conversion and selectivity determined by ^{1}H NMR spectroscopy with 1,4-dioxane as the internal standard. Selectivity for *n*-butyl levulinate = [% *n*-butyl levulinate / (% *n*-butyl levulinate + % 2-butoxymethylfuran)]. Average of 3 runs.

First, a blank experiment using a cartridge filled with silica and no catalyst was conducted to eliminate any catalytic effects by the reactor itself and this resulted in no conversion of FFA. Figure 4.25 shows that the use of 0.1 or 0.5 g of catalyst gave low conversions and moderate selectivities while an increase in the catalyst loading to 1.0 g resulted in a significant improvement in both conversion and selectivity. For example, **4.11** and **Amberlyst-15** gave conversions of 76% and 77%, respectively and selectivities of 82% and 84% butyl levulinate, respectively. Notably, a further increase in the catalyst amount to 1.5 g did not greatly change the yield of BL compared with that for 1 g, therefore all further optimisation studies used 1 g of catalyst.

4.4.2 Temperature

The effect of temperature in batch reactions is not the same as the effect of the temperature in segmented and continuous flow as the reactors back-pressure regulator allows for more control over the pressure of the reaction. Reactions can therefore be conducted at higher temperatures, above the boiling point of *n*-butanol (bp 117 ℃), which results in improved yields and shorter reaction times. With the added advantage of flow reactors possessing high heat transfer efficiency and the heat released from the reaction can be removed in time to avoid the formation of unwanted side products, therefore, consecutive by-products can be inhibited or at least minimised by the process. A series of segmented flow reactions were conducted at 90 °C, 110 °C, 130 °C and 150 °C using 1.0 g of catalyst with a flow rate of 1.1 mL min^{-1} and a reaction time of 1 hour, the results of which are shown graphically in Figure 4.26. At 90 ℃ low conversions were obtained which is consistent with the batch studies (Figure 4.20). Above 90 ℃ conversion improved for each catalyst, **4.11** proved to be the more efficient catalyst ultimately giving near quantitative conversions at 150 °C.

Figure 4.26: Influence of the temperature on the selectivity and conversion for the segmented alcoholysis of FFA in *n*-butanol catalysed by **4.10**/SiO$_2$, **4.11**/SiO$_2$ or **Amberlyst-15**/SiO$_2$. Reaction conditions: catalyst, 1 g of POM@PIIL or resin on 1 g SiO$_2$; 0.32 M FFA in *n*-butanol; temperature, 110 ℃, flow rate, 1.1 mL min^{-1}; time, 60 mins. Conversion and selectivity determined by ^{1}H NMR spectroscopy with 1,4-dioxane as the internal standard. Selectivity for *n*-butyl levulinate = [% *n*-butyl levulinate / (% *n*-butyl levulinate + % 2-butoxymethylfuran)]. Average of 3 runs.

Light-orange samples were recovered from the reactions conducted at 90 °C and 110 °C , an indication that no apparent catalyst fouling/deactivation had occurred; however, at this temperature lower conversions of FFA were obtained (Figure 4.27). Darker coloured samples were recovered after the first 10 minutes of operation for reactions conducted above 110 ℃ which indicated a degree of catalyst leaching/fouling had occurred. In addition, the catalyst cartridge after the reaction at 130 °C and 150 ℃ appeared dark-grey which also further indicated that either catalyst deactivation or the saturation of the acid sites with polyfurfuryl alcohol at these temperatures had occurred. However, the poor conversion and low yield of butyl levulinate obtained at 90 and 110 ℃ prompted us to conduct further investigations at 130 °C.


Figure 4.27: Photograph of collected post reaction samples at 150, 130, 110 and 90 ℃ (from left to right).

4.4.3 Flow Rate and Residence Time

In flow chemistry, the contact or residence time is the ratio of the volume of the reactor and the flow rate of the reactant solution. This measures the time in which the reactants stay in contact with the catalyst. In general, the higher the contact time or the longer the residence time of a reactant inside the reactor, the higher should be the conversion of a reactant into the expected products. However, deactivation or decomposition of the catalyst and/or undesired acid-catalysed transformations often occur with prolonged contact or residence times which can poison the catalyst.

Following the determination of an optimum reaction temperature, the effect of the reactions flow rate was investigated and therefore the effect of the residence time on the yield of butyl levulinate was also studied the results of which are shown in figure 4.28.
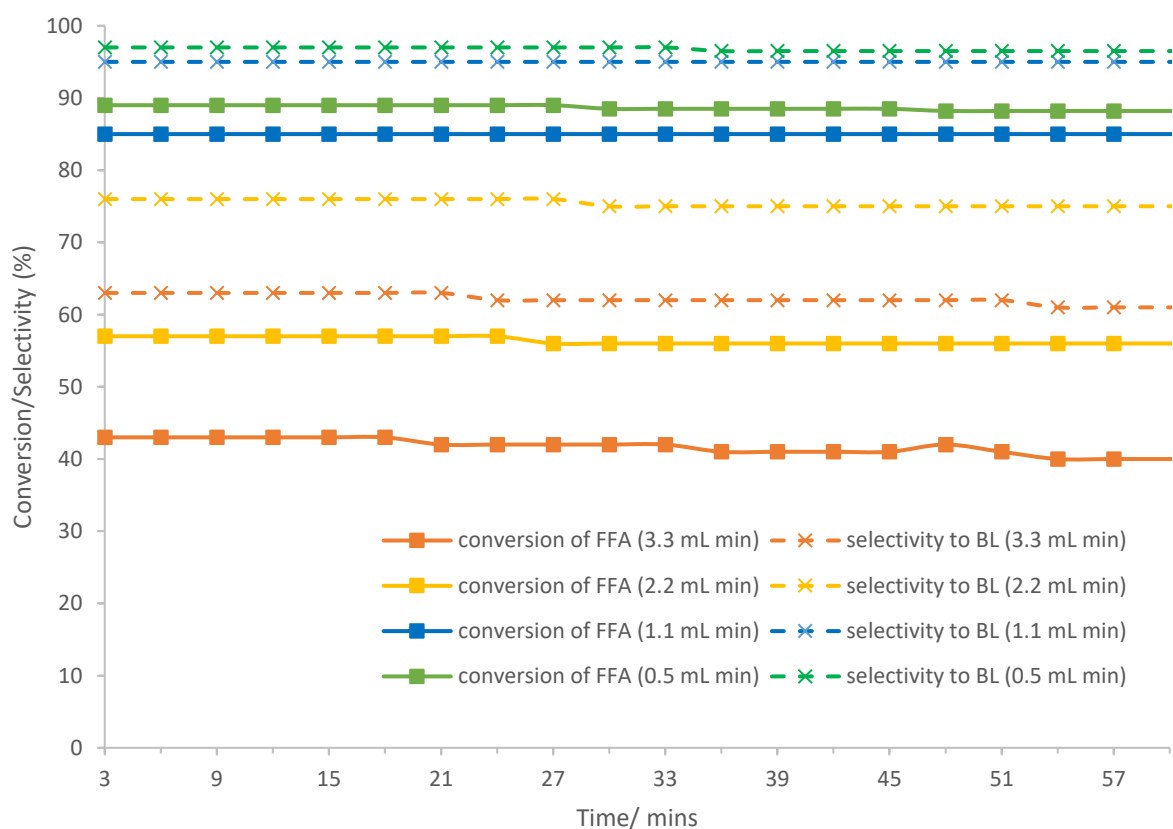

Figure 4.28: Influence of the flow rate and the residence time (R_t) on the selectivity and conversion in the segmented flow alcoholysis of FFA in *n*-butanol catalysed by **4.11**/SiO$_2$. Reaction conditions: catalyst, 1.0 g of **4.11** on 1.0 g of silica; 0.32 M FFA in *n*-butanol; temperature, 130 ℃; flow rate, (specified FR); injection volume, 60 mL. Conversion and selectivity determined by ^{1}H NMR spectroscopy with 1,4-dioxane as

the internal standard. Selectivity for *n*-butyl levulinate = [% *n*-butyl levulinate / (% *n*-butyl levulinate + % 2-butoxymethylfuran)]. Average of 2 runs.

Figure 4.28 shows the effect of the flow rates and the residence times on the conversion of FFA and the selectivity towards butyl levulinate. A flow rate of 3.3 mL min^{-1} (R_t = 1.3 minutes) resulted in a decrease in the conversion of FFA to 43%, as the reaction required a certain amount of contact time with the catalyst cartridge in order to achieve high conversions of FFA. A slightly higher conversion of 57% was obtained when the reaction was conducted with a flow rate of 2.2 mL min^{-1} (R_t = 2 minutes). For this reaction, low flow rates and a longer substrate residence time of 4 minutes (1.1 mL min^{-1}) gave 85% conversion and high selectivity for butyl levulinate. The conversion and selectivity improved slightly when the residence time was increased to 8.8 minutes (0.5 mL min^{-1}). The substrate mixture was added at a rate of 0.5 mL min^{-1} (R_t = 8.8 minutes), however, it is inherent that the errors in the pressure are significantly higher at lower flow rates, in particular at flow rates < 1 mL min^{-1}. In addition, longer residence times than 1.1 mL min^{-1} were considered to be less productive in terms of the improvement in conversion/selectivity and as such a residence time of 1.1 mL min^{-1} was considered to be the best compromise for further studies. Gratifyingly, the conversions and the selectivity for butyl levulinate showed stable profiles over the entire experiment.

4.4.4 Kinetic Studies

In the next set of reactions the effect of the reaction temperature was studied with a comparative set of life-time studies at 130 ℃ and 150 ℃ using a cartridge packed with either **4.10**/SiO$_2$, **4.11**/SiO$_2$ or **Amberlyst-15**/SiO$_2$ (Figure 4.29).
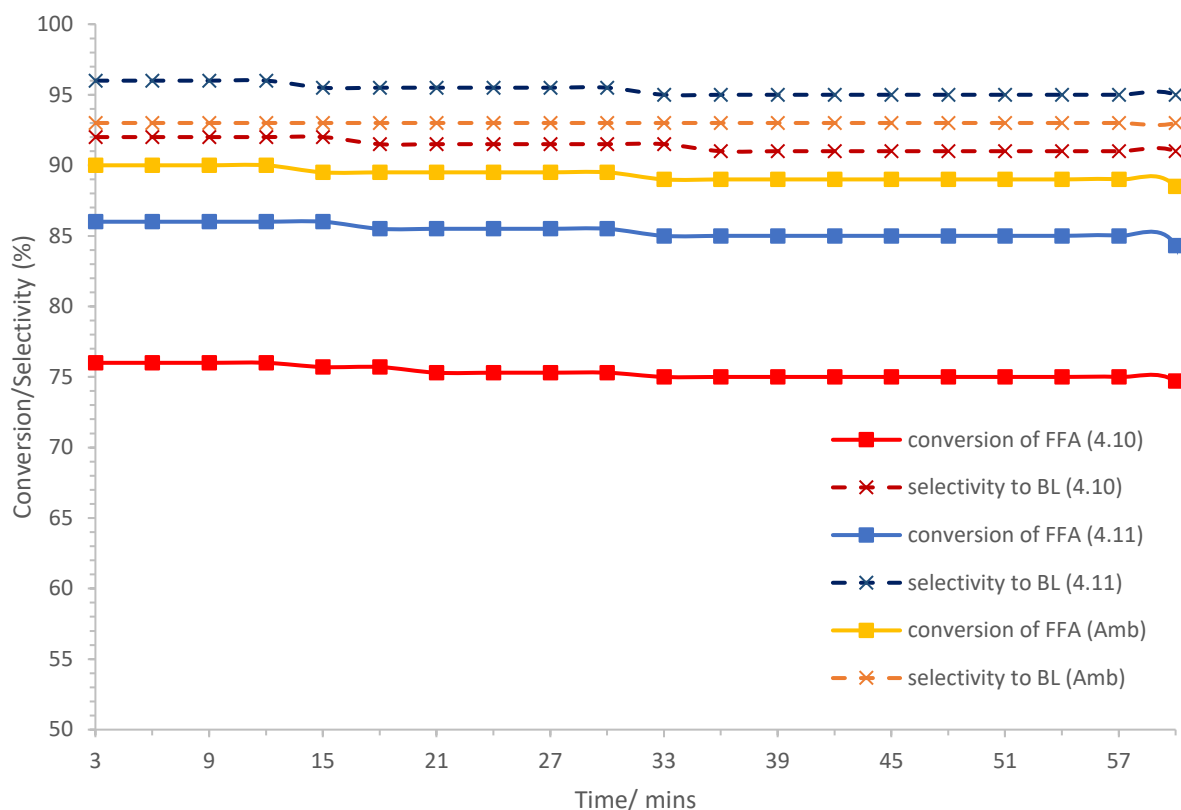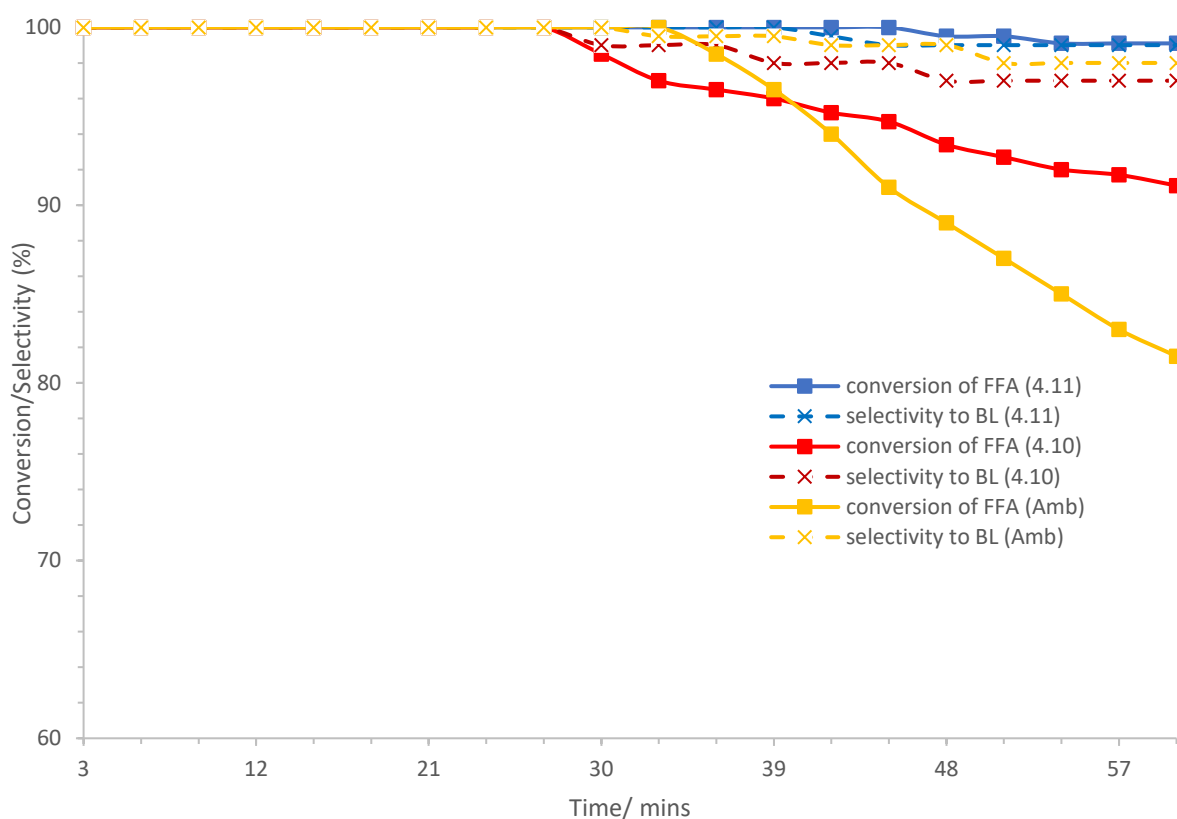
Figure 4.29: Conversion-selectivity profile as a function of the time-on-stream (1 h) for the segmented flow alcoholysis of FFA catalysed by **4.10**/SiO$_2$, **4.11**/SiO$_2$ and **Amberlyst-15**/SiO$_2$. Reaction conditions: catalyst, 1 g of POM@PIIL or resin on 1 g of silica; 0.32 M FFA in *n*-butanol; temperature, 130 ℃; flow rate, 1.1 mL min^{-1}; injection volume, 60 mL. Conversion and selectivity determined by ^{1}H NMR spectroscopy with 1,4-dioxane as the internal standard. Selectivity for *n*-butyl levulinate = [% *n*-butyl levulinate / (% *n*-butyl levulinate + % 2-butoxymethylfuran)]. Average of 2 runs.

The resulting time-composition profile in figure 4.29 revealed that the conversion and selectivity remained relatively constant over the one-hour. Catalysts **4.10** and **4.11** gave conversions of 75 and 85%, respectively, at 130 ℃ with high selectivity for butyl levulinate. Moreover, all of the catalyst cartridges could be stored overnight and reused with only a minor reduction in the catalyst performance (~1%) the following day indicating the system may be stable and suitable for use in continuous flow and semi-quantitative scale-up reactions.

` The temperature was then raised to 150 ℃ to explore the effect of an increase in temperature on the alcoholysis of FFA.


Figure 4.30: Conversion-selectivity profile as a function of the time-on-stream (1 h) for the segmented flow alcoholysis of FFA catalysed by **4.10**/SiO$_2$, **4.11**/SiO$_2$ and **Amberlyst-15**/SiO$_2$. Reaction conditions: catalyst, 1.0 g of POM@PIIL or resin on 1.0 g of silica; 0.32 M FFA in *n*-butanol; temperature, 150 ℃; flow rate, 1.1 mL min^{-1}; injection volume, 60 mL. Conversion and selectivity determined by ^{1}H NMR spectroscopy with 1,4-dioxane as the internal standard. Selectivity for *n*-butyl levulinate = [% *n*-butyl levulinate / (% *n*-butyl levulinate + % 2-butoxymethylfuran)]. Average of 2 runs.

The time-composition profile in figure 4.30 demonstrated a marked contrast to that at 130 ℃ in Figure 4.29 as the 20 ℃ increase resulted in complete conversion of the FFA for all 3 catalysts but at the same time the systems appeared to suffer from catalyst deactivation and/or leaching. The pressure within the system also increased

significantly which may be due to leached insoluble species blocking the Teflon tubing. A similar blocking result was observed with **4.11** after 70 minutes of operation. In addition, **Amberlyst-15** is hydrothermally unstable at temperatures above 150 ℃ and therefore after ion exchange the resin support started to degrade. The beneficial influence of the IL functionality within the PIIL support is further demonstrated by the long-term operation of **4.10** and **4.11** under the reaction conditions compared to a commercial sample of **Amberlyst-15**. These considerations suggest that **4.10** and **4.11** may be suitable candidates for use in a continuous flow processes based around efficient product scale-up and heterogeneous catalysis.

Furthermore, the influence of the POM is more difficult to justify, it can be postulated that a silicate is more likely to make stronger and more electrostatic interactions to silica than phosphates which was reflected by the appearance of less leaching of the active POM in the analogous **4.11** system. Both of the POM@PIIL/SiO$_2$ catalysts which were initially ivory in appearance became grey by the end of the reaction which further confirmed the idea of a certain extent of polyfurfuryl alcohol formation, leaching of the catalyst and/or catalyst decomposition (Figure 4.31). However, the higher reaction temperature could significantly shorten the reaction time.
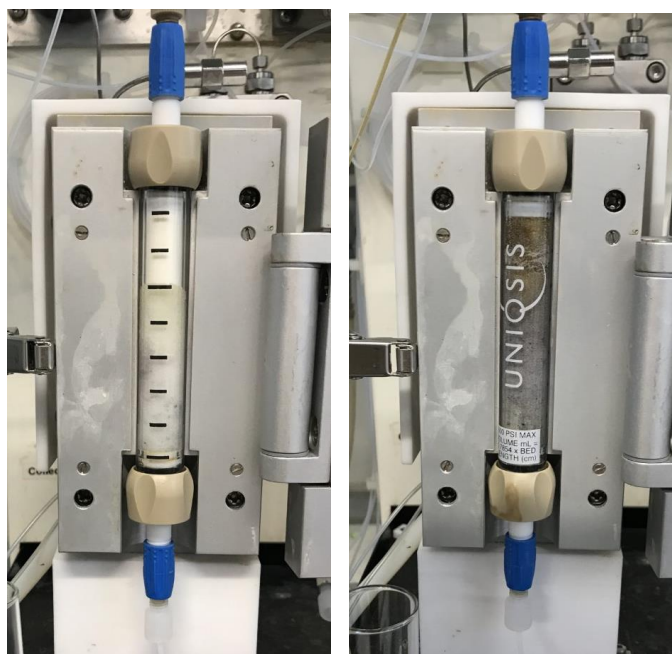
Figure 4.31: Picture of the **4.11** catalyst column of POM@PIIL/SiO$_2$ before (left) and after (right) the reaction in segmented flow.

Although the profile at 130 ℃ was relatively consistent compared to 150 ℃, the higher temperature was required in order to achieve full conversion of FFA. However, the increase in temperature may cause the catalyst to leach faster and therefore conversions drop quite rapidly. 150 ℃ gave the perfect reaction profile for the initial (1.1 mL min^{-1}), but was not stable on this support at that temperature for long periods of time (> 30 minutes). To suppress the formation of the undesired side-products, a lower temperature should be employed. This leaves two options, either the reaction can be operated at 130 ℃ which would limit the conversion of FFA to 85 % or, develop a more stable catalyst support. Therefore, further adaptations and investigations will need to be carried out to improve these systems and to fully understand their nature.

The assessment of **4.10** and **4.11** under these reaction conditions illustrates the robustness of these POM@PIIL based catalysts. Supported by the high activity and selectivity for *n*-butyl levulinate, further studies were conducted to demonstrate the favourable effect of the IL functionality within the PIIL support of **4.10** and **4.11**. In this regard, the homogeneous analogue of **4.10** and **4.11**, for comparison, [**POM@TBA**], was prepared by the anion exchange of $[PO_4\{WO(O_2)_2\}_4]^{3-}$ with tetrabutylammonium bromide and adsorbed onto silica as a heterogeneous SILP-type catalyst. A substantial reduction in the conversion of FFA was observed after only 12 minutes of operation and the catalyst became completely inactive after 40 minutes (Figure 4.32a). Figure 4.32b shows that the **POM@TBA** catalyst had leached from the silica support and blocked the PTFE tubing which caused a pressure build-up within the flow reactor. The degree of POM leaching can be directly associated to the poor performance of **POM@TBA**/SiO$_2$ in comparison to the recyclable **4.10** and **4.11** which again highlights the positive effect of the IL support in retaining the active POM/acid sites. This outcome would suggest that additional stabilisation effects are present within the PIIL supports over a period of time and as such further studies will be required to determine the nature of this positive effect.
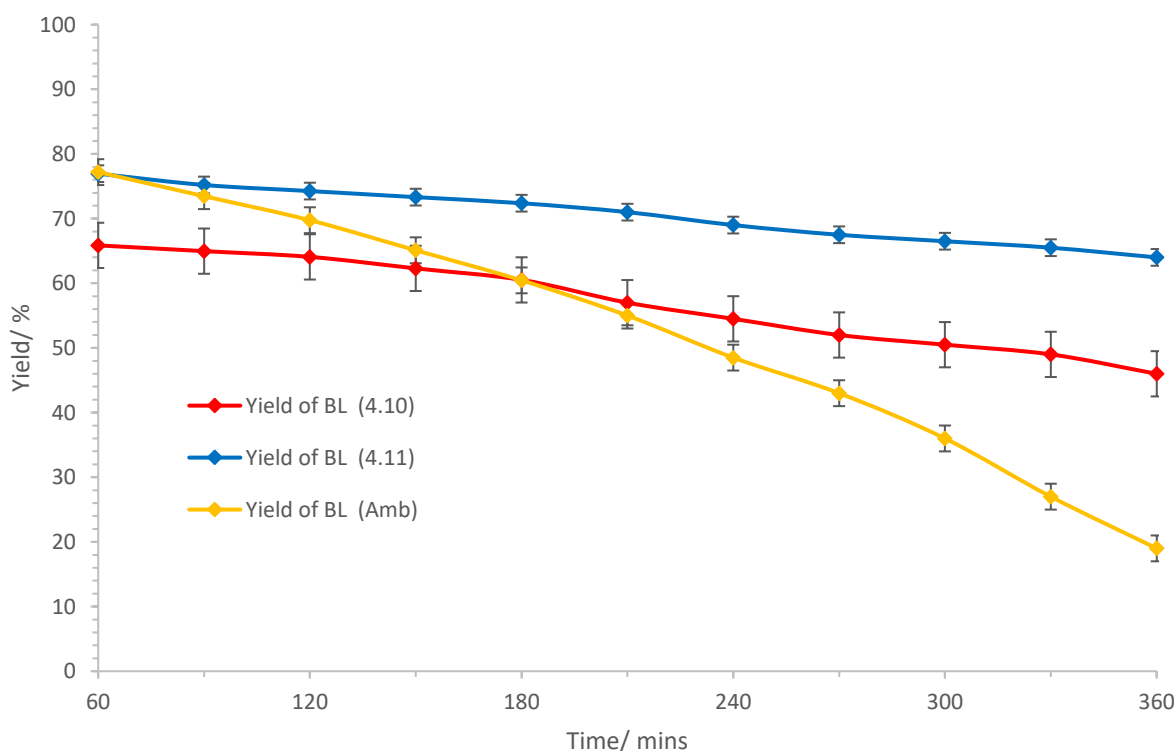
a)

b)
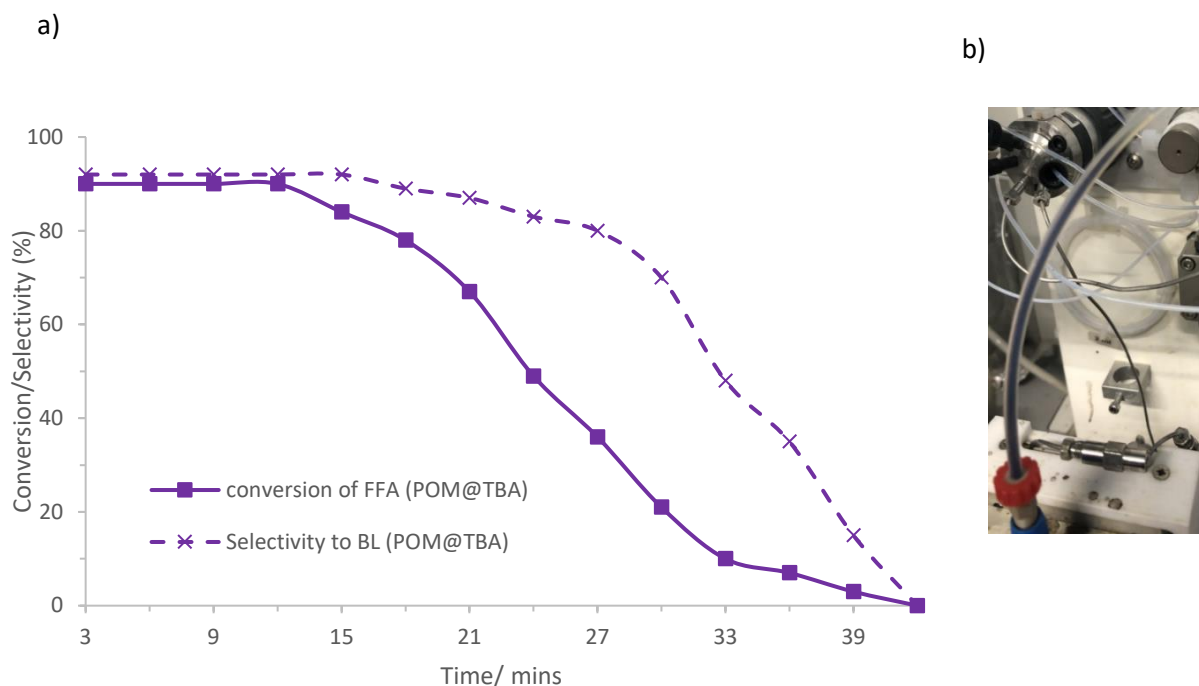
Figure 4.32: a) conversion-selectivity profile as a function of the time-on-stream (36 minutes) for the segmented flow alcoholysis of FFA catalysed by **POM@TBA**/SiO₂. Reaction conditions: catalyst, 1.0 g of **POM@TBA** on 1.0 g of silica; 0.32 M FFA in *n*-butanol; temperature, 130 ℃; flow rate, 1.1 mL min⁻¹; injection volume, 44 mL. Conversion and selectivity determined by ¹H NMR spectroscopy with 1,4-dioxane as the internal standard. Selectivity for *n*-butyl levulinate = [% *n*-butyl levulinate / (% *n*-butyl levulinate + % 2-butoxymethylfuran)]. Average of 2 runs.

4.4.5 Continuous Flow and Scale Up Reactions

Encouraged by the efficiency of **4.10**, **4.11** and **Amberlyst-15** under the segmented flow conditions a series of scale-up continuous flow studies were conducted to assess the catalysts' long-term stability. The use of continuous flow means that the practical issues involved with the catalyst recovery are avoided. One of the key features for the use of an immobilised catalyst in continuous flow applications is a stable activity profile so that it can be used over extended times. The POM@PIIL catalysed alcoholysis of FFA was monitored over prolonged times. Each experiment was conducted with a fresh catalyst cartridge. To this end, the optimum conditions which were identified under the segmented flow conditions were, 1.1 mL min⁻¹ at 130 ℃ and 0.32 M of furfuryl alcohol in *n*-butanol. Under these conditions a semi-quantitative scale-up flow experiment using a 0.32 M solution of FFA continuously processed 8.4 g of FFA over

the course of 6 hours (~1.4 g h^{-1}). During this time, 3 mL samples are taken from the exit stream every 30 minutes, concentrated and analysed by ^{1}H NMR spectroscopy to assess the catalyst performance (Figure 4.33).

IR analysis of the samples collected over 60 minutes from catalytic reactions with **4.10** and **4.11** showed the presence of polyoxotungstate; this leaching would account for the gradual loss in activity over 360 minutes of reaction. All of the catalyst systems, even the commercial ion exchange resin, **Amberlyst-15**, were susceptible to catalyst deactivation either due to the formation of polyfurfuryl alcohol or by the loss of the active acid, be it the form of POM in POM@PIIL or the H$^+$ ions from **Amberlyst-15**. While the scale-up continuous flow catalysed **4.10**/SiO$_2$ gave 56% yield of butyl levulinate after 6 hours, the same reaction with **4.11**/SiO$_2$ achieved a 70% yield of butyl levulinate in the same time.

Figure 4.33: Conversion-selectivity profile as a function of the time-on-stream (6 hours) for the continuous flow alcoholysis of FFA catalysed by **4.10**/SiO$_2$, **4.11**/SiO$_2$ and **Amberlyst-15**/SiO$_2$. Reaction conditions: catalyst, 1.0 g on 1.0 g of silica; 0.32 M FFA in *n*-butanol; temperature, 130 ℃; flow rate, 1.1 mL min^{-1}; injection volume, 360 mL. Conversion and selectivity determined by ^{1}H NMR spectroscopy with 1,4-dioxane

as the internal standard. Selectivity for *n*-butyl levulinate = [% *n*-butyl levulinate / (% *n*-butyl levulinate + % 2-butoxymethylfuran)]. Average of 2 runs.

The gradual decrease in catalyst performance after the first 60 minutes of reaction could be due to leaching of the POM. This could be due to the hydrogen bonding capability of the solvent that would facilitate 'extraction' of the charged tungsten species from the cartridge. In addition, the change in the catalyst performance over time could be due to the progressive deposition over time of the polyfurfuryl alcohol on the catalyst/silica surface especially at the high temperature and acid content of the catalyst cartridge which would gradually block the catalysts' active sites. It should be possible to achieve more efficient substrate processing by fine-tuning the architecture of the PIIL and the ionic microenvironment in order to limit the substrate-support interaction. Thus could enable the successful implementation of PIIL catalysts under continuous operation which would allow for the further optimisation of these catalytic systems.

Interestingly, **4.11**/SiO$_2$ was markedly more stable than its phosphorus POM-derived counterpart **4.10**/SiO$_2$ which experienced a 19% drop in the yield of butyl levulinate after 6 hours of continuous operation. Conversions of FFA steadily dropped with time during the 6 hours of operation. This was associated with the leaching of the active peroxotungstate. The exchange of the H$^+$ ions from **Amberlyst-15** over the 6 hours led to a drop in the initial yield of 77% to 19%.

Encouraged by the long-term stability of **4.10** and **4.11** under the continuous flow alcoholysis of FFA, a study was conducted to determine if the POM-based PIIL loaded catalyst columns could be employed for the alcoholysis of different substrates. To this end, a proof of principle operation was carried out by processing FFA under the optimum segmented flow conditions described above at a residence time of 4.4 minutes, but at 100 ℃ for the ethanolysis of FFA (Appendix R). **4.10** and **4.11** achieved a similar high activity (92% yield for **4.10** and 98% yield for ethyl levulinate) for the ethanolysis which further highlights the POM@PIIL stability and application.

4.5 Conclusion

The PIIL-immobilised POMs **4.10** and **4.11** proved to be highly efficient catalysts for the alcoholysis of furfuryl alcohol in batch with various alcohols and outperformed comparable literature catalysts. While high catalytic performances were achieved the modulated nature of the PIIL support should enable more efficient systems to be developed by tuning the hydrophilicity/hydrophobicity as well as the structural integrity of the support.

Moreover, the same catalysts proved to be remarkably efficient under continuous flow operation and showed encouraging stability profiles for the alcoholysis of furfuryl alcohol allowing 8.4 g of furfuryl alcohol to be processed in 6 hours. The yield of *n*-butyl levulinate increased with higher catalyst loadings, higher reaction temperature and longer residence times. However, leaching of the active POM and/or catalyst deactivation under continuous flow operation at high temperatures over long periods of time resulted in a gradual drop in efficacy. In addition, a significantly higher catalyst loading was required to shorten the reaction times, however the reaction time was decreased from 40 minutes to 3 minutes to obtain 90% conversion of furfuryl alcohol at 130 ℃ for **4.11** which is a value that is more suited to a continuous flow system. It was shown that the presence of an IL in the SILP system is vital otherwise the catalyst leached out of the reactor too quickly as demonstrated by **POM@TBA**. Flow chemistry has also been shown to have a high degree of reproducibility. The use of a back-pressure regulator enabled super heating of *n*-butanol which allowed segmented and continuous flow processes to be carried out at temperatures above the boiling point of the solvent which is usually a limiting factor in process design. The flow path and the variety in the combinations of the catalyst cartridges and reactors yields a flexible system, the different configurations may also provide a different approach to improve a process compared to the corresponding batch reactions.

In addition, these studies have highlighted the complex nature of the relationship between the substrate, support and catalyst, therefore further investigations are necessary to explore the nature of the catalyst interactions with its surrounding environment. As with the previously reported batch studies it will be challenging but necessary to fully examine and understand the nature of this relationship to fully utilise the concept of PIIL supported catalysis. The encouraging initial results imply that the PIIL materials could be a viable way of generating highly active and stable catalysts,

as such the reaction and substrate scope under continuous flow conditions should be extended to fully assess the merits of the PIIL support systems. The processes described in this chapter are in no way ideal for long-term operations and there is considerable scope for further improvement and optimisation. Regardless, the performance of **4.10** and **4.11** under continuous flow conditions demonstrates that the PIIL methodology may potentially be implemented in industrially relevant processes.

4.6   References

1. D. Balsalobre-Lorente, M Shahbaz, D. Roubaud and S. Farhani, *Energy Policy*, 2018, **113**, 356-367.

2. C. Xu, R. A. D. Arancon, J. Labidi and R. Luque, *Chem. Soc. Rev.*, 2014, **43**, 7485-7500.

3. P. Zhai, G. Lv, Z. Cai, Y. Zhu, H. Li, X. Zhang and F. Wang, *ChemistrySelect*, 2019, **4**, 3940–3947.

4. K. J. Zeitsch, *The Chemistry and Technology of Furfural and its Many Byproducts*, Elsevier, Amsterdam, 2000.

5. B. M. Nagajara, A. H. Padmasri, P. Seetharamulu, K. Hari Prasad Reddy, B. David Raju and K. S. Rama Rao, *J. Mol. Catal. A: Chem.*, 2007, **278**, 29.

6. Y. Yan, C. Bu, Q. He, Z. Zheng and J. Ouyang, *RSC Adv.*, 2018, **8**, 26720-26727.

7. Y. Kuwahara, H. Kango and H. Yamashita, *ACS Sustainable Chem. Eng.*, 2017, **5**, 1141-1152.

8. US Department of Energy, Top Value Added Chemicals from Biomass, Volume 1, Results of Screening for Potential Candidates from Sugars and Synthesis Gas, 2004, Report NREL/TP-510-355532.

9. F. Su, L. Ma, D. Song, X. Zhang and Y. Guo, *Green Chem.*, 2013, **15**, 885-890.

10. C. J. Clarke, W.-C. Tu, O. Levers, A. Brohl and J. P. Hallett, *Chem. Rev.*, 2018, **118**, 747-800.

11. A. Demolis, N. Essayem and F. Rataboul, *ACS Sustainable Chem. Eng.*, 2014, **2**, 1338-1352.

12. E. Christensen, A. Williams, S. Paul, S. Burton and R. L. McCormick, *Energy Fuels*, 2011, **25**, 5422-5428.

13. H. Joshi, B. R. Moser, J. Toler, W. F. Smith and T. Walker, *Biomass Bioenergy*, 2011, **35**, 3262-3266.

14. A. P. Grove, C. Morely, J. Smith and A. Stevenson, US Pat. Application 2005/0144835 A1, 2005.

15. A. Démolis, N. Essayem and F. Rataboul, *ACS Sustainable Chem. Eng.*, 2014, **2**, 1338-1352.

16. A. Ran, X. Guizhuan, C. Chun, B. Jing and F. Shuqi, *J. Energy Chem.*, 2017, **26**, 556-563.

17. R. H. Clark, A. P. Groves, C. Morley and J. Smith, Fuel Compositions, Patent WO2004035713, 2004.

18. M. S. Tiwari, A. B. Gawade, G. D. Yadav, *Green Chem.*, 2017, **19**, 963–976.

19. G. Wang, Z. Zhang, L. Song, *Green Chem.*, 2014, **16**, 1436–1443.

20. D. Song, S. An, B. Lu, Y. Guo, J. Leng, *Appl. Catal. B: Environ.,* 2015, **179**, 445–457.

21. a) E. Ahmad, M. I. Alam, K. K. Pant, M. A. Haider, *Green Chem.*, 2016, **18**, 4804–4823; b) C. R. Patil, P. S. Niphadkar, V. V. Bokade, P. N. Joshi, *Catal. Commun.*, 2014, **43**, 188–191.

22. X. F. Chen, H. X. Li, H. S. Luo and M. H. Qiao, *Appl. Catal., A*, 2002, **233**, 13-20.

23. F. Rataboul and N. Essayem, *Ind. Eng. Chem. Res.*, 2011, **50**, 799-805.

24. S. S. Enumula, K. S. Koppadi, V. R. B. Gurram, D. R. Burri and S. R. R. Kamaraju, *Sustainable Energy Fuels*, 2017,**1**, 644-651.

25. Y. Leng, J. Wang, D. Zhu, X. Ren, H. Ge and L.Shen, Angew. *Chem. Int. Ed.*, 2009, **48**, 168-171.

26. a) F. Su, Q. Wu, D. Song, X. Zhang, M. Wang, Y. Guo, *J. Mat. Chem. A*, 2013, **1**, 13209; b) D. Song, S. An, Y. Sun, Y. Guo, *J. Catal.*, 2016, **333**, 184–199.

27. P. Sudarsanam, R. Zhong, S. V. d. Bosch, S. M. Coman, V. I. Parvulescu and B. F. Sels, *Chem. Soc. Rev.,* 2018, **47**, 8349-8402.

28. G. A. Kraus and T. Guney, *Green Chem.*, 2012, **14**, 1593-1596.

29. L. Peng, X. Gao, X. Yu, H. Li, J. Zhang and L. He, *Energy Fuels*, 2019, **33**, 330-339.

30. J. Wu, Y. Shao, G. Jing, Z. Zhang, Z. Ye and X. Hu, *J. Chem. Technol. Biotechnol.*, 2019, **94**, 3093-3101.

31. P. Neves, S. Lima, M. Pillinger, S. M. Rocha, J. Rocha, A. A. Valente, *Catal. Today*, 2013, **218**, 76–84.

32. J. Dong, J. Hu, Y. Chi, Z. Lin, B. Zou, S. Yang, C. L. Hill, C. Hu, *Angew. Chem. Int. Ed.*, 2017, **56**, 4473–4477.

33. R. Hao, J. He, L. Zhao and Y. Zhang, *ChemistrySelect*, 2017, **2**, 7918-7924.

34. K. Y. Nandiwale, S. K. Sonar, P. S. Niphadkar, P. N. Joshi, S. S. Deshpande, V. S. Patil, and V. V. Bokade, *Appl. Catal. A: Gen.*, 2013, **461**, 90–98.

35. S. Dharne and V. V. Bokade, V.V. *J. Nat. Gas Chem.*, 2011, **20**, 18–24.

36. P. D. Carà, R. Ciriminna, N. R. Shiju, G. Rothenberg and M. Pagliaro, *ChemSusChem.*, 2014, **7**, 835-840.

37. X. Z. Liang and J. G. Yang, *Green Chem.*, 2010, **12**, 201-204.

38. G. Wang, Z. Zhang and L. Song, *Green Chem.*, 2014, **16**, 1436-1443.

39. J. P. Lange, W. D. Van de Graff and R. J. Haan, *ChemSusChem*, 2009, **2**, 437-441.

40. a) R. Kreitner, M. Rietkerk, H. L. Castricum, H. M. van Veen, J. E. ten Elshof and J. F. Vente, *ChemSusChem*, 2009, **2**, 158-160; b) M. J. dos Reis, V. Prevot, F. Leroux, F. Silverio, J. B. Valim, *J. Porous Mater.*, 2010, **17**, 443-451.

41. Y. Leng, J. Wang, D. R. Zhu, X. Q. Ren, H. Q. Ge, L. Shen, *Angew. Chem.*, 2009, **121**, 174-177; *Angew Chem. Int. Ed.*, 2009, **48**, 168-171.

42. J.-P. Lange, E. van der Heide, J. van Buijtenen, R. Price, *ChemSusChem*, 2012, **5**, 150–166.

43. B. Capai, G. Lartigau, US Patent 5.175.358, 1992.

44. Z. Zhang, K. Dong, Z. K. Zhao, *ChemSusChem*, 2011, **4**, 112–118.

45. H. P. Gregor, J. I. Bregman, F. Gutoff, R. D. Broadley, D. E. Baldwin and C. G. Overberger, *J. Colloid Sci.*, 1951, **6**, 20-32.

46. V. S. Chandane, A. P. Rathod, K. L. Wasewar and S. S. Sonawane, *J. Chem. Eng.,* 2017, 34, 269-258.

47. Prasenjit Bhaumik and Paresh Laxmikant Dhepe, Chapter 1: Conversion of Biomass into Sugars, in *Biomass Sugars for Non-Fuel Applications*, 2015, pp. 1-53

48. P. Zhao, Y. Leng and J. Wang, *J. Chem. Eng.*, 2012, **205**, 72-78.

49. C. Song, S. Liu, X. Peng, J. Long, W. Lou and X. Li, *ChemSusChem*, 2016, **9**, 3307-3316.

50. a) B. M. Devassy, G. V. Shanbhag, F. Lefebvre, W. Bohringer, J. Fletcher and S. B. Halligudi, *J. Mol. Catal. A Chem.*, 2005, **230**, 113-119; b) G. A. Tsigdinos, *Top. Curr. Chem.*, 1978, **76**, 1-60.

51. M. N. Timofeeva, *Appl. Catal. A*, 2003, **256**, 19–35.

52. D. Song, S. An, Y. Sun, P. Zhang, Y. Guo and D. Zhou, *ChemCatChem*, 2016, **8**, 2037-2048.

53. N. Guigo, A. Mija, L. Vincent and N. Sbirrazzuoli, *Phys. Chem. Chem. Phys.*, 2007, **9**, 5359–5366.

54. Z. Zhang, K. Dong, and Z. Zhao, *ChemSusChem*, 2011, **4**, 112-118.

55. G. M. G. Maldonado, R. S. Assary, J. Dumesic and L. A. Curtiss, *Energy Environ. Sci.*, 2012, **20**, 8990-8997.

56. R. I. Khusnutdinov, A. R. Baiguzina, A. A. Smirnov, R. R. Mukminov, U. M. Whemilev, Russ. *J. Appl. Chem.*, 2007, **80**, 1687–1690.

57. D. Song, S. An, B. Lu, Y. Guo and J. Leng, *Appl. Catal. B: Environ.*, 2015, **179**, 445-457.

58. M. Hronec, K. Fulajtrov, T. Sotk, *J. Ind. Eng. Chem.*, 2014, **20**, 650–655.

59. L. Pranger, R. Tannenbaum, *Macromolecules*, 2008, **41**, 8682–8687.

60. M. S. Tiwari, J. S. Dicks, J. Keogh, V. V. Ranade and H. G. Manyar, *Mol. Catal.*, 2020, **488**, 110918.

61. B. S. Rao, P. K. Kumari, D. Dhanalakshmi and N. Lingaiah, *J. Mol. Catal. A: Chem.*, 2017, **427**, 80-86.

62. J. N. Appaturi, M. R. Johan, R. J. Ramalingam, H. A. Al-Lohedan and J. J. Vihjaya, *RSC Adv.*, 2017, **7**, 55206-55214.

63. E. S. Sankar, K. S. Reddy, Y. Jyothi, B. D. Raju and K. S. R. Rao, *Catal. Lett.*, 2017, **147**, 2807-2816.

64. R. Bringué, E. Ramírez, M. Iborra, J. Tejero and F. Cunill, *Fuel*, 2019, **257**, 116010.

65. Z. Mohammadbagheri and A. N. Chermahini, *J. Ind. Eng. Chem.*, 2018, **62**, 401-408.

66. X. Zhao, N. Sun, S. Wang, F. Li and Y. Wang, *Ind. Eng. Chem. Res.*, 2008, **47**, 1365-1369.

67. A. Carrero, G. Vicente, R. Rodríguez, G. L. del Peso, C. Santos, *Biochem. Eng. J.*, 2015, **97**, 119−124.

Chapter 5

Future Work

Future Work

Chapter 2 describes the synthesis of highly active ultra-small monodisperse ruthenium nanoparticles for the selective hydrogenation of α,β-unsaturated ketones and aldehydes. An extension of this project could involve preparing a set of RuNPs using different catalyst preparation methods which would be useful to establish how variations in the nanoparticles' dispersion affects the activity, selectivity, and stability. For instance, the particle's size is crucial to enhance the strong metal to support interaction and consequently govern the activity and stability of the nanoparticle.[1] The completion of this work will involve further characterisation studies such as TEM and DRIFTS to fully understand the nature and variety of the catalytic systems that were studied which would aid the optimisation and the understanding of the reaction mechanisms.

Chapter 3 describes the application of RuNPs for the reduction of nitroarenes. An extension of this project could involve applying the catalyst system in continuous flow to scaleup the reaction or to further explore and optimise the reaction conditions to selectively prepare either *N*-phenylhydroxylamine or azoxybenzene. The completion of this work will involve in-depth mechanistic studies such as primary kinetic isotope effects (KIEs) and Hammett-type kinetic studies to fully understand and study the nature of the mechanism of these catalytic systems.[2]

Chapter 4 describes the optimisation of the reaction conditions both in batch and under continuous flow to synthesise *n*-butyl levulinate selectively. Very promising results were obtained in flow, in which, the lifetime of the catalyst was greatly extended in comparison to when the reaction was conducted under batch regime. These studies were only preliminary, but provided a good basis to investigate going forward. POM@PIIL catalysts have been shown to be extremely active and highly selective for the alcoholysis of furfuryl alcohol, which make them good candidates for further investigation. The catalysts were not reusable after catalyst recovery from the reaction medium, therefore these issues need to be addressed in an attempt to improve and optimise the whole process. In particular, problems of polyoxometalate leaching and/ catalyst deactivation must be overcome. The reason for deactivation was probably the adsorption of polyfurfuryl alcohol and/or the reaction intermediates. Therefore, the immediate first step to continue with this area of research would be to attempt to avoid

the adsorption of such species onto the active sites, which has become one of the most important objectives for any future research in this area. To try to overcome this, one possible solution may lie in modifying the catalyst bed or catalyst volume. Minor changes of the temperature around 130-150 °C under flow would also be of interest to maximise the activity and selectivity to *n*-butyl levulinate. This may also require the screening of a wider range of preparation methods, support materials and/or treatment procedures. To do this, a new catalyst recovery procedure should be developed in order to retain the active species. Alternatively, a re-activation procedure step could be attempted to recover the initial activity. Preliminary studies were conducted to regenerate the Amberlyst resin, which in general showed good activity could be obtained after catalytic cycles. There are various further studies that could be pursued. Further catalyst characterisation should be undertaken to obtain a better understanding of the reaction mechanism. Although, there has been progress in improving the catalyst stability in segmented flow for this reaction in this thesis, it is far from ideal. Further work in this area should be focused on developing a more stable catalyst which could probe the use of other catalysts supports. Further testing for different catalytic reactions is required in order to demonstrate the applicability of these materials in a broader range of processes. Another possibility is to prepare magnetic core-shell iron-based supports which will facilitate more efficient catalyst recycling.[3] It is postulated that these types of magnetic NP systems greatly benefit from improved recyclability, as they can be magnetically separated from the reaction mixture at the end of a process with an external magnet.
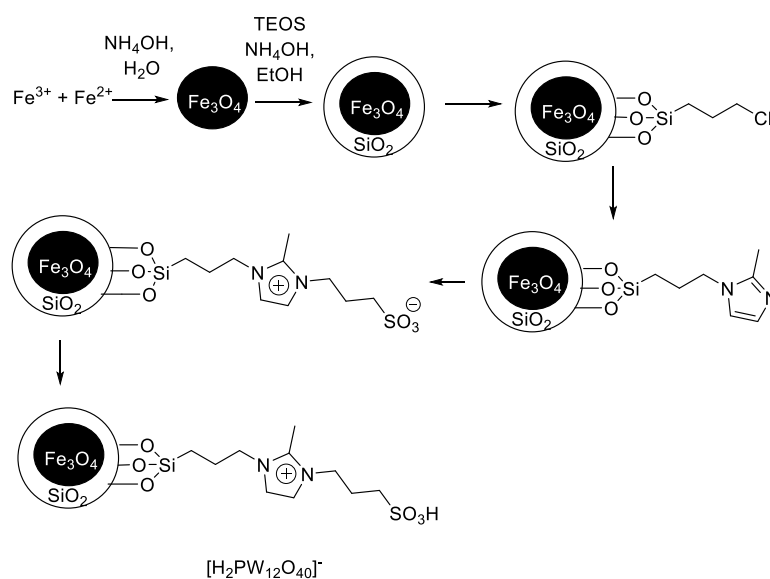
Figure 6.1: Synthetic plan for the synthesis of magnetic iron core-shell nanoparticles
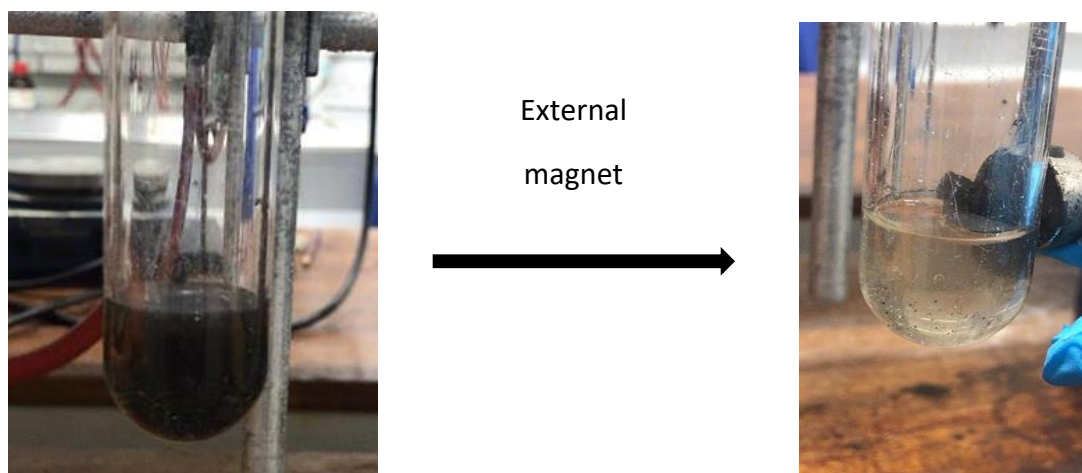
External

magnet

Figure 6.2: Image of magnetic core-shell iron nanoparticles being separated from solution using an external magnet.

References

1. F. P. de Silva, J. L. Fiorio and L. M. Rossi, *ACS Omega*, 2017, **2**, 6014-6022.

2. S. Fountoulaki, V. Daikopoulou, P. L. Gkizis, I. Tamiolakis, G. S. Armatas and I. N. Lykakis, *ACS Catal.*, 2014, **4**, 3504-3511.

3. E. S. D. T. de Mendonca, A. C. B. de Faria, S. C. L. Dias, F. F. H. Aragon, J. C. Mantilla, J. A. H. Coaquira and J. A. Dias, *Surf. Interfaces*, 2019, **14**, 34-43.

Chapter 6

Experimental

General comments

All reagents were purchased and used without further purification from commercial suppliers. $RuCl_3.xH_2O$ (Alfa Aesar, P02C024). All dry solvents (THF and diethyl ether) were distilled under a N_2 atmosphere and over sodium. ^1H and $^{13}C\{^1H\}$ NMR spectra were recorded on either JEOL LAMBDA-500 or ECS-400 spectrometers. All ^1H and ^{13}C NMR were referenced relative to $CDCl_3$ (δ_H = 7.26, δ_C = 77.16), MeOD (δ_H = 4.87, δ_C = 49.00) or D_2O (δ_H = 4.79). FT-IR spectroscopy was performed with a Varian 800 FT-IR instrument (Varian Inc.). CHN analysis was performed on a Carlo Erba 1108 Elemental Analyser. Solid-state ^{13}C and ^{31}P spectra were recorded at 100.56 MHz and 161.87 MHz, respectively using a Varian VNMRS 400 spectrometer and a rotor (o.d. = 4 mm) magic-angle spinning probe. Thermogravimetric analysis (TGA) was performed on a PerkinElmer Thermogravimetric Analyser, at a heating rate of 10 °C min^{-1} in air. SEM images were collected on a Tescan Vega 3LMU scanning electron microscope. XPS measurements were conducted on a Theta Probe system (Thermo Scientific, UK). TEM images were obtained using a FEI Tecnai TF20 field emission gun microscope. Powder X-ray diffraction patterns (XRD) were recorded using a PANalytical X'Pert Pro Multipurpose Diffractometer (MPD). Inductively coupled plasma (ICP) analysis to calculate metal loadings was conducted using a Perkin-Elmer Optima 4300.
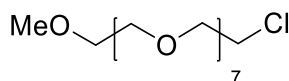
6.1 Chapter 2 Experimental.

6.1.1 Synthesis of 1,2-dimethyl-3-(4-vinylbenzyl)imidazol-3-ium chloride (2.1).[1]
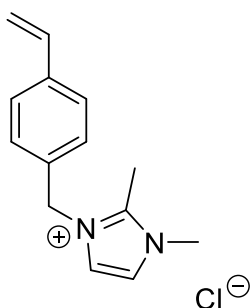
An oven-dried Schlenk flask under N_2 was charged with 1,2-dimethylimidazole (6 g, 62.4 mmol), 4-chloromethylstyrene (8.8 mL, 62.4 mmol) and chloroform (60 mL), the resultant mixture was stirred at 60 °C for 12 hours. After this time, the solution was cooled to room temperature and the solvent was reduced *in vacuo* to ca. 15-20 mL. The resultant viscous yellow residue was precipitated into ethyl acetate (200 mL), filtered and dried under high vacuum to afford **2.1** as a pale-yellow solid (14.6 g, 58.6 mmol) in 94% yield.

¹H NMR (300 MHz, CDCl₃, *δ*): 7.74 (2H, s, N-C<u>H</u>=C<u>H</u>-N), 6.83-6.74 (4H, dd, J = 9 Hz, 17 Hz, C₆<u>H</u>₄), 6.05-6.15 (1H, dd, J = 11 Hz, 18 Hz, CH₂=C<u>H</u>-C), 5.21-5.15 (1H, d, J = 18 Hz, C<u>H</u>₂=CH-C), 5.04 (2H, s, N-C<u>H</u>₂-C), 4.74-4.70 (1H, d, J = 12 Hz, C<u>H</u>₂=CH-C), 3.41 (3H, s, N-C<u>H</u>₃), 2.21 (3H, s, N=C(C<u>H</u>₃)-N); **¹³C {¹H} NMR** (75 MHz CDCl₃, *δ*): 143.93, 138.08, 135.62, 132.40, 128.38, 126.84, 122.82, 121.85, 115.11, 10.68, 51.82, 35.66; **Anal. Calc**. for C₁₄H₁₇ClN₂ (248.75): C, 67.60; H, 6.89; N, 11.26 %. Found: C, 67.35; H, 7.24; N, 11.60%.

6.1.2 Synthesis of 2-methyl-1-(4-vinylbenzyl)imidazole (2.2).[1]
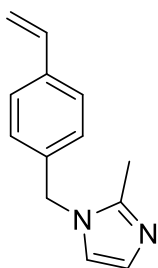
An oven-dried Schlenk flask under N_2 was charged with sodium hydride (3.7 g (wet mass, dispersed in mineral oil), 2.28 g (dry), 95 mmol, 1.3 equiv.). To remove the mineral oil, anhydrous hexane (15 mL) was added and the suspension was stirred under N_2 for 5 minutes at room temperature. The hexane was then removed *via* cannula filtration and the process was repeated and then this solid was dried under high vacuum. The resultant off-white solid was suspended in anhydrous dimethylformamide (70 mL) under a N_2 atmosphere. The suspension was then cooled to 0 °C and 2-methylimidazole (6 g, 73.1 mmol, 1 equiv.) was added slowly portion-wise which resulted in the liberation of gas. After complete addition and when the exotherm had subsided, 4-chloromethylstyrene (12.4 mL, 87.7 mmol, 1.2 equiv.) was added slowly and the ice bath was removed and the brown solution was heated to 75 °C and stirred for 1 hour. After this, the reaction was cooled to room temperature, water (15 mL) was added to the mixture and the product was extracted with ethyl acetate (3 x 100 mL). The combined organic layer was then reduced *in vacuo* ca. 40 mL, 6N HCl (50 mL) was added and the aqueous layer was washed with diethyl ether (2 x 80 mL) and then the aqueous layer was treated with 1M NaOH solution until pH 12 was obtained. The product was then extracted with diethyl ether (3 x 100 mL), the combined organic layers from the base-extraction were then dried over $MgSO_4$ and the solvent removed *in vacuo* to give **2.2** as a pale-yellow oil (13.8 g, 69.6 mmol) in 95% yield.

^{1}H NMR (300 MHz, CDCl$_3$, δ): 7.27-7.25 (2H, d, J = 8 Hz, N-C<u>H</u>=C<u>H</u>-N), 6.80-6.77 (2H, d, J = 8 Hz, C$_6$<u>H</u>$_4$), 6.75 (1H, d, J = 8 Hz, C$_6$<u>H</u>$_4$), 6.60 (1H, d, J = 8 Hz, C$_6$<u>H</u>$_4$), 6.50-6.41 (1H, dd, *J* = 11 Hz, 18 Hz, CH$_2$=C<u>H</u>-C), 5.55-5.49 (1H, d, *J* = 18 Hz, C<u>H</u>$_2$=CH-C), 5.05-5.01 (1H, d, *J* = 11 Hz, C<u>H</u>$_2$=CH-C), 4.73 (2H, s, N-C<u>H</u>$_2$-C), 2.08 (3H, s, N=C(C<u>H</u>$_3$)-N);

^{13}C{^{1}H} NMR (75 MHz, CDCl$_3$, δ): 144.40, 136.83, 135.67, 135.47, 126.71, 126.50, 126.28, 119.50, 114.01, 48.98, 12.57; **Anal. Calc**. for C$_{13}$H$_{14}$N$_2$ (198.27): C, 78.75; H, 7.12; N, 14.13%. Found: C, 79.11; H, 7.47; N, 14.47%.

6.1.3 Synthesis of 2-methyl-1,3-bis(4-vinylbenzyl)-imidazol-3-ium chloride (2.3).[1]
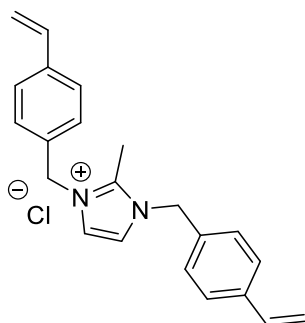
An oven-dried Schlenk flask under N_2 was charged with **2.2** (9 g, 45.4 mmol, 1 equiv.) and anhydrous chloroform (60 mL) under a N_2 atmosphere. 4-chloromethylstyrene (6.34 mL, 45.4 mmol, 1 equiv.) was added to the solution and the resulting mixture was heated to 60 °C and stirred for 16 hours. After this time, the solution was cooled to room temperature, concentrated *in vacuo* (to ca. 10 mL), diethyl ether (200 mL) was added and the resulting mixture was vigorously stirred for 1 hour. After this time, the mixture was left to settle and the solid product was isolated *via* frit filtration, washed with diethyl ether (2 x 80 mL) and dried under high vacuum to afford the **2.3** as a white solid (14.5 g, 41.3 mmol) in 91 % yield.

¹H NMR (300 MHz, CDCl₃, *δ*): 7.57 (2H, d, *J* = 5.9 Hz, N-C<u>H</u>=C<u>H</u>-N), 7.36 (4H, d, *J* = 5.9 Hz, C₆<u>H</u>₄), 7.27 (4H, *J* = 5.9 Hz, C₆<u>H</u>₄), 6.66 (2H, dd, *J* = 11.9 Hz, 17.9 Hz, CH₂=C<u>H</u>-C), 5.76 (2H, d, *J* = 17.9 Hz, C<u>H</u>₂=CH-C), 5.51 (4H, s, =C-C<u>H</u>₂-N), 5.30 (2H, d, *J* = 11.9 Hz, C<u>H</u>₂=CH-C), 2.76 (3H , s, N=C(C<u>H</u>₃)-N); **¹³C{¹H} NMR** (75 MHz, CDCl₃, *δ*): 152.97, 135.99, 134.04, 133.55, 128.77, 128.41, 122.73, 113.18, 52.55, 11.32; **Anal. Calc**. for C₂₂H₂₃ClN₂ (350.1): C, 75.31; H, 6.61; N, 7.98%. Found: C, 75.08; H, 6.38; N, 7.75%.

6.1.4 Synthesis of methyl octaethylene glycol chloride (2.5).[1]

An oven-dried Schlenk flask under N_2 was charged with poly(ethylene glycol) monomethyl ether (20 g, 57.2 mmol, 1 equiv.), pyridine (4.52 g, 57.2 mmol, 1 equiv.) and anhydrous toluene (70 mL). The solution was stirred and heated to 80 °C, at which

point thionyl chloride (6.8 g, 57.2 mmol, 1 equiv.) was added dropwise. Following the addition, the mixture was heated to 110 °C and stirred for 2 days. After this, the crude mixture was cooled to room temperature and poured onto ice water (5 mL) and the organics were extracted with toluene (3 x 60 mL). The organic phases were combined, dried over $MgSO_4$, filtered and the solvent was removed *in vacuo.* The residue was dissolved in methanol (20 mL) and passed through a silica column and the solvent was removed *in vacuo* to give **2.5** as a pale-yellow liquid (18.84 g, 50.3 mmol) in 88% yield.

^{1}H NMR (300 MHz, CDCl$_3$, δ): 3.64 (t, *J* = 5.6 Hz, 2H, -C$\underline{H}_2$Cl), 3.57 – 3.49 (m, 24H, C$\underline{H}_2$-O-C$\underline{H}_2$), 3.42 (t, *J* = 4.8 Hz, 2H, -C$\underline{H}_2$O), 3.25 (s, 3H, -OC$\underline{H}_3$); **^{13}C{^{1}H} NMR** (75 MHz, CDCl$_3$, δ): 71.64, 71.05, 70.35, 70.29, 70.20, 58.68, 42.49. **Anal. Calc**. for C$_{15}$H$_{31}$ClO$_8$ (374.91): C, 50.21; H, 8.71. Found: C, 49.73; H, 8.58.

6.1.5 Synthesis of 2-methyl-1-(2,5,8,11,14,17,20,23-octaoxapentacosan-25-yl)-imidazole (2.6).[1]

An oven-dried Schlenk flask under N$_2$ was charged with sodium hydride (2.13 g (wet mass, dispersed in mineral oil), 1.33 g (dry mass), 55.4 mmol, 1.3 equiv.). To remove the mineral oil, anhydrous hexane (15 mL) was added and the suspension was stirred at room temperature. The hexane was removed *via* cannula filtration and the process was repeated and then dried under high vacuum. The resultant off-white solid was suspended in anhydrous THF (70 mL) under a N$_2$ atmosphere. The suspension was then cooled to 0 °C and 2-methylimidazole (3.5 g, 42.6 mmol, 1 equiv.) was added slowly portion-wise which resulted in the liberation of gas. After the exotherm had subsided, **2.5** (18.3 g, 58.8 mmol, 1.2 equiv.) was added slowly and the brown solution was heated to 75 °C and stirred for 16 hours. After this, once the solution had cooled down to room temperature the solvent was removed *in vacuo* and water (5 mL) was added. The product was extracted with diethyl ether (3 x 40 mL) and the organic layers

were combined, dried over MgSO$_4$, filtered and the solvent removed *in vacuo* to give **2.6** as a viscous yellow oil (15.8 g, 38.8 mmol) in 91% yield.

^{1}H NMR (300 MHz, CDCl$_3$, δ): 6.81 (d, *J* = 1.2 Hz, 2H, N-C<u>H=CH</u>-N), 3.61 (t, *J* = 4.7 Hz, 2H, N-C<u>H$_2$</u>-CH$_2$), 3.56 – 3.50 (m, 24H, C<u>H$_2$</u>-O-C<u>H$_2$</u>), 3.45 (t, *J* = 4.9 Hz, 2H, O-C<u>H$_2$</u>), 3.26 (s, 3H, -OC<u>H$_3$</u>), 2.29 (s, 3H, N=C(C<u>H$_3$</u>)-N); **^{13}C{^{1}H} NMR** (75 MHz, CDCl$_3$, δ): 144.31, 121.09, 71.67, 71.65, 71.11, 71.08, 70.38, 70.31, 58.75, 58.42, 58.70, 42.49, 13.64; **Anal. Calc.** for C$_{19}$H$_{37}$N$_2$O$_8$ (407.56): C, 56.23; H, 8.99; N, 6.25%. Found: C, 56.02; H, 8.78; N, 6.04%.

6.1.6 Synthesis of 1-bromomethyl-4-vinyl-benzene (2.7).[1]
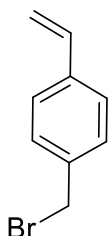
An oven-dried Schlenk flask under N$_2$ was charged with 4-chloromethyl styrene (9.23 mL, 65.5 mmol, 1 equiv.), acetonitrile (70 mL) and sodium bromide (27 g, 262.1 mmol, 4 equiv.). The solution was heated to 80 °C and stirred for 16 hours. After this time, the reaction was left to cool to room temperature and then filtered to remove any solids. The filtrate was concentrated *in vacuo* to give a yellow oil (11.7 g, 59.6 mmol) in 91% yield.

^{1}H NMR (300 MHz, CDCl$_3$, δ): 7.34 (m, 4H, C$_6$<u>H$_4$</u>), 6.73 (dd, *J* = 17.3, 10.4 Hz, 1H, CH$_2$=C<u>H</u>-C), 5.78 (d, *J* = 17.3 Hz, 1H, C<u>H$_2$</u>=CH-C), 5.30 (d, *J* = 10.4 Hz, 1H, C<u>H$_2$</u>=CH-C), 4.52 (s, 2H, -C<u>H$_2$</u>Br). **^{13}C{^{1}H} NMR** (75 MHz, CDCl$_3$, δ): 137.01, 136.93, 135.82, 128.64, 126.28, 113.89, 33.12 (-<u>C</u>H$_2$Br). **Anal. Calc.** for C$_9$H$_9$Br (195.99): C, 54.85; H, 4.60. Found: C, 54.56; H, 4.31.

6.1.7 Synthesis of 2-methyl-1-(2,5,8,11,14,17,20,23-octaoxapentacosan-25-yl)-3-(4-vinylbenzyl)-imidazolium bromide (2.8).[1]
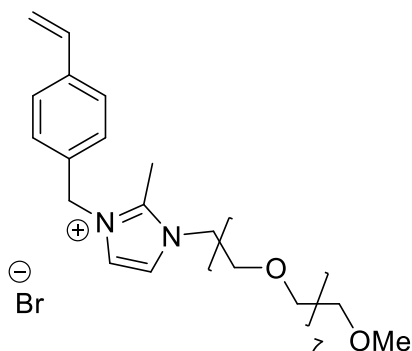
An oven-dried Schlenk flask under N_2 was charged with **2.6** (12.5 g, 27.9 mmol, 1 equiv.), **2.7** (5.47 g, 27.9 mmol, 1 equiv.) and dichloromethane (30 mL). The resulting solution was heated to 35 °C and stirred for 16 hours. After this time, the solvent was removed with an external trap under reduced pressure, the crude product was then washed with diethyl ether (3 x 30 mL), the diethyl ether was decanted off and the remaining residue was dried under reduced pressure to afford **2.8** as a viscous yellow oil (15.07 g, 24.9 mmol) in 89% yield.

¹H NMR (300 MHz, CDCl₃, δ): 7.80 (s, 1H, N-C$\underline{H}$=CH-N), 7.42 (s, 1H, N-CH=C$\underline{H}$-N), 7.31 (d, J = 8.0 Hz, 2H, C₆$\underline{H}$₄), 7.20 (d, J = 7.8 Hz, 2H, C₆$\underline{H}$₄), 6.61 (dd, J = 17.5, 10.8 Hz, 1H, CH₂=C$\underline{H}$-C), 5.68 (d, J = 17.5 Hz, 1H, C$\underline{H}$₂=CH-C), 5.30 (d, 2H, J = 11.3 Hz, C$\underline{H}$₂=CH-C), 5.22 (d, 2H, N-C$\underline{H}$₂-C), 4.44 (t, J = 4.7 Hz, 2H, C$\underline{H}$₂-OCH₃), 3.81 (t, J = 4.7 Hz, 2H, N-C$\underline{H}$₂-CH₂), 3.57 – 3.39 (m, 24H, C$\underline{H}$₂-O-C$\underline{H}$₂), 3.28 (s, 3H, -OC$\underline{H}$₃), 2.71 (s, 3H, N=C(C$\underline{H}$₃)-N); **¹³C{¹H} NMR** (75 MHz, CDCl₃, δ): 144.37, 144.34, 137.69, 135.38, 132.33, 132.30, 128.13, 127.97, 127.14, 126.67, 122.48, 121.68, 121.33, 114.69, 71.42, 71.17, 70.79, 70.13, 70.01, 69.55, 69.03, 58.25, 57.62, 51.22, 48.21, 10.49, 10.07, 9.95; **Anal. Calc**. for C₂₈H₄₆BrN₂O₈ (604.64): C, 59.94; H, 8.22; N, 4.66%. Found: C, 60.21; H, 8.49; N, 4.93%.

6.1.8 Synthesis of diphenyl(4-vinylphenyl)phosphine (2.9).[1]
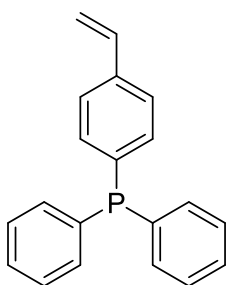
A round bottom flask under N_2 was charged with Mg turnings (3 g, 123.5 mmol, 2.4 equiv.) suspended in anhydrous THF (60 mL) and a crystal of iodine was added to the flask. The mixture was then cooled to 0 °C and stirred for 15 minutes. An oven-dried Schlenk flask was charged with 4-chlorostyrene (8 mL, 67 mmol, 1.3 equiv.) dissolved in anhydrous THF (30 mL) and 25% of the solution was added dropwise to the round bottom flask containing the Mg turnings. Once the reaction was initiated and started to generate heat, the remaining 75% of the 4-chlorostyrene solution was added dropwise over a 10-minute period before heating to 65 °C for 5 hours to generate the Grignard solution. A separate round bottomed flask was charged with chlorodiphenylphosphine (9.5 mL, 51.5 mmol, 1 equiv.) dissolved in anhydrous THF (30 mL) which was then cooled to 0 °C. The Grignard solution was then added dropwise to the phosphine-solution and the resultant mixture was stirred for 16 hours at room temperature. After this time, the reaction was quenched with degassed water (100 mL) and the product extracted with degassed diethyl ether (3 x 100 mL). The combined organic layers stored under N_2 were dried over $MgSO_4$, filtered and the solvent removed using an external trap to afford **2.9** as a white solid (10 g, 31.9 mmol) in 62% yield. The product was stored under N_2.

^{1}H NMR (300 MHz, CDCl$_3$, δ): 7.26-7.30 (m, 14H, C$_6$H$_4$), 6.62 (dd, J = 17.5, J = 10.8 Hz, 1H, CH$_2$=CH-C), 5.72 (d, J = 17.4 Hz, 1H, CH$_2$=CH-C) 5.19 (d, J = 10.8 Hz, 1H, CH$_2$=CH-C); **^{13}C{^{1}H} NMR** (75 MHz, CDCl$_3$, δ): 137.45, 137.03, 136.87, 136.34, 134.01, 133.88, 133.33, 133.00, 128.45, 126.05; **^{31}P{^{1}H} NMR** (121 MHz, CDCl$_3$, δ): -5.82.

6.1.9   *General procedure for polymerisations.*

An oven-dried Schlenk flask under N_2 was charged with the appropriate monomers (mole ratio of 1.86:1:0.14 imidazolium: phosphine: crosslinker) dissolved in a 1:1 anhydrous ethanol and anhydrous THF mixture (8 mL solvent/g monomer). To this solution, AIBN (5 mol %) was added and the reaction mixture was degassed using the freeze-thaw method six times prior to heating to 70 °C for 3 days. After this time, the mixture was cooled to room temperature and an additional 5 mol% AIBN was added before the degassing process was repeated and heated to 70 °C for a further 16 hours.

The solution was then cooled to room temperature and the solvent was concentrated under reduced pressure *ca.* 10 mL. The resulting residue was added dropwise to diethyl ether (300 mL) and vigorously stirred for 1 hour. After this time, the solution was left to settle, filtered through a frit and the solid was washed with diethyl ether (2 x 50 mL) and dried under vacuum to afford the corresponding PIL as an off-white solid. Yield of **2.10** (PPh$_2$-PEGPIL) = 92% and **2.11** (PPh$_2$-PIL) = 90%.

6.1.10 Synthesis of PEG-PIL (2.12).

PEGylated functionalised PIL **2.12** was prepared following the general protocol in section **6.*1.9*** (mole ratio of 1.86:1:0.14 imidazolium-PEG: styrene: crosslinker) and was obtained as a pale-yellow solid in 91% yield.

6.1.11 Synthesis of PIL (2.13).

PIL **2.13** was prepared following the general protocol in section **6.1.9** (mole ratio of 1.86:1:0.14 imidazolium: styrene: crosslinker) and was obtained as a pale-yellow solid in 90% yield.

6.1.12 General procedure for the oxidation of PILs with H$_2$O$_2$.

An oven-dried Schlenk flask under N$_2$ was charged with the appropriate PIL (2 mmol) dissolved in dichloromethane (20 mL) and an aqueous solution of H$_2$O$_2$ (35% w/w, 0.7 mL, 8.4 mmol) and stirred for 16 hours at room temperature. The reaction mixture was then diluted with dichloromethane (30 mL) and stirred with 5-8 g of MgSO$_4$ for 10 minutes. The reaction mixture was then filtered with a funnel and the filtrate was reduced in vacuo to obtain **2.19** as a white solid. For **2.10** (PPh$_2$-PEG), the MgSO$_4$ filter was stirred with methanol for 10 minutes and filtered and the filtrate solvent was removed *in vacuo* to give **2.18** as a white solid. Yield of **2.18** ((O)PPh$_2$-PEGPIL) = 90%, and **2.19** ((O)PPh$_2$-PIL) = 92%.

6.1.13 General procedure for the synthesis of RuNPs from RuCl₃.

An oven-dried Schlenk flask under N_2 was charged with the appropriate PIL (0.5 mmol) suspended in ethanol (25 mL). To this, $RuCl_3 \cdot 3H_2O$ (0.13 g, 0.5 mmol) was added in a single portion and the mixture was stirred vigorously at room temperature for 4 hours. After this, the mixture was cooled to 0 ℃ and an aqueous solution of $NaBH_4$ (0.15 g, 4 mmol, 8 equiv.) dissolved in water (5 mL) was added dropwise. The mixture rapidly turned from dark brown to green then to black and the resulting mixture was stirred vigorously for 16 hours at room temperature under a N_2 atmosphere. After this, the solvent was removed to dryness under reduced pressure and acetone was added to triturate, the solids were collected by filtration through a sintered frit and washed with water (10 mL), ethanol (2 x 20 mL) and diethyl ether (3 x 30 mL) to obtain RuNPs as black powders. Yield of **2.14** (PPh₂-PEG) = 82%, **2.15** (PPh₂) = 81%, **2.16** (PEG) = 84% and **2.17** (PIIL) = 90%, **2.20** ((O)PPh₂-PEG) = 83% and **2.21** ((O)PPh₂) = 81%.

6.1.14 General procedure for the synthesis of RuNPs from Ru(COD)(COT).

A 50 mL glass insert was charged with the appropriate PIL (0.1 mmol), [Ru(COD)(COT)] (0.035 g, 0.1 mmol) and anhydrous THF (25 mL). The reduction reaction was conducted in a 50 mL temperature-controlled Parr benchtop reactor with a gas ballast and a magnetically coupled stirrer. After the reactor was assembled it was pressurised to 100 psi of hydrogen and left for 10 seconds before the gas is released through the outlet valve. The sequence was repeated five times then the reactor was pressurised to 150 psi and the solution was stirred at 70 °C for 16 hours. After this time, the reactor was cooled to room temperature and the gas was released through the outlet valve. The vessel was removed from the reactor and the reaction mixture was transferred to a 50 mL round bottom flask. An external trap was used to remove the solvent, triturated with anhydrous hexane (10 mL) then dried under reduced pressure to obtain the RuNPs as black powders. Yield of **2.22** (PPh₂-PEG) = 80% and **2.23** (PPh₂) = 82%.

6.1.15 *General procedure for the selective carbonyl hydrogenation of model aldehydes and ketones.*

All hydrogenation reactions were conducted in a 50 mL temperature-controlled Parr benchtop reactor with a gas ballast and a magnetically coupled stirrer. In a standard procedure, a 50 mL glass vessel was charged with substrate (1 mmol), 12 mL of the appropriate solvent and the appropriate catalyst (0.1 mol % based on Ru content calculated from ICP-OES analysis). Reactions were conducted under 70 psi of hydrogen at 50 °C unless stated otherwise. After the reactor was assembled it was pressurised to 100 psi of hydrogen and left for 10 seconds before the gas is released through the outlet valve. The sequence was repeated five times then the reactor was pressurised to 70 psi and heated to 50 °C for the desired reaction time. For the reactions conducted in ethanol, 2-methyl-THF or toluene, the mixture was passed through a silica plug and then the solvent removed *in vacuo*. Reactions conducted in aqueous medium were transferred to a dropping funnel and extracted with ethyl acetate (2 x 20 mL). The combined organic phases were dried over $MgSO_4$, filtered and the solvent removed *in vacuo*. Conversion and selectivity were determined using ^{1}H NMR spectroscopy of the remaining starting material and the reaction products against 1,3-dinitrobenzene. Well-defined resonances were used to determine the composition of the mixture by standardising the relative integrations based on the number of protons that are associated with the chosen peaks.

6.1.16 *General procedure for the complete hydrogenation of substituted acetophenone to the corresponding substituted cyclohexylethanol.*

In a standard procedure, a 50 mL glass vessel was charged with the catalyst (0.1 mol % based on Ru content calculated from ICP-OES analysis), ethanol/water (1:1) (12 mL), K_2CO_3 (0.014 g, 0.1 mmol) and substrate (1 mmol). Reactions were conducted under 400 psi of hydrogen at 70 °C unless stated otherwise. After the reactor was assembled it was pressurised to 100 psi of hydrogen and left for 10 seconds, before the gas is released through the outlet valve. The sequence was repeated five times then the reactor was pressurised to 400 psi and heated to 70 °C for the desired reaction time. Following this, the reactor was cooled down to room temperature and the reaction mixture transferred to a dropping funnel and extracted with ethyl acetate (2 x 20 mL). The combined organic phases were dried over $MgSO_4$, filtered and the solvent removed *in vacuo*. Conversion and selectivity were determined

using ^{1}H NMR spectroscopy of the remaining starting material and the reaction products against 1,3-dinitrobenzene. Well-defined resonances were used to determine the composition of the mixture by standardising the relative integrations based on the number of protons that are associated with the chosen peaks.

6.1.17 *General procedure for the selective carbonyl hydrogenation of furfural to furfuryl alcohol.*

In a standard procedure, a 50 mL glass vessel was charged with the catalyst (0.1 mol % based on Ru content calculated from ICP-OES analysis), water (12 mL) and furfural (0.083 mL, 1 mmol). Reactions were conducted under 70 psi of hydrogen at 50 °C unless stated otherwise. After the reactor was assembled it was pressurised to 100 psi of hydrogen and left for 10 seconds before the gas was released through the outlet valve. The sequence was repeated five times then the reactor was pressurised to 70 psi and heated to 50 °C for the desired reaction time. Following this, the reactor was cooled down to room temperature and the reaction mixture transferred to a dropping funnel and extracted with ethyl acetate (2 x 20 mL). The combined organic phases were dried over MgSO$_4$, filtered and the solvent removed *in vacuo.* Conversion and selectivity were determined using ^{1}H NMR spectroscopy of the remaining starting material and the reaction products against 1,3-dinitrobenzene. Well-defined resonances were used to determine the composition of the mixture by standardising the relative integrations based on the number of protons that are associated with the chosen peaks.

6.1.18 *General procedure for the hydrogenation of levulinic acid to γ-valerolactone.*

In a standard procedure, a 50 mL glass vessel was charged with the catalyst (0.1 mol % based on Ru content calculated from ICP-OES analysis), water (12 mL) and levulinic acid (0.1 mL, 1 mmol). Reactions were conducted under 400 psi of hydrogen at 110 °C unless stated otherwise. After the reactor was assembled it was pressurised to 100 psi of hydrogen and left for 10 seconds before the gas was released through the outlet valve. The sequence was repeated five times then the reactor was pressurised to 400 psi and heated to 110 °C for the desired reaction time. Following

this, the reactor was cooled down to room temperature and the reaction mixture transferred to a dropping funnel and extracted with ethyl acetate (2 x 20 mL). The combined organic phases were dried over MgSO$_4$, filtered and the solvent removed *in vacuo*. Conversion and selectivity were determined using ^{1}H NMR spectroscopy of the remaining starting material and the reaction products against 1,3-dinitrobenzene. Well-defined resonances were used to determine the composition of the mixture by standardising the relative integrations based on the number of protons that are associated with the chosen peaks.

6.1.19 *General procedure for the hydrogenation of ethyl levulinate to γ-valerolactone.*

In a standard procedure, a 50 mL glass vessel was charged with the catalyst (0.1 mol % based on Ru content calculated from ICP-OES analysis), water (12 mL) and ethyl levulinate (0.14 mL, 1 mmol). Reactions were conducted under 400 psi of hydrogen at 110 °C unless stated otherwise. After the reactor was assembled it was pressurised to 100 psi of hydrogen and left for 10 seconds, before the gas was released through the outlet valve. The sequence was repeated five times then the reactor was pressurised to 400 psi and heated to 110 °C for the desired reaction time. Following this, the reactor was cooled down to room temperature and the reaction mixture transferred to a dropping funnel and extracted with ethyl acetate (2 x 20 mL). The combined organic phases were dried over MgSO$_4$, filtered and the solvent removed *in vacuo*. Conversion and selectivity were determined using ^{1}H NMR spectroscopy of the remaining starting material and the reaction products against 1,3-dinitrobenzene. Well-defined resonances were used to determine the composition of the mixture by standardising the relative integrations based on the number of protons that are associated with the chosen peaks.

6.2   Chapter 3 Experimental.

6.2.1 *General procedure for the selective reduction of nitroarenes.*

An oven-dried Schlenk under N$_2$ was charged with nitrobenzene (1 mmol, 0.10 mL), solvent (2 mL) and catalyst (0.1 mol%). Hydrazine hydrate (3 mmol, 0.094 mL) was added into the reaction mixture. The mixture was stirred at the specified temperature for the specified time. After completion of the reaction the mixture was passed through

a silica plug to remove hydrazine or water and the solvent was removed *in vacuo*. The conversion and selectivity were determined by ^{1}H NMR spectroscopy using dioxane as an internal standard.

6.2.2   *General procedure for the nitroarene reduction recycle.*

An oven-dried Schlenk under N_2 was charged with nitrobenzene (1 mmol, 0.10 mL), solvent (2 mL) and catalyst (0.1 mol%). Hydrazine hydrate (3 mmol, 0.094 mL) was added into the reaction mixture. The mixture was stirred at 40 ℃ for the 90 minutes. After completion, the solution was transferred to a dropping funnel and extracted with ethyl acetate (10 mL). The catalyst-containing aqueous phase was transferred into a new oven-dried Schlenk flask and recharged with 1 equivalent of nitrobenzene and 3 equivalents of N_2H_4 and the reaction repeated.

6.3   Chapter 4 Experimental.

6.3.1   *Synthesis of 4-(2-methyl-1-(4-vinylbenzyl)-1H-imidazol-3-ium-3-yl)butane-1-sulfonate (4.1).*
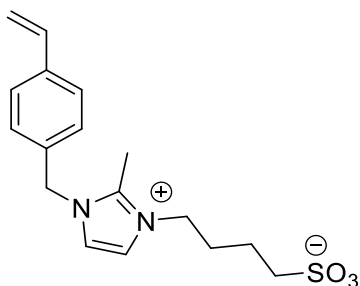
An oven-dried Schlenk flask under N_2 was charged with 2-methyl-1-(4-vinylbenzyl)-1H-imidazole, **2.2** (8 g, 40.3 mmol), 1,4-butane sultone (4.13 mL, 40.3 mmol) and acetonitrile (70 mL). The reaction was stirred and heated to 70 ℃ for 48 hours. The reaction mixture was concentrated to *ca.* 15 mL and added dropwise into vigorously stirred acetone (400 mL) and filtered to afford **4.1** as a white powder (10.8 g, 32.3 mmol) in 80 % yield.

^{1}H NMR (300 MHz D$_2$O/NaCl, *δ*): 7.54 (1H, d, J = 2 Hz, N-<u>CH</u>=CH-N), 7.45 (1H, d, J = 2 Hz, N-CH=<u>CH</u>-N), 7.45-7.42 (2H, d, J = 8 Hz), 7.23-7.20 (1H, d, J = 8 Hz), 6.73-6.63 (1H, dd, J = 11 Hz, 18 Hz), 5.78-5.73 (1H, d, J = 17 Hz), 5.23-5.20 (1H, d, J = 11 Hz), 5.32 (2H, s, C-<u>CH$_2$</u>-N), 4.17-4.12 (2H, t, J = 7 Hz, N-<u>CH$_2$</u>-CH$_2$), 2.80-2.75 (2H, t, J = 7

Hz), 1.99-1.89 (2H, m, S-C$\underline{H_2}$-CH$_2$). 2.59 (3H, s, =C(C$\underline{H_3}$)-N), 2.00-1.90 (2H, m, N-CH$_2$-C$\underline{H_2}$), 1.79-1.69 (2H, m, S-CH$_2$-C$\underline{H_2}$); ^{13}C {^{1}H} NMR (75 MHz D$_2$O/NaCl, δ): 138.37, 135.84, 133.01, 127.83, 126.72, 121.52, 121.40, 113.98, 51.05, 49.95, 29.30, 27.96, 21.47, 8.53; **Anal. Calc**. for C$_{17}$H$_{22}$N$_2$O$_3$S (334.43): C, 61.05; H, 6.63; N, 8.38%. Found: C, 61.41; H, 6.98; N, 8.72%.

6.3.2 Synthesis of 4-(2-methyl-1H-imidazol-3-ium-3-yl)butane-1-sulfonate (4.2).
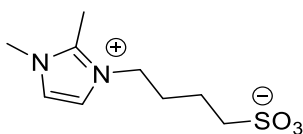
An oven dried Schlenk flask under N$_2$ was charged with 1,2-dimethylimidazole (8 g, 83.2 mmol), 1,4-butane sultone (8.5 mL, 83.2 mmol) and acetonitrile (70 mL). The reaction was stirred and heated to 70 ℃ for 48 hours. The reaction mixture was added dropwise into acetone (150 mL) and filtered to afford a white powder (16.4 g, 70.6 mmol) in 85 % yield.

^{1}**H NMR** (300 MHz, D$_2$O/NaCl, δ): 7.55-7.47 (2H, dd, J = 2 Hz, 21 Hz, N-C$\underline{H}$=C$\underline{H}$-N), 4.26-4.21 (2H, t, J = 7 Hz, N-C$\underline{H_2}$-CH$_2$), 3.85 (3H, s, N-C$\underline{H_3}$), 2.90-2.85 (2H, t, J = 7 Hz. S-C$\underline{H_2}$-CH$_2$), 2.68 (3H, s, =C(C$\underline{H_3}$)-N), 2.07-1.97 (2H, m, N-CH$_2$-C$\underline{H_2}$), 1.88-1.77 (2H, m, S-CH$_2$-C$\underline{H_2}$); ^{13}**C {^{1}H} NMR** (75 MHz, D$_2$O/NaCl, δ): 121.52, 121.40, 113.98, 51.05, 49.95, 32.10, 27.96, 21.47, 8.53; **Anal. Calc**. for C$_9$H$_{16}$N$_2$O$_3$S (232.30): C, 46.53; H, 6.94; N, 12.06%. Found: C, 46.89; H, 7.29; N, 12.40%.

6.3.3 General procedure for the homopolymerisations.

An oven-dried Schlenk flask under N$_2$ was charged with the appropriate imidazolium monomer dissolved in anhydrous ethanol (10 mL solvent/g monomer). To this solution, AIBN (5 mol %) was added and the reaction mixture was degassed using the freeze-thaw method six times prior to heating to 80 °C for three days. The solution was then cooled to room temperature and the solvent was concentrated under reduced pressure *ca.* 5-10 mL. The resulting residue was added dropwise to diethyl ether (200 mL) and vigorously stirred for 30 minutes. After this time, the solution was left to settle, filtered through a frit and the solid was washed with diethyl ether (2 x 30 mL) and dried under

vacuum to afford the corresponding PIL as a pale-yellow solid. Yield of **4.3** (PIL) = 94% and **4.4** (SO_3-PIL) = 89%.

6.3.4 General procedure for the copolymerisation.[3]

An oven-dried Schlenk flask under N_2 was charged with the appropriate monomers (mole ratio of 2:1 imidazolium: styrene) dissolved in anhydrous ethanol (8 mL solvent/g monomer). To this solution, AIBN (5 mol %) was added and the reaction mixture was degassed using the freeze-thaw method six times prior to heating to 80 °C for three days. The solution was then cooled to room temperature and the solvent was concentrated under reduced pressure *ca.* 5-10 mL. The resulting residue was added dropwise to diethyl ether (200 mL) and vigorously stirred for 30 minutes. After this time, the solution was left to settle, filtered through a frit and the solid was washed with diethyl ether (2 x 30 mL) and dried under vacuum to afford the corresponding PIL as an pale-yellow solid. Yield of **4.5** (PIL) = 88% and **4.6** (SO_3-PIL) = 89%.

6.3.5 General procedure for the impregnation of PILs with polyoxometalate.

A round bottom flask under N_2 was charged with the appropriate polyoxometalate dissolved in the minimum volume of water (5-10 mL) and stirred at room temperature for 30 minutes. After this time, a 1:1 concentrated methanolic solution of PIL/NEt_3 (mole ratio 1:1 imidazolium to polyoxometalate) was added and the resultant mixture was stirred for 16 hours at room temperature. The mixture was then filtered through a sintered glass frit and the collected solid was washed with water (2 x 20 mL), ethanol (3 x 20 mL) and diethyl ether (3 x 30mL) and dried to yield free flowing pale-orange powders. Yield of **3.7** = 87%, **3.8** = 71%, **3.9** = 84%, **3.10** = 80%, **3.11** = 82% and **3.12** = 91%.

6.3.6 General procedure for the impregnation of PILs with H_2SO_4.

A round bottom flask under N_2 was charged with the appropriate PIL dissolved in methanol (40 mL) at room temperature. To this was added sulphuric acid (1:1 equiv. SO_3:H_2SO_4) and the resultant mixture was stirred for 16 hours at room temperature. The mixture was then cooled to 0 ℃ and then filtered through a sintered glass frit and the collected solid was washed with water (2 x 20 mL), ethanol (3 x 20 mL) and diethyl

ether (3 x 30mL) and dried to yield free flowing pale-yellow powders. Yield of **3.13** = 90%, **4.14** = 87% and **4.15** = 93%

6.3.7 General procedure for catalytic furfuryl alcohol alcoholysis in batch.

In a standard procedure, an oven-dried Schlenk flask under N_2 was charged with the appropriate catalyst (2.5 mol% based on W content determined by CHN analysis), alcohol (3 mL) and furfuryl alcohol (0.087 mL, 1 mmol). The reaction mixtures were heated at the desired reaction temperature under continuous magnetic stirring at 800 rpm for the given reaction time. After this time, the reaction was removed from the oil bath, cooled in a cold-water bath, sampled (~0.1 mL) diluted with butanol (0.5 mL). The aliquot was analysed by ^1H NMR spectroscopy using 1.3-dioxane as an internal standard to quantify the conversion and determine the selectivity. Relative percentages of starting material and products were determined using integrals in the 1H NMR spectra.

6.3.8 General procedure for catalytic alcoholysis recycle studies.

An oven-dried Schlenk flask under N_2 was charged with furfuryl alcohol (1 mmol), the appropriate PIIL@POM (2.5 mol% based on W content determined by CHN analysis) or resin and *n*-butanol (3 mL) and stirred at 110 ℃ for 40 minutes. After this time, the solution was transferred to a PTFE centrifuge tube and centrifuged (10 min, 12000 rpm), the solution was decanted using a pipette and the catalyst washed with ethyl acetate (15 mL), filtered and dried under high vacuum prior to reuse under the same reaction conditions. The remaining solution was analysed as described above.

6.3.9 General procedure for segmented catalytic alcoholysis using the Uniqsis FlowSyn™
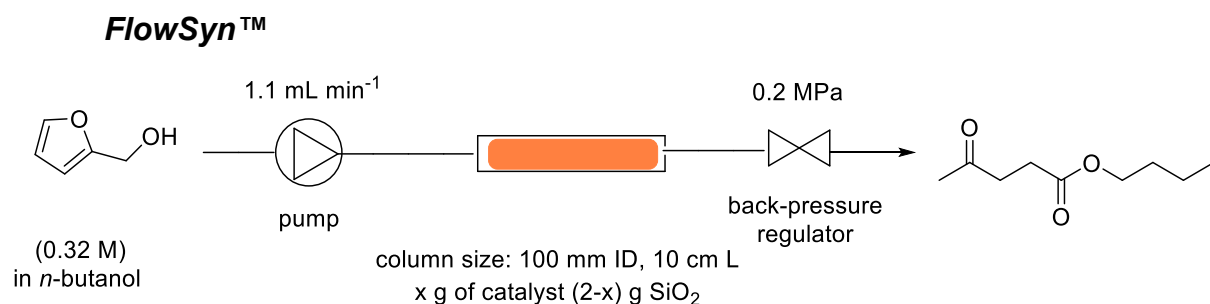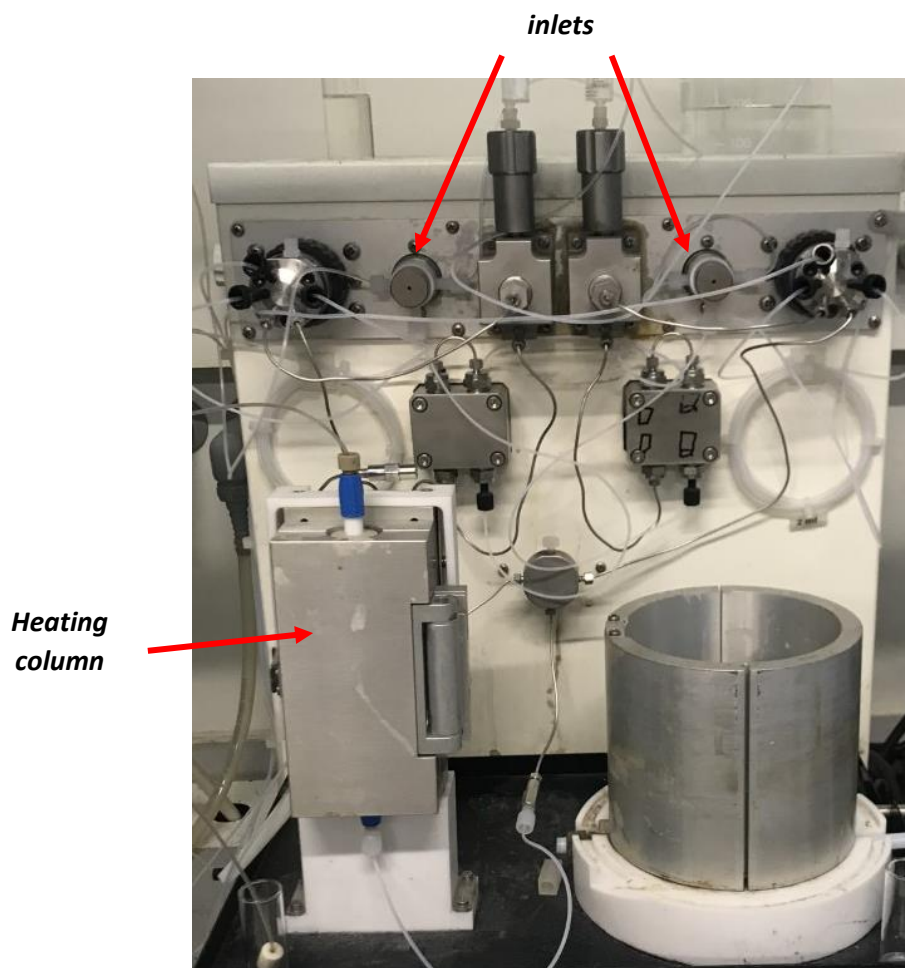
Figure 6.1: Uniqsis FlowSyn™ set-up.

A series of experiments were performed under manual control using the Uniqsis FlowSyn™ at different temperatures of 90, 110, 130 and 150 °C. The FlowSyn™ was fitted with a heating column (Figure 6.1) and both inlets were set to the solvent and the outlet was set to waste. A glass OMNIFIT® column (l, 100 mm; i.d.10 mm) was filled with catalyst (x g) or resin mixed in (Geduran® Si60 (43-60 µm)) silica (2-x g) and the ends of the column were sealed with adjustable PTFE flow adaptors before the catalyst column was placed into a cartridge heater. The reagent lines were primed with solvent e.g. *n*-butanol, for 5 minutes between each run. The system was pressurised to the desired pressure (~100 psi), checked for any leaks and then the reactor was heated to the desired reaction temperature. The liquid pump was then purged with the (0.32 M) reagent stock solution of furfuryl alcohol in *n*-butanol under N_2. When the pressure, temperature and flows were stable, the reagent mixture was pumped through at the desired flow rate. The reactor was maintained with a fixed 100 psi back-pressure regulator. The exiting stream was collected into separate vials in 3 mL fractions. Each

sample was sampled and analysed by ^{1}H NMR spectroscopy using 1,4-dioxane as an internal standard to quantify the amount of starting material and product composition.

Table 6.1: System manual setup.

Manual setup			
Inlet A	Reagent	Pump A	1.00 mL/min
Inlet B	Reagent	Pump B	0 mL/min
Outlet	Collect	Total flow rate	1.00 mL/min
Loop A	Load	Coil temperature	RT
Loop B	Load	Column temp	90, 110, 130, 150

6.3.10 General procedure for continuous flow alcoholysis.

A glass OMNIFIT® column (l, 100 mm; i.d. 10 mm) was packed with catalyst or resin (x g) mixed with silica (ca. 2-x g, Geduran® Si60 (43-60 µm)) and the ends of the column were sealed with adjustable PTFE flow adaptors before the catalyst column was placed into a cartridge heater. The system was pressurised to the desired pressure (~100 psi), checked for any leaks and then the reactor was heated to 130 ℃. The liquid pump was then purged with the (0.32 M) stock solution of furfuryl alcohol in *n*-butanol under N_2. When the pressure, temperature and flows were stable, the reagent mixture was pumped through at 1 mL min^{-1}. The reactor was maintained with a fixed 100 psi back-pressure regulator. The exiting stream was collected into separate vials in 3 mL fractions every 30 minutes. Each collected sample was sampled and analysed by ^{1}H NMR spectroscopy using 1,4-dioxane as an internal standard to quantify the amount of starting material and product composition.

Characterisation of alcohol, 2-butoxymethyl furan and levulinate.
[1]H and ^{13}C signals that are used for calculation of conversion of furfuryl alcohol and/or the selectivity for each substrate:
Furfuryl alcohol

^{1}H NMR (300 MHz, BuOH, δ): 7.65 (d, 1H), 6.59 (m, 2H), 4.81 (m, 2H).

Intermediate 2-butoxymethyl furan

^{1}H NMR (300 MHz, BuOH, δ): 7.70 (m, 1H), 6.63 (m, 2H), 4..71 (m, 2H), 3.75 (t, 2H), 1.49 (m, 4H), 0.96 (t, 3H).

n-butyl levulinate

¹H NMR (300 MHz, BuOH, δ): 4.36 (t, 2H), 3.88 (t, 2H), 3.06 (t, 2H), 2.83 (s, 3H), 1.81 (m, 2H), 1.71 (m, 2H), 1.25 (t, 3H).

References

1. S. Doherty, J. G. Knight, T. Backhouse, E. Abood, H. Alshaikh, I. J. S. Fairlamb, R. A. Bourne, T. W. Chamberlain and R. Stones, *Green Chem.*, 2017, **19**, 1635-1641.

2. C. Pan, K. Pelzer, K. Philippot, B. Chaudret, F. Dassenoy, P. Lecante and M.-J. Casanove, *J. Am. Chem. Soc.*, 2001, **31**, 7584-7593.

3. S. Doherty, J. G. Knight, M. A. Carroll, A. R. Clemmet, J. R. Ellison, T. Backhouse, N. Holmes and R. A. Bourne, *RSC Adv.*, 2016, **6**, 73118-73131.

Appendices

Appendix for Chapter 2

Appendix A: NMR spectras for the monomers

A1: Solution ^{1}H NMR spectrum of 1,2-dimethyl-3-(4-vinylbenzyl)-1H-imidazol-3-ium chloride (**2.1**) in CDCl$_3$
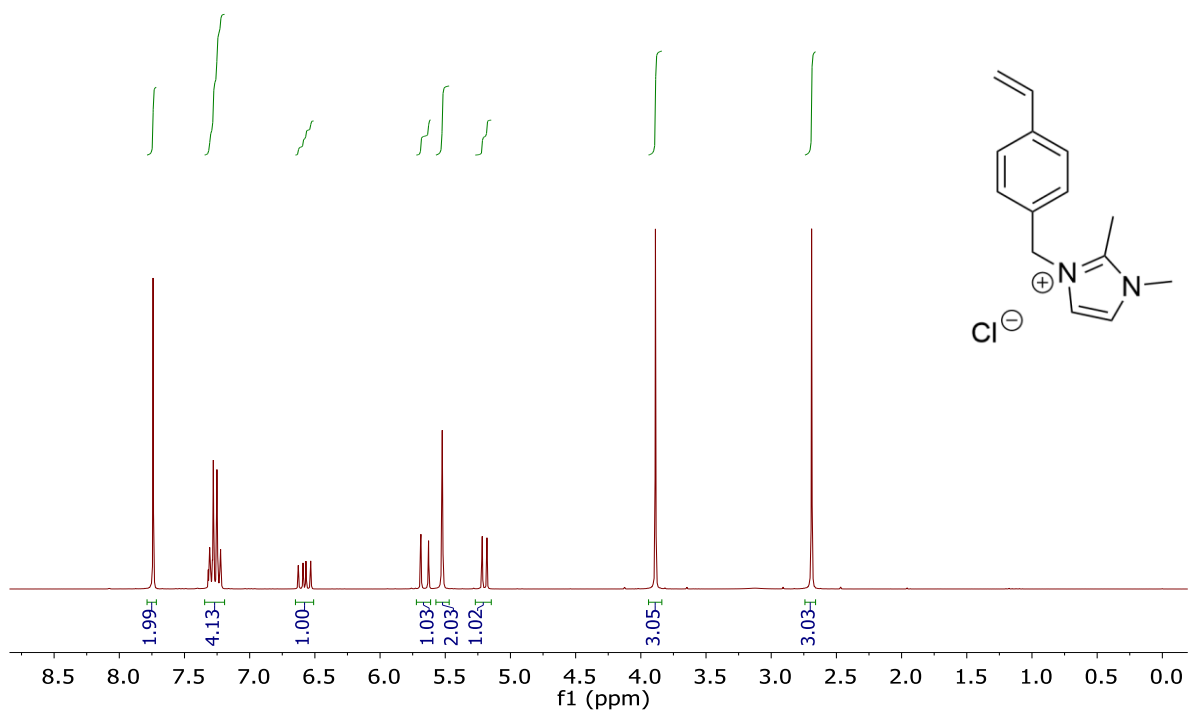
A2: Solution ^{1}H NMR spectrum of 2-methyl-1,3-bis(4-vinylbenzyl)-1H-imidazol-3-ium chloride (**2.3**) in CDCl$_3$
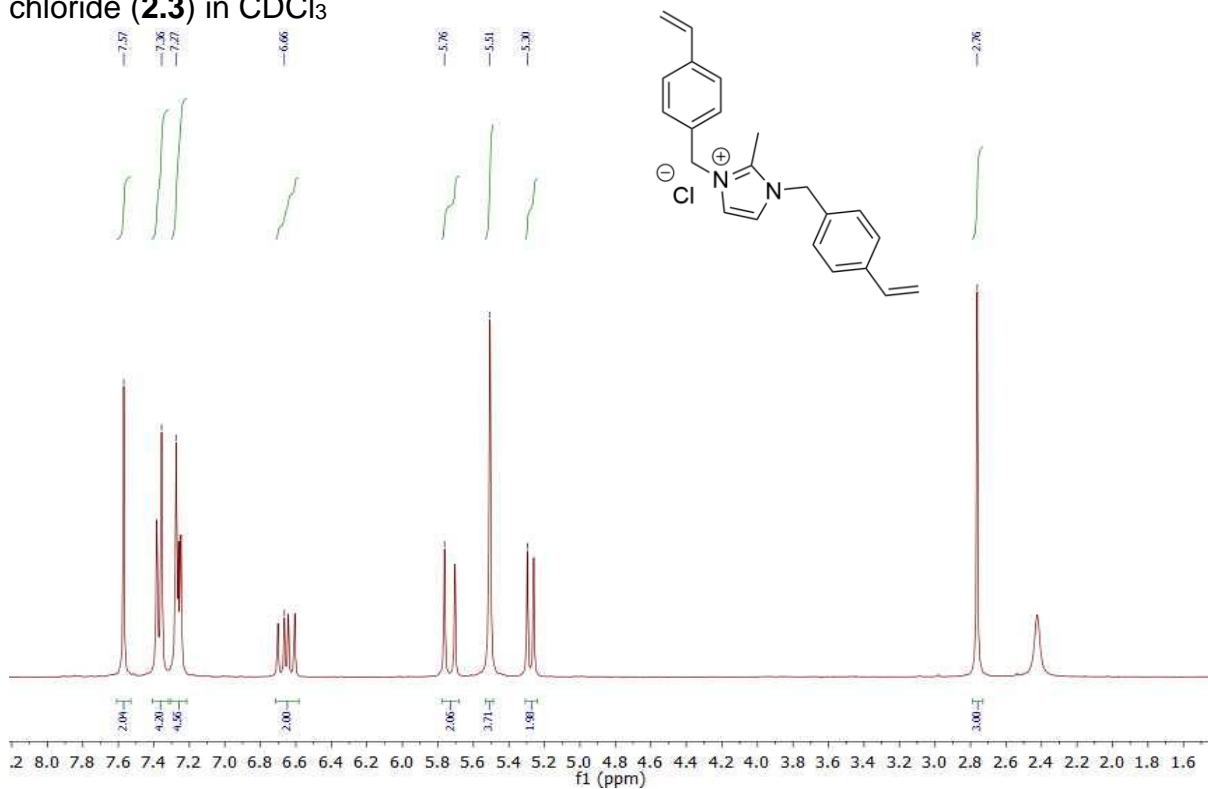
A3: Solution ^{1}H NMR spectrum of 1-bromomethyl-4-vinyl-benzene (**2.7**) in CDCl$_3$
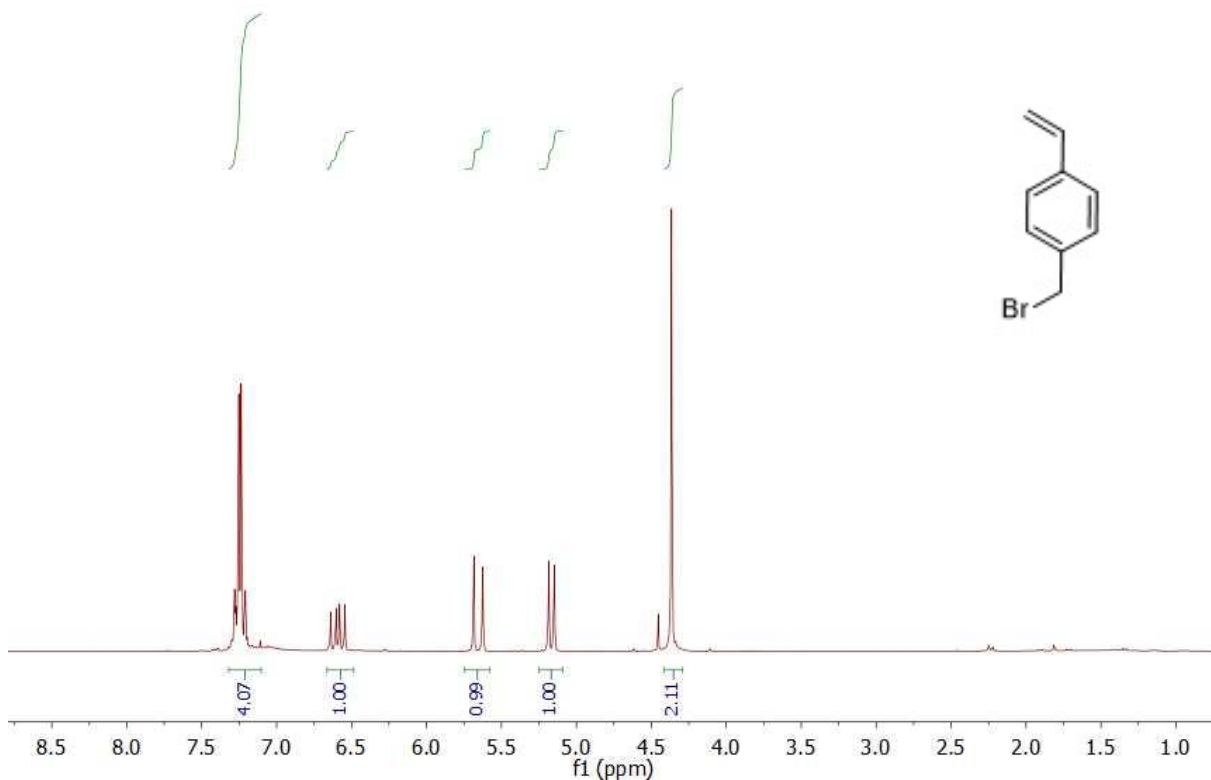
A4: Solution ^{1}H NMR spectrum of 2-methyl-1-(2,5,8,11,14,17,20,23-octaoxa pentacosan-25-yl)-3-(4-vinylbenzyl)-1H-3λ4-imidazolium bromide **2.8** in CDCl$_3$
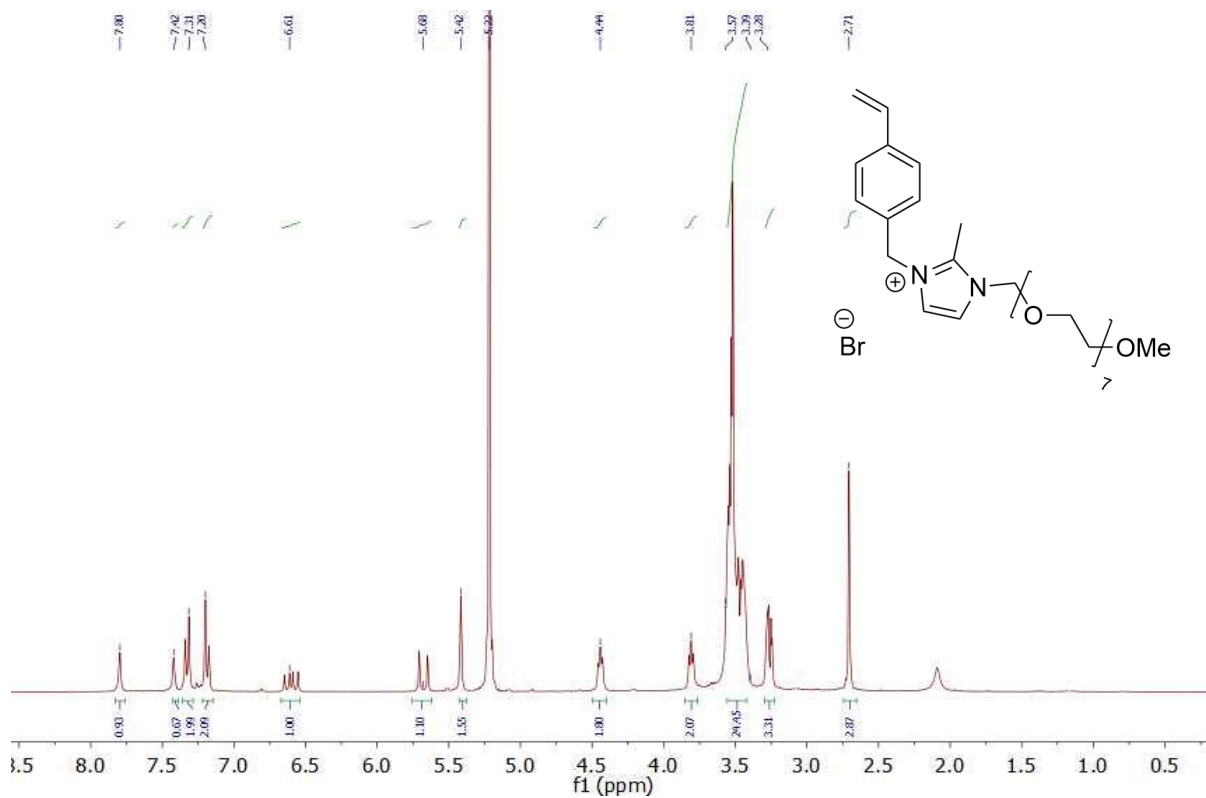
A: Solution ^{1}H NMR spectrum of diphenyl(4-vinylphenyl)phosphine **2.9** in CDCl$_3$
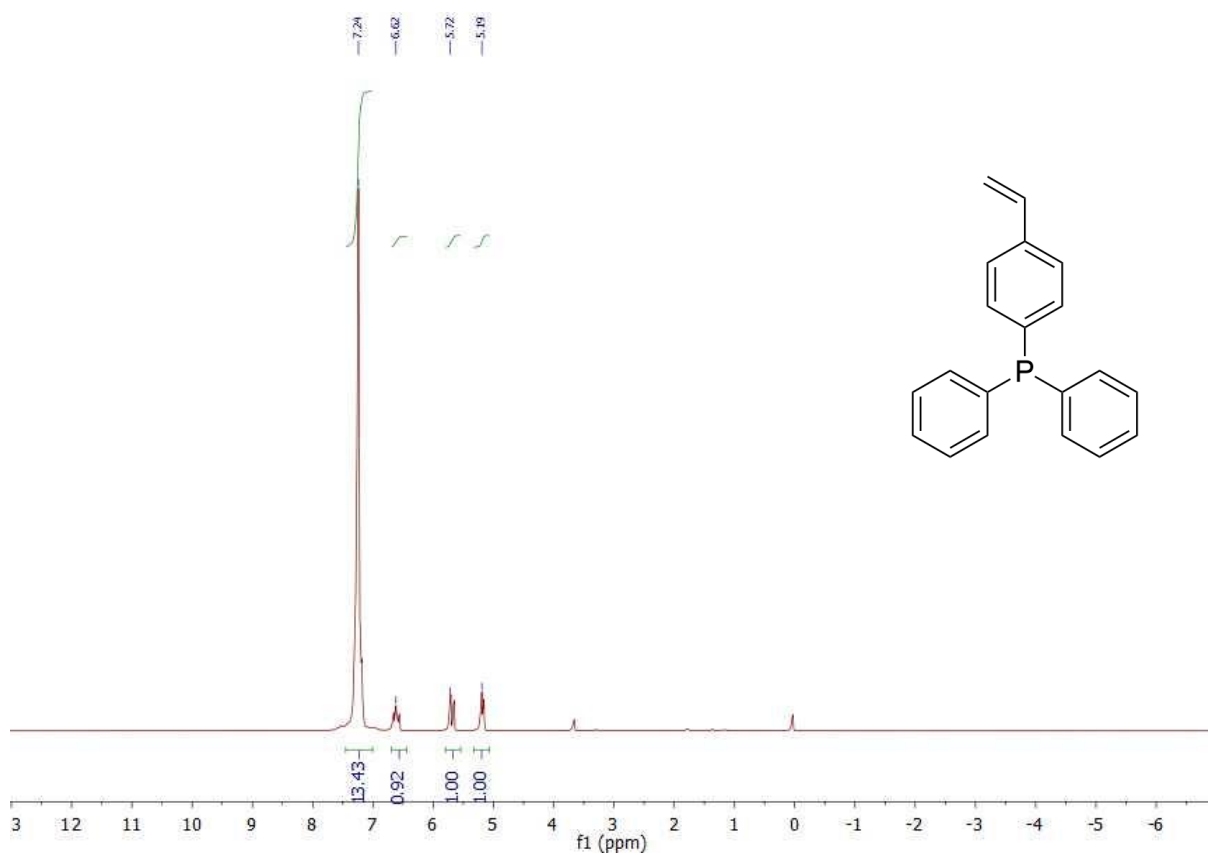
A5: Solution ^{31}P NMR spectrum of diphenyl(4-vinylphenyl)phosphine **2.9** in CDCl$_3$
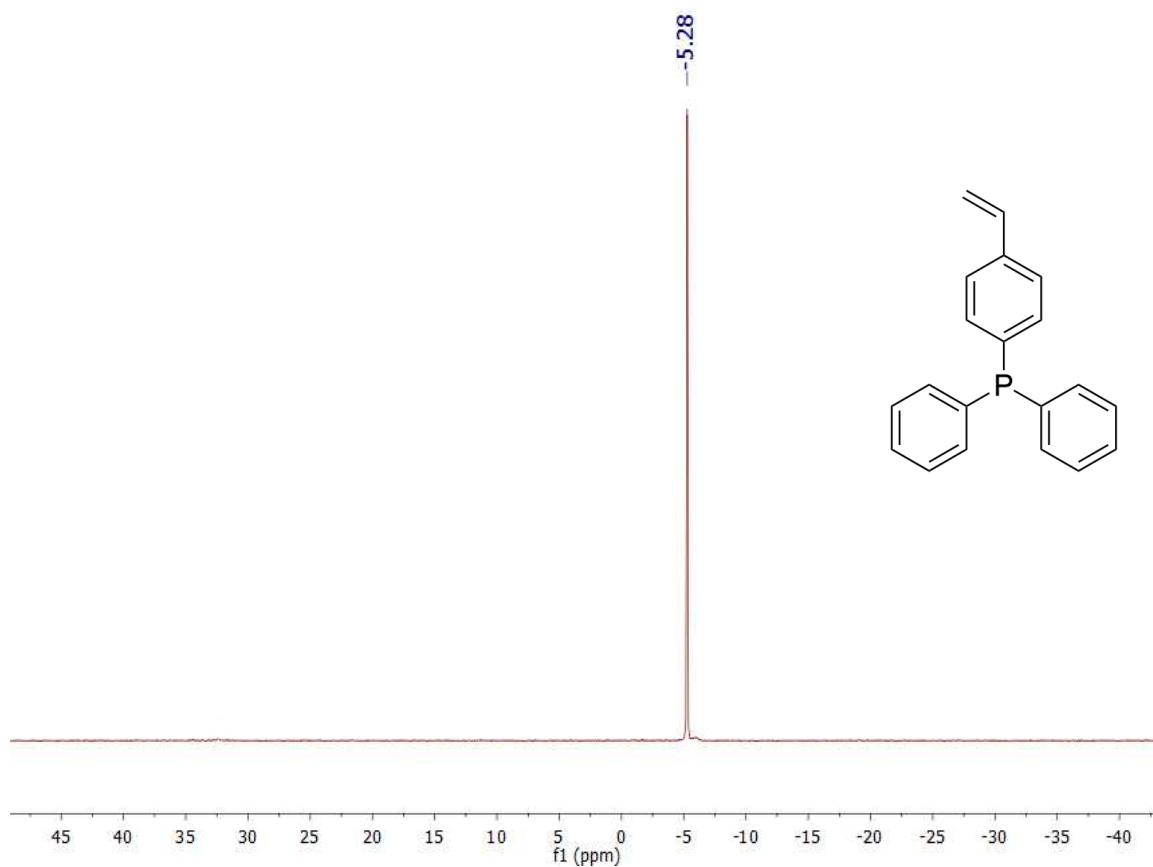
Appendix B: SEM images of polymers

B1: SEM of PIL **2.12**
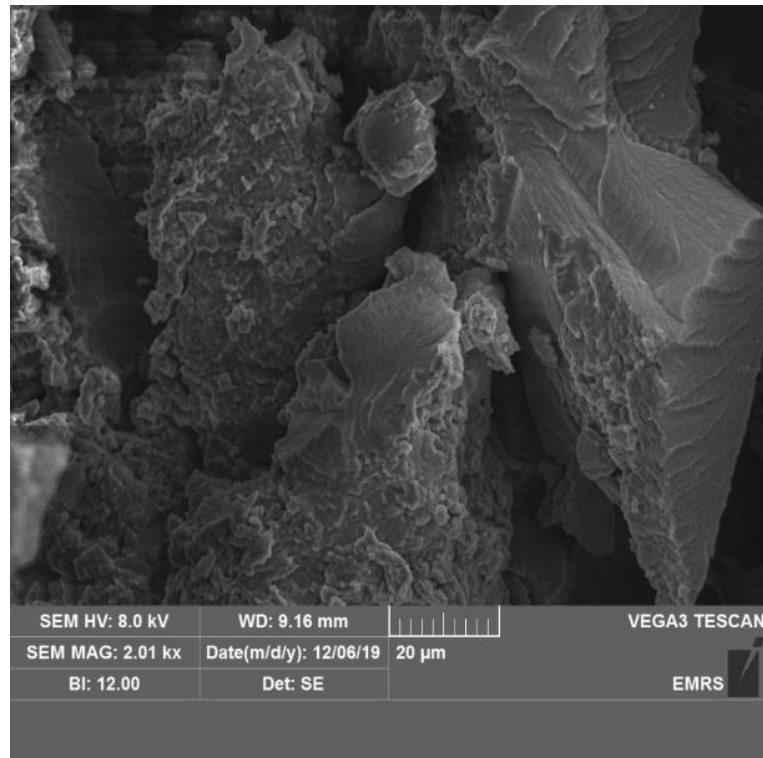
B2: SEM of PEG-PIL **2.13**
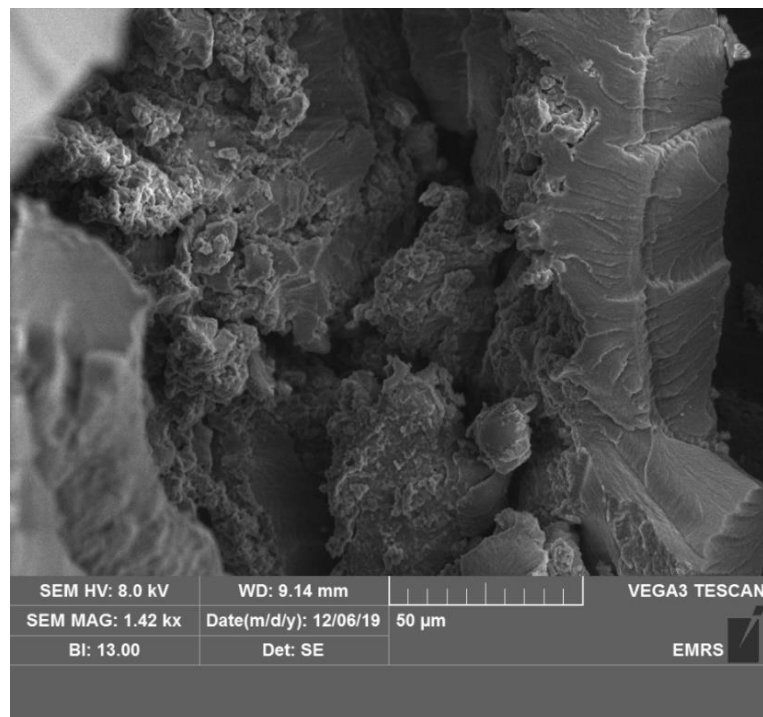
Appendix C: TGA of polymers

C1: TGA of PIL **2.12**
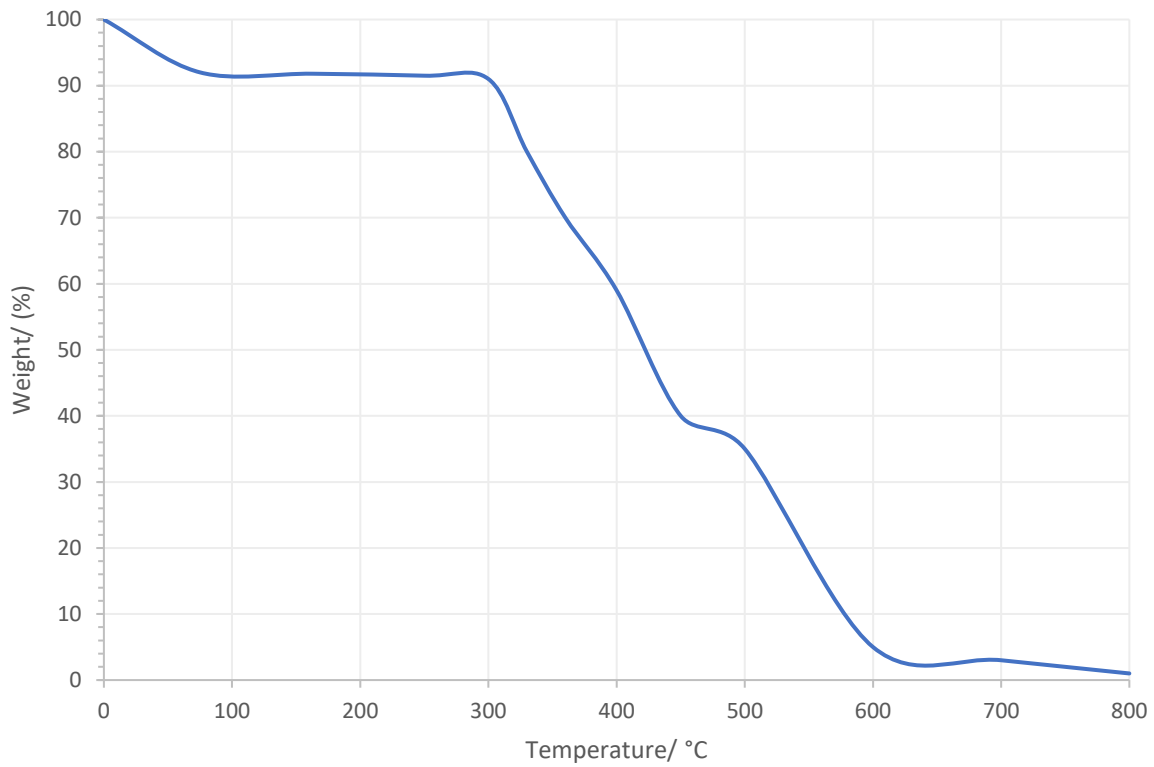
C2: TGA of PEG-PIL **2.13**
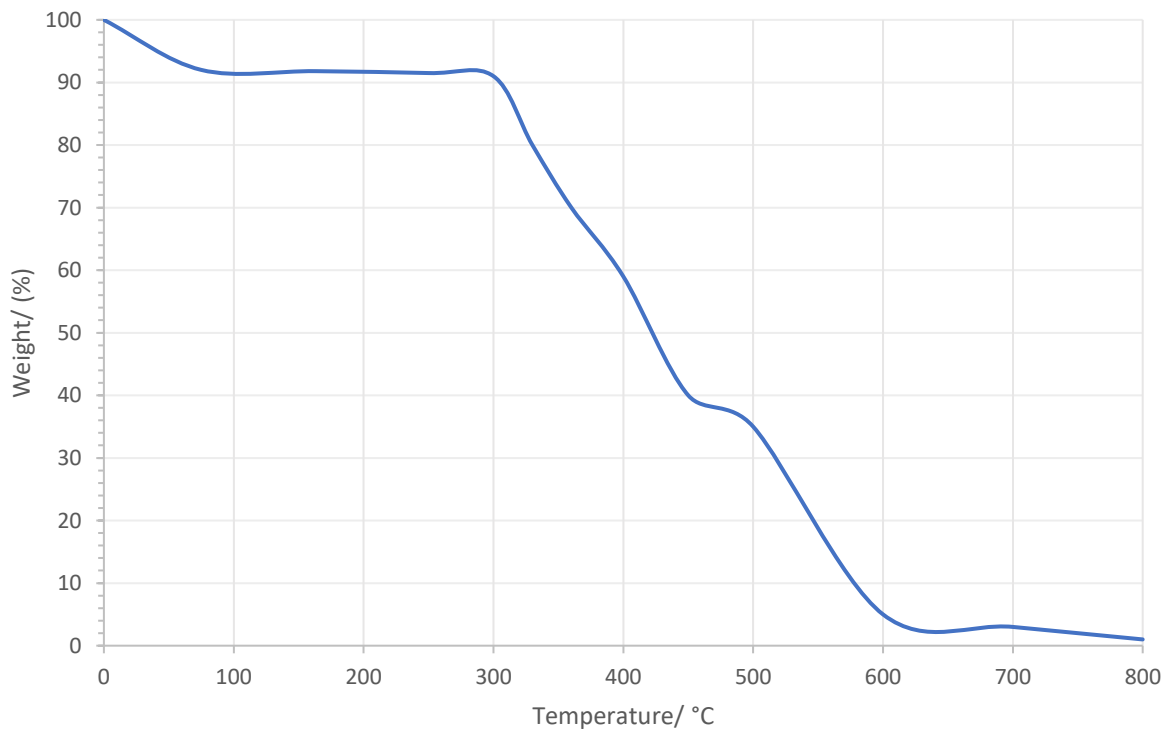
Appendix D: FTIR of RuNPs

D1: FTIR of (O)PPh₂-PIIL 2.19
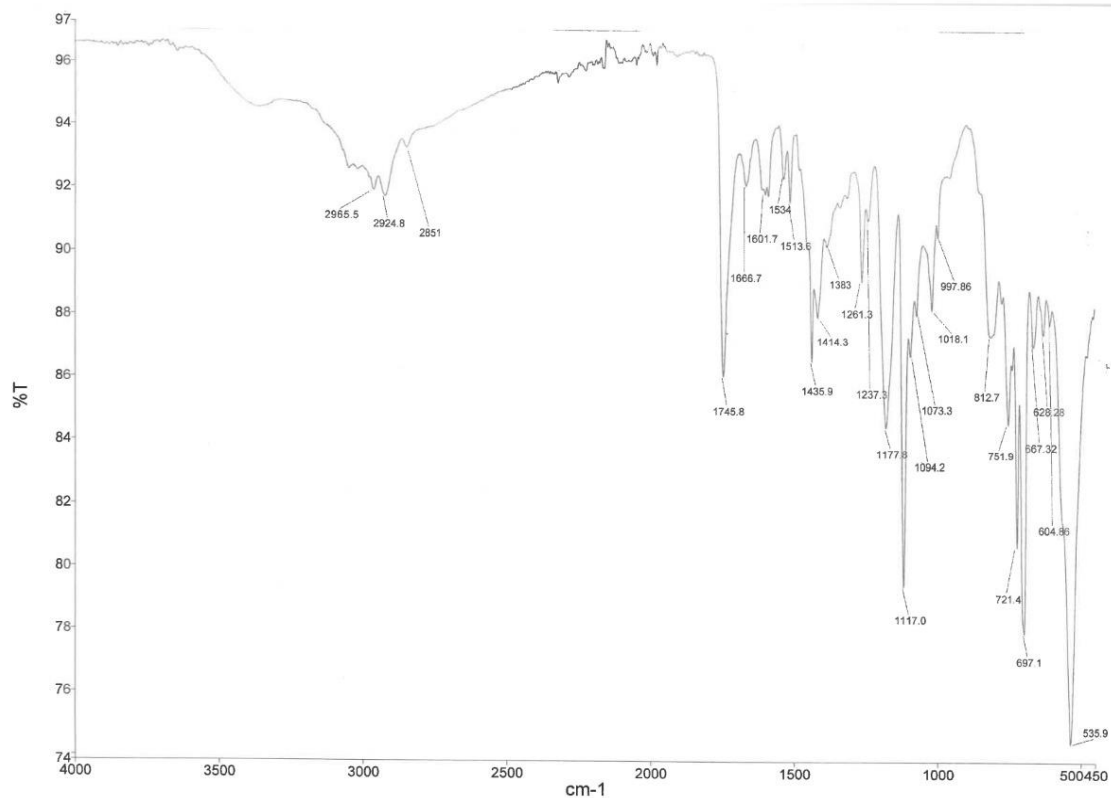
D2: FTIR of RuNP@(O)PPh₂-PEGPIIL 2.20
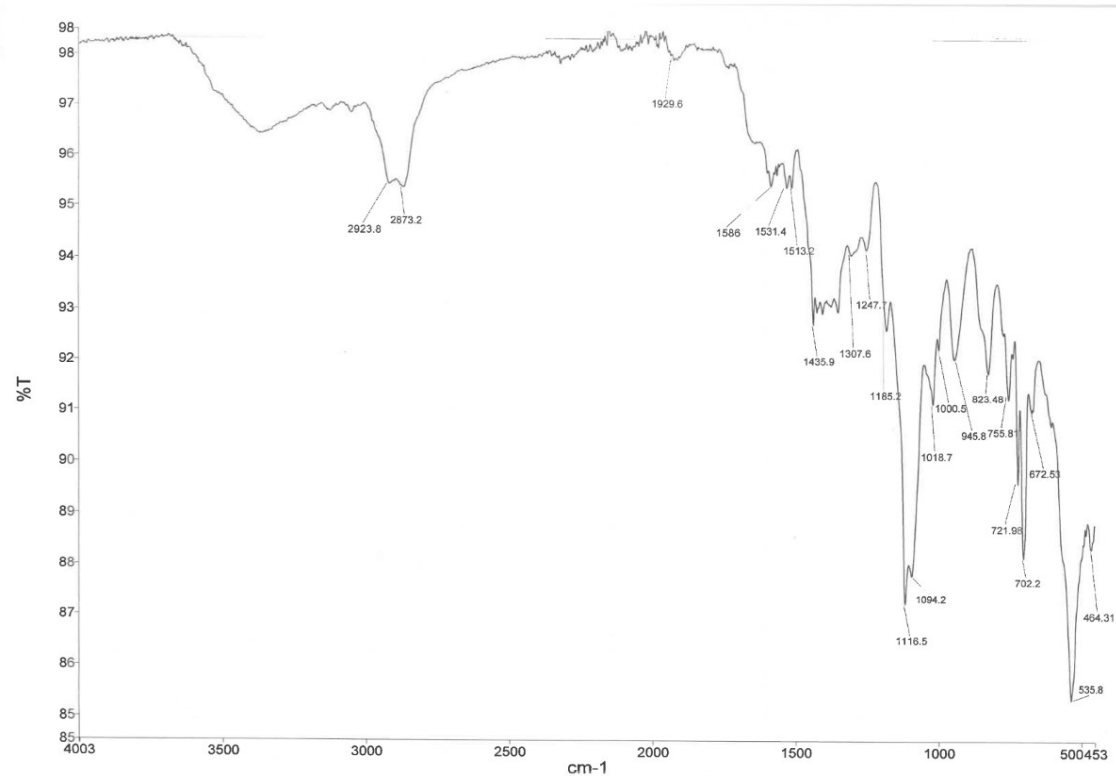
D3: FTIR of Ru(COD)(COT)@PPh$_2$-PEGPIIL **2.22**
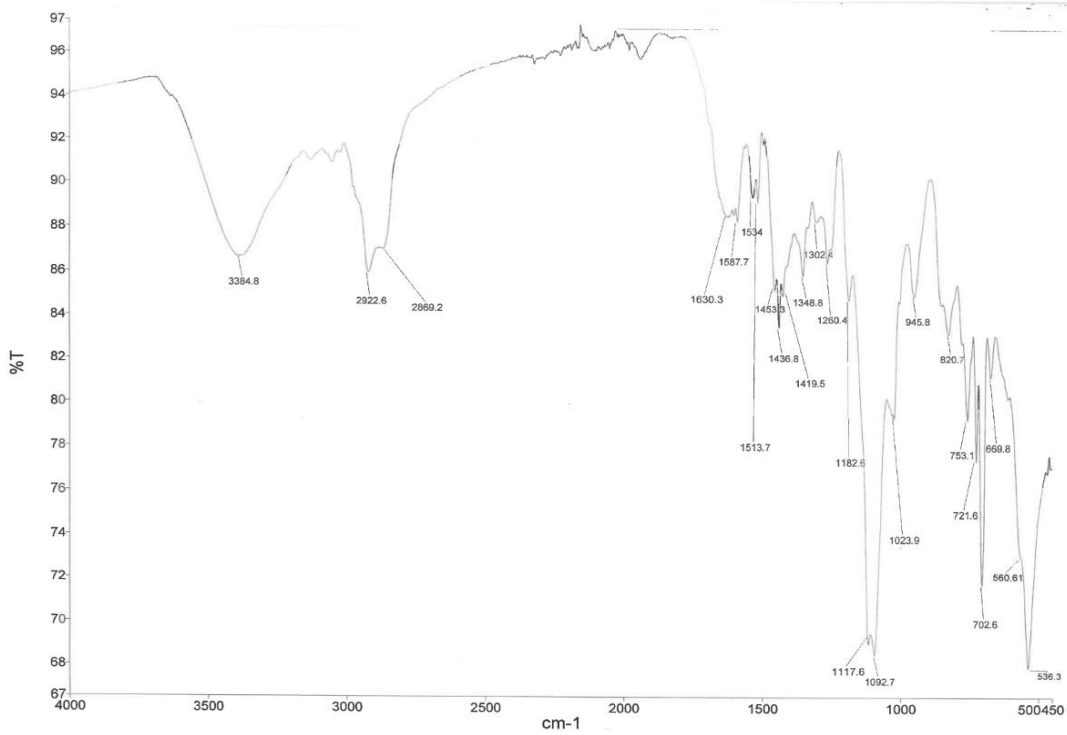
D4: FTIR of the collected organic fractions from the POM@TBA experiment
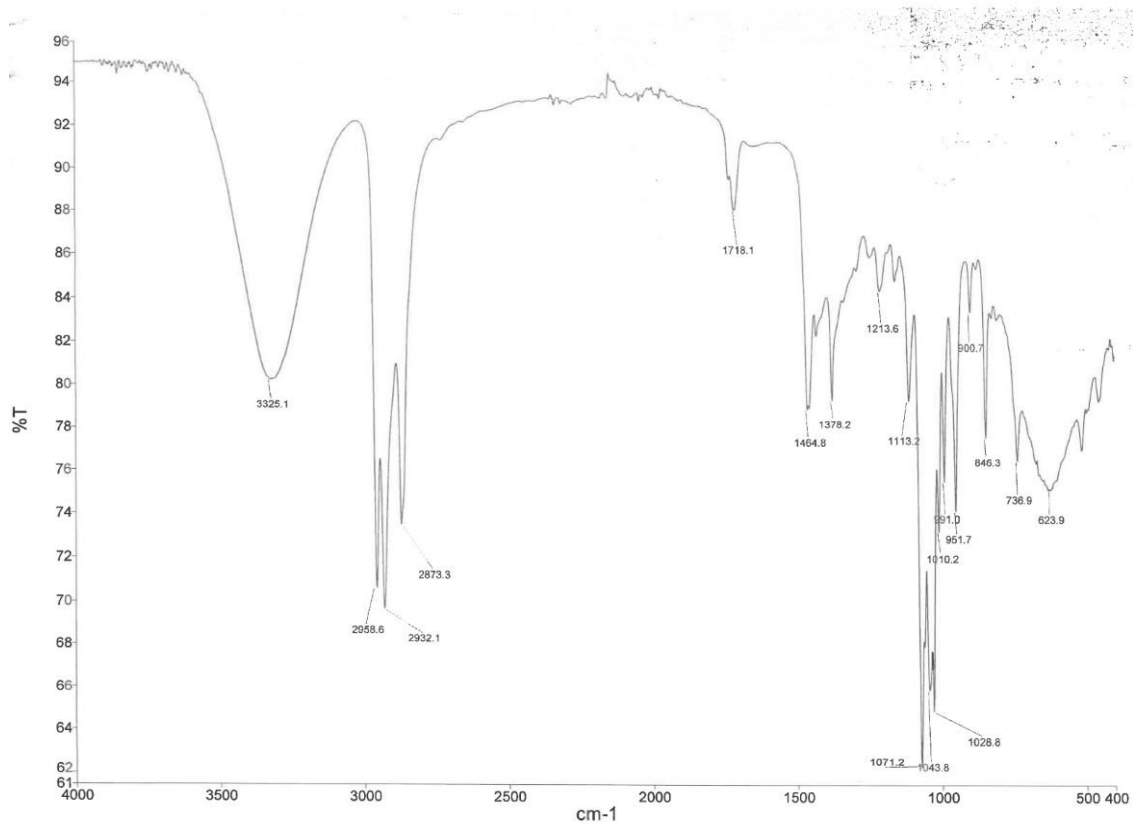
Appendix E: SEM images of RuNPs

E1: SEM images of RuNP@PPh$_2$-PEGPIIL (**2.12**)
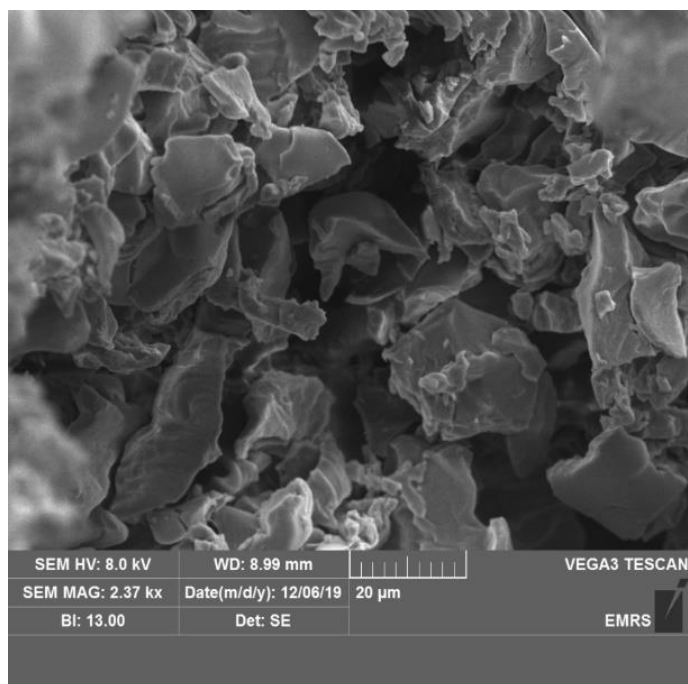
E2: SEM images of RuNP@PPh$_2$-PIIL (**2.13**)
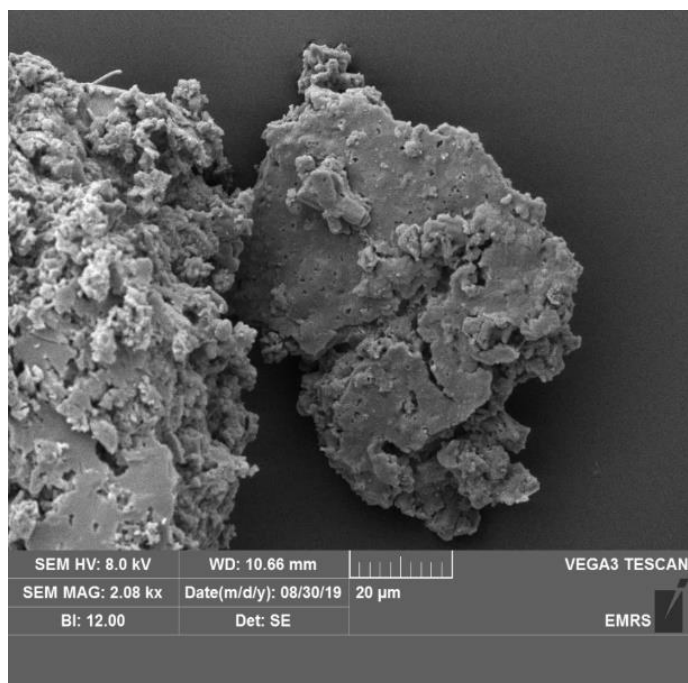
E3: SEM images of RuNP@PEGPIIL (**2.16**)
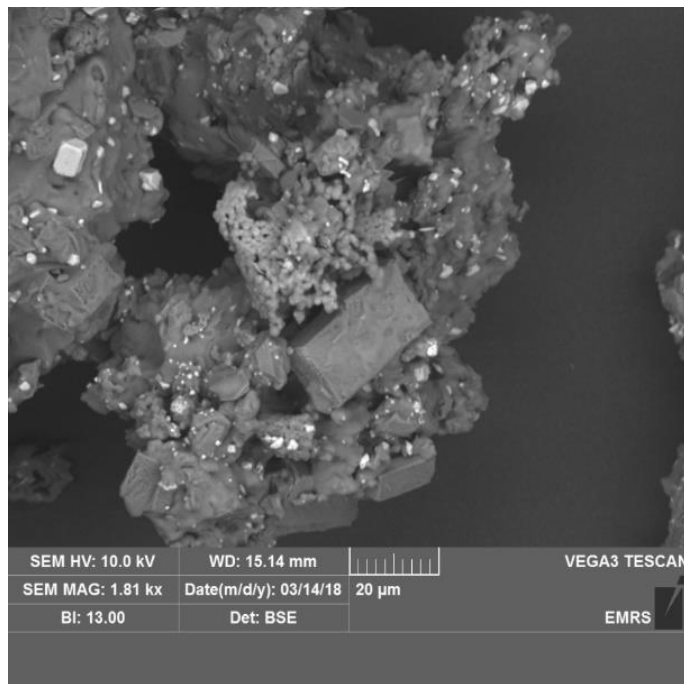
E4: SEM images of RuNP@PIIL (**2.17**)
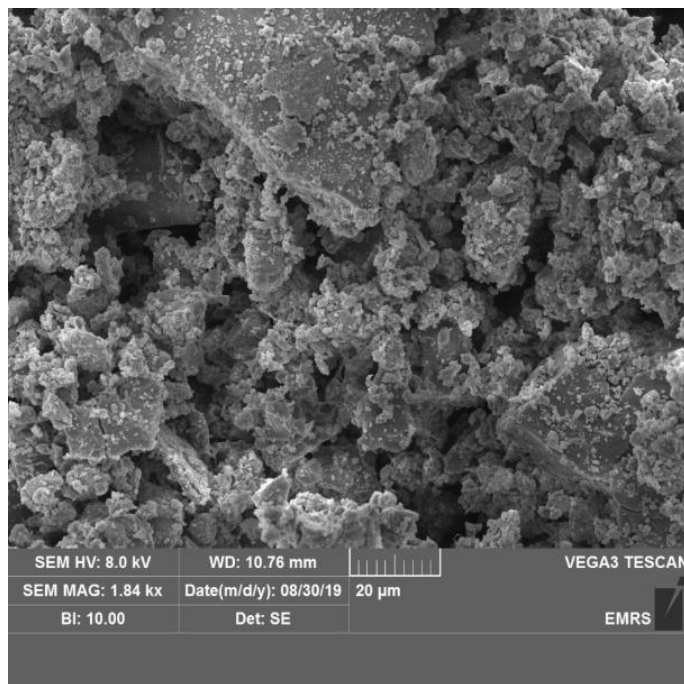
E5: SEM images of RuCODCOT@PPh$_2$-PEGPIIL (**2.22**)
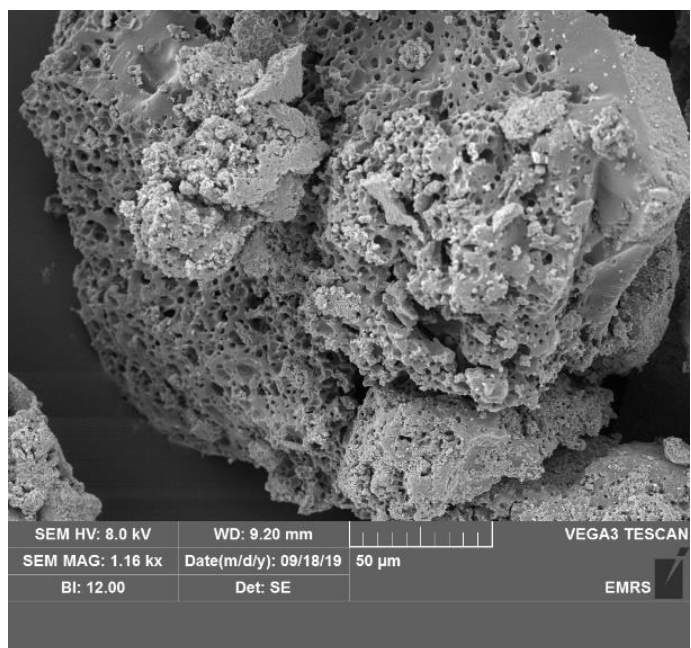
E6: SEM images of RuCODCOT@PPh$_2$-PIIL (**2.23**)
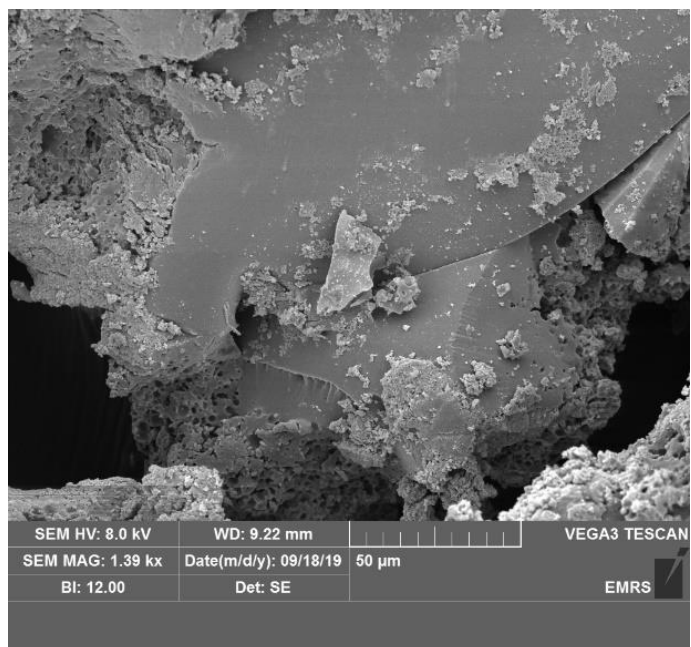
Appendix F: XPS of RuNPs

F1: XPS spectra of **2.14** and **2.20** P 2p.
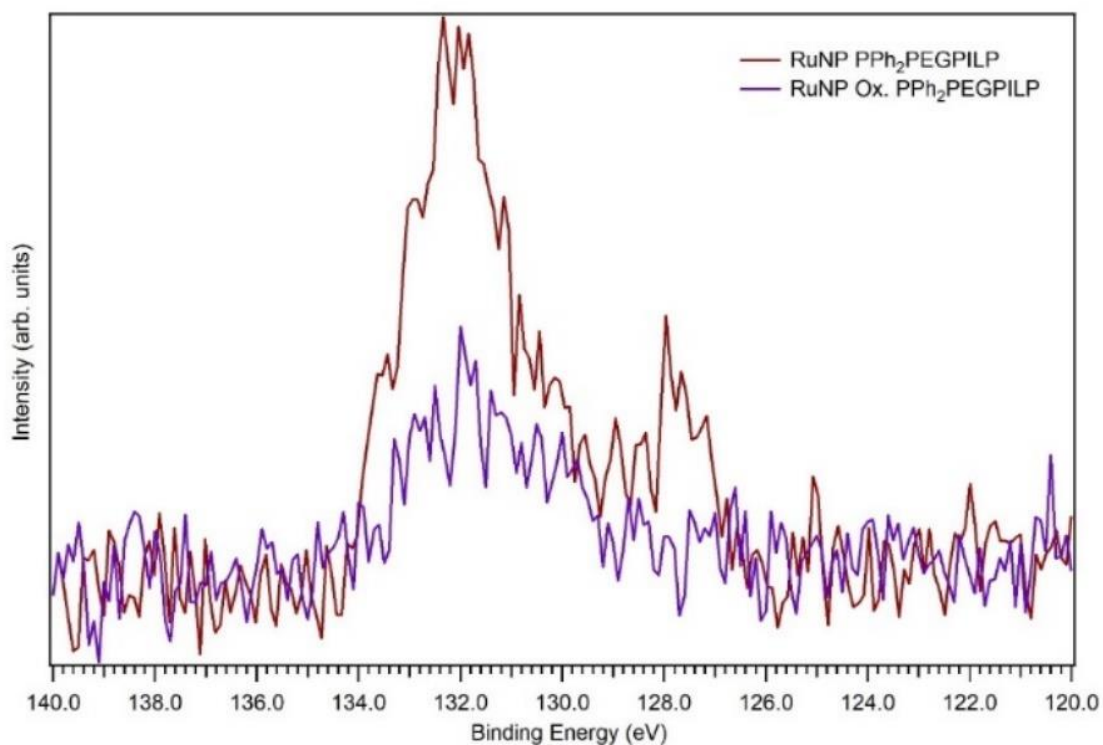
F2: XPS spectra of **2.14**, **2.16** and **2.20** O 1s.
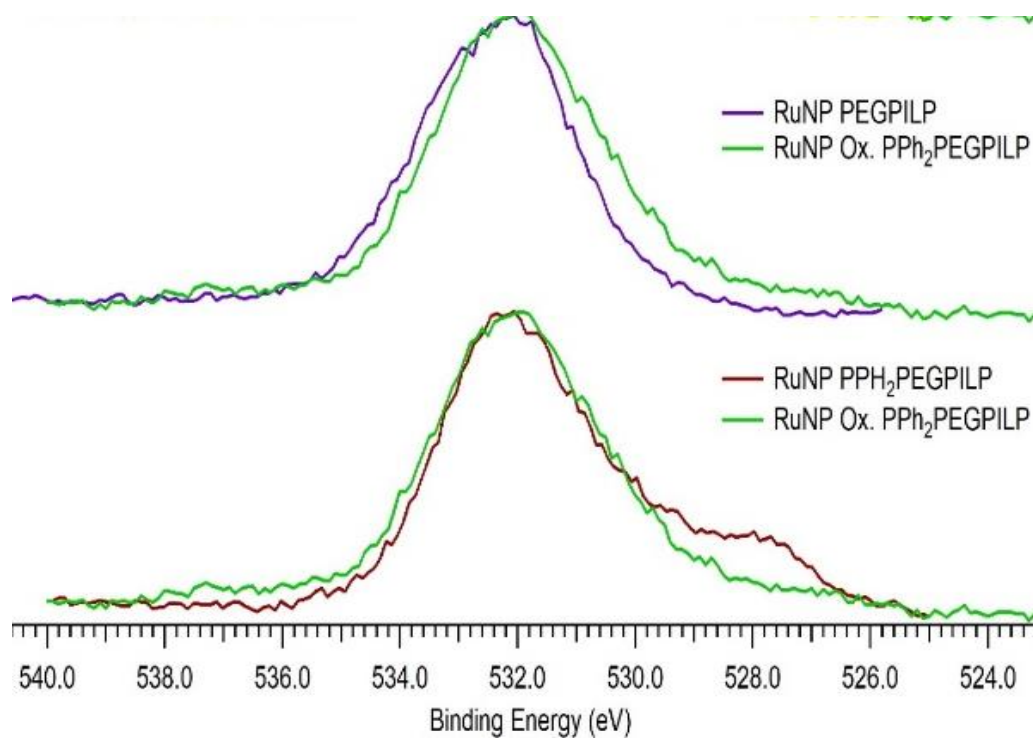
Appendix G: TEM of RuNPs

G1 TEM images (a) and the associated particle size distribution (b) of RuNPs generated by the *in-situ* reduction of RuNP@PPh$_2$-PIILP (**2.15**) with RuCl$_3$. Black and white scale bars are 25 and 1 nm, respectively.

(i)
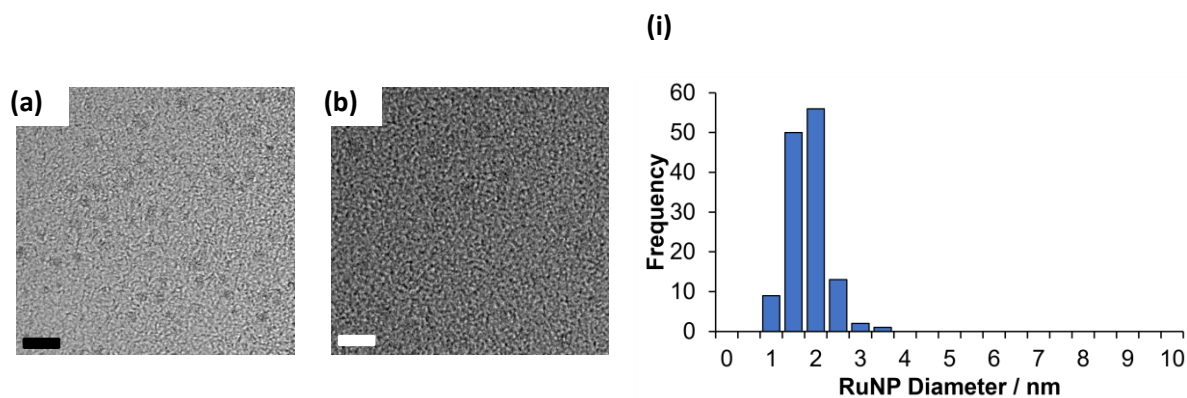
G2 TEM images (a) and the associated particle size distribution (b) of RuNPs generated by the *in-situ* reduction of RuNP@PPh$_2$-PEGPIILP (**2.14**) with RuCl$_3$. Black and white scale bars are 25 and 1 nm, respectively.

(j)
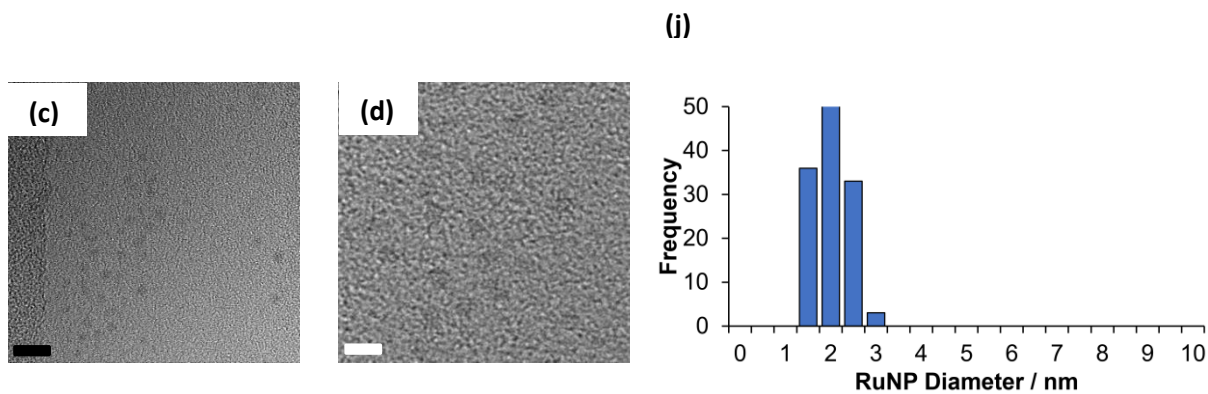
Appendix for Chapter 3

Appendix H: ¹H NMR for the substituted nitroarene reduction reaction mixtures

H1: Reduction of 1-methyl-2-nitrobenzene

Reduction of 1-methyl-2-nitrobenzene
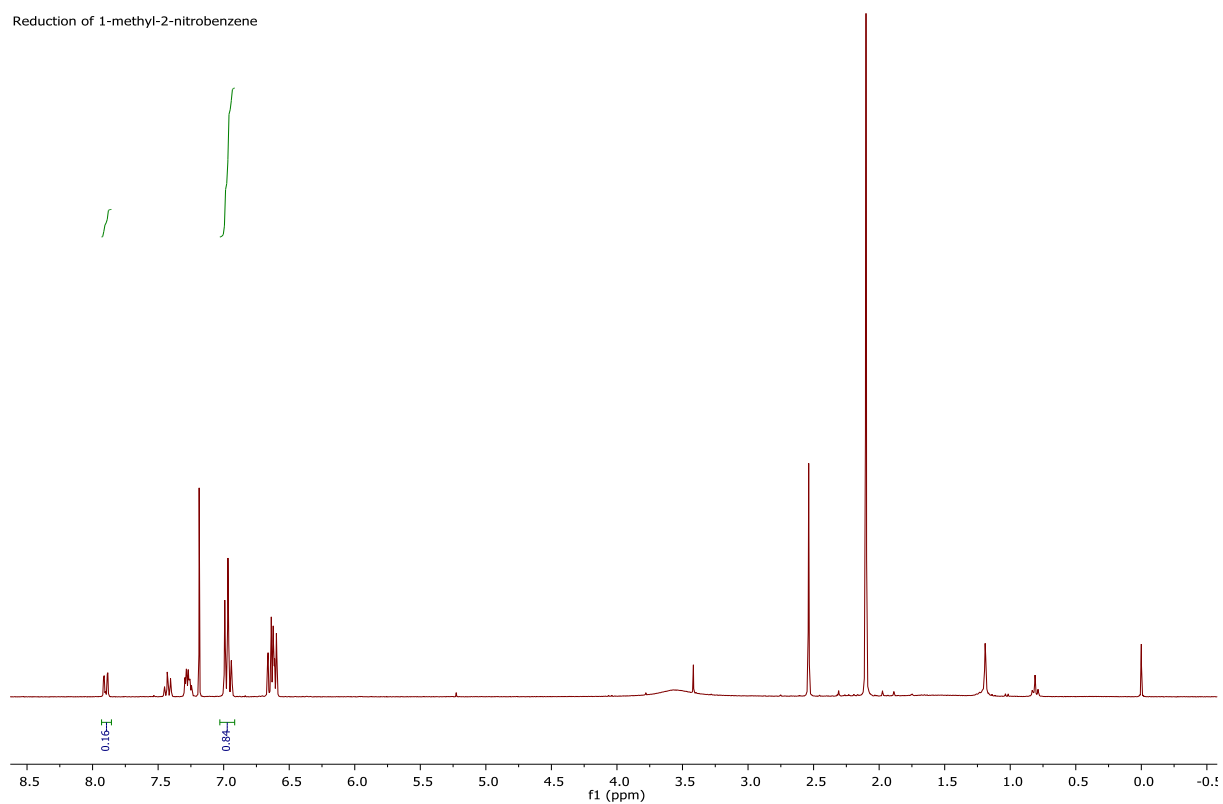
H2: Reduction of 2-nitroanisole

reduction of 2-nitroanisole
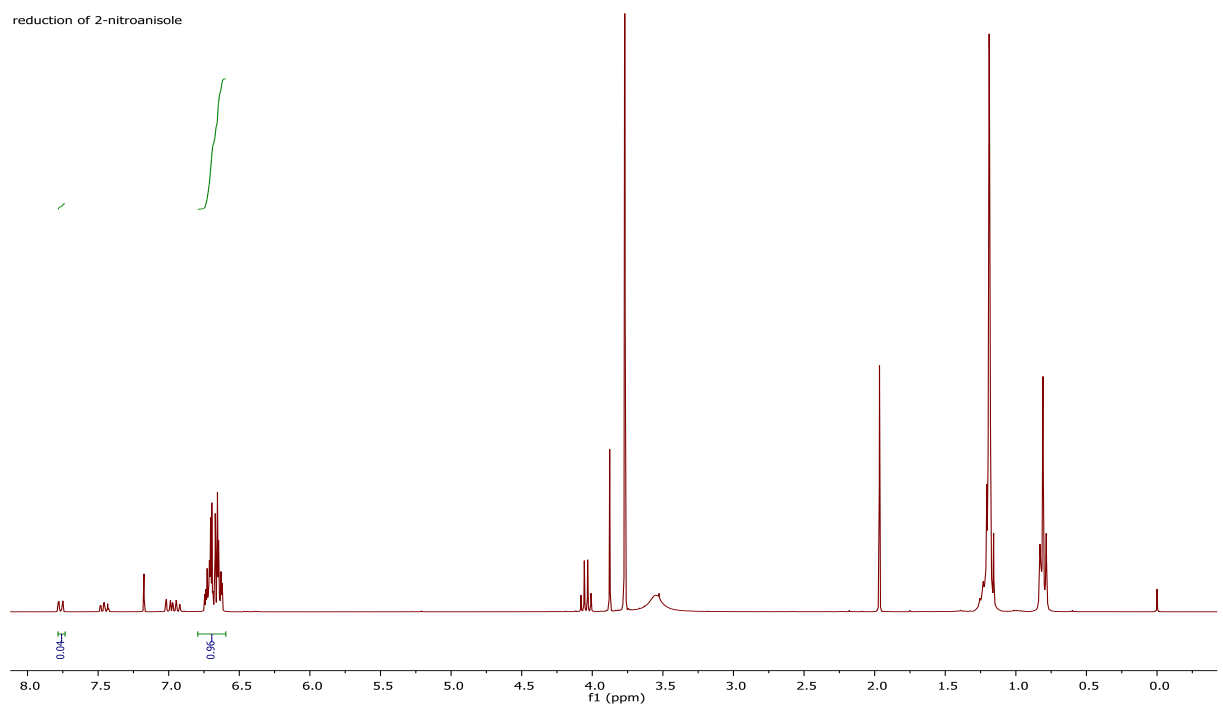
H3: Reduction of 4-nitroanisole

reduction of 4-nitroanisole
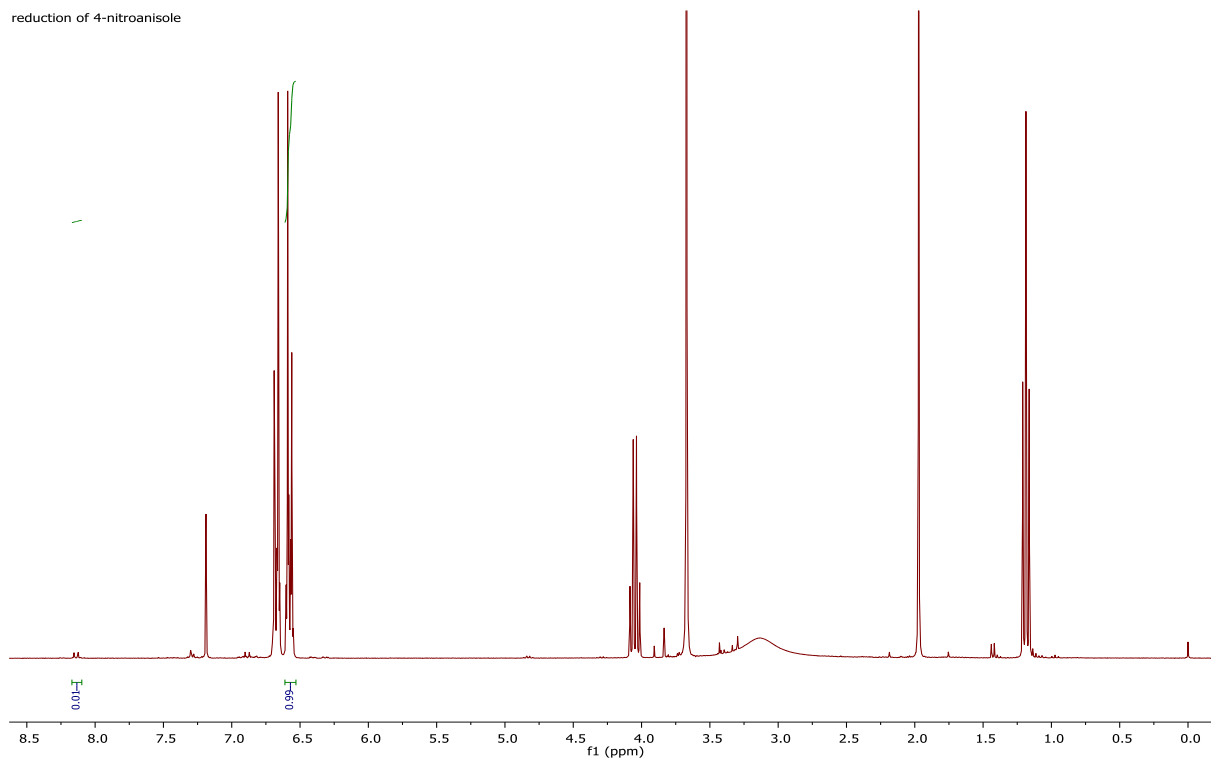
H4: Reduction of 2-bromo-nitrobenzene

reduction of 2-bromo-nitrobenzene
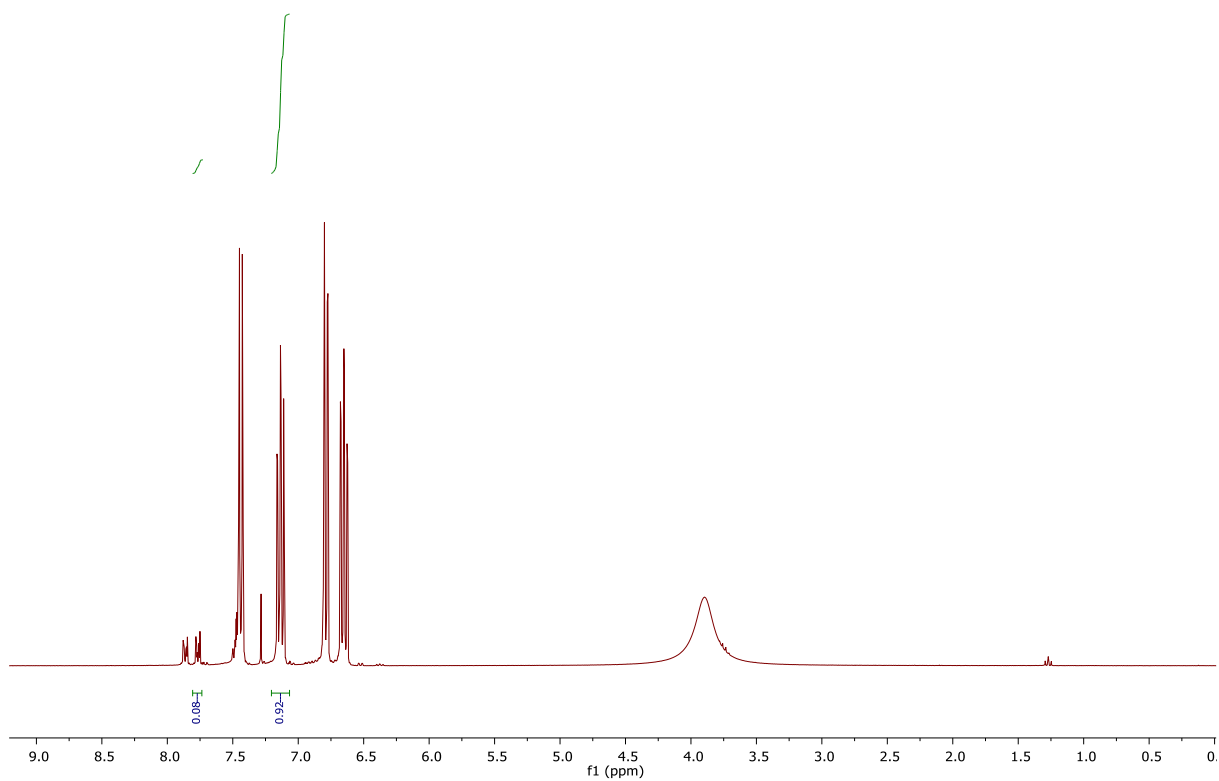
H5: Reduction of 6-nitroquinoline

Reduction oof 6-nitroquinoline
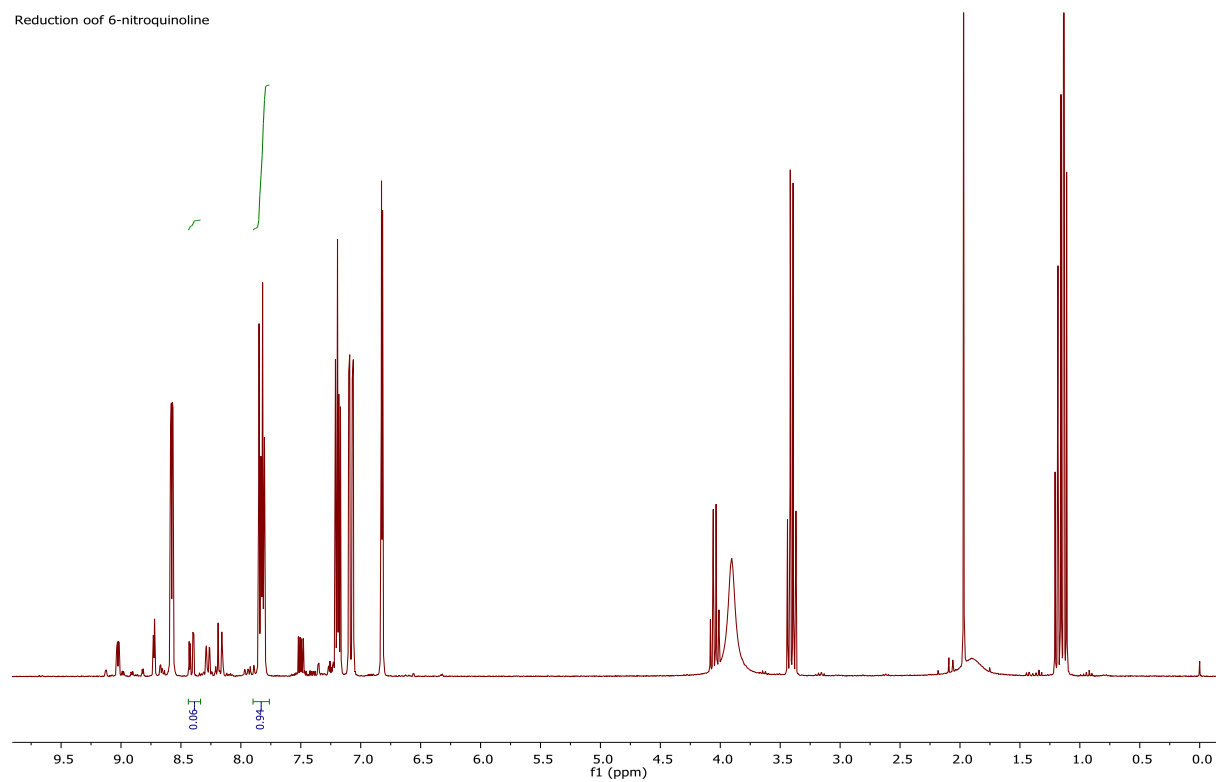
Appendix for Chapter 4

Appendix I: Properties of Amberlyst-15

	Amberlyst-15
Manufacturer	Dow Chemical Co.
Physical form	Gray coloured spherical beads
Matrix type	Styrene-DVB
Crosslinkage (%DVB)	20-25
Ionic form	H^+
Functional group	Sulfonic acid
Operating pH	0-14
Ion exchange capacity (eq $L^{-1)}$)	1.8
Particle size (mm)	0.600-0.800
Thermal stability (℃)	120
Moisture holding capacity (%)	52-57

Table 4.1: Physico-chemical properties of **Amberlyst-15** cation exchange resin used in these comparison studies.

Appendix J: NMR for the Monomers and Polymers

J1: Solution ^1H NMR and $^{13}C\{^1H\}$ spectrum of 4-(2-methyl-1-(4-vinylbenzyl)-1H-imidazol-3-ium-3-yl)butane-1-sulfonate **4.1** in D$_2$O/NaCl
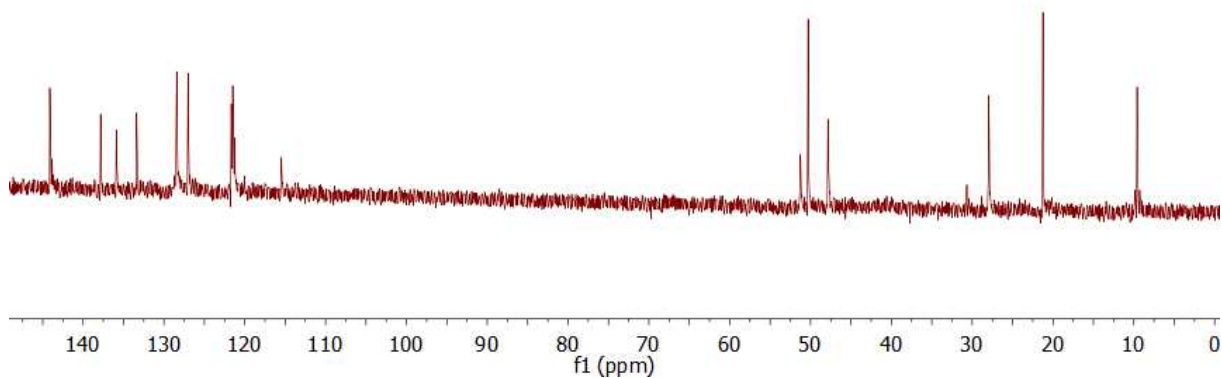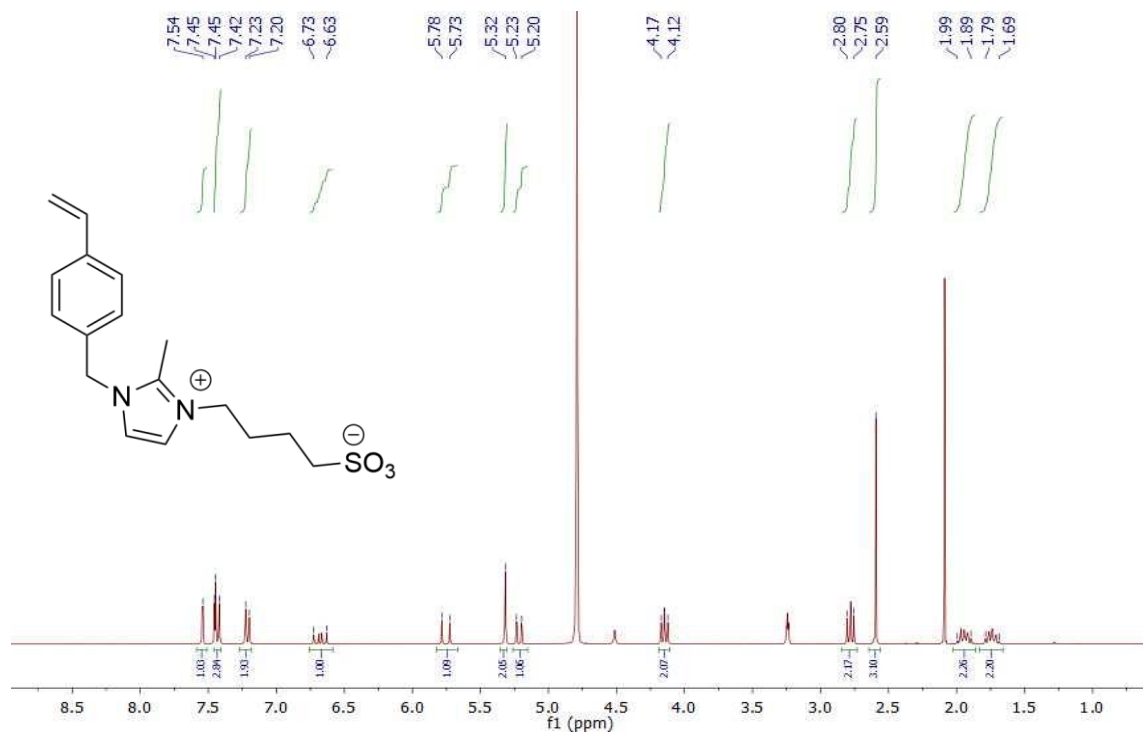
J2: Solution ^1H and $^{13}C\{^1H\}$ NMR spectrum of 4-(2-methyl-1H-imidazol-3-ium-3-yl)butane-1-sulfonate **4.2** in D_2O/NaCl
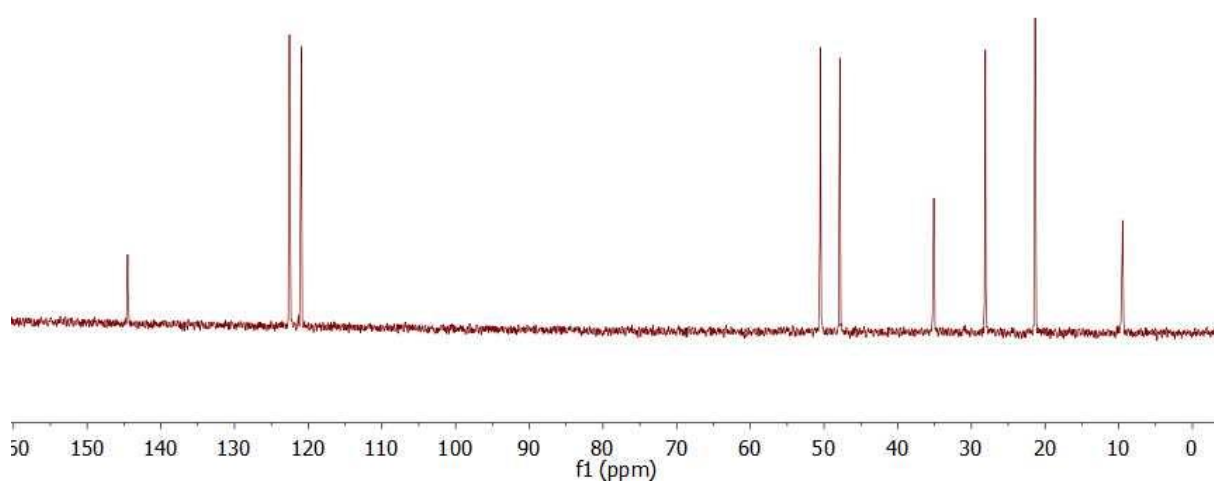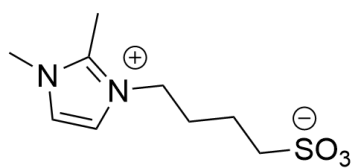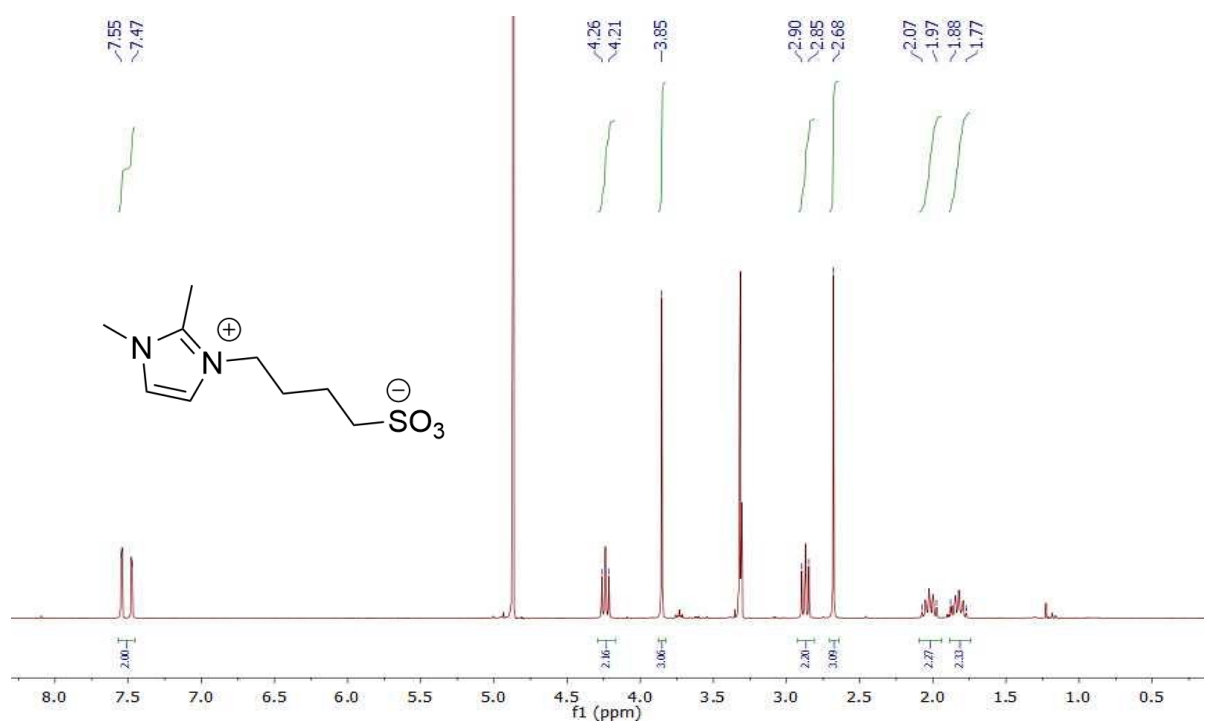
J3: Solution ^{1}H NMR spectrum of PIL **4.5** in MeOD
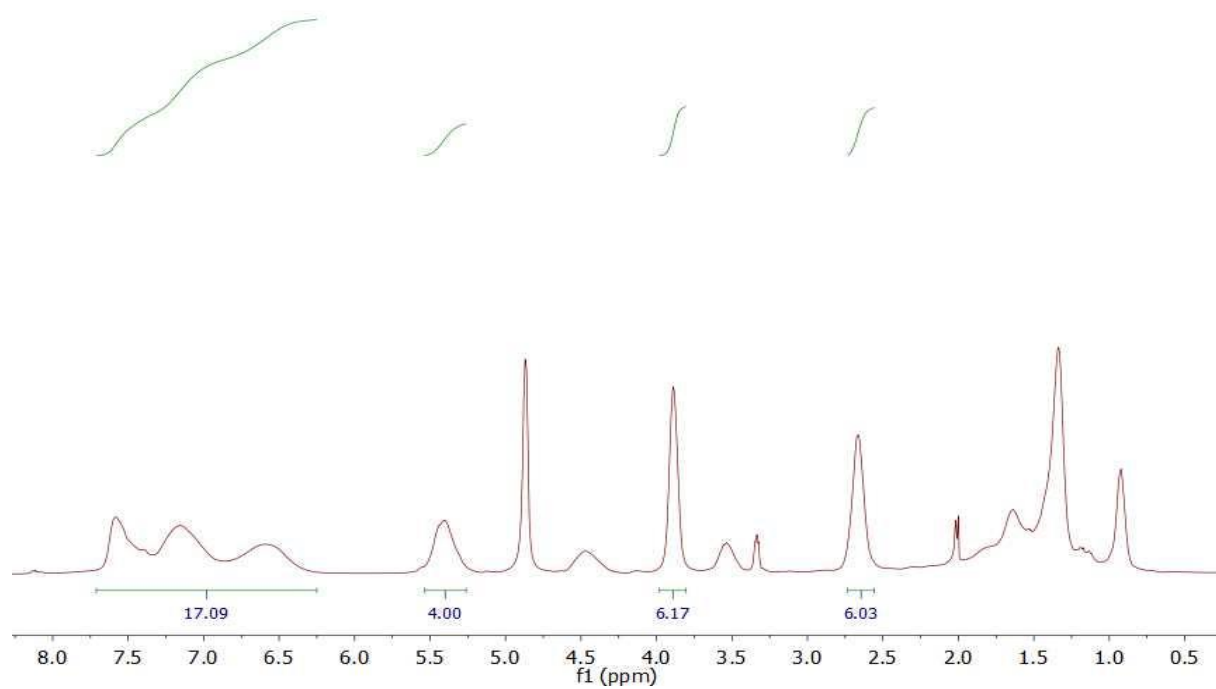
J4: Solution ^{1}H NMR spectrum of PIL **4.6** in D$_2$O/NaCl
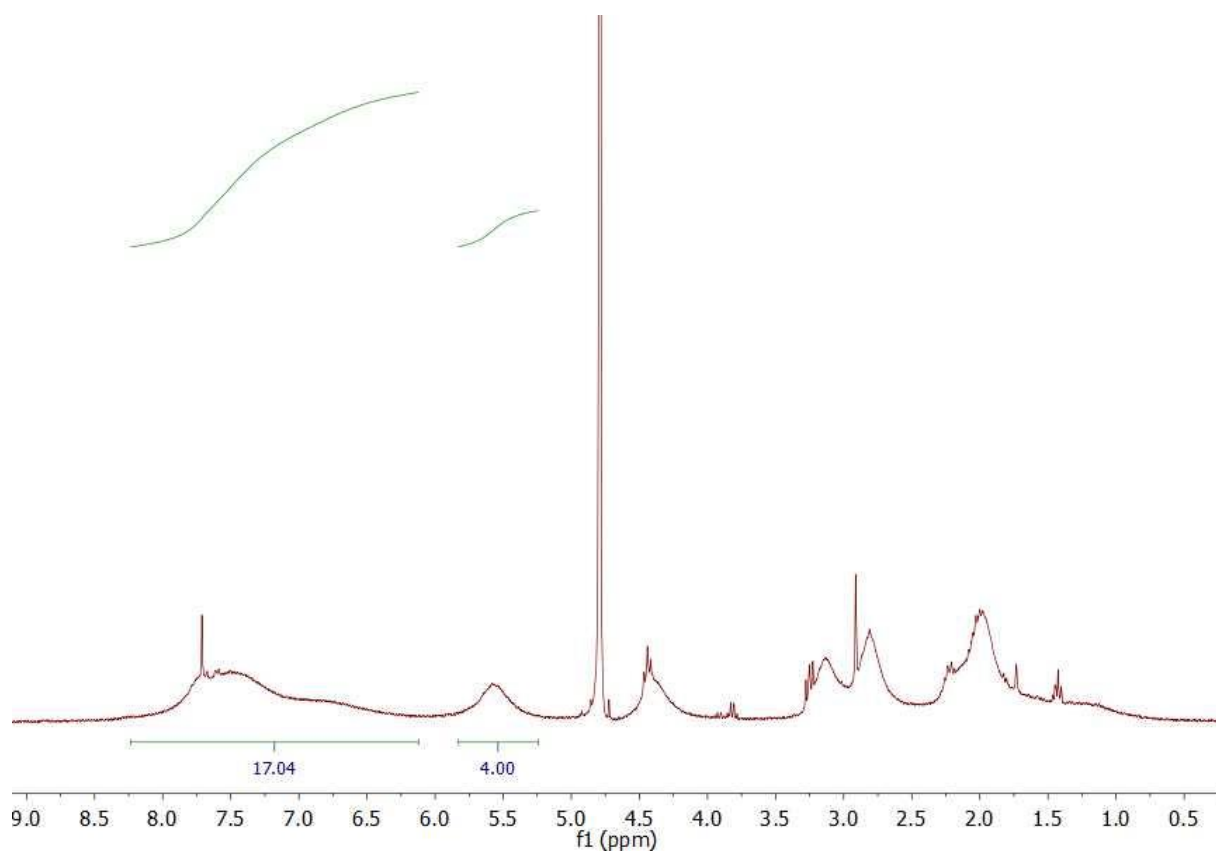
J5: Solid state ^{31}P NMR for POM@PIIL:
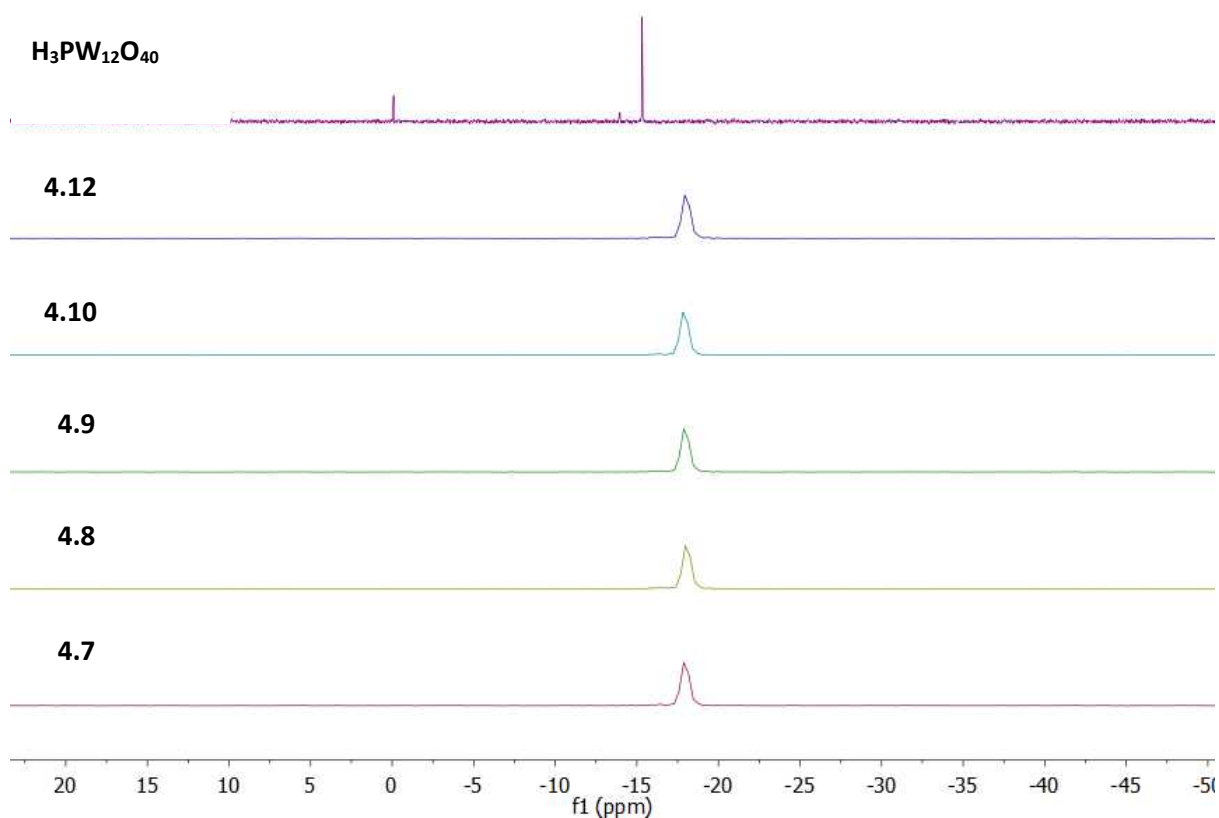
	$H_3PW_{12}O_{40}$	4.7	4.8	4.9	4.10	4.12
δ / ppm	-15.37	-17.94	-18.04	-17.94	-17.89	-18.00

Appendix K: TGA of polymers and PIIL materials.

K1: TGA of Polymer **4.3**:
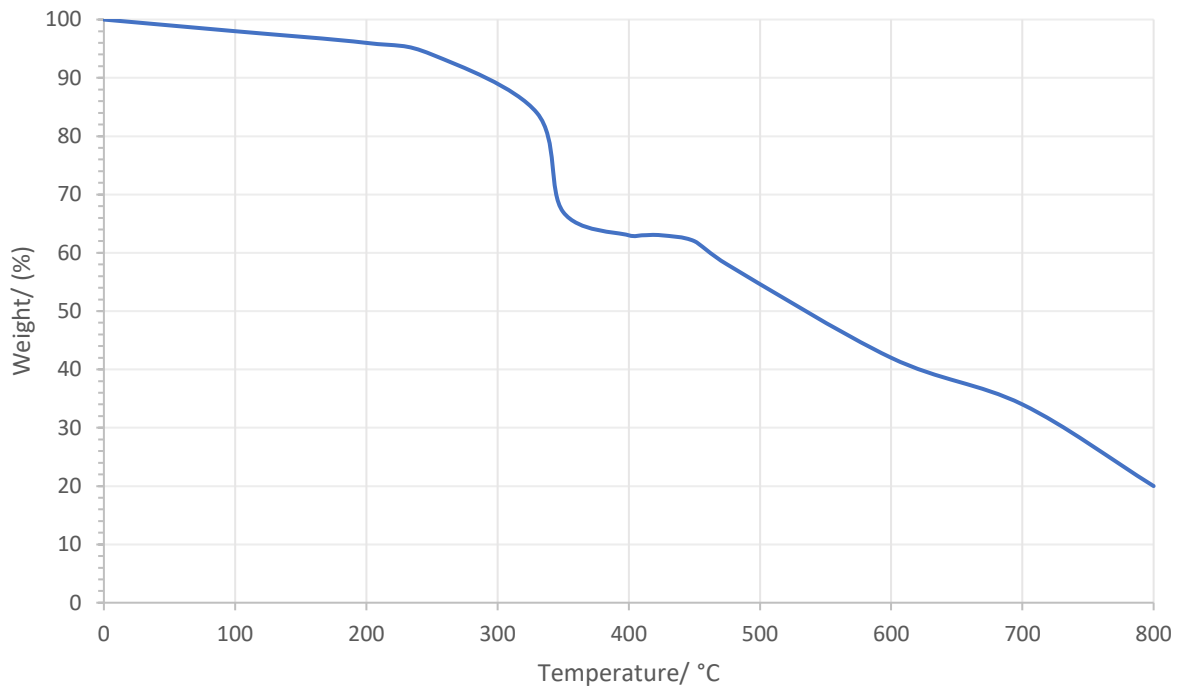
K2: TGA of Polymer **4.4**:
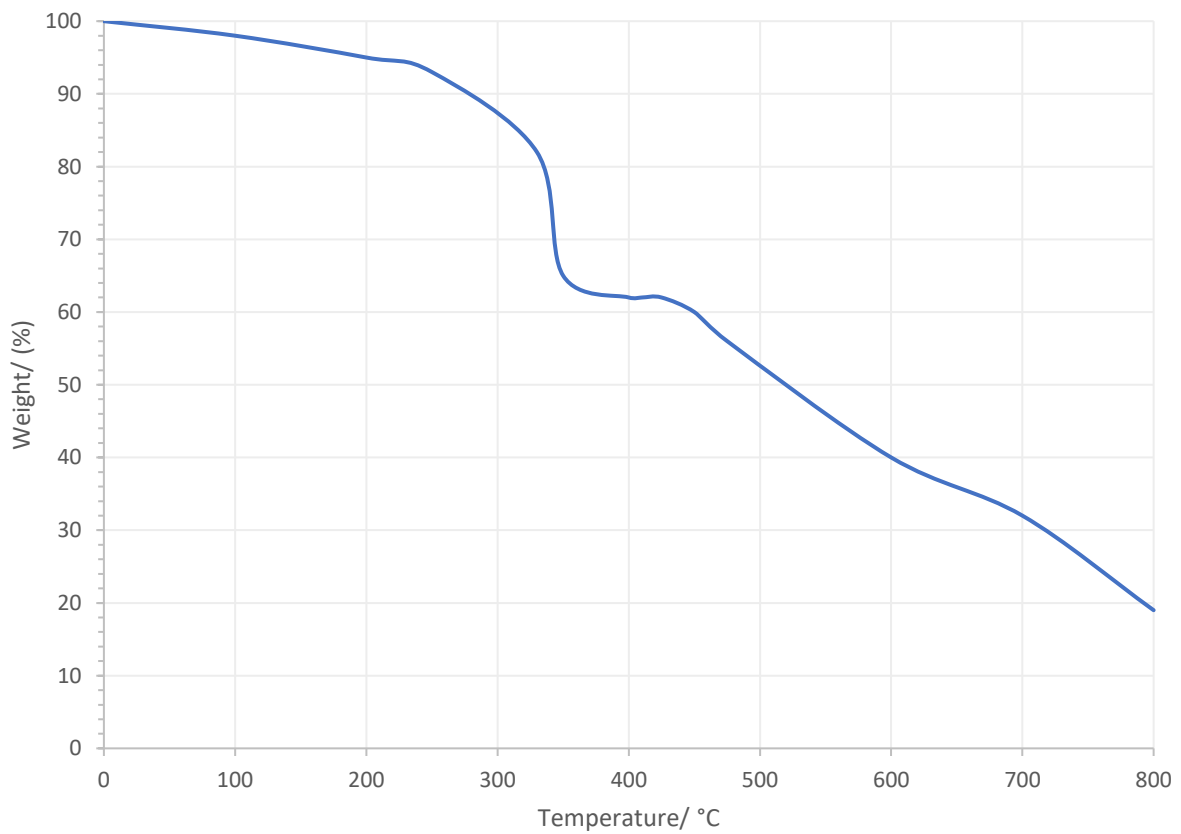
K3: TGA of Polymer **4.5**:
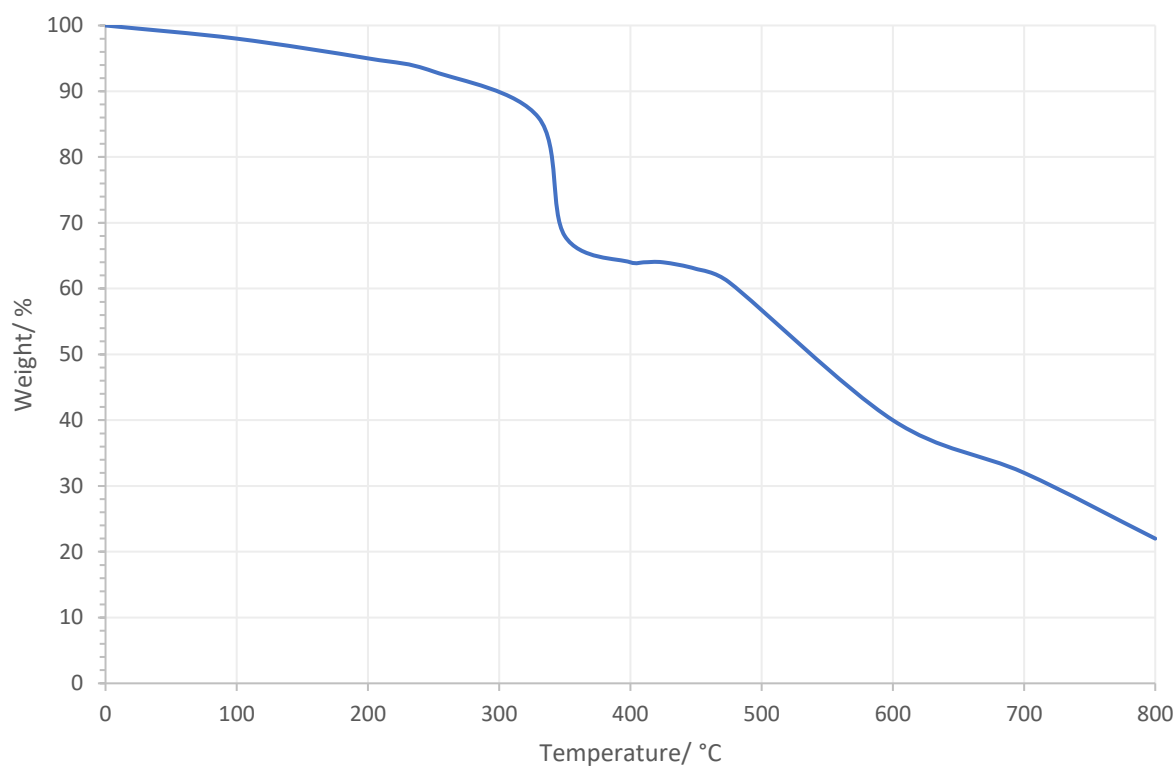
K4: TGA of POM@PIIL **4.7**:
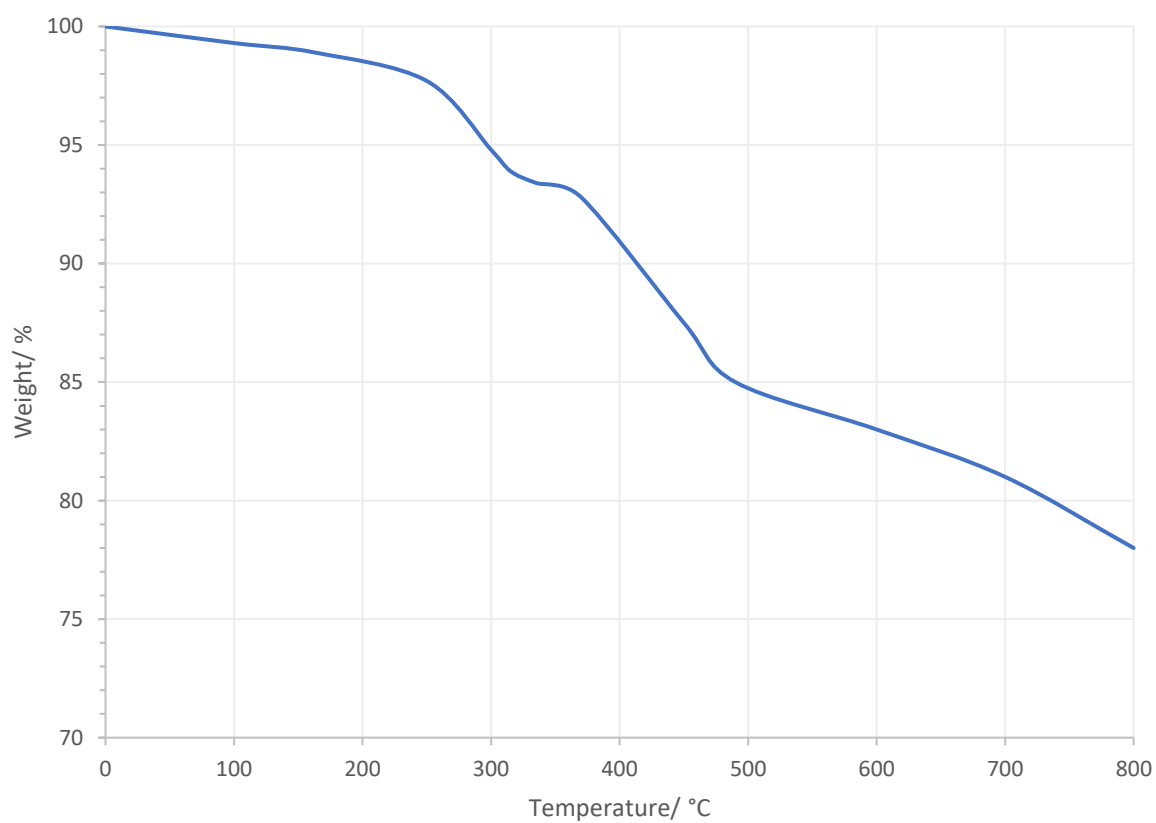
K5: TGA of POM@PIIL **4.8**:
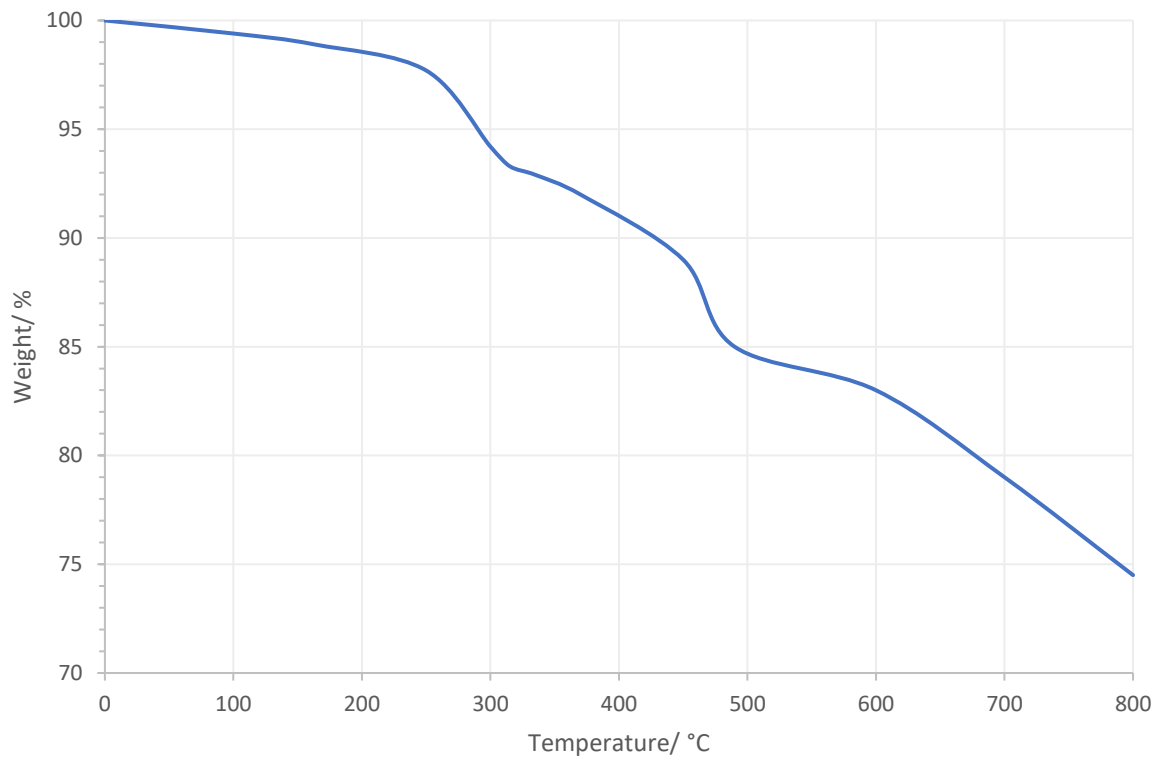
K6: TGA of POM@PIIL **4.9**:
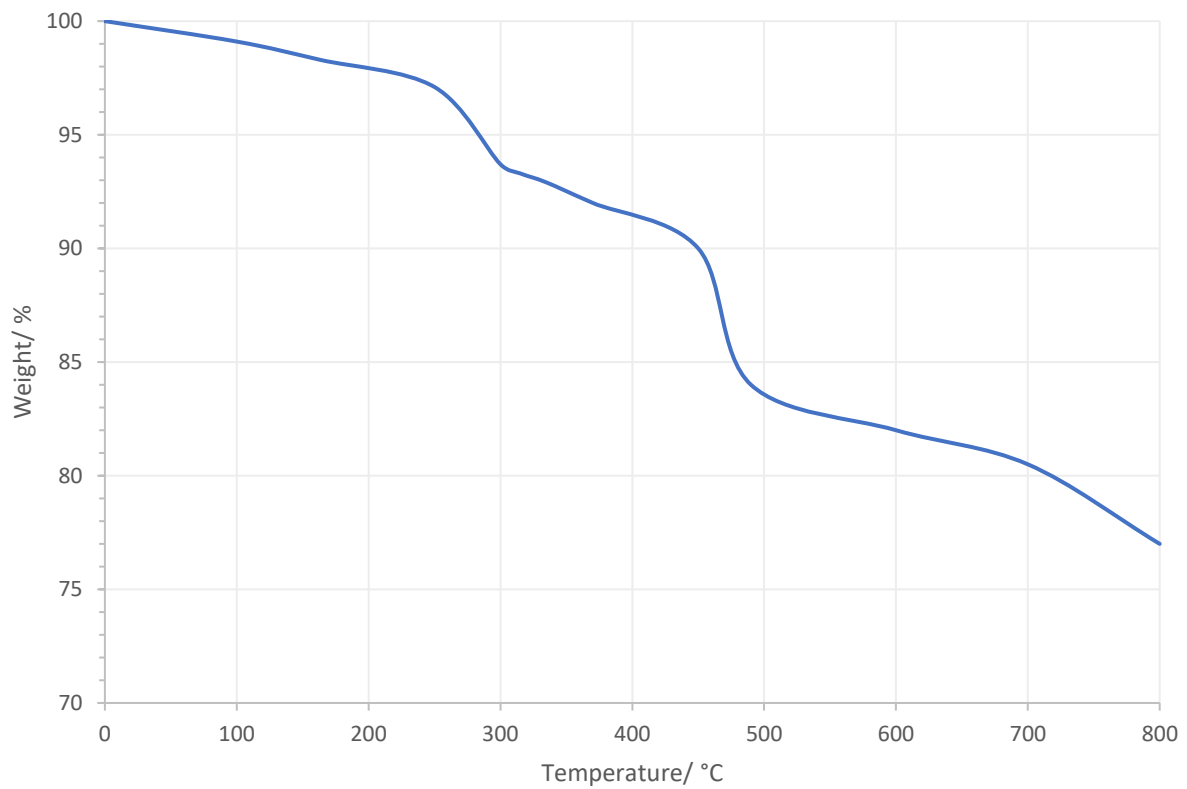
K7: TGA of HSO$_4$@PIIL **4.13**:
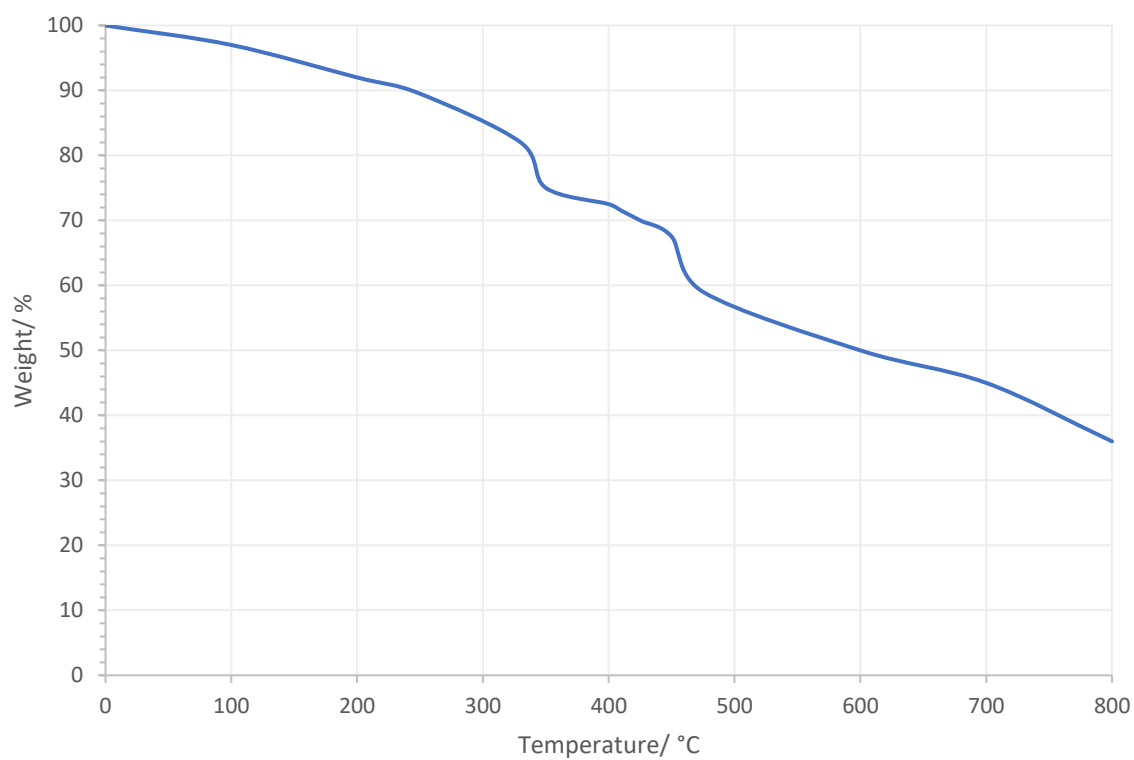
K8: TGA of HSO$_4$@PIIL **4.14**:
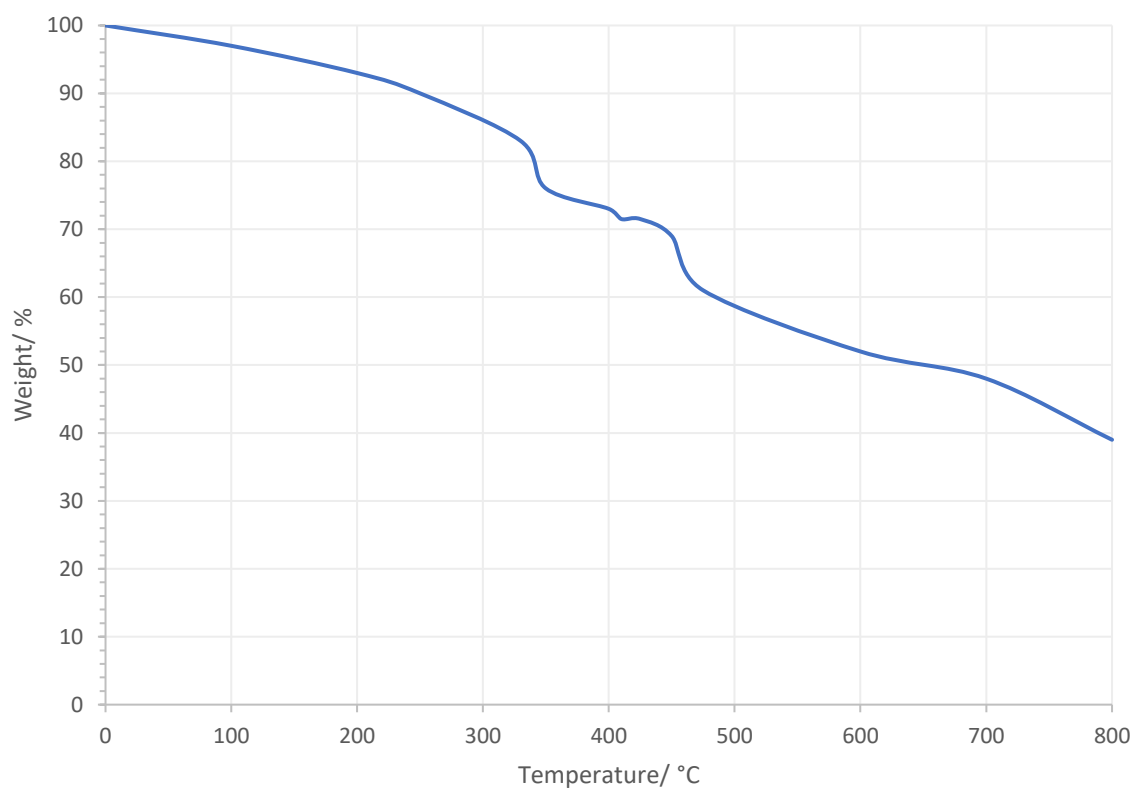
Appendix L. Determination of the POM loading for the POM@PIIL materials from CHN analysis.

L1: CHN analysis of POM@PIIL **4.7**:

CHN Anal. Calc. for:

- Polymer, $C_{16}H_{23}N_2Cl$ (278.82 g/mol): C, 68.9 ;H, 8.25 ; N, 10.0 %
- POM@PIILP, $C_{16}H_{25}N_2 \bullet [H_2PW12O40]^-$ (3137.2 g/mol): C, 5.35 ; H, 0.00697 ; N, 0.0781

Found:

- Polymer, $C_{16}H_{23}N_2Cl$ (278.82 g/mol): C, 65.12 ;H, 7.83 ; N, 11.92 %
- POM@PIILP, $C_{16}H_{25}N_2 \bullet [H_2PW_{12}O_{40}]^-$ (3137.2 g/mol): C, 13.22 ; H, 1.49; N, 1.84

Therefore: 1 g of polymer contains $0.1192/14.0 = 8.51 \times 10^{-3}$ moles N

1 g POM@PIILP = $0.0184/14 = 1.31 \times 10^{-3}$ moles N

$\frac{moles\ of\ N\ on\ 1\ g\ polymer}{moles\ of\ N\ on\ 1g\ POM@PIILP}$ = 8.51×10^{-3} / 1.31×10^{-3} = 6.50

6.50 g of POM@PIILP contains 8.51×10^{-3} moles of N (see above) = 1 g polymer

Therefore 6.5 g of polymer (6.5-1g) of PIILP contain POM only

5.5 g extra mass is from POM = ((2811 g/mol)) = 2881 g/mol

5.5 g/ 2881 $gmol^{-1}$ = 1.91×10^{-3} moles of POM = 1.91×10^{-3} mol x 2881 $gmol^{-1}$ (=MW of POM) = 5.5 g POM on 6.5 g PIILP

Therefore 1 g PIILP contains, 1 / 6.5 g x 5.5 g = 0.846 g POM = 2.94×10^{-4} moles POM

$\frac{moles\ of\ N\ on\ 1g\ of\ POM@PIILP}{2}$ = 1.31×10^{-3} moles of N/2 = 6.55×10^{-4} moles of SO_3H

$\frac{moles\ of\ SO3H}{moles\ of\ POM}$ = $\frac{0.000655}{0.000294}$ = 2.23 therefore 1:2.23 of POM to SO_3H polymer

---

L2: CHN analysis POM@PIIL **4.8**:

CHN Anal. Calc. for:

- Polymer, $C_{18}H_{28}N_2O_3S$ (334.43 g/mol): C, 64.6 ;H, 8.37 ; N, 8.37 %
- POM@PIIL $C_{18}H_{29}N_2O_3S \cdot H_2PW_{12}O_{40}$ (3245.51 g/mol): C, 5.55; H, 0.745; N, 0.72.

Found:

- Polymer, $C_{43}H_{60}N_4O_6S_2$ (334.43 g/mol): C, 58.5 ;H, 7.21 ; N, 8.13 %
- POM@PIIL $C_{18}H_{29}N_2O_3S \cdot H_2PW_{12}O_{40}$ (3245.51 g/mol): C, 15.62; H, 2.02; N, 2.15.

Therefore: 1 g of polymer contains 0.0813/14.0 = 5.81 x 10^{-3} moles N

1 g POM@PIIL = 0.0215/ 14 = 1.54 x 10^{-3} moles N

$\frac{moles\ of\ N\ on\ 1\ g\ polymer}{moles\ of\ N\ on\ 1g\ POM@PIIL}$ = 5.81 x 10^{-3} / 1.54 x 10^{-3} = 3.773

3.773 g of POM@PIIL contains 5.18 x 10^{-3} moles of N (see above) = 1 g polymer

Therefore 2.773 g of polymer (3.773-1g) of PIIL contain POM only

2.773 g extra mass is from POM = ((2881 gmol^{-1})) = 2881 gmol^{-1}

2.773 g/ 2881 gmol^{-1} = 0.96 x10^{-3} moles of POM = 0.96 x 10^{-3} mol x 2881 gmol^{-1} (=MW of POM) = 2.773 g POM on 3.773 g PIIL

Therefore 1 g PIIL contains, 1 / 3.773 g x 2.905 g = 0.735 g POM = 2.55 x 10^{-4} moles $[PW_{12}O_{40}]^{3-}$

$\frac{moles\ of\ N\ on\ 1g\ of\ POM@PIIL}{2}$ = 1.54 x 10^{-3} moles of N/2 = 7.7 x 10^{-4} moles of SO$_3$H

$\frac{moles\ of\ SO3H}{moles\ of\ POM}$ = $\frac{0.000770}{0.000255}$ = 2.75 therefore 1:2.75 of POM to SO$_3$H polymer

L3: CHN analysis of POM@PIIL **4.9**:

CHN Anal. Calc. for:

- Polymer, $C_{34}H_{42}N_4Cl_2$ (576 g/mol): C, 70.8 ; H, 7.29 ; N, 9.72 %
- POM@PIIL, $C_{34}H_{42}N_4 \cdot 2[HPW_{12}O_{40}]^-$ (6336 g/mol): C, 5.63 ; H, 0.00607 ; N, 0.00774

Found:

- Polymer, $C_{34}H_{42}N_4Cl_2$ (576 g/mol): C, 68.15 ; H, 8.45; N, 9.89 %
- POM@PILL, $C_{34}H_{42}N_4 \cdot 2[HPW_{12}O_{40}]^-$ (6336 g/mol): C, 12.1 ; H, 1.43 ; N, 2.19

Therefore: 1 g of polymer contains $0.0989/14.0 = 7.06 \times 10^{-3}$ moles N

1 g POM@PIIL $= 0.0219/14 = 1.56 \times 10^{-3}$ moles N

$$\frac{moles\ of\ N\ on\ 1\ g\ polymer}{moles\ of\ N\ on\ 1g\ POM@PIIL} = 7.06 \times 10^{-3} / 1.56 \times 10^{-3} = 4.526$$

4.526 g of POM@PIIL contains 7.06×10^{-3} moles of N (see above) = 1 g polymer

Therefore 3.526 g of polymer (4.526-1g) of PIIL contain POM only

3.526 g extra mass is from POM $= ((2811\ gmol^{-1})) = 2881\ gmol^{-1}$

3.526 g/ 2881 $gmol^{-1} = 1.22 \times 10^{-3}$ moles of POM $= 1.22 \times 10^{-3}$ mol x 2881 $gmol^{-1}$ (=MW of POM) = 3.526 g POM on 4.526 g PIIL

Therefore 1 g PIIL contains, 1 / 4.526 g x 3.526 g = 0.779 g POM $= 2.70 \times 10^{-4}$ moles POM

$$\frac{moles\ of\ N\ on\ 1g\ of\ POM@PIIL}{2} = 1.56 \times 10^{-3}\ \text{moles of N/2} = 0.78 \times 10^{-3}\ \text{moles of }SO_3H$$

$$\frac{moles\ of\ SO3H}{moles\ of\ POM} = \frac{0.00270}{0.00078} = 3.46\ \text{therefore 1:3.46 of POM to }SO_3H\ \text{polymer}$$

L4: CHN analysis of POM@PIIL **4.11**:

CHN Anal. Calc. for:

- Polymer, $C_{43}H_{60}N_4O_6S_2$ (792 g/mol): C, 64.6 ;H, 8.37 ; N, 8.37 %
- POM@PIIL, $C_{43}H_{66}N_4O_{86}S_2Si_2W_{24}$ (6552.34 g/mol): C, 6.45; H, 0.826; N, 0.70.

Found:

- Polymer, $C_{43}H_{60}N_4O_6S_2$ (792 g/mol): C, 59.6 ;H, 6.35 ; N, 6.95 %
- POM@PIIL, $C_{43}H_{66}N_4O_{86}S_2Si_2W_{24}$ (6552.34 g/mol): C, 10.05; H, 1.48; N, 0.90.

Therefore: 1 g of polymer contains $0.0695/14.0 = 4.96 \times 10^{-3}$ moles N

1 g POM@PIIL $= 0.0090/14 = 6.42 \times 10^{-4}$ moles N

$\dfrac{moles\ of\ N\ on\ 1\ g\ polymer}{moles\ of\ N\ on\ 1g\ POM@PIIL} = 4.96 \times 10^{-3} / 6.42 \times 10^{-4} = 7.73$

7.73 g of POM@PIIL contains 4.96×10^{-3} moles of N (see above) = 1 g polymer

Therefore 6.73 g of polymer (7.73-1g) of PIIL contain POM only

6.73 g extra mass is from POM = $((2881\ gmol^{-1})) = 2881\ gmol^{-1}$

6.73 g/ 2881 $gmol^{-1} = 2.34 \times 10^{-3}$ moles of POM = 2.34×10^{-3} mol x 2881 $gmol^{-1}$ (=MW of POM) = 6.73 g POM on 7.73 g PIIL

Therefore 1 g PIIL contains, 1 / 7.73 g x 6.73 g = 0.871 g POM = 3.02×10^{-4} moles $[SiW_{12}O_{40}]^{4-}$

$\dfrac{moles\ of\ N\ on\ 1g\ of\ POM@PIIL}{2} = 6.42 \times 10^{-4}$ moles of N/2 = 3.21×10^{-4} moles of SO_3H

$\dfrac{moles\ of\ SO3H}{moles\ of\ POM} = \dfrac{0.000321}{0.000302} = 1.06$ therefore 1:1.06 of POM to SO_3H polymer

L5: CHN analysis of HSO$_4$@PIIL **4.13**:

CHN Anal. Calc. for:

- Polymer, C$_{18}$H$_{28}$N$_2$O$_3$S (334.43 g/mol): C, 64.6 ;H, 8.37 ; N, 8.37 %
- HSO$_4$@PIIL, C$_{18}$H$_{29}$N$_2$O$_3$S• HSO$_4^-$ (462.58 g/mol): C, 15.6; H, 2.09; N, 2.02.

Found:

- Polymer, C$_{18}$H$_{28}$N$_2$O$_3$S (334.43 g/mol): C, 58.5 ;H, 7.21 ; N, 8.13 %
- HSO$_4$@PIIL, C$_{18}$H$_{29}$N$_2$O$_3$S• HSO$_4^-$ (462.58 g/mol): C, 53.53; H, 6.83; N, 7.32.

Therefore: 1 g of polymer contains 0.0813/14.0 = 5.81 x 10^{-3} moles N

1 g HSO$_4$@PIIL = 0.0732/ 14 = 5.22 x 10^{-3} moles N

$\frac{moles\ of\ N\ on\ 1\ g\ polymer}{moles\ of\ N\ on\ 1g\ HSO4@PIIL}$ = 5.81 x 10^{-3} / 5.22 x 10^{-3} = 1.113

1.113 g of HSO$_4$@PIIL contains 5.81 x 10^{-3} moles of N (see above) = 1 g polymer

Therefore 0.113 g of polymer (1.113-1g) of PIIL contain HSO$_4$ only

0.113 g extra mass is from HSO$_4$ = ((97.07 gmol^{-1})) = 97.07 gmol^{-1}

0.113 g/ 97.07 gmol^{-1} = 1.16 x10^{-3} moles of HSO$_4$ = 1.16 x 10^{-3} mol x 97.07 gmol^{-1} (=MW of HSO$_4$) = 0.113 g POM on 1.113 g PIIL

Therefore 1 g PIIL contains, 1 / 1.113 g x 0.113 g = 0.1015 g HSO$_4$ = 1.05 x 10^{-3} moles HSO$_4^-$

$\frac{moles\ of\ N\ on\ 1g\ of\ HSO4@PIIL}{2}$ = 5.22 x 10^{-3} moles of N/2 = 2.61 x 10^{-3} moles of SO$_3$H

$\frac{moles\ of\ SO3H}{moles\ of\ HSO4}$ = $\frac{0.00261}{0.00522}$ = 0.5 therefore 1:0.5 of HSO$_4$ to SO$_3$H polymer

L6: CHN analysis of HSO_4@PIIL **4.14**:

CHN Anal. Calc. for:

- Polymer, $C_{43}H_{60}N_4O_6S_2$ (792 g/mol): C, 65.2 ;H, 7.58 ; N, 7.07 %
- HSO_4@PIIL, $C_{43}H_{66}N_4O_6S_2 \cdot 2HSO_4^-$ (969.12 g/mol): C, 15.2; H, 1.83; N, 1.65.

Found:

- Polymer, $C_{43}H_{60}N_4O_6S_2$ (792 g/mol): C, 59.6 ;H, 6.35 ; N, 6.95 %
- HSO_4@PIIL, $C_{43}H_{66}N_4O_6S_2 \cdot 2HSO_4^-$ (969.12 g/mol): C, 50.9; H, 6.89; N, 6.22.

Therefore: 1 g of polymer contains $0.0695/14.0 = 4.96 \times 10^{-3}$ moles N

1 g HSO_4@PIIL $= 0.0622/ 14 = 4.44 \times 10^{-3}$ moles N

$\frac{moles\ of\ N\ on\ 1\ g\ polymer}{moles\ of\ N\ on\ 1g\ HSO4@PIIL} = 4.96 \times 10^{-3} / 4.44 \times 10^{-3} = 1.117$

1.117 g of HSO_4@PIIL contains 4.96×10^{-3} moles of N (see above) = 1 g polymer

Therefore 0.117 g of polymer (1.117-1g) of PIIL contain HSO_4 only

0.117 g extra mass is from $HSO_4 = ((97.07\ gmol^{-1})) = 97.07\ gmol^{-1}$

0.117 g/ 97.07 $gmol^{-1} = 1.21 \times 10^{-3}$ moles of $HSO_4 = 1.21 \times 10^{-3}$ mol x 97.07 $gmol^{-1}$ (=MW of HSO_4) = 0.117 g POM on 1.117 g PIIL

Therefore 1 g PIIL contains, 1 / 1.117 g x 0.117 g = 0.105 g $HSO_4 = 1.08 \times 10^{-3}$ moles HSO_4^-

$\frac{moles\ of\ N\ on\ 1g\ of\ HSO4@PIIL}{2} = 4.44 \times 10^{-3}$ moles of N/2 $= 2.22 \times 10^{-3}$ moles of SO_3H

$\frac{moles\ of\ SO3H}{moles\ of\ HSO4} = \frac{0.00222}{0.00108} = 2.05$ therefore 1:2.05 of HSO_4 to SO_3H polymer

Appendix M. SEM images of the polymers and PIIL materials.

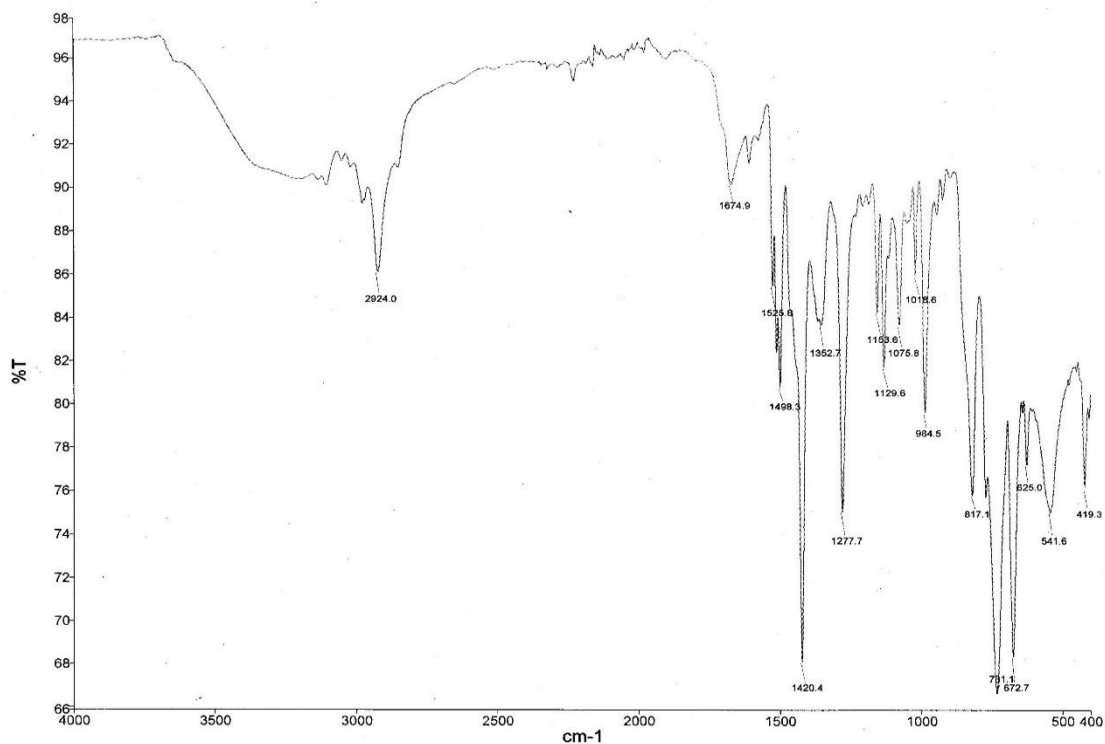M1: SEM image of HSO$_4$@PIIL **4.13**
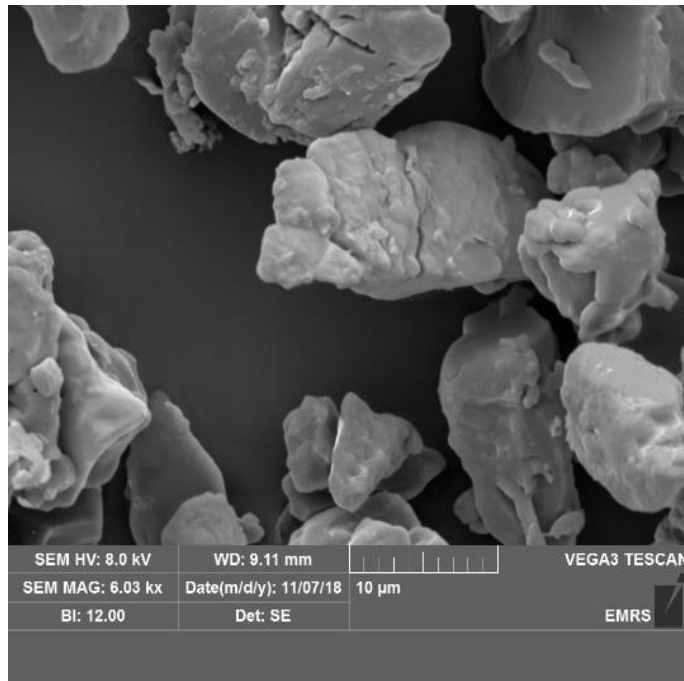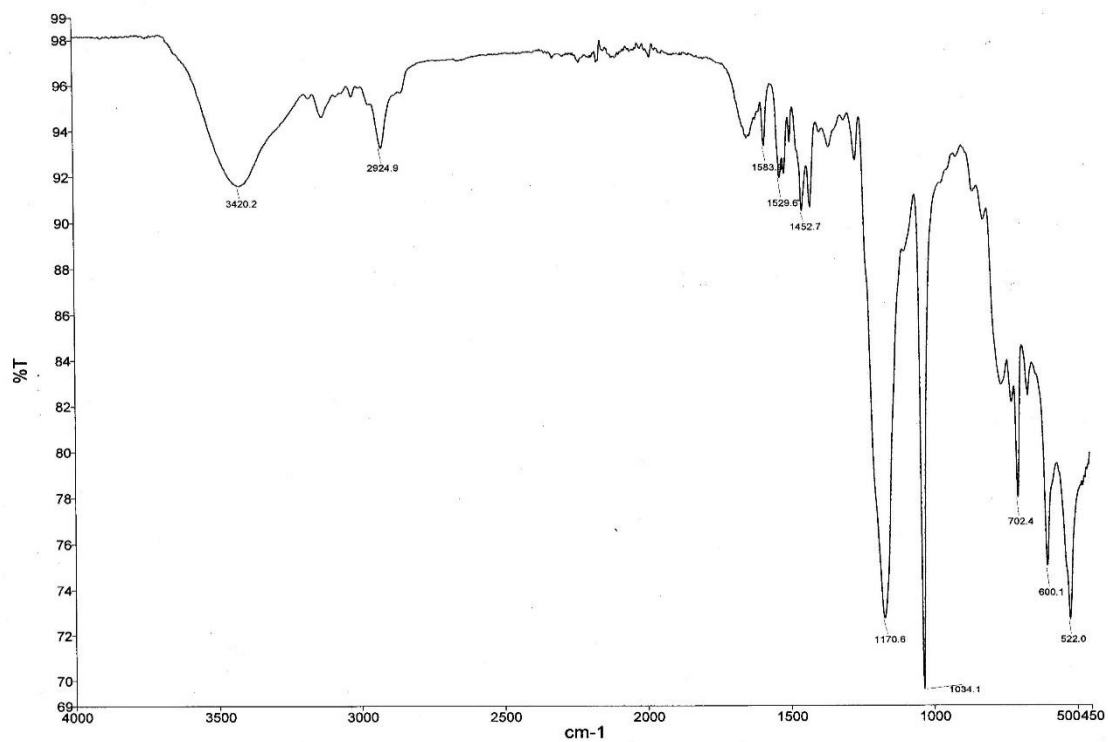

M1: SEM image of HSO$_4$@PIIL **4.14**:
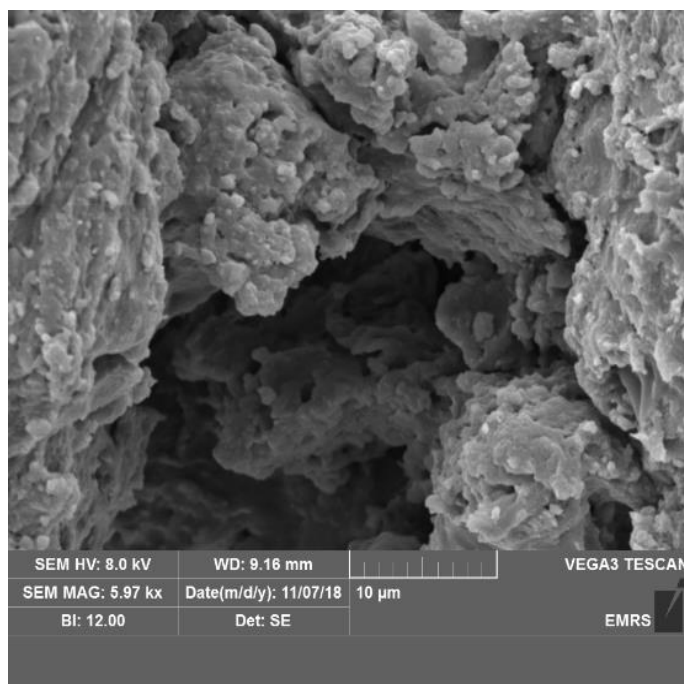
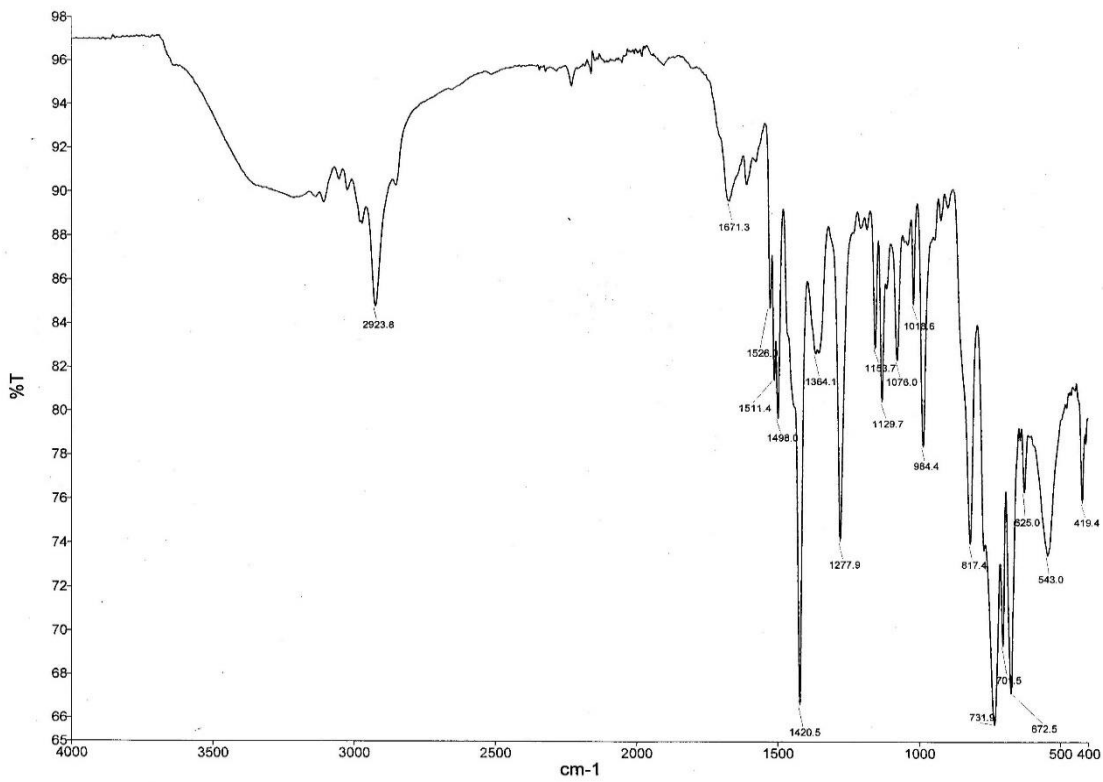## Appendix N: FTIR of polymers and POM@PIIL
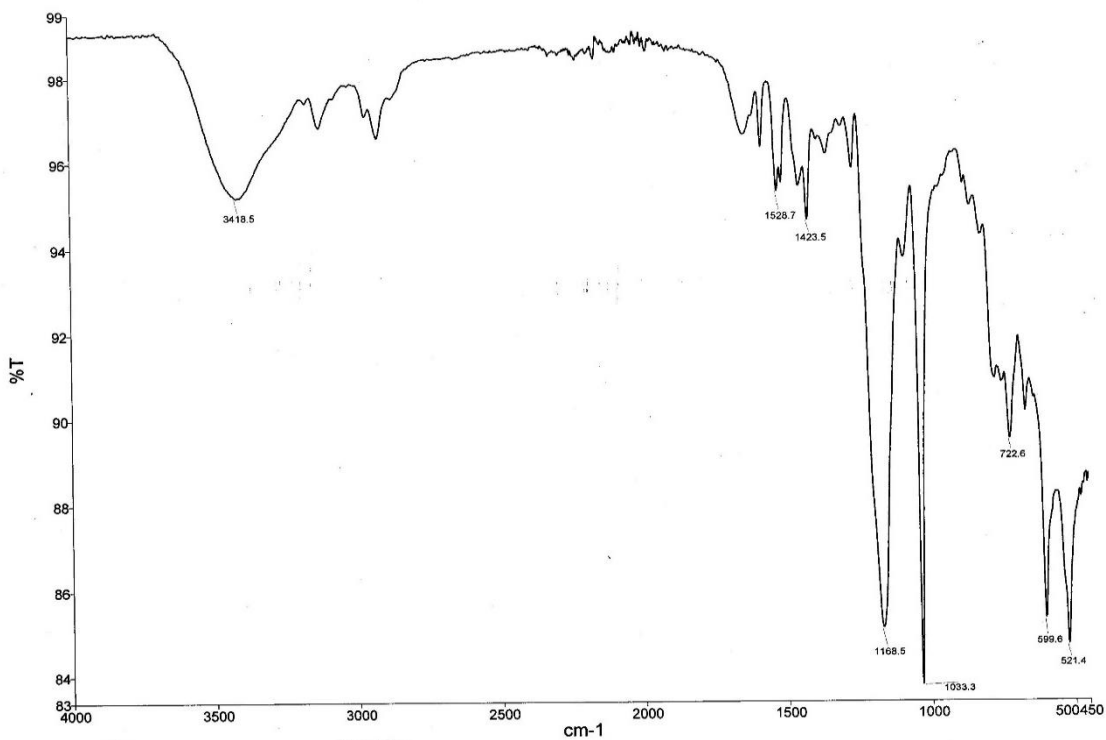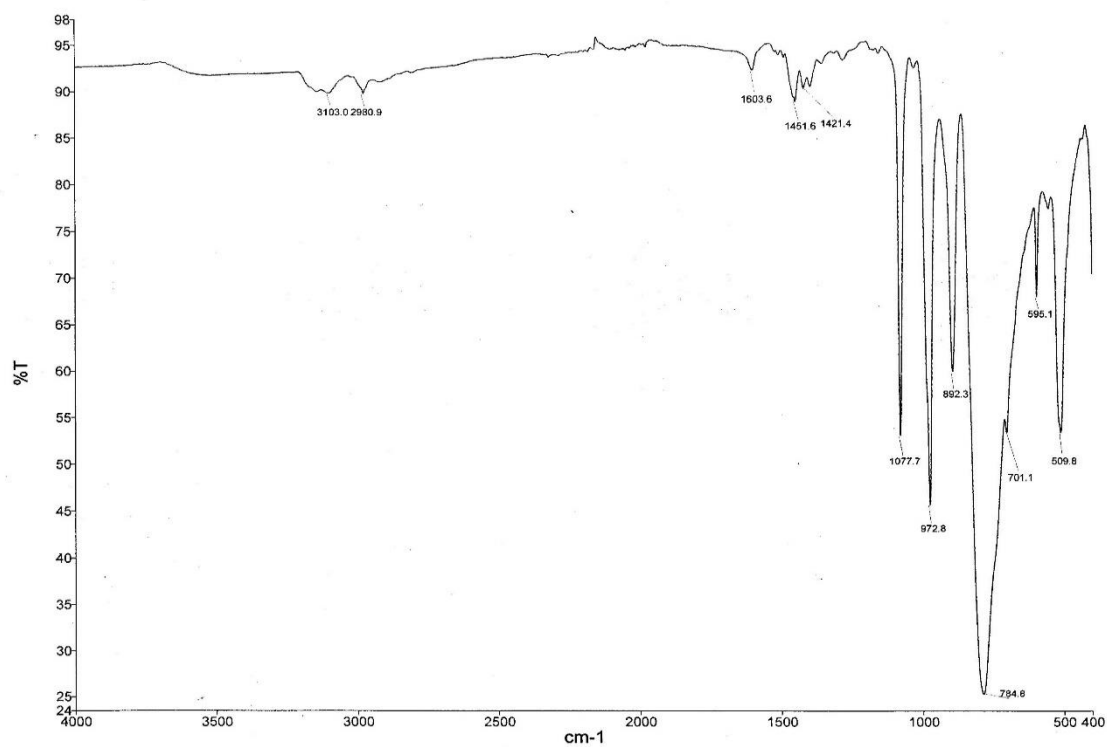
N1: FTIR of Polymer **4.3**:

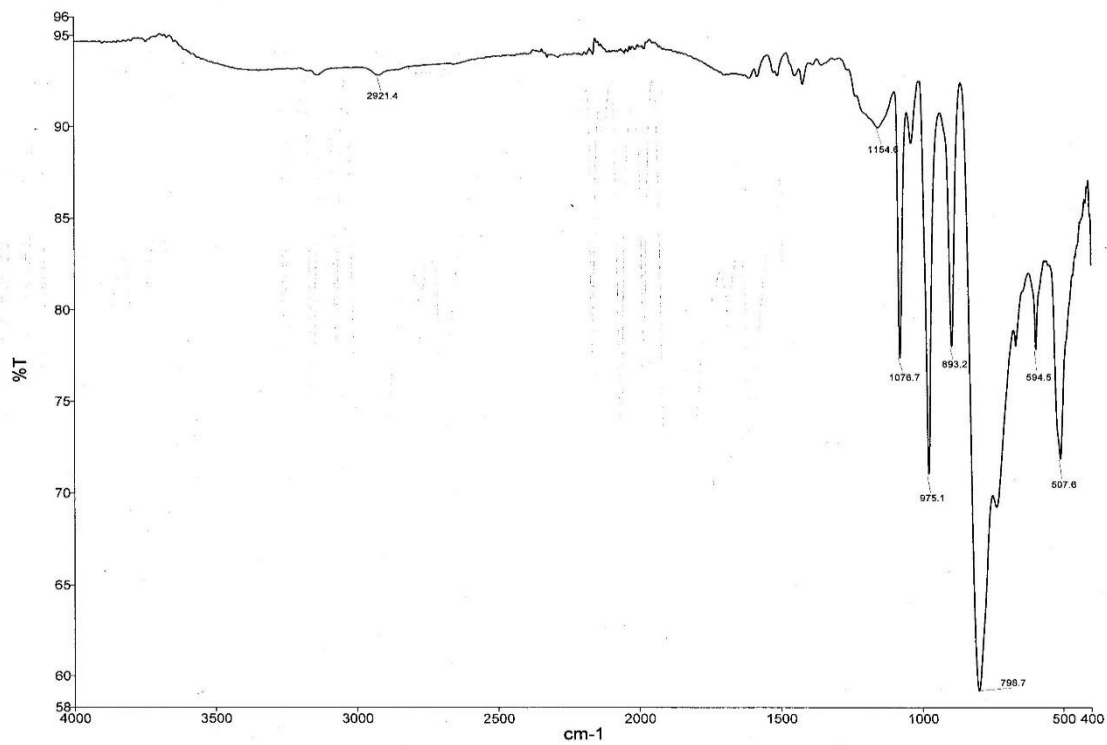N2: FTIR of Polymer **4.4**:

N3: FTIR of Polymer **4.5**:
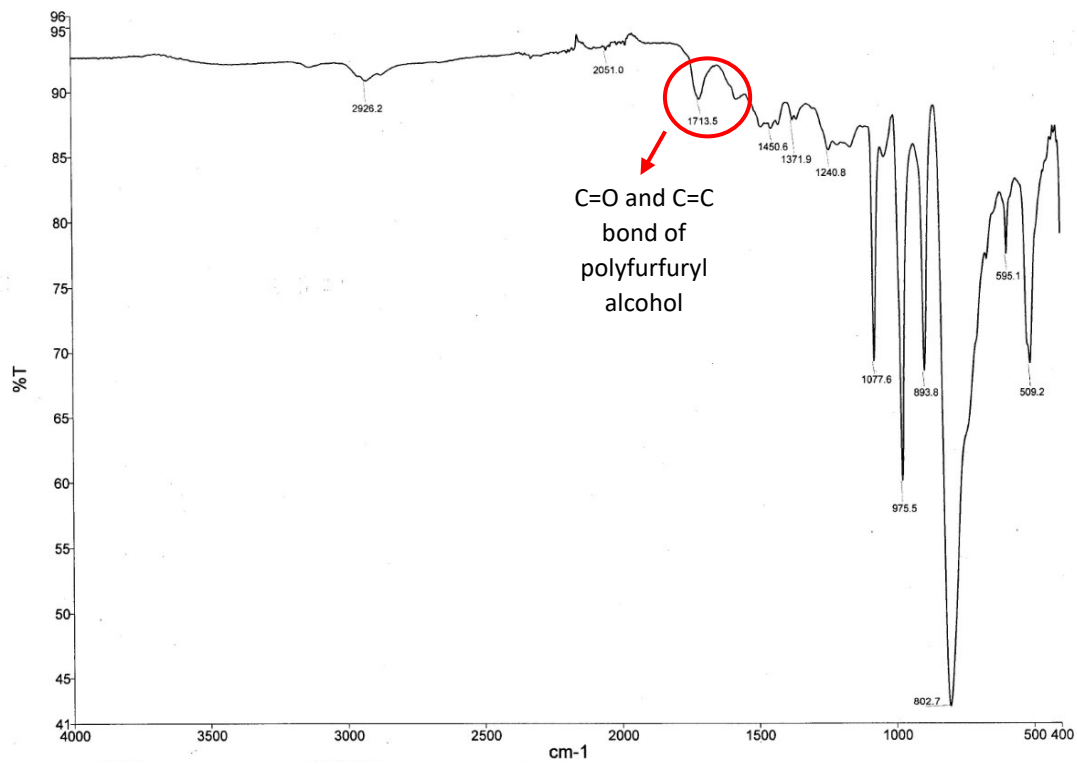

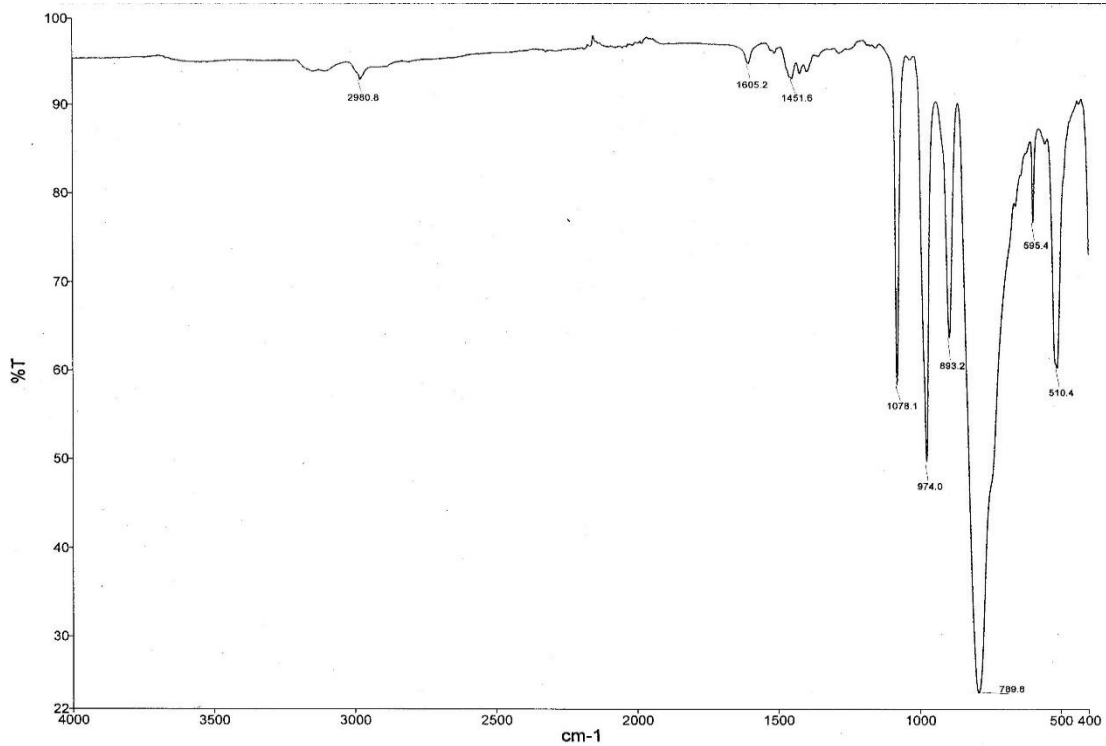N4: FTIR of Polymer **4.6**:
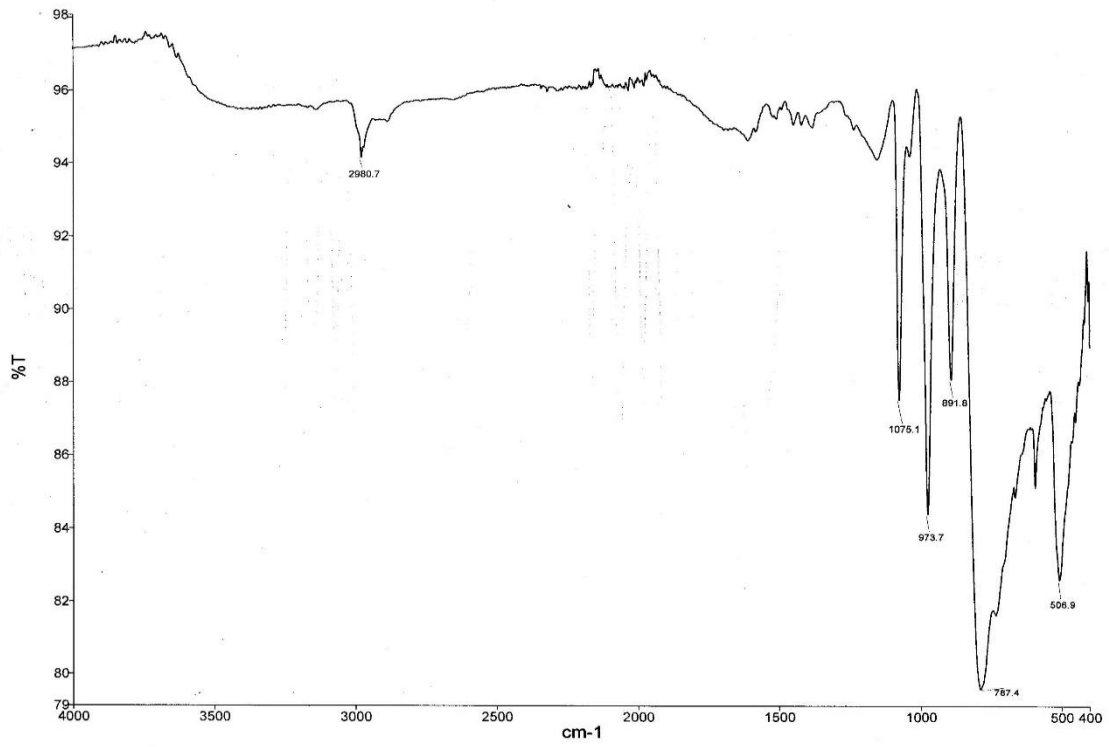
N5: FTIR of POM@PIIL **4.7**:

N6: FTIR of POM@PIIL **4.8**:

N7: FTIR of Recovered POM@PIIL **4.11** from catalyst recycle study:

C=O and C=C bond of polyfurfuryl alcohol
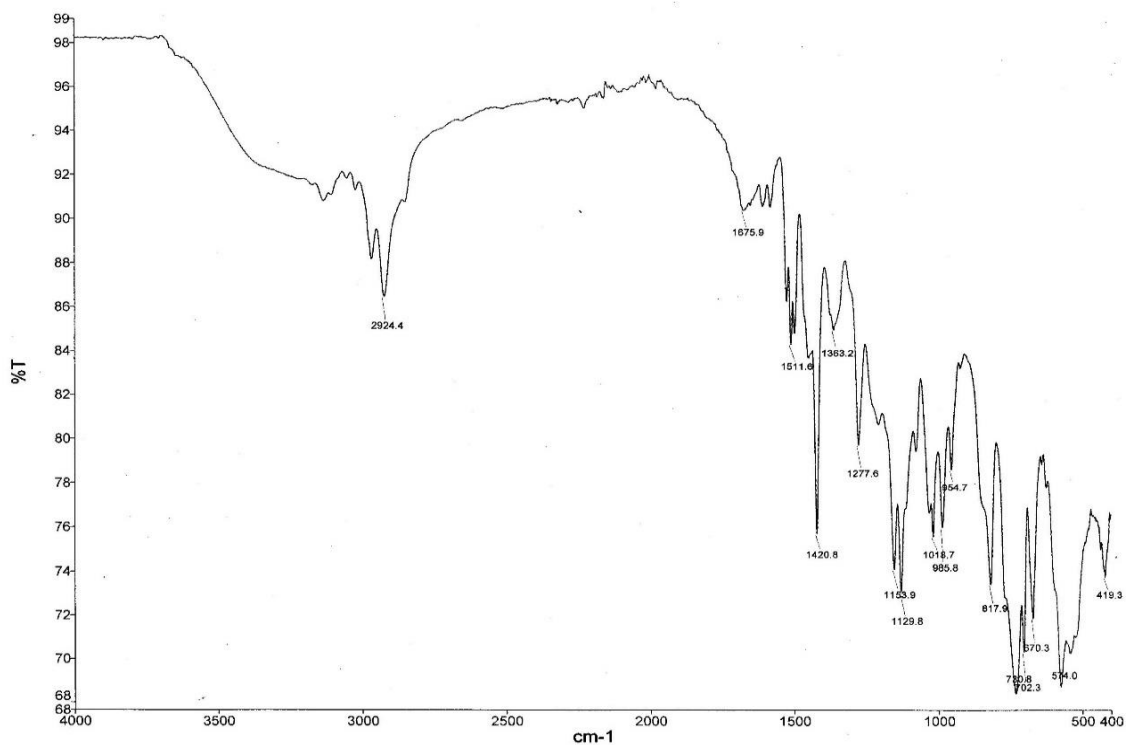
N8: FTIR of POM@PIIL **4.9**:
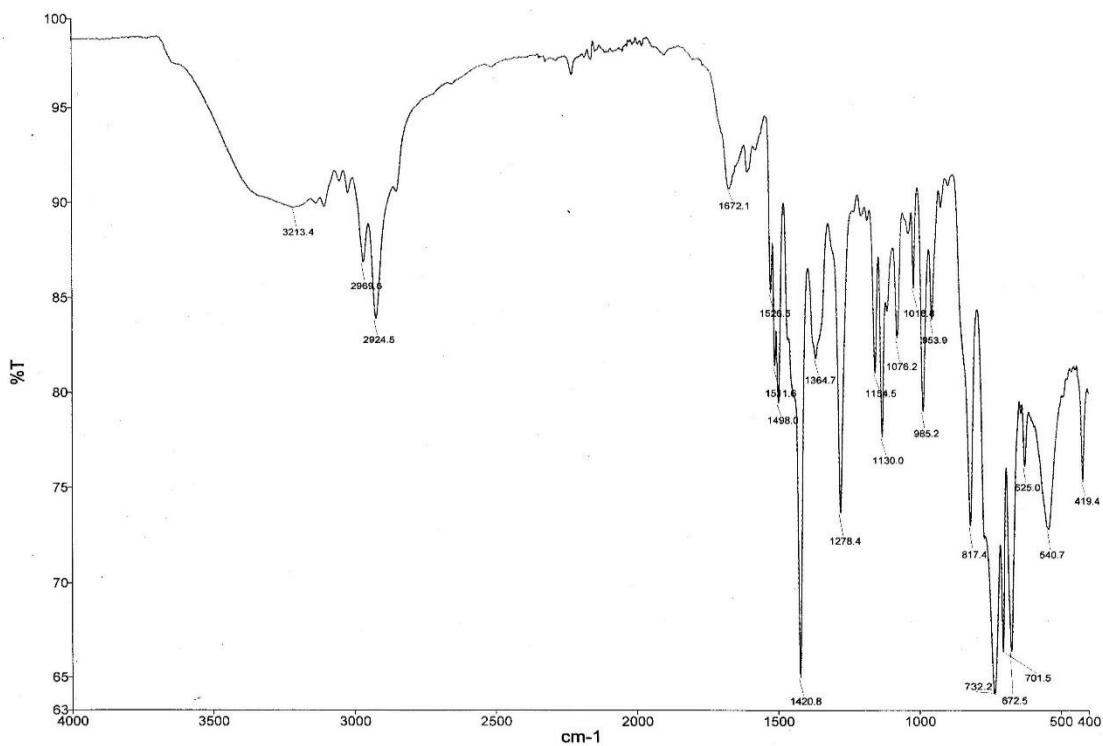
N9: FTIR of POM@PIIL **4.10**:

N10: FTIR of POM@PIIL **4.11**:
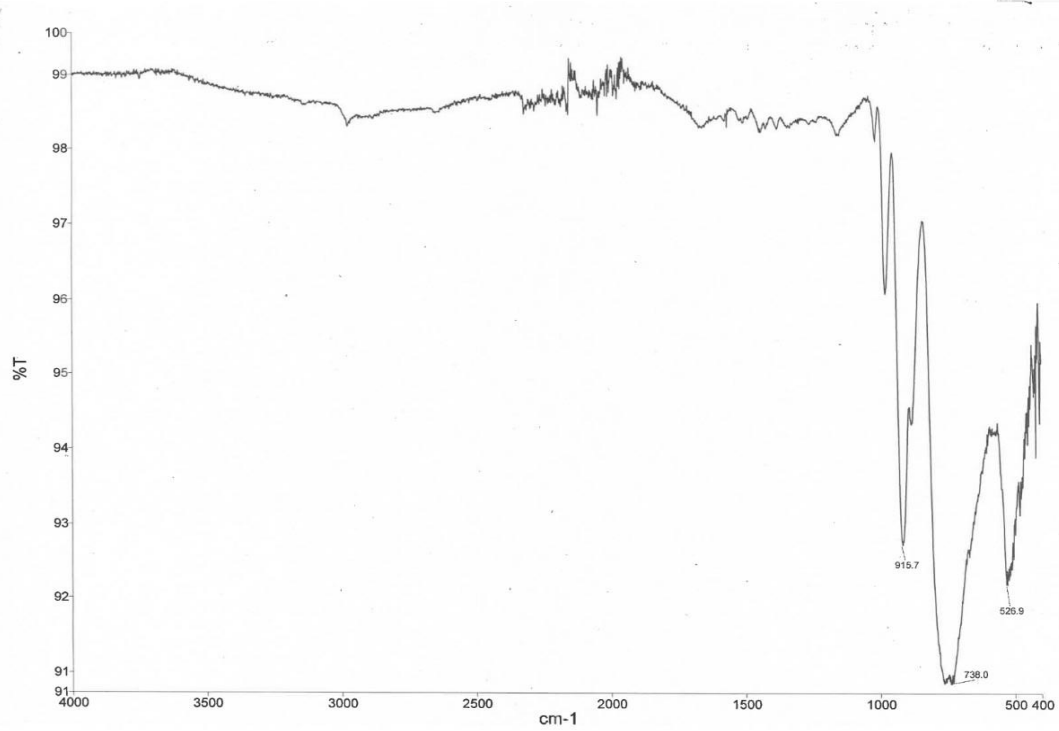
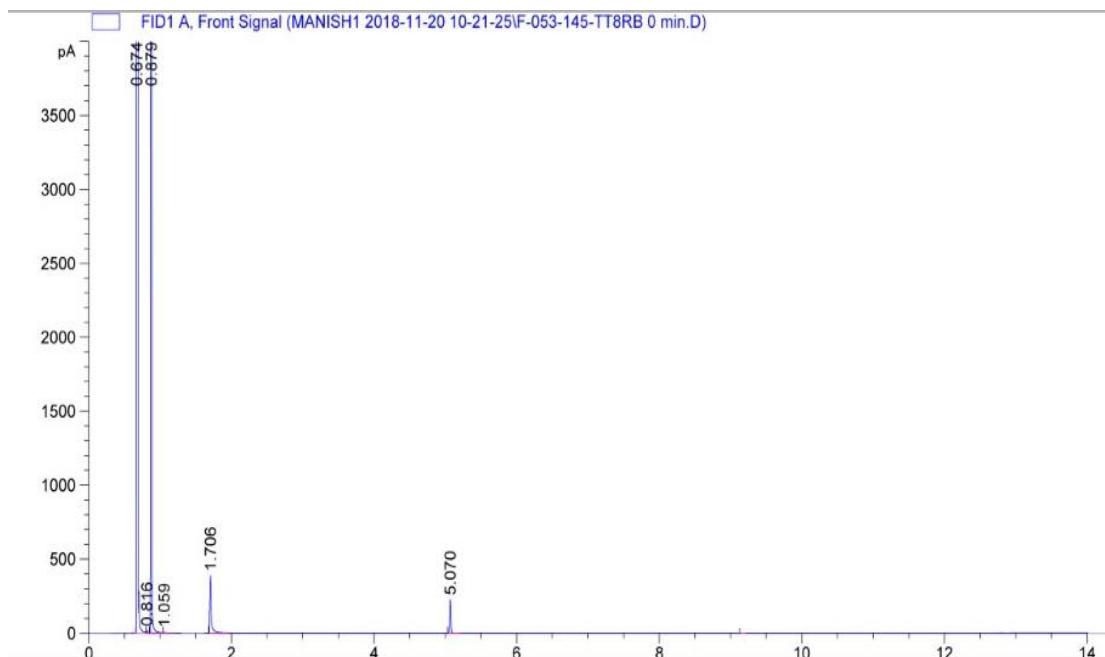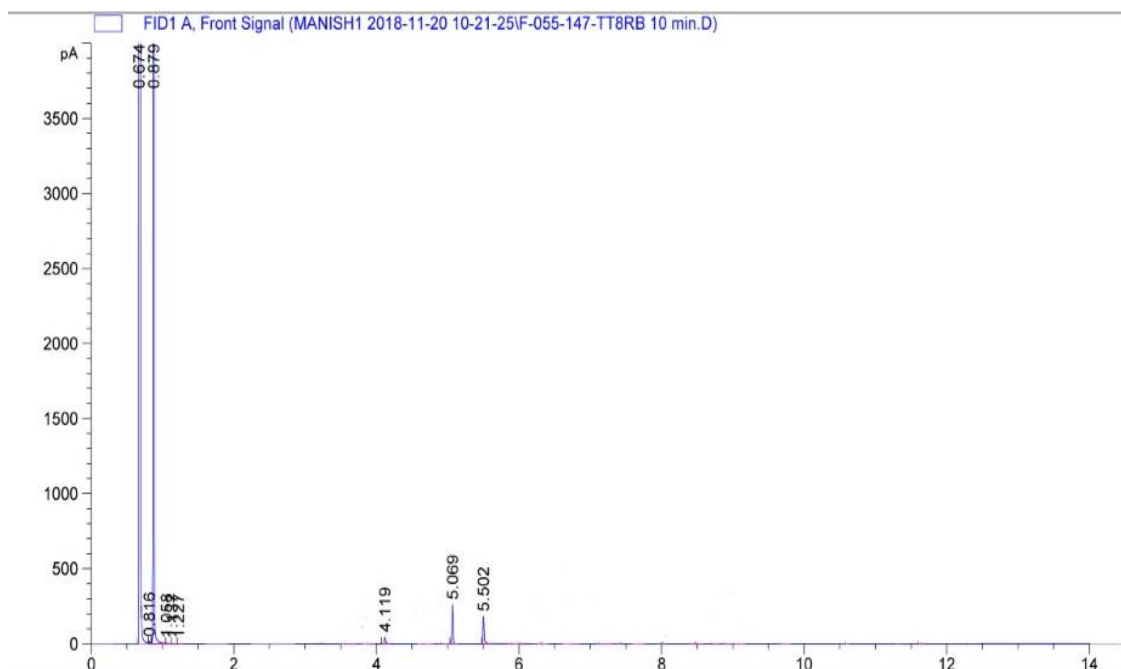N11: FTIR of HSO₄@PIIL **4.13**:

N12: FTIR of HSO₄@PIIL **4.14**:

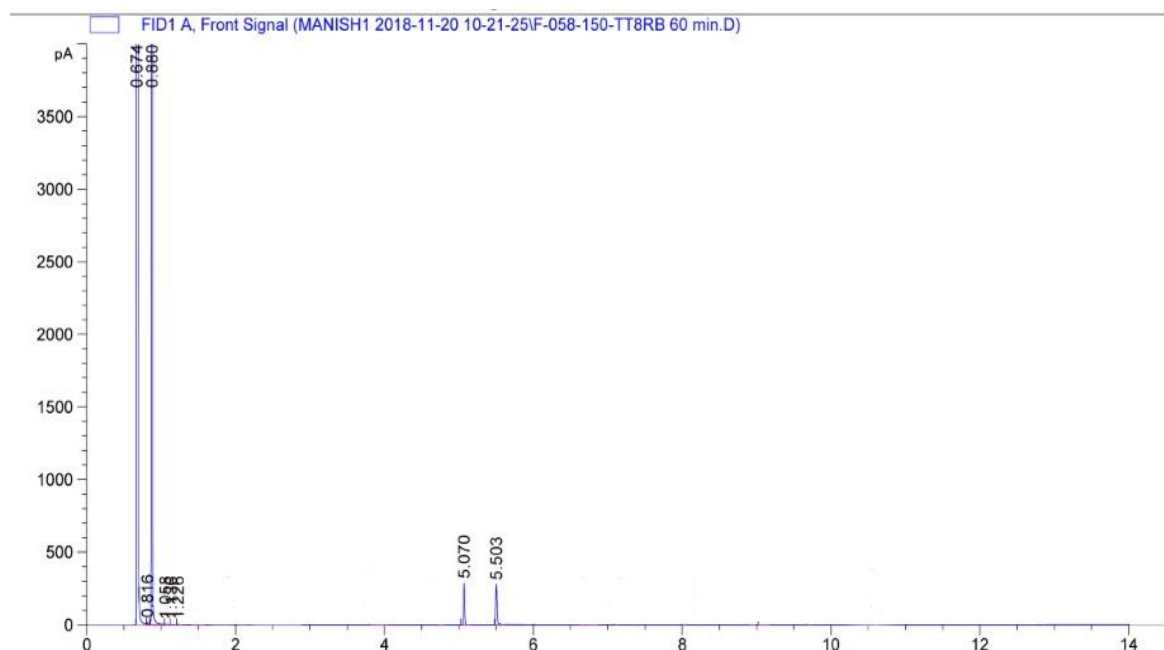## Appendix O: GC for the butanolysis of furfuryl alcohol

O1: GC of the reaction mixture, t_0

O2: GC of **4.11** catalysed reaction mixture after 10 minutes

O3: GC of **4.11** catalysed reaction mixture after 60 minutes

FID1 A, Front Signal (MANISH1 2018-11-20 10-21-25\F-058-150-TT8RB 60 min.D)

Relaxation times:

- n-butanol: 0.674 and 0.880 minutes
- furfuryl alcohol: 1.706 minutes
- 2-butoxymethylfuran: 4.119 minutes
- Dodecane: 5.070 minutes
- *n*-butyl levulinate: 5.503 minutes

Appendix P: Catalyst regeneration studies for the catalyst recycling:

a) Calcined at 300 ℃:

Recycle	4.10 conv. of FFA (%)	4.10 sel. to BL (%)	4.11 conv. of FFA (%)	4.10 sel. to BL (%)
0	80	77	85	96
1	67	76	81	93
2	55	72	66	90
3	36	69	52	82
4	29	65	43	80

b) Soaked in a 2M HCl solution:

| Recycle	Amb. conv. of FFA (%)	Amb. sel. to BL (%)
0	77	79
1	74	78
2	70	75
3	67	74
4	65	72

Reaction conditions: 2.5 mol% catalyst; FFA, 1 mmol; n-butanol, 3 mL; temperature, 110 ℃; time, 30 mins; agitation, 800 rpm. Conversion and selectivity determined by ^{1}H NMR spectroscopy with 1, 4-dioxane as the internal standard. Selectivity for *n*-butyl levulinate = [% *n*-butyl levulinate / (% *n*-butyl levulinate + % 2-butoxymethylfuran)]. Average of 2 runs.

Appendix Q: Time on-line data (TOL) for continuous flow for the butanolysis of furfuryl alcohol:

TOL (h)	4.10 conv.of FFA (%)	4.10 sel. to BL (%)	4.11 conv.of FFA (%)	4.11 sel. to BL (%)	Amb conv.of FFA (%)	Amb sel. to BL (%)
1	74	89	81	95	83	93
2	72	89	79	94	75	93
3	68	89	77	94	65	93
4	62	88	74	93	54	90
5	58	87	72	92	41	88
6	54	85	70	92	22	85

Reaction conditions: catalyst, 1 g on 1 g of silica; 0.32 M FFA in *n*-butanol; temperature, 130 ℃; flow rate, 1.1 mL min^{-1}; injection volume, 360 mL. Conversion and selectivity determined by ^{1}H NMR spectroscopy with 1,4-dioxane as the internal standard. Selectivity for *n*-butyl levulinate = [% *n*-butyl levulinate / (% *n*-butyl levulinate + % 2-butoxymethylfuran)]. Average of 2 runs.

Appendix R: Continuous Flow for the ethanolysis of furfuryl alcohol:
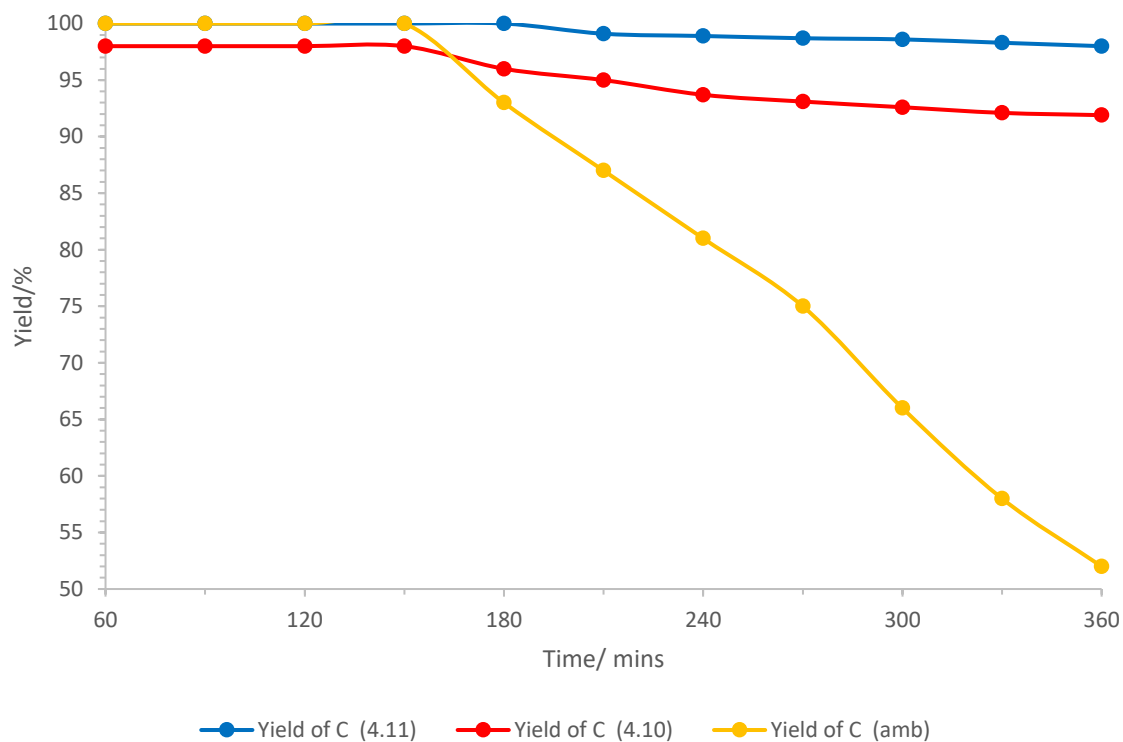
Reaction conditions: catalyst, 1 g of POM@PIIL or resin on 1 g of silica; 0.32 M FFA in ethanol; temperature, 100 ℃; flow rate, 1.1 mL min^{-1}; injection volume, 360 mL. Conversion and selectivity determined by ^{1}H NMR spectroscopy with 1,4-dioxane as the internal standard.